Detection of Freezing of Gait in Patients with Parkinson's Disease using Electroencephalography and Computational Intelligence

By

Aluysius Maria Ardi Handojoseno

A thesis submitted in partial fulfilment of the requirements for the degree of Doctor of Philosophy

Faculty of Engineering and Information Technology

2015

Certificate of Authorship/Originality

I, Aluysius Maria Ardi Handojoseno, certify that the work in this thesis has not previously been submitted for a degree, nor has it been submitted as part of the requirements of a degree, except as fully acknowledged within the text.

I also certify that this thesis has been written by me. Any help that I have received in my research work and in the preparation of the thesis itself has been acknowledged. In addition, I certify that all information sources and literature used are indicated in the thesis.

Signature of Candidate:

Production Note:
Signature removed prior to publication.

Date: 26 November 2015

“Teach us to give and not to count the cost”

St. Ignatius Loyola

Acknowledgements

First and foremost, I thank God, whose many blessings have made me who I am today, and enabled me to complete the research.

I would like to express my heartfelt appreciation and sincere gratitude to my principal supervisor, Professor Hung Tan Nguyen, Professor and Director, Centre for Health Technologies, University of Technology, Sydney, for the opportunity to carry out this research and for his invaluable guidance throughout. His experience and expertise in Health Technologies provided crucial insights for the research presented in this work.

I would also like to express my thanks to Dr Yvonne Tran and Dr Tuan Nghia Nguyen, my co-supervisors. Their guidance and support were exceptional. Their advice always enlightened and encouraged.

My sincere gratitude also goes to Dr Simon J.G. Lewis, Dr James 'Mac' Shine, and Moran Gilat at the Parkinson's Disease Research Clinic, Brain and Mind Research Institute, University of Sydney, for their collaboration in collecting data, analyzing results, and writing papers for journals and conferences. I hope we can further our collaboration on new projects in the near future.

My special thanks to all my colleagues and staff members at the Centre for Health Technology, University of Technology, Sydney, especially Dr. Mitchell Yuwono for his compelling enthusiasm and support, and to Quynh Tran Ly who will continue to work on this project.

Finally and importantly, my deep appreciation goes to the Indonesian and Australian Jesuits for the mission and all support of doing this research, my Jesuit community in St. Mary's North Sydney especially to Father Daven Day, and to my Indonesian Jesuit friends, and to Mum and my family, for their constant love, understanding, encouragement, moral support and prayer throughout. And special thanks also to my friends especially Reena Maria Francesca Tolmik, Penny Ho, Gracelyn Vega, Gems Surya and family, Fenty Terihardjo and Bernadette Soesanto.

Contents

List of Figures

List of Tables

Nomenclature

3D-SSP	:	3-dimensional Stereotactic Surface Projections
AD	:	Alzheimer Disease
ANN	:	Artificial Neural Networks
APSD	:	Auto-Power Spectral Densities
AR	:	Autoregressive
BA	:	Brodmann Area
BSS	:	Blind Source Separation
CPSD	:	Cross Power Spectral Density
CS	:	Centroid Scale
CWT	:	Continuous Wavelet Transform
DALY	:	Disability Adjusted Life Years
dDTF	:	Direct Directed Transfer Function
DNN	:	Dynamic Neural Network
DSM-IV	:	Diagnostic and Statistical Manual of Mental Disorder, Fourth Edition
DTF	:	Directed Transfer Function
DWT	:	Discrete Wavelet Transforms
EEG	:	Electroencephalography
EMG	:	Electromyography
EOG	:	Electrooculography
ffDTF	:	Full Frequency Directed Transfer Function
FFT	:	Fast Fourier Transform
FI	:	Freeze Index
fMRI	:	Function Magnetic Resonance Imaging
FOG	:	Freezing of Gait
FOG-Q	:	Freezing of Gait Questionnaire
H&Y	:	Hoehn and Yahr

ICA	:	Independent Component Analysis
MEG	:	Magnetoencephalography
MGAP	:	Microbe Genome Annotation Platform
MLP-NN	:	Multi Layer Perceptron Neural Networks
MMSE	:	Mini Mental State Examination
MRP	:	Movement-Related potentials
MSC	:	Magnitude Squared Coherence
MVAR	:	Multivariate Autoregressive
NFOG-Q	:	New Freezing of Gait Questionnaire
PCA	:	Principle Components Analysis
Pcc	:	Pearson's Correlation Coefficient
PD	:	Parkinson's Disease
PDC	:	Partial Directed Coherence
PLV	:	Phase Locking Value
PSD	:	Power Spectral Density
PSE	:	Power Spectral Entropy
PWF	:	Patient with PD with FOG
PWoF	:	Patient with PD without FOG
PWP	:	Patient with PD
RAS	:	Rhythmic Auditory Stimulation
ROI	:	Region of Interest
RT	:	Reaction Time
SCF	:	Spectral Centroid Frequency
sGPDC	:	Squared Generalized Partial Directed Coherence
SMA	:	Supplementary Motor Area
SPECT	:	Single Photon Emission Computed Tomography
TUG	:	Timed Up and Go
UPDRS	:	Unified Parkinson's Disease Rating Scale
VBM	:	Voxel-Based Morphometry
WCO	:	Wavelet Coherence
WCS	:	Wavelet Cross Spectrum
WE	:	Wavelet Energy
WEE	:	Wavelet Energy Entropy
WPLI	:	Weighted Phase Lag Index
WPS	:	Wavelet Power Spectrum

Abstract

Freezing of Gait (FOG) is a common movement disorder affecting patients with Parkinson's disease in the advanced stage. Patients often describe it as feeling like their feet are "glued to the floor" which suppresses their ability to start walking or to continue moving forward. It significantly affects patients' quality of life since the sudden and unpredictable characteristic of FOG is a common cause of falls and related injuries. It interferes with daily activities, and leads to a loss of independence. Freezing of gait is mainly perceived as an alteration in the pattern of movement, and the accelerometer, which senses movement, speed and direction, can be used as the main sensor in the detection of FOG in research studies.

Although the accelerometer has been successfully applied in the detection of FOG, it is only able to detect FOG as it occurs, which is often too late for prevention of injuries such as falls. The research in this thesis introduces electroencephalography (EEG) as a novel technique to address this problem. The EEG provides a window to see the transition episode *before* a freezing episode. Freezing of gait occurs as a result of complex, dynamic neurophysiology in the brain related to motor control as well as cognition and emotions, and the EEG signal can capture the electrical activity of the brain while this is occurring. In addition, scalp EEG has many other benefits, such as its portability, non-invasive nature, relative inexpensive cost and simple operation, whilst providing high precision in time measurements.

The study examined 16 patients (age 70.88 ± 6.92 years) with idiopathic Parkinson's disease and significant FOG, consisted of 9 patients at Hoehn and Yahr (H&Y) stages 2 and 2.5 - the early stages (56.25%), 5 patients at stage 3 - the moderate stage (31.25%), and

2 patients at stage 4 - the advanced stage (12.5%). This research studied the various features of EEG which can be used as indicators of FOG and aims to introduce the effective features as inputs for the FOG.

The first analysis was based on the classical power spectral density (extracted using Fast Fourier Transform) and its counterpart (extracted using wavelet transform). By using centroid frequency extracted from channel central zero (Cz) as input and artificial neural network as the classifier, the classification of two episodes (normal walking and 5 s transition before freezing) in the in-group was obtained with a sensitivity, specificity and accuracy of 77.0%, 74.1% and 79.5%, respectively.

The second analysis studied the cross correlation and coherence based features, aiming to improve the performance of the FOG detection and to obtain a better understanding of FOG. These features provide spatial properties of EEG which complement the time-frequency characterization gained from classical power spectral analysis.

Beyond correlation of two brain locations, in the third analysis, the brain connectivity dynamic analysis was explored further using the analysis of the causal influence between the brain locations of interest. A squared Generalized Partial Directed Coherence was used to evaluate this causal connectivity. This approach modelled effectively the inherently multivariate nature of neuronal networks. All the features were investigated with clinical EEG data. After the optimization using Independent Component Analysis and Bayesian regularization, and applying squared Generalized Partial Directed Coherence connectivity estimation, in the in-group the classifier achieved a sensitivity, specificity and accuracy of 89.1%, 91.2%, and 90.2% , respectively. The results in the out-group were relatively similar with a sensitivity, specificity and accuracy of 86.5%, 92.8% and 89.5%, respectively.

In addition, the physiology analysis provided the characterization of FOG. Beta oscillations in central lead were found to underlie the neural activity in transition to the freezing episode in power spectral measurement. In coherence study, pairwise frontocentral showed significant change, especially in the theta frequency. Effective connectivity also showed significant alteration on the causality measurement in this area. This finding lead

to the development of the predicted mechanism underlying FOG.

In summary, the techniques proposed in this dissertation contribute to the development of the detection system of FOG that can be used by patients with PD to improve their symptoms with satisfactory classification performance. In addition, the results of the experiment provide the electrophysiological signature of FOG in PD lead to novel insights into the pattern of spatiotemporal dynamic of the brain underlying this debilitating symptom of PD.

Chapter 1

Introduction

"I turned myself around. In fact, Parkinson's has made me a better person. A better husband, father and overall human being. Life delivered me a catastrophe, but I found a richness of soul."
-Michael J. Fox

1.1 Motivation

After Alzheimer's disease (AD), Parkinson's disease (PD) is the second most prevalent neurodegenerative disorder which increases with age (Factor & Weiner, 2007a). It is a slowly progressive, incurable, and complex neurodegenerative disorder, which mainly but not only involves motor systems. In addition to the main motor symptomatology (tremor, rigidity, akinesia, and postural disturbance) and the late onset motor symptoms (such as gait disturbance including festinating gait and freezing of gait (FOG), speech and swallowing disorders, gastrointestinal motor functions disturbance, postural instability and falls), some non-motor symptoms such as depression, dementia, hallucinations, sleep disorder, and personality change may be present and may become troublesome after several years of the disease.

Identified clinically as idiopathic PD to distinguish it from more general Parkinsonism, PD is widely understood to be caused mainly by the degeneration of a neurotransmitter

which controls movement, called dopamine, in the substantia nigra, an area in the basal ganglia of the brain (Wichmann *et al.*, 2007). Developments in the study of the pathological process, reveal new insights into the complex and multi system abnormalities in the neurotransmitter systems, which cause a wide range of non-motor symptoms, such as cognitive and affective problems (Wolters & Bosboom, 2007). As a result, non dopaminergic hypotheses have been developed along with the finding that the neurodegeneration in PD also affects most of the brain neuromediators, such as acetylcholine (chemicals which are stimulates muscle cells), noradrenaline-epinephrine (chemicals which are responsible for vigilant concentration, in an anti-stress hormone in the body), serotoninergic (chemicals related to serotonin, a contributor to feeling of well-being and happiness, positive and negative moods), cholinergic (chemicals related to acetylcholine which has an important role in the sensory perceptions, learning and memory), and glutamate (a neurotransmitter which is involved in most aspects of normal brain function, including cognition, memory and learning) (Devos *et al.*, 2010).

PD is a relatively common disorder which affects between 4.1 and 4.6 million individuals over age 50 in the Western Europe's 5 most populous nations (Germany, France, the United Kingdom, Italy, and Spain) and the world's 10 most populous nations (China, India, United States, Indonesia, Brazil, Pakistan, Bangladesh, Russia, Nigeria, and Japan) in 2005 (Dorsey *et al.*, 2007). The number of people with PD (PWP) has been predicted to double over the next 20 years along with the ageing of the general population and the increasing of life expectancy (Factor & Weiner, 2007a). It is estimated that over 64,000 Australians had a diagnosis of PD in 2011, approximately one in every 350 people, with nearly 30 newly diagnosed PD cases each day (DeloitteAccessEconomicsPtyLtd, 2011). One in five of those affected is estimated to be of working age (15-64) with 12.2 years the median living years from onset to death.

Currently, neurological diseases, including PD, lead to 1% of deaths worldwide. Neurological diseases are predicted to become the second most common cause of death in the world by 2040 (WHO *et al.*, 2004). While PD by itself is not fatal, life expectancy of PWP decreased due to the degrading impact of PD on the physical disabilities. A nine-year follow up study on 170 PWP in Sweden reveals premature death due to cerebrovascular

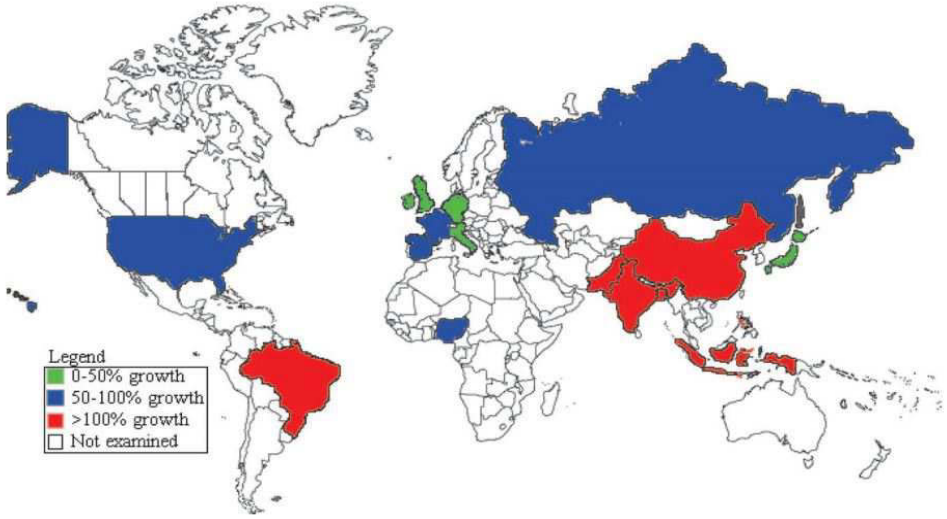

Figure 1.1: Projected growth rates in number of individuals over 50 with PD in the most populous nations in Western Europe and the world from 2005 to 2030 (Dorsey *et al.*, 2007).

diseases and swallowing problems led to pneumonia (Fall *et al.*, 2003).

Society also pays an enormous price for PD. The personal financial cost impact of PD in Australia in 2011 was estimated to be around $12,000, and the average life time financial cost to be around $144,000 for PWP who lives for 12 years (DeloitteAccessEconomicsPtyLtd, 2011). The impact of the disease on an individual and societal basis was also measured through the "healthy life" lost year due to disability and early death, which is called Disability Adjusted Life Years, DALYs. For PD, the burden of the disease in Australia in 2011 was estimated to be 46,069 DALYs. A recent Finnish study also found PD to have the greatest negative impact on health-related quality of life among 29 major chronic conditions including stroke, heart failure and cancer (Saarni *et al.*, 2006).

The progression of motor symptoms becomes the main bases for the clinical diagnosis of PD. The Hoehn and Yahr scale of PD, introduced in 1967, has wide utilization and acceptance because it is very easy to administer to rate the progression of PD symptoms. Its modified forms are still used in practice and clinical trials (Gancher, 2008). It applies 5 neuropathologic stages of PD as illustrated in Table 1.1. As the Hoehn and Yahr scale rating system measures motor movement impairment only, the Unified Parkinson's Disease Rating Scale (UPDRS) which is more complicated but covers more factors (for example

behavior, mood and activities of daily living), has largely supplanted it.

Table 1.1: The Hoehn & Yahr Scale (1967)

Stage	Characteristics
1	Unilateral involvement only. Usually minimal or no functional impairment. Symptoms include tremor of one limb, and change in posture, locomotion and facial expression.
2	Bilateral symptoms with minimal disability. Posture and gait affected.
3	Significant slowing of body movements. First signs of postural instability of walking or standing, Mild to moderate disability.
4	Severe symptoms: walking limited, rigidity and bradykinesia. Severely disabling, individual is markedly incapacitated and is unable to live alone.
5	Cachectic stage. Restricted to bed or wheelchair unless aided.

Freezing of Gait (FOG) is common in idiopathic PD and is found in a majority of advanced PD patients, generally accepted as related to those with Hoehn Yahr stages 3 and 4, with prevalence of FOG occurring in up to 53% of the population after 5 years of illness (Niewboer *et al.*, 2004; Okuma, 2006; Giladi & Niewboer, 2008). However, other studies show that FOG occurs in very early stages of idiopathic PD (Bloem *et al.*, 2004), with up to one quarter of the patients experiencing FOG in the early stages of PD (Moore *et al.*, 2008). A survey of 6620 PWP in Germany reported that 28% of the cohort experienced FOG daily, whilst 13% and 6% of the cohort experienced FOG weekly and monthly, respectively (Macht *et al.*, 2007).

Described by patients as a feeling like their feet are “glued to the floor”, this episodic gait disorder suppresses patient ability to start walking or continue moving forward. The alternating tremble of the leg and hastening or increase in cadence with a decrease in step length (festination), often accompanies FOG. The sudden and unpredictable character of FOG makes it a common cause of falls, interferes with daily activities, and significantly impairs quality of life (Backer, 2006). FOG happened both in the “on” state (when medication is functioning effectively), but more frequently in the “off” state (when medications has no effect). FOG was found to be the most distressing symptom and the least understood symptom in PD. The poor efficacy of empirical treatments present the condition as an important clinical issue (Nutt *et al.*, 2011a; Shine *et al.*, 2011).

That patients do not have a proper understanding of what actual freezing looks like is a challenge for clinicians, as this causes them to deny having FOG (Snijders, 2012). The challenge for researchers lies in the difficulty to provoke FOG because during physical examination, compared with normal daily life when FOG happens naturally, patients can temporarily suppress FOG in a formal testing environment, simply through their extra attention to gait.

FOG is difficult to measure because it is highly sensitive to environmental triggers, cognitive input, and medication. The manifestation of FOG is intimately related to the external environment of the individual. Several specific scenarios have been found to initiate FOG, including dual tasking, passing through doorways or crowded areas, and stress and anxiety, with turning around and fatigue found to be the strongest provoking factor (Rahman *et al.*, 2008). Together, the multifactorial nature of these triggers indicates a multi system deficit in FOG, in which impaired information processing across cognitive, affective, and motor domains leads to overwhelming inhibition over the brainstem structures that control gait (Shine *et al.*, 2013a; Nieuwboer & Giladi, 2013a). This proposal is supported by the results of functional neuroimaging (Bartels & Leenders, 2009; Shine *et al.*, 2013b; Almeida & Lebold, 2010).

As dopaminergic replacement therapy only partially alleviates FOG, different strategies have been developed to trigger alternative neural circuits in behavioral control. Somatosensory cues have been found to improve walking, with visual cues offering the strongest influence, followed by tactile, emotional and auditory cues (Rahman *et al.*, 2008). A recent investigation on the effect of visual cues using laser on 7 PD patients with FOG showed that “on-demand” cueing (only given when FOG episodes were observed) is more efficient for reducing the duration of FOG periods than continuous cueing (Velik *et al.*, 2012) which indicates the importance of a FOG detection system.

1.2 Problem Statement

In recent years, few attempts to detect or predict the onset of FOG have been reported. Because leg oscillations are so common in an episodes of freezing, they are used as a

sign of the onset of freezing and as an indication for immediate special treatment to "un-freeze" (Nutt *et al.*, 2011a; Jovanov *et al.*, 2009). There are 2 major approaches: that based on characterizing FOG using a spatiotemporal kinematic parameter of gait (an increased cadence, decreased stride length, and decreased angular excursion of leg joints) (Connor *et al.*, 2007); and that based on frequency analysis of leg movement (Delval *et al.*, 2010). Some research have reported Electromyography (EMG) patterns to detect the onset of FOG (Niewboer *et al.*, 2004; Popovic *et al.*, 2010). A wearable device using "on-body" acceleration sensors to measure patient's movements has also been developed (Bachlin *et al.*, 2010).

While the above research give insight to the physiological characteristic signs, their reliability as an indicator of FOG are limited by their large variability in data measurements due to different walking styles among patients. Besides, the research cannot differentiate akinesia of FOG and non-FOG gait disturbance during normal walking, which may include stopping voluntarily, due to the similarity in characteristic of related motor performance (Moore *et al.*, 2008; Mazilu *et al.*, 2012; Niazmand *et al.*, 2011a). Furthermore, applying the intervention after indicating gait problem makes it less effective to un-freeze. Thus there is need for a different approach to solve all of these problems, and using a brain signal appears to be a potential effective solution, as it can provide information on the motor progression before the onset of FOG, and it is not determine by the personal gait movement styles.

Despite extensive research on the Electroencephalography (EEG) to identify and analyze brain dysfunctions including AD (Trambaiolli *et al.*, 2011), epilepsy (Adeli *et al.*, 2007), monitoring cerebral injury and recovery (Shin *et al.*, 2008), there are very few studies on EEG and PD (Velu *et al.*, 2013). While EEGs have been used to study PD, including symptoms relating to FOG, no implementation of EEG for FOG detection has taken place. With the development of the EEG signal preprocessing (better sensor, amplifier and filtering), EEG signal transmission data mode (wireless), EEG signal processing (artifact handling, features of extraction and selection), and EEG signal classification, EEG appears as a promising device in the detection of FOG in PD's patients due to its portability and convenience of use.

This research project have emerged as a further development of an initial discussion in understanding and predicting FOG in PD patients using EEG signals, between Professor Hung Nguyen, the Director of the Centre for Health Technologies, University of Technology Sydney, and Associate Professor Dr Simon J.G. Lewis, the Director of the Parkinson's Disease Research Clinic, Brain and Mind Research Institute, University of Sydney.

1.3 Thesis Objective

The aim of this research is to develop new methodologies for FOG detection through the development of algorithms which automatically interpret brain data associated with FOG in PD patients. This research used a 4-channel wireless EEG system developed by Centre for Health Technologies - UTS research team. Brain signal dynamics were chosen to predict the onset of freezing at the earliest time due to its ability to measure dynamic physiological change in the brain *before* the occurrence of movement disturbances. Using EEG, both cortical and subcortical activity can be studied through the time-varying changes in certain spectral bands, which also allow insights into the mechanism of FOG. Hence, 3 areas are explored.

First, the feasibility of this novel method of using EEG for detecting FOG is assessed. This research includes the extraction of valuable information from each single separated channel measures, and the study of the potential use of EEG to discriminate between normal walking and transition to freezing of PD patients with FOG. An Artificial Neural Networks (ANN) is implemented to classify the EEG signals from those 2 conditions using the representation of the time frequency domain characteristic of EEG signals, extracted using Fast Fourier Transform and wavelet transform.

Second, the functional interactions of pairwise EEG channels related to the freezing episode as indicators of FOG (which also can be used as features for a classification system) are investigated. Moving further from analysis on single separated channel measures, this study observes the statistical dependencies among spatially remote neurophysiological measurement characterized by their correlations and coherences. The implementation of ANN as a classifier for FOG detection with these features as inputs and its physiology

was researched.

Third, the influence one neural system exerts over another in 4 different cortical levels was studied and used to give insight for the neurophysiological explanation of FOG and as inputs for classification system. The classification system is optimized by maximizing separation between signals which represent different conditions (i.e. minimizing the mutual information between the components of the input) using the independent component analysis (ICA) and by building more robust training for ANN using Bayesian regularization.

1.4 Thesis Contribution

The contributions of this doctoral research are presented as follows:

- Firstly, a method for extracting valuable information from EEG signals, and study of the potential use of EEG to predict FOG, by discriminating the pattern of EEG signals characterized by single channel measurement based during normal walking and transition to FOG. This novel application of EEG signals classification for detecting FOG includes data collection and signal processing from 16 PD patients with FOG. The preliminary study that showed the feasibility of using this new approach in FOG treatment has been reported in (Handojoseno *et al.*, 2012).

- Second, neural networks predictive classification of FOG was augmented by connectivity measures reflecting the functional interaction between pairwise electrode taken from 4 locations of interest. This study of coupling and cross talk between different locations of EEG channel lead to further exploration of the FOG physiology mechanisms associated with motor, cognition and emotional systems and parameters related to those mechanisms captured using EEG signals. This part of the research has been presented in (Handojoseno *et al.* 2013; 2015a). The interpretation on the pathophysiology underlying FOG based on the finding in the connectivity proposed further insight into the understanding of this mysterious symptom of PD (Shine *et al.*, 2014).

- Third, the direction of information flow on the pair of time series was determined using partial directed coherence and used as inputs for FOG detection. An optimization of the source information separation by implementing ICA to this effective feature was investigated and proved. It was found to increase the performance significantly when combined with the application of Bayesian regularization as the training methods for artificial neural networks using brain effective connectivity estimation as inputs, as has been reported in (Handojoseno *et al.* 2014; 2015c).

1.5 Outline of Thesis

This thesis consists of 6 chapters, a bibliography and appendices. The following chapters of this thesis are organized as below:

Chapter 2 reviews literature associated with the FOG detection. It covers the fundamental keys to understanding of PD including the history, the pathophysiology, specially related to gait movement, diagnosis and treatment. It also provides an explanation of FOG including current research related to 5 hypotheses on the pathophysiology of FOG, especially those which explore the brain dynamic during that episodic gait disorder. Then, the scope is narrowed to focus on the existing strategies of FOG detection, and to provide a brief outline of the proposed FOG detection strategy.

Chapter 3 presents the initial works on FOG detection based on power spectral analysis. The classical Fourier transform based univariate feature is compared to its counterpart extracted using wavelet transform based features. This part includes EEG acquisition through timed up and go (TUG) test and the basic EEG signal analysis. It presents a study of the characteristic of EEG data from 3 different episodes, that are normal walking, transition to freezing, and freezing, followed by the classification of the data for the detection of freezing using artificial neural networks. This chapter is completed with a discussion and conclusion.

Chapter 4 presents an investigation on brain functional connectivity of EEG signals from PD patients with FOG. Although basic spectral analysis already indicates a different pattern of EEG signal during transition to freezing compared to normal walking, extracting more information beyond the classical approach provides more insight into the physiological dynamic of the brain following the growing interest of neuroscientists on the brain networking. This analysis also provides additional information of EEG signals as inputs for a classification system to improve the performance of FOG detection. The optimal characterizations of the differences between normal walking and transition to freezing were searched by combining different features based on their ranking, and their performances when used as inputs of artificial neural networks, are evaluated. This chapter is completed with a discussion and conclusion.

Chapter 5 presents the FOG detection strategy using brain effective connectivity analysis which captures causality beyond correlation in multivariate analysis. Optimization of the features was investigated using a combination of ICA and brain effective connectivity measurement. Optimization of the classifier was investigated by using Bayesian regularization instead of early stopping. Also presented in this chapter is the predicted mechanism underlying FOG, which has been proposed, through the analysis of brain activity, related with abnormal patterns of theta frequency oscillations during the FOG episode. This chapter is completed with a discussion and conclusion.

Chapter 6 presents the overall discussion and conclusions for this research. The discussion covers the advantages and the limitation of different methods utilized in the study as well as their performance in achieving the objectives of developing methodologies for FOG detection in patient with PD using EEG signals and computational intelligence. The chapter ends with suggestions of possible directions for future works in FOG detection.

1.6 Publications

Journal papers:

- A. M. A. Handojoseno, J. M. Shine, T. N. Nguyen, Y. Tran, S. J. G. Lewis, and H.

T. Nguyen, 2015, "Analysis and Prediction of the Freezing of Gait using EEG Brain Dynamics," in *IEEE Transactions on Neural Systems and Rehabilitation Engineering*, vol 23, no.5, pp. 887-896.

- J. M. Shine, A. M. A. Handojoseno, T. N. Nguyen, Y. Tran, S. L. Naismith, H. Nguyen, and S. J. G. Lewis, 2014, "Abnormal patterns of theta frequency oscillations during the temporal evolution of freezing of gait in Parkinson's disease", *Clinical Neurophysiology*, vol. 125, pp. 569-576.

Conference papers:

- A. M. A. Handojoseno, M. Gilat, Q. Tran, H. Chamtie, J. M. Shine, T. N. Nguyen, Y. Tran, S. J. G. Lewis, and H. T. Nguyen, 2015, "An EEG Study of Turning Freeze in Parkinson's Disease Patients: The Alteration of Brain Dynamic on the Motor and Visual Cortex", *Proceeding of the 37th Annual International Conference of the IEEE Engineering in Medicine and Biology Society*, Milano, Italy, pp. 6618-6621.

- A. M. A. Handojoseno, J. M. Shine, M. Gilat, T. N. Nguyen, Y. Tran, S. J. G. Lewis, and H. T. Nguyen, 2014, "Prediction of Freezing of Gait using analysis of brain effective connectivity", *Proceeding of the 36th Annual International Conference of the IEEE Engineering in Medicine and Biology Society*, Chicago, Illinois, USA, pp. 4119-4122.

- A. M. A. Handojoseno, J. M. Shine, T. N. Nguyen, Y. Tran, S. J. G. Lewis, and H. T. Nguyen, 2013, "Using EEG spatial correlation, cross frequency energy, and wavelet coefficients for the prediction of Freezing of Gait in Parkinson's Disease patients", *Proceeding of the 35th Annual International Conference of the IEEE Engineering in Medicine and Biology Society*, Osaka, Japan, pp. 4263-4266.

- A. M. A. Handojoseno, J. M. Shine, T. N. Nguyen, Y. Tran, S. J. G. Lewis, and H. T. Nguyen, 2012, "The detection of Freezing of Gait in Parkinson's disease patients using EEG signals based on wavelet decomposition", *Proceeding of the 34th Annual International Conference of the IEEE Engineering in Medicine and Biology Society*, San Diego, California, USA, pp. 69-72.

Submitted papers:

- A. M. A. Handojoseno, G. R. Naik, M. Gilat, J. M. Shine, T. N. Nguyen, Y. Tran, S. J. G. Lewis, and H. T. Nguyen, 2015, "Detection of Freezing of Gait based on combination of Independent Component Analysis and Brain Effective Connectivity," in *Journal of Biomedical and Health Informatics*, submitted.

Chapter 2

Literature Review

"The disease, respecting which the present inquiry is made, is of a nature highly afflictive. Notwithstanding which, it has not yet obtained a place in the classification of nosologists; some have regarded its characteristic symptoms as distinct and different diseases, and others have given its name to diseases differing essentially from it; whilst the unhappy sufferer has considered it as an evil, from the domination of which he had no prospect of escape."
-James Parkinson

2.1 Parkinson's Disease

Parkinson's disease (PD) occurs worldwide and very likely was known thousands of years ago (Goldstein, 2009). The description of a disease closely resembling PD was found in ancient Sanskrit writing in India from around 2.500 B.C, and in ancient Egyptian papyrus text from around 1150 years later. It also appeared in the study on tremors of the Greek physician Galen in the second century A.D., and the observation of the Italian artist Leonardo da Vinci in the fifteenth century. However, it was not until early in the nineteenth century (1817) that we have accurate descriptions of the sequence of PD symptoms by the English physician James Parkinson in his "An Essay on the Shaking Palsy". This

work received little initial attention until a French physician, Jean-Martin Charcot, continued the research, dissecting the 4 cardinal features of PD (tremor, rigidity, akinesia and postural instability - gait disturbance) and naming the condition which mainly affected the motor system, as Parkinson's disease.

In the early 1960s, researchers identified the deficiency of an important chemical, dopamine, as a hallmark of the disease. A 90% reduction in the concentration of dopamine was found in the striatum and substantia nigra in the basal ganglia in the brains of patients dying of PD (Simuni & Hurtig, 2008). Dopamine is one of the neurotransmitters which help transmit messages to the striatum in the central area of the brain to initiate and control movement and balance (see Fig. 2.1). Working with acetylcholine, the dopamine system guarantees that muscles work smoothly without unintended movement.

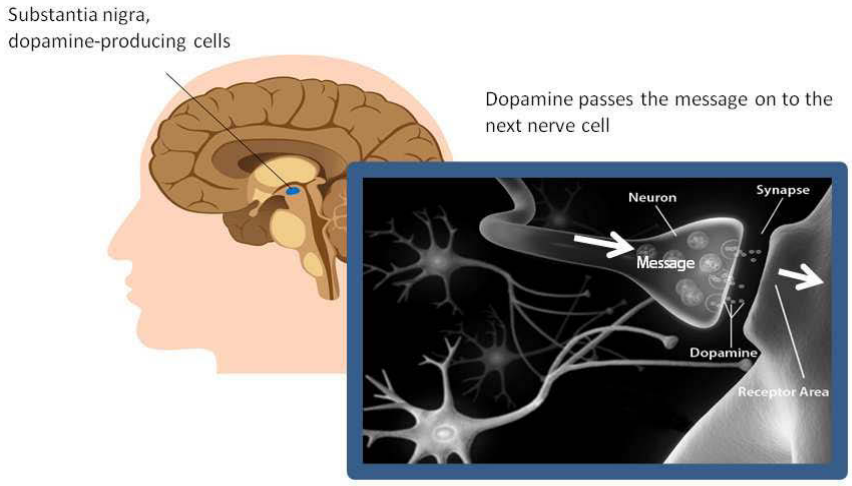

Figure 2.1: Dopamine roles in the movement production as a neurotransmitter.

Fig. 2.2 shows the comparison between a healthy state and PD. Signals pass from the brain's cortex through the reticular formation and spinal cord (Pathway A) to the muscles to make them contract. Other signals pass along Pathway B through the basal ganglia to damp on the signal in Pathway A, reducing muscle tone to avoid jerky movements. In PD, decreasing amounts of dopamine prevent modification of the nerve pathways that control muscles contraction. The loss of damping effect makes the muscles overly tense, causing tremor, joint rigidity, slow movement and freezing.

The motor control system can be seen as having 3 aspects: planning, programming and

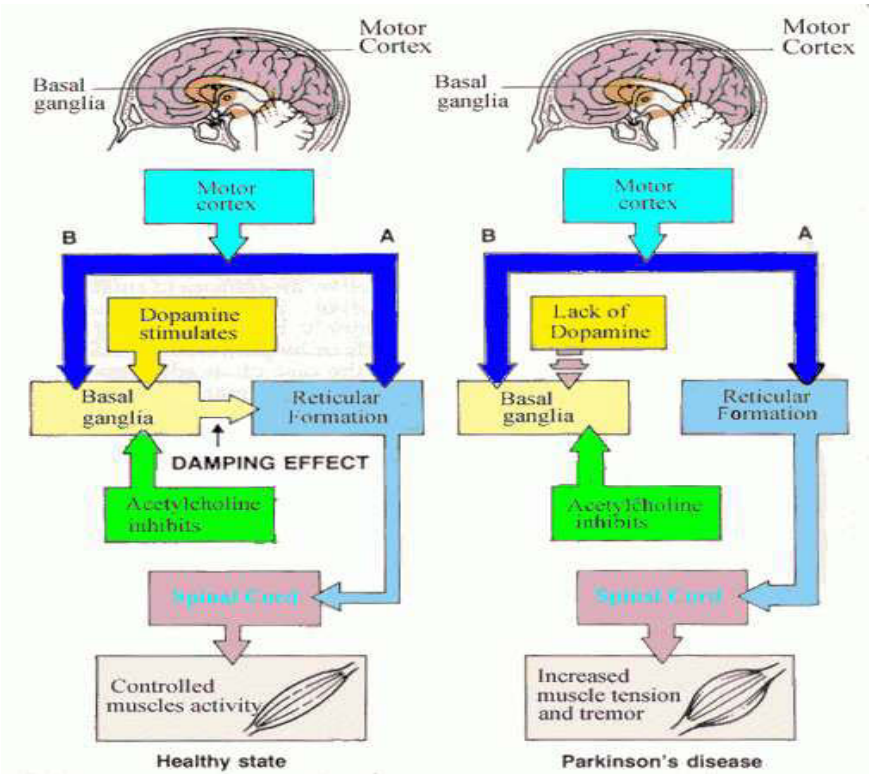

Figure 2.2: Comparison of control movement between healthy state and PD (Arthur & Brown, 2009).

executing related mainly with 3 parts of brain: motor cortex, basal ganglia and cerebellum (Reed, 1998)(Fig.2.3). While lack of motor execution is known as a major sign of PD, researchers have different opinions whether the problem of voluntary movement in PD occurs in motor programming or planning. Mixed findings have been reported, perhaps due to different patient groups disease severity and the wide variation of PD symptoms among patients.

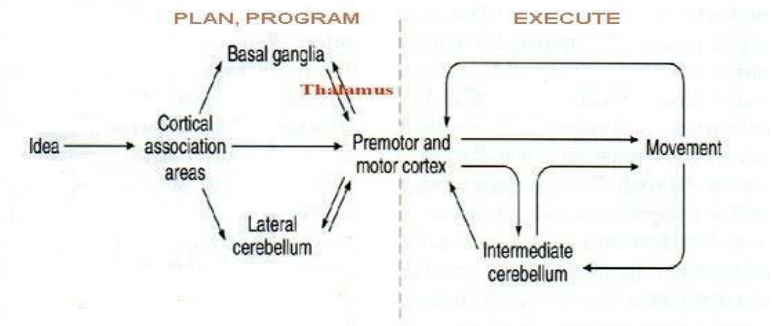

Figure 2.3: Schematic diagram of the nervous system for normal movement (Reed, 1998).

A study of speeded sequential movements in a reaction time (RT) task, to consider the cognitive processes that occur during the time period between the onset of a target stimulus and the initiation of movement, proved that PD does not impair the response selection, programming or execution processes themselves, but affects the smooth coordination of those processes (Jennings, 1995). Research on the differences between preprogrammed movements and those prepared online, found the increase of RT for more complex movements, the variability of RT due to disease severity, and that complex movement needs more online programming. This result supported the explanation of the disruption in the motor planning process influenced by the basal ganglia (Reed, 1998). The different task with a different amounts of attention assigned to the motor task, resulted in varying the sign (i.e. increase or decrease in activation) in the frontal motor areas which are abnormally activated in PD patients as they perform manual motor tasks (Rowe & Siebner, 2012).

In spite of difficulties of specifying which part of the process of movement is most affected by PD, there is a general understanding on the movement process. To initiate movement, the brain must have current information about the environment to determine the positions of the body parts that are to be moved and the positions of any external objects with which the body is going to interact with. Through the sensory organs, this information is collected, projected to its proper location in the brain, and analyzed. As seen in Fig.2.4, the inferior and posterior parietal cortex simultaneously receive highly processed somaesthetic (parietal lobe), visual (occipital lobe), auditory (temporal lobe) and movement-related input from the various association areas.

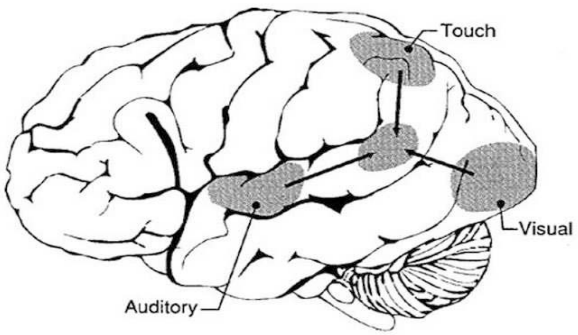

Figure 2.4: Schematic diagram of converging sensory flow to the inferior-posterior parietal lobule (Joseph, 1996).

Initial information about the position of the body parts and its environment from the parietal lobe is sent to the frontal lobe and is used to plan movements. It is analyzed at the prefrontal cortex (planning) and then projected to the premotor cortex and supplementary motor area (programming) and to the primary motor cortex (executing)(Fig.2.5). From the primary motor cortex, the signal is transmitted to the spinal cord and then to the primary regions where it is acted upon, so that neurons in the primary area also become active before and during movement. Based on functional imaging, it is known that actual movement increases activation of the primary motor compared to merely preparing to make movement, showing its significant role in executing the plan (Carlson, 2013).

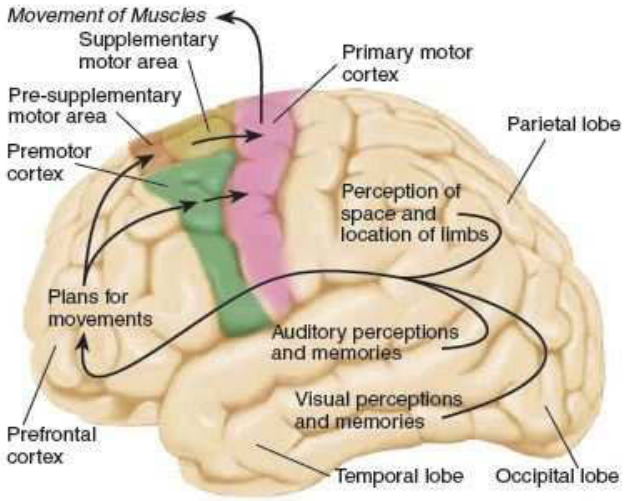

Figure 2.5: Schematic diagram of the motor control flow (Carlson, 2013).

Since classically PD has been considered as a motor disorder, the motor circuit became the focus of its studies. However, numerous studies have shown the influence of non-motoric aspects in the movement disorders in PD including FOG. Anatomical and functional studies on the basal ganglia, the main part of the brain affected by PD, show a more complex system rather than simply motor control, as it also involves activities such as learning, decision making, habit formation, temporal estimation, reward-related behavior, and emotions.

A recent model of basal ganglia proposed that certain parallel cortico-subcortical “loops” are responsible for specific behavioral aspects: motor (the putamen, projecting back to motor cortices, that is the primary motor cortex, supplementary motor area, and premotor

cortex), associative/cognitive (the dorsal caudate nucleus projecting to the prefrontal cortex) and limbic/emotional (the ventral striatum projecting to the anterior cingulate cortex and the medial orbitofrontal cortices) (Juri *et al.*, 2010) (Fig.2.6). Another model subdivided it into 5 loops including those 3 loops and 2 additional loops, the oculomotor and the lateral orbitofrontal (Yelnik, 2002).

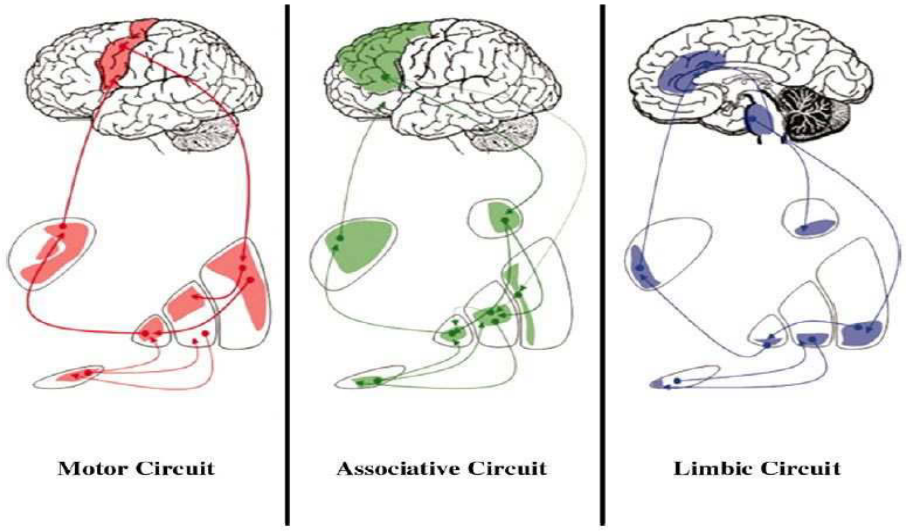

Figure 2.6: Main functional division of the cortio-basal connections (Juri *et al.*, 2010).

At present the diagnosis of PD is made clinically on the basis of history and clinical examination. Laboratory tests and imaging techniques are helpful in excluding other processes that may present with Parkinsonian symptoms, but none can definitively diagnose PD. The difficulties come from the fact that PD affects people differently (Wieler, 2003): some people have almost no symptoms while others have many. Moreover, the constellation of motor impairments can be caused not only by PD, but by any number of conditions that decrease available dopamine, for example metabolic disorder, exposure to toxins, drugs that interfere with the dopamine pathways in the basal ganglia and heredity disorders.

However, while there is no early detection screening test for PD at this time, research continues with many different approaches. A wide range of possible markers studied include: olfactory identification deficits, combine motor/smell/mood disorder, progression of clinical scales, blood/cerebrospinal fluid/tissue indicators, neuroimaging indicators and genetic indicators (Morgan *et al.*, 2010). The drive is based on the progression is likely to be fastest at the beginning of the disease. As a consequence, neuroprotective treatment

should be given as soon as possible after the onset of signs and symptoms in order to slow down or even prevent the degenerative progress of this disease.

2.2 Freezing of Gait

2.2.1 Gait Disturbance and Freezing of Gait in PD

In his paper An Essay on the Shaking Palsy in 1817, James Parkinson described the gait disturbances characteristics integral of Parkinson's disease (Giladi & Niewboer, 2008):

"The propensity to lean forward becomes invincible, and the patient is thereby forced to step on the toes and fore part of the feet, whilst the upper part of the body is thrown so far forward as to render it difficult to avoid falling on the face. In some cases, when the state of the malady is attained, the patient can no longer exercise himself by walking in his usual manner, but is thrown on the toes and forepart of the feet; being, at the same time, irresistibly impelled to make much quicker and short steps, and thereby to adopt unwillingly a running pace."

This notation, recorded in the early research on PD, describes gait festination, a unique disorder of locomotion highly associated with freezing of gait (FOG). Festination can be seen as a kind of gait disturbance which often presents with FOG in PD patients. While Charcot might have described a FOG episode in 1877, it was Souques who at 1921, created a description of "a patient being glued to the floor", which was used widely subsequently as a surrogate marker to diagnose FOG (Snijders, 2012):

"Un parkinsonien que j'ai observe, malade depuis dix ans, ne pouvait marcher que très péniblement, les pieds collés au sol. Or, parfois, il pouvait courir et même soulever les pieds assez haut pour sauter un obstacle."

Based on the observation of its process, characterized as a loss of efficient forward movement generation, FOG can be classified in 3 subtypes (Giladi & Niewboer, 2008): first, a complete akinesia (no limbs or trunk movement, the most severe subtype), second, trembling in place (no effective forward motion whilst the patient makes an effort to overcome the block), and third, a very small shuffling forward steps (the least severe subtype). Commonly in daily life, it occurs in 5 situations: starting, turning, walking in tight quarters, upon reaching destination and during mental overload, where start hesitation has been reported as the most common type of FOG (Giladi & Niewboer, 2008). In relation to dopaminergic treatment, commonly FOG is classified as "off" freezing (which improved with dopaminergic treatment) or "on" freezing (which does not improve with dopaminergic treatment, and can be even worse given the treatment) (Linazasoro, 1996).

The sudden disability to start walking or continue moving forward causes regular falls and related injuries, leading to a loss of independence with a strong negative impact on patient quality of life (Walton *et al.*, 2015). This vicious cycle of FOG can be seen in Figures 2.7.

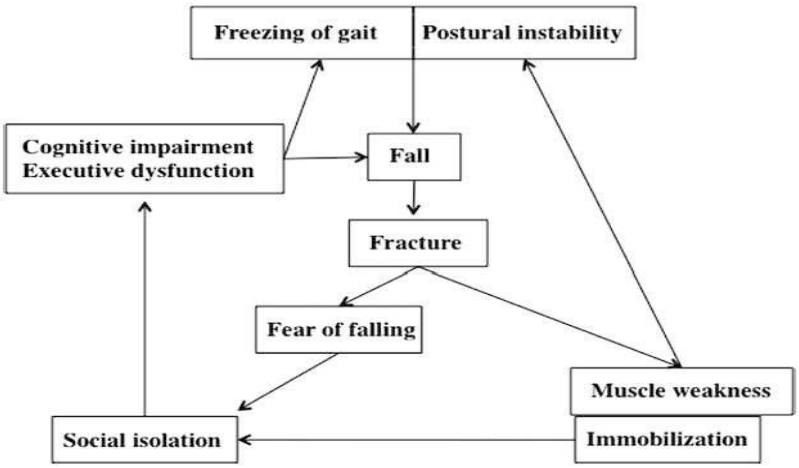

Figure 2.7: Clinical impact of FOG (Okuma, 2014).

Current clinical evaluation and quantification of FOG conducted by experienced examiners in the gait laboratory has challenges because the medical environment improves FOG (Giladi & Niewboer, 2008). Besides, the classification of the patient's severity is based on their subjective description of FOG, through the Freezing of Gait Questionnaire (FOG-Q) (Giladi *et al.*, 2009), the New Freezing of Gait Questionnaire (NFOG-Q) (Nieuwboer

et al., 2009) or the Unified Parkinson's Disease Rating Scale (UPDRS)(Factor & Weiner, 2007b). This standard approach has the limitation that not all patients are able to give a correct assessment of their own freezing problems (Nieuwboer *et al.*, 2009).

A recent review, based on an National Institute of Health - U.S. Department of Health and Human Services sponsored gathering of experts, describes FOG as a mysterious phenomenon (Nutt *et al.*, 2011a) and proposes 5 directions for developing hypotheses on the pathophysiology of FOG, based on publications between January 1966 and April 2011. These 5 hypotheses attribute FOG to (1) abnormal gait pattern generation, (2) a problem with central drive and automaticity of movement, (3) abnormal coupling of posture with gait, (4) perceptual malfunction, and (5) frontal executive dysfunction. Table 2.1 shows the contribution of recent studies to each of these hypotheses (Heremans *et al.*, 2013).

Research has identified the areas of the brain that are affected by FOG (Table 2.2). Recent study on gait planning in PD patients using motor imagery of walking in combination with function Magnetic Resonance Imaging (fMRI) shows cerebral activity reduction in the right superior parietal lobule in PD patients with FOG and PD patients without FOG compared with controls in activity for motor imagery versus visual imagery (Snijders *et al.*, 2011) (Fig.2.8). It suggests the impairment of patients with PD in integrating the prediction of the somatosensory consequences of a motor plan in Brodmann areas (BA) 5 and 7. The similar result with less motor imagery-related activity in PD patients than control also happened in a deeper area of the brain, the anterior cingulate cortex (BA 24).

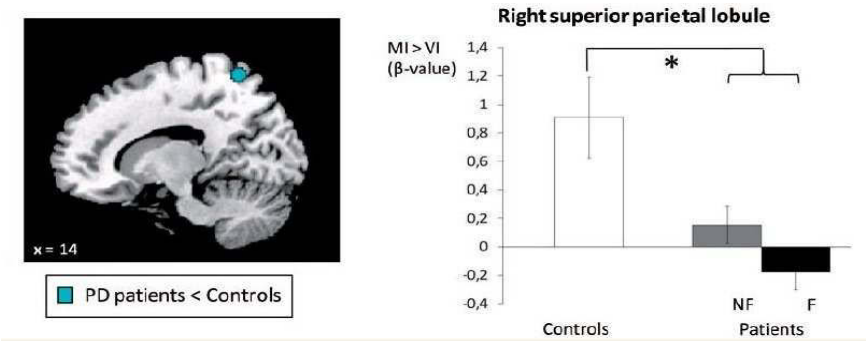

Figure 2.8: Imagery-related brain activity in right superior parietal area. PD=Parkinson's disease; F=patients with FOG; NF=patients without FOG; *=significant difference of $P \leq 0.05$ (Snijders *et al.*, 2011).

Table 2.1: Studies on pathophysiology of FOG
(Heremans *et al.*, 2013)

Hypothesis on the origins of FOG	Study	Methodology	Main results
1. Abnormal gait pattern generation	Peterson et al, in press	Gait analysis	Stepping coordination is worse in freezers.
	Williams et al, in press	Gait analysis	Manipulation of step amplitude and rhythm affects coordination in PD.
	Bhatt et al,2013	Gait analysis	Freezers have an abnormal gait pattern during turning.
	Cowie et al, 2012	Gait analysis	Freezing is related to high stride time variability but not to reduced stride length.
	Snijders et al, 2011	fMRI + VBM	Freezers show altered brain activity in areas involved in regulation of step amplitude.
2. Problem with central drive (automaticity) of movement	Spildooren et al, 2012a	Gait analysis central drive	Freezers benefit more from cueing than nonfreezers during turning.
	Lee et al, 2012	Gait analysis	Visual and auditory cues improve gait in freezers.
	Snijders et al, 2012	Gait analysis	Dual tasking during gait augments the risk to induce FOG.
	Nanhoe-Mahabier et al, 2012	Gait analysis	Auditory cueing improves gait in PD patients with and without FOG.
3. Abnormal coupling posture & gait	Spildooren et al, in press	Gait analysis	Freezers have an abnormal head-pelvis coupling during turning.
4. Perceptual malfunction	Cowie et al, 2012	Gait analysis	The number of freeze-like events increases when walking through narrow doorways.
	Kostic et al, 2012	VBM	Freezers show GM atrophy in regions involved in visuomotor functioning.
	Lord et al, 2012	Visuospatial tests	Freezers have a dysfunction of dorsal occipito-parietal pathways.
	Nantel et al, 2012	Visuospatial tests	Freezers have a dysfunction in visuospatial perception and reasoning.
	Tessitore et al, 2012	fMRI	Freezers show reduced functional connectivity in visual networks in freezers.
5. Frontal executive dysfunction	Shine et al, 2013	fMRI	Freezers showed reduced activation in cognitive control network during virtual walking.
	Imamura et al, 2012	rCBF	Freezers show decreased brain perfusion in areas involved in cognitive functioning.
	Tessitore et al, 2012	rsfMRI	Freezers have reduced functional connectivity in executive attention networks.
	Kostic et al, 2012	VBM	Freezers show GM atrophy in regions involved in executive functioning.
	Vandenbossche et al, 2011	Cognitive tests	Freezers showed impairment in conflict resolution.
	Vandenbossche et al, 2012	Cognitive tests	Freezers have a deficit in response selection.

Table 2.2: Overview of selected studies of lower gait movement, FOG, and related brain location

Authors	Subjects	Methodology	Results	Location of interest
J. Youn et al., 2015	42 PWP: 19 PWF, 23 PWoF, and 33 normal control	MRI and whole Voxel-based analysis	The microstructural changes in the pedunculopontine nucleus and connected subcortical structures: basal ganglia, thalamus and cerebellum	Fz, Cz
J. B. Toledo et al., 2014	22 PWP with subthalamic nucleus (STN) deep brain stimulation electrodes implanted bilaterally	local field potentials, EEG	The increase of high-beta STN oscillations and cortico STN coherence	C3, Cz, C4, F3, F4
D.S. Peterson et al., 2014	9 PWF and 9 PWoF	fMRI with imagined task	The reducing activity in SMA region on the right side of the brain	C4
P.D. Velu et al., 2013	2 PWF and 6 normal control	EEG, EOG, and EMG with virtual reality glasses	The decreasing power in alpha band power due to visual cues and the increasing information flow from Oz to Cz and P4 in beta band power.	P4, Oz, Cz
J. Cremers et al., 2012	15 PWP and 15 normal control	fMRI with imagined task & Microbe Genome Annotation Platform (MGAP)	The right posterior parietal cortex was hypoactivated within patients MGAP and its mental gait-related activation decreased with increasing severity of gait disturbances	C1, P1-P2(Pz), F1-F2(Fz)
A.H. Snijders et al., 2011	25 PWP: 13 PWF and 12 PWoF	fMRI & EMG with imagined task	Increased activity in the right superior parietal lobule and right anterior cingulate cortex, decreased activity in the SMA and increased activity in the MLR	C1, P1-P2(Pz), F1-F2(Fz)
M. Shoushtarian et al., 2011	20 normal control (8 young, 12 older), 20 PWP: 9 PWF, and 11 PWoF	EEG, EMG & EOG	A significant larger early slope and peak amplitudes at Cz for the HYA group compared to PD groups, and also the PWoF compared to PWF	Cz
M. Bakker et al., 2008	16 healthy men	fMRI & EMG with imagined task	The increasing of the cerebral activity in Superior Parietal Lobule and superior middle occipital gyrus	P3-P1-P2-P4, P6
H. Matsui et al., 2005	55 PWP: 24 PWF and 31 PWoF	SPECT	The medial frontal area perfusion of the FOG group decreased compared to that of no FOG group	AF7, FPz

PWP: patient with PD; PWF: patient with FOG; PWoF= patient without FOG

According to recent brain activation studies (Snijders *et al.*, 2011; Hashimoto, 2006; Crémers *et al.*, 2012), the medial frontoparietal cortex (the supplementary motor area or SMA, and the adjacent areas: lateral premotor areas, medial primary sensory motor areas, anterior cingulate cortex, and superior parietal cortex) is assumed as the brain site responsible for FOG in PD patients because lesions here cause identical FOG in gait apraxia. In the study using motor imagery and visual imagery of walking, decreased activity in the SMA was detected in PD patients with FOG (see Fig.2.9).

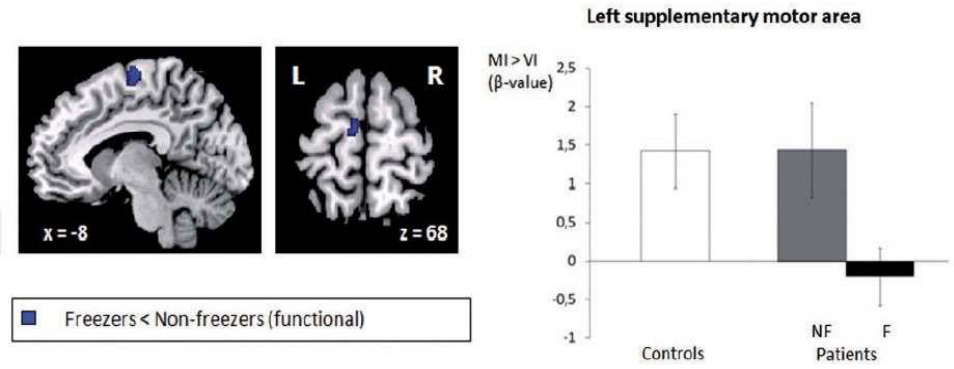

Figure 2.9: Imagery-related brain activity in the left supplementary motor area. F=patients with FOG; NF=patients without FOG; *=significant difference of P 0.05 (Snijders *et al.*, 2011).

In an experiment of motor imagery walking along a narrow path, Bakker *et al.* (2008) found increasing cerebral activity in the left and right superior parietal lobule and in the right middle occipital gyrus, structures with strong sensory afferences (Fig.2.10). This study revealed an increased activity in the dorsal premotor cortex caudal, right rostral cingulate zone posterior, superior parietal lobule and putamen during motor imagery of gait in general along a broad path. It suggests that cerebral activity in the cerebellum and SMA increases with increasing path length and the involvement of the structures in a timing function is specific for motor imagery of gait, such as the timing of walking movements.

Some studies of the central mechanisms underlying the organization of motor function and its impairments involved analysis of cortical movement-related potentials (MRP) acquired by averaging EEG activity prior to and during voluntary movements (Fig.2.11). The comparison of MRP of healthy young adult and healthy older adult patients with PD

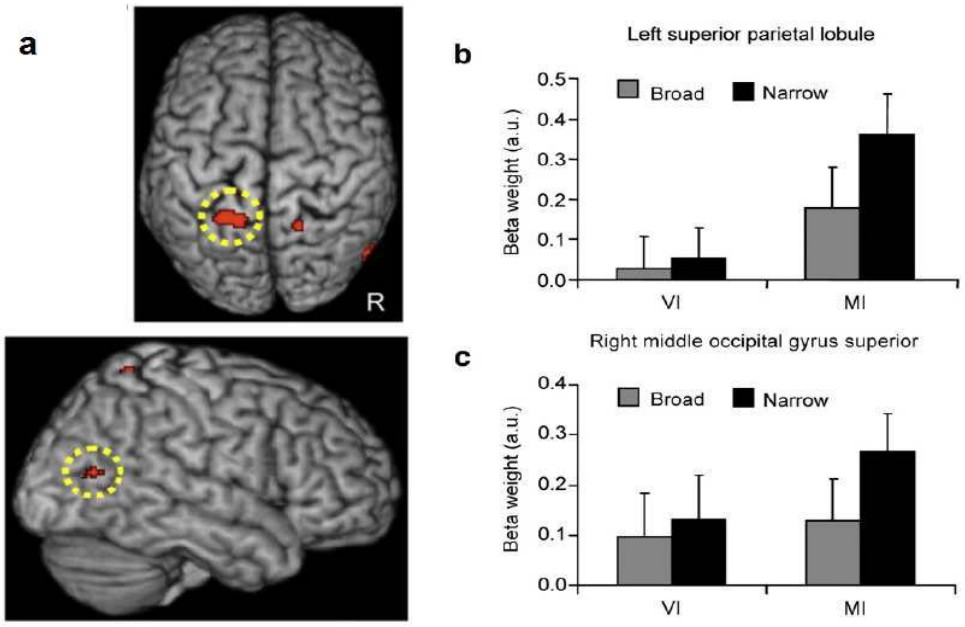

Figure 2.10: Imagery-related brain activity during motor imagery of gait along a narrow path (Bakker *et al.*, 2008).

(PWP) without gait initiation difficulties/FOG (PWoF), and of young and older healthy adult patients with gait initiation difficulties/FOG (PWF) in a study by Shoushtarian *et al.* (2011) showed that significant group differences on early slope and peak amplitudes were mainly found at central zero. It showed gait-generated MRPs malfunction in both preparatory and execution stage.

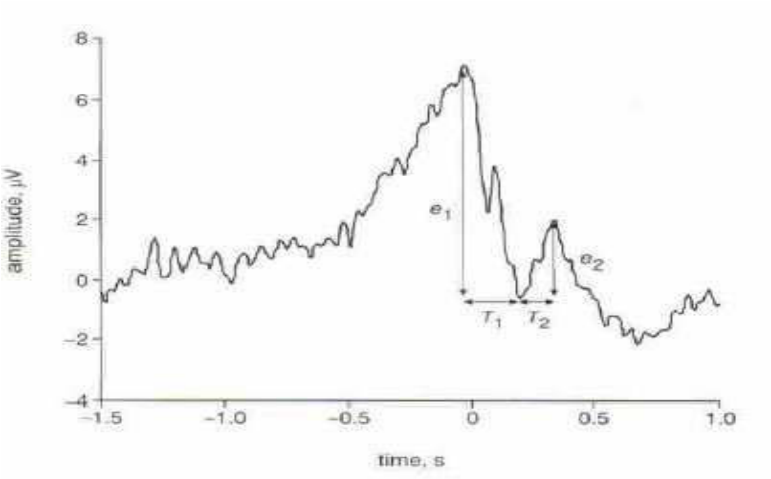

Figure 2.11: Sample averaged MRP with two prominent peaks (Yom-Tov & Inbar, 2003).

Using three-dimensional Stereotactic Surface Projections (3D-SSP) for analyzing Single

Photon Emission Computed Tomography (SPECT), Matsui *et al.* (2005) located the brain area affected by FOG in the bilateral BA 11 (Fig.2.12). This spot was reported as related with emotional or affective information (motivation, depression, panic attack) and also with cognition (decision making). The Amboni *et al.* (2008) study which focused on the executive functions in PD patients, found that FOG correlated with lower scores at frontal tests in patients with early-stage PD. It supports the hypothesis that "on" state FOG is associated with cognitive frontal dysfunction and shows that the severity of FOG is related to the severity of cognitive impairment.

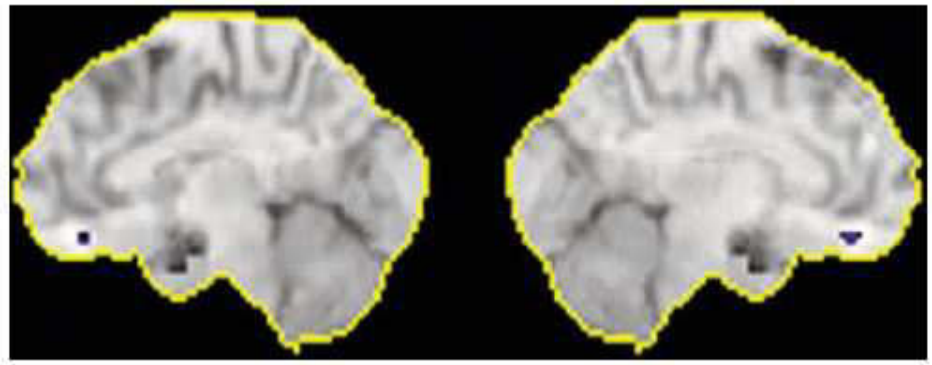

Figure 2.12: Three-dimensional stereotactic surface projection image colouring in BA 11 where perfusion decreased in FOG group compared with that of the no FOG group (Matsui *et al.*, 2005).

With the understanding that dysfunction in FOG occurs in the preparation period before any movement, Velu *et al.* (2013) used portable EEG to examine how the effect of visual cues in increasing the information flow from visual and parietal areas to the motor cortex. Based on anatomical findings from prior functional magnetic resonance imaging (fMRI) and positron emission tomography (PET) experiments, they focused on analysis of spectral power and connectivity in occipital (Oz), parietal (P4) and motor (Cz) channels. The result of their study on two subjects suggests that visual feedback cues have an important role in the activity and information flow via the nodes of an occipital-parietal-motor network.

2.2.2 Treatment of FOG

The medical treatment of FOG is complicated due to the multifactorial mechanism related with FOG, and that the pathogenesis of FOG is poorly understood (Nutt *et al.*, 2011b). Different stages of the disease and different types of FOG need different strategies to improve FOG. As can be seen in Fig. 2.13, there should be no wearing off where dopaminergic medication is increased in the under-treated patient. FOG is also improved in the "off" state and in the "on" state in "pseudo-on" cases. However, reducing dopaminergic medication is necessary in the "true-on" freezing.

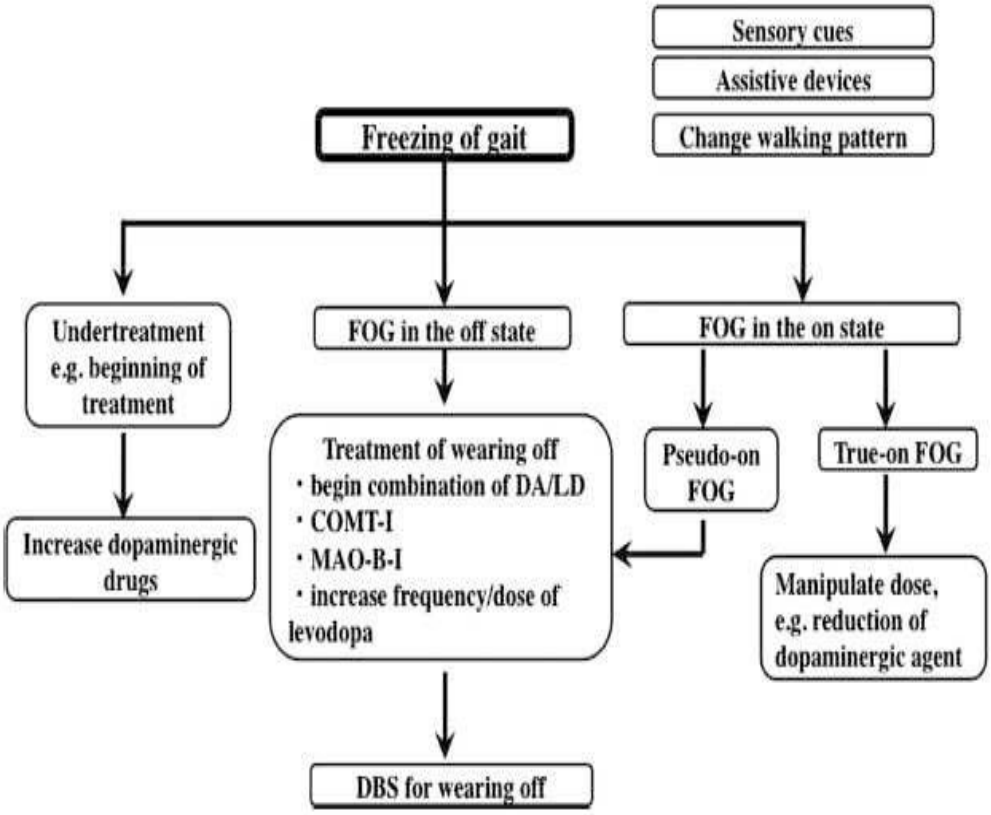

Figure 2.13: Treatment of FOG (Okuma, 2014).

Compensation strategies to prevent or lessen FOG have been developed based on rhythmical cueing on gait, the development of assistive devices and behavioural approach (Okuma, 2014). The integration of the emotional activation as well as the aesthetic qualities of music to auditory cuing instead of only metronome reduced the impairment of perceptual and motor timing abilities of 15 PD patients from 73% into 40% (Benoit *et al.*,

2014). Cognitive cuing using Virtual Reality improved dual-tasking ability in 13 PD patients with FOG measured by stepping time, rhythmicity and reaction time (Killane *et al.*, 2015).

Combination of a laser light cue with a cane or walker has been reported to improve freezing, and has been commercialized while mobility and safety have been improved using assistive devices such as a 4-wheeled walker (Okuma, 2014). The improvement of freezing can be achieved also by various "tricks", as seen from over 30% of responders in a FOG study to improve walking, through paying attention to each steps, taking longer steps, altering the distribution of body weight, going up stairs, consciously lifting one limb higher, stamping of feet, and counting silently (Rahman *et al.*, 2008).

Improvement of FOG in the "off" state can be obtained also by stimulating the subthalamic nucleus, and alternatively the globus pallidus, using deep brain stimulation surgery (Okuma, 2014). Optimization of this treatment can be achieved by reducing the frequency of deep brain stimulation. However, this method works only where the dopaminergic treatment improves the FOG and only in the FOG "off" state, and may lead to postural deficit postoperatively after several years (Snijders, 2012).

2.3 Current Strategies of FOG Detection

The existence of FOG in PD is often observed based on 3 different presentations of the movement (Bloem *et al.*, 2004). The most common FOG is associated with an effort to overcome the block which causes the legs to "tremble in place". Yet, the best-known FOG is connected to symptoms of akinesia as the patient becomes unable to start walking or fails to continue to move forward. Shuffling forward with small steps is the third type of FOG. Studies of impairment on the initiation and termination of gait as well as a sudden interruption of walking lead to the finding of the changes in the PD patients compared to healthy person, for example the reduced movement speed, stride length, step amplitudes, decreased ground reaction forces, and increased cadence at the onset of gait (Niewboer *et al.*, 2004). This finding becomes a fundamental aspect for many FOG detection strategies as can be seen in Table 2.3.

Table 2.3: Studies on the detection of FOG

Authors	Subjects	Methodology	Characteristic features	Results
Han et. al., 2003, 2006	5 healthy control and 2 PWP;5 healthy control and 5 PWP	3D-accelerometer, foot pressure system, camcoder	$\frac{WE(0-2.5Hz)}{WE(10-20Hz)}$; A stopping threshold (Tst)	Increased of high frequency component during FOG
Moore et al., 2008	11 PWF and 10 healthy control	Accelerometer, videotape, Bayesian classifier	$FI = \frac{PS(3-8Hz)}{PS(0.5-3Hz)}$ episode > 3 s	A significantly higher 'freeze' band power (3-8 Hz) during FOG
Johanov et al., 2009	1 PWF and simulation data	3D-accelerometer, gyroscope, in real-time	FI	Average detection latency was 332 ms
Bachlin et al., 2009, 2010	10 PWF	Accelerometer, wearable device, online, window lenght=4.5s	FI	Se=78.1%, Sp=86.9%
Delval et al., 2010	10 PWoF, 10 PWF, 10 healthy control	3D motion analysis system, goniometers, videotape	FI	Se=75-83%; Sp=95%
Popovic et al., 2010	9 PWF	Force Sensitive Resistors, accelerometer, videotape	The Pearson's correlation coefficient	A decreasing of the correlation between a normal step and the "freezing" steps
Cole et al., 2011	10 PWF and 2 healthy control	3D accelerometer, electromyograph, dynamic neural networks	PSD $<$ 2.5Hz), PSD $>$ 2.5Hz), ratio height of peak of highpass signal	Se=82.9%; Sp=97.3%
Niazmand et al., 2011	6 PWF	3D-accelerometer integrated into smart pants, videotape	the number of pulses, the shaking foot time, FI	Se=88.3%; Sp=85.3%; limitation to identify akinesia of FOG
Mazilu et al., 2012, 2014	10 PWF; 23 PWF	Accelerometer, with smartphone and rhytmic auditory cuing, online, PCA for dimension reduction, various classifier	FI, mean, std, entropy, Signal Magnitude Vector, Averaged Acceleration Energy, etc.	Se=99.69%, Sp=99.96%, latency=340 ms
Mancini et al., 2012	21 PWP, 27 PWoF, 21 healthy control	3D acceleromter, 3D gyroscopes	PSD, Frequency Ratio	Increase power in the "freeze" band (3-8 Hz)
Tripoliti et al., 2013	5 healthy control, 5 PWF, 6 PWoF,	Accelerometer, gyroscope, 4 classifier	Entropy	Se=81.94%, Sp=96.11%, Acc=96.11%, AUC=98.6%
Coste et al., 2014	4 PWF	3D accelerometer, 3D magnometer, 3D gyrometer, videotape	$FOGC_n = \frac{C_n.L_{min}}{C_{max}.(L_n+L_{min})}$ $C = frequency(cadence)$ $L = stridelength$	$FOGC_n$ is more sensitive to festination than FI

PWP: patient with PD; PWF: patient with FOG; PWoF= patient without FOG
WE: wavelet energy; PSD: power spectral density; FI= Freezing Index
Se=sensitivity; Sp=specificity; Acc=accuracy; AUC=area under receiver operating characteristic curve

2.3.1 The Beginning of the FOG Detection Research: the Search for the Indicators of FOG

Based on those clinical observations, to detect the onset of FOG and to ascertain the need for "un-freeze" treatment, Han *et al.* (2003) pioneered a research in the detection of FOG using 2 biaxial accelerometers to measure the leg oscillations. Collecting data from 5 healthy controls and 2 patients with FOG (PWF), the study found that a freezing gait has a higher main frequency acceleration (6 - 8 Hz) compared with a normal gait (2 Hz) (Fig. 2.14). Then, the normal, FOG and resting state were classified based on the comparison of the wavelet power level on different frequency bands. The group continued their preliminary work by developing the wearable activity monitoring system using a 3 dimensional accelerometer with foot pressure system, and the camcorder for the reference of gait detection (Han *et al.*, 2006). They developed a general gait detection algorithm beyond FOG to detect any abnormality, such as toe-walking and slowness. Based on the sequential evaluation of gait signals parameters, it has detection accuracies of 94% (47 gaits of 50 gaits were correctly detected) and 93% (116 gaits of 125 gaits were correctly detected) for normal and PD gait, respectively.

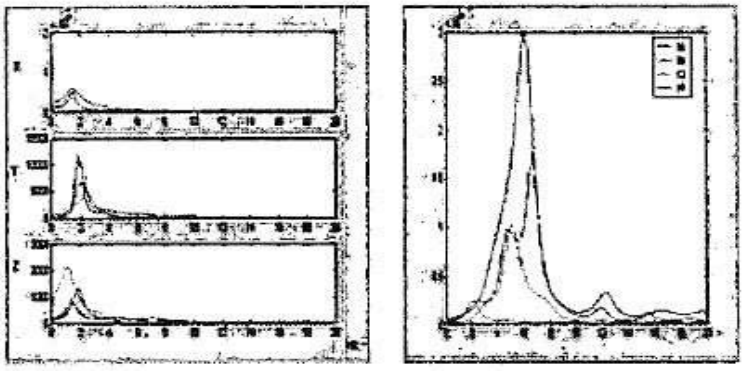

Figure 2.14: Frequency characteristics of normal (near 2 Hz) and FOG (6-8 Hz) of the 3 dimensional acceleration measurement (x: horizontal, Y: vertical, z: transverse) (Han *et al.*, 2003).

A 3-axis accelerometer emerges as the most popular sensor for FOG detection. In their study of an ambulatory FOG in 11 PD patients and 10 healthy controls, Moore *et al.* (2008) introduced the freeze index (FI) as the power of the considered body segment acceleration signal in the freeze band (38 Hz) divided by the power of the signal in the

"locomotor" band (0.53 Hz) (Fig. 2.15). For each instance t, FI(t) was defined as the square of the area under the power spectra of a 6-s window of data (centred at time t) in the freeze band, divided by the square of the area under the power spectra in the locomotor band. The width of the sliding window was based on FOG duration. The optimal window width was determined to be approximately twice the duration of the shortest FOG event detected. Also, an individual FI threshold found to increase the accuracy and sensitivity of the detection, was calculated as the mean plus one standard deviation of the peak FI from data of volitional standing.

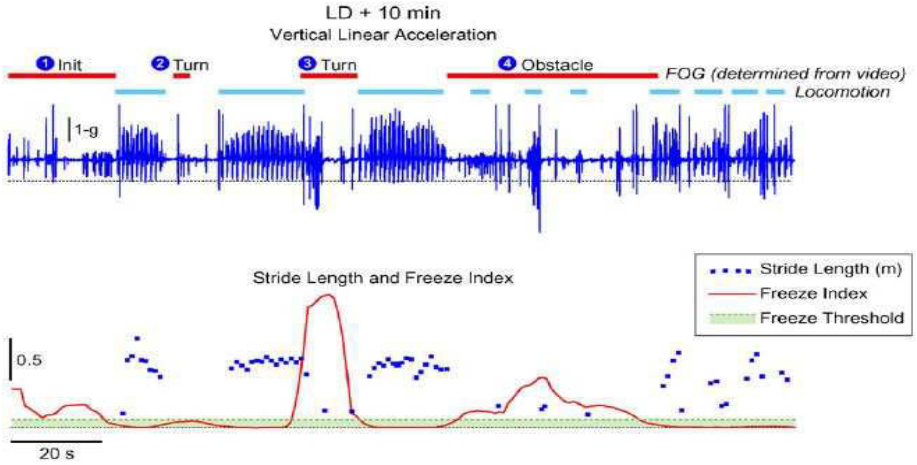

Figure 2.15: The freeze index (FI=red trace) was calculated from the power in the freeze band (38 Hz) divided by power in the locomotor band (0.53 Hz). Large peaks occurred during FOG (Moore *et al.*, 2008).

Delval *et al.* (2010) introduced goniometer as a kinematic sensor located in the patient's knee in studying subtle FOG. They evaluated gait parameters in 10 PWF, 10 PWoF and 10 controls who walked on a motorized treadmill while avoiding obstacles dropped randomly. They used the concept of FI from Moore *et al.* (2008) in their time-frequency analysis using sliding windowed FFT with window size 4.1 s. A significant decrease was found in step duration, minimum step length, and FI between trials with FOG and trials without FOG of all 3 groups, revealing them as significant parameters associated with FOG with sensitivity of 75 - 88% and specificity of >95%. While they presented interesting observation on the presence of high frequencies in freezers during festination linked to the FOG phenomenon and claim of the ability to detect subtle FOG episodes using frequency analysis, they acknowledged their limitation for using an artificial form

of "freezing" rather than FOG in "real life".

The idea of ambulatory monitoring of FOG lead Popovic *et al.* (2010) to assess FOG in 9 PWF in the "on" state using a force sensitive resistor insoles and Pearson's correlation coefficient (Pcc). Accelerometer data was taken as a comparison. Bluetooth technology was implemented for remote recording and processing of the sensor data. Aiming to complement clinical examination of FOG, it claimed success in detecting all the FOG episodes, when compared with those 24 FOG episodes estimated from the video. Pcc values of less than $\pm$ 1 were signalled as "small steps" in FOG. This method claimed to be equally sensitive to various freezing patterns. However, it is unclear how the system would recognize various non-FOG pattern of walking which may be different from normal walking.

Different groups continued to explore this method including Niazmand *et al.* (2011a), Mancini *et al.* (2012) and Azevedo Coste *et al.* (2014). In their proposed MiMed-Pants using five 3D acceleration sensors with the algorithm based on the frequency dominant threshold, Niazmand et al. achieved a sensitivity of 88.3% and specificity of 85.3% from experiment with 6 PWF, acknowledging that the system could not classify stillness and could not detect akinesia of FOG. Mancini *et al.* (2012) verified an increased in power in the 'freeze' band and the usefulness of frequency ratio FI as an indicator of gait disturbance during a freezing episode. Most recently, Azevedo Coste *et al.* (2014) proposed as a new criterion, FOG frequency cadence ($FOGC_n$), put forward as providing a better indicator of freezing compared with FI.

2.3.2 Unfreeze Attempt and Online Detection of FOG

To improve the function of PWP using non medication means, researchers developed various assistive devices such as canes or walking sticks, walkers and power wheelchairs. External stimuli were found to improve gait performance in PWP (Rubinstein *et al.*, 2002). The modified inverted stick with an attached visual cue to abort freezing episodes was found to help 2 of 8 PWP with "off" freezing during walking and in number of freezing episodes (Dietz *et al.*, 1990). Based on this idea, the Laser Cane was produced and

commercialized (Fig. 2.16). However, resistance to this visual cue walking device was reported in the "on" freezing in the majority of 28 PWP in the Kompoliti *et al.* (2000) research. Moreover, these assistive devices may lead to falling when the device slips or "catches" objects (Constantinescu *et al.*, 2007).

Visual cue strategy has also been developed by giving visual feedback using virtual reality device as a training device. This closed-loop apparatus generated a virtual tiled floor in a checkerboard arrangement whilst responding dynamically to the patient's self movement (Fig. 2.16). The improvement in walking abilities of 68% of 20 PWP in 15 minutes after device removal, and 36% of the patients after one week of the first test showed the effectiveness of this approach in the therapy for PWP by creating a "cue memory" to improve their stride length and walking speed (Baram *et al.*, 2006).

Figure 2.16: Laser Cane, a walking stick with a bright red line laser beam projection to help the PD patient overcome freezing episodes (Constantinescu *et al.*, 2007).

The importance of cueing in the FOG treatment inspired Jovanov *et al.* (2009) to propose a new direction in the research of FOG by introducing the first real-time system for detection of FOG system, complemented with the on-demand un-freeze using acoustic stimulation. A prototype FOG sensor module with an accelerometer and a gyroscope sensor in a small ARM7 processor based board which can be attached to the belt, knee, ankle, or a shoe, was build. Then the Bluetooth module sends digital audio stimulus to the wireless headset when freeze was detected. Borrowing the concept of FI from Moore *et al.* (2008), the algorithm was optimized using 320 ms window instead of 6 s window with the average detection latency of 332 ms for 5 experiments. While the results look

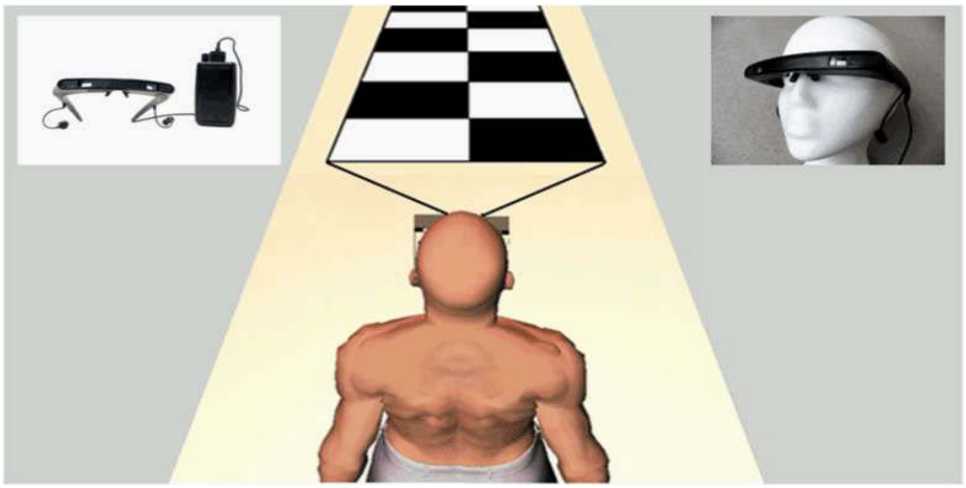

Figure 2.17: The GaitAid Virtual Walker visual cueing device transmits image of tiled floor to a projector fitted to glasses. The tiles image moves in response to the patient's movements, prompting the brain to keep the leg muscles going. Earphones provide additional help to improve walking, by giving auditory feedback
(Chong *et al.*, 2011)

promising, they were very limited recorded experiments from 4 simulated FOG events and from 1 patient. No real-time detection experiment was conducted and no further development of the proposed system has been made.

A similar real-time wearable device for FOG detection was reported from a study involving 10 PWF at the Movement Disorders Unit, Department of Neurology at the Tel Aviv Sourasky Medical Center (TAMSC) (Bächlin *et al.*, 2009). The system consisted of a 3D accelerometer and a 3D gyroscope, with data transmitted over a wireless Bluetooth linked to a light wearable computing system based on the Intel XScale processor and a complementary on demand rhythmic auditory stimulation (RAS) system (Fig. 2.18). The main computational algorithm was based on FFT calculation of a 32 sample window (0.5 s) and the extraction of FI following Moore *et al.* (2008). A maximum delay of 2 s was chosen as the detection tolerance.

The average sensitivity and specificity were reported as 73.1% and 81.6% respectively. However, there were a large variations due to the different walking styles of patients with patient 8 achieving only 34.1% sensitivity (with specificity of 88.9%) and patient 1 achieving only 39.7% specificity (with 99.1% sensitivity) (Fig. 2.19). Optimization of the system developed by subject dependent parameter, increased detection performance

up to 88.6% and 92.4% sensitivity and specificity, respectively (Bachlin *et al.*, 2010). The system performance also increased significantly with the worst result in patient 8 achieving both sensitivity and specificity at 80% (Fig. 2.19). Optimal window length was 4.5 s for the best detection performance.

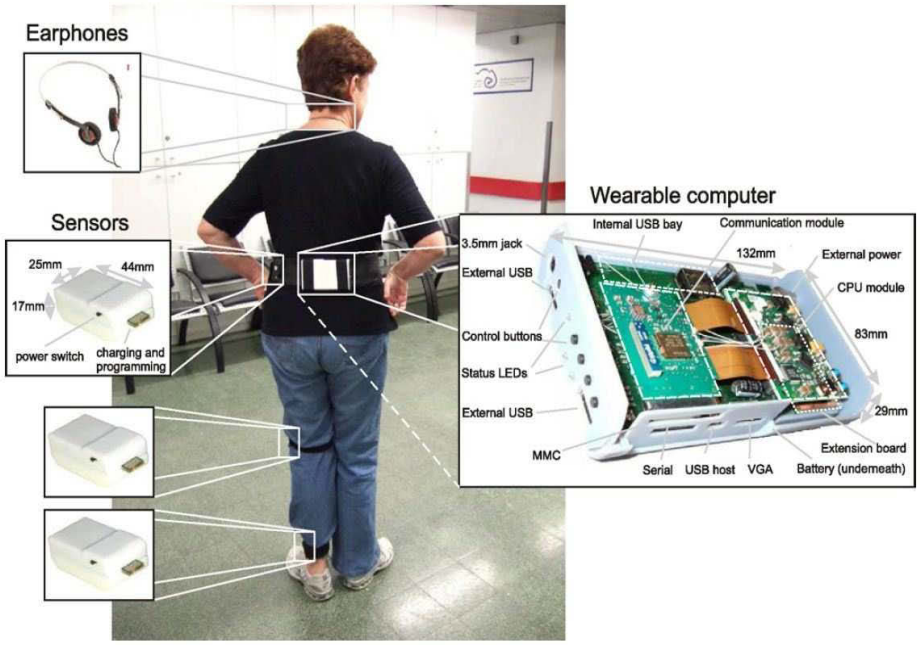

Figure 2.18: FOG detection and feedback device developed by Bächlin *et al.* (2009) with sensors attached to the shank, the thigh and the lower back .

2.3.3 Machine Learning in FOG Detection

Cole *et al.* (2011) integrated machine learning into a FOG detection. A dynamic neural network (DNN) classified the input features derived from the outputs of 3 triaxial accelerometer sensors and a surface EMG sensor worn by patients. The DNN consisted of a 2-stage linear classifier FOG detection algorithm. The first stage of the algorithm determined when the patient was upright using two inputs features from the Y-channel and the Z-channel of accelerometer, where the subject was upright when the Y-channel was dominant over the Z-channel. The second stage of the algorithm was applied in the interval when the patient was upright. A multilayer perceptron neural network comprising 11 nodes input layers with various features extracted from 2 s windowed sections of the accelerometer and EMG sensor signals, and 4 nodes hidden layers used the weights of a

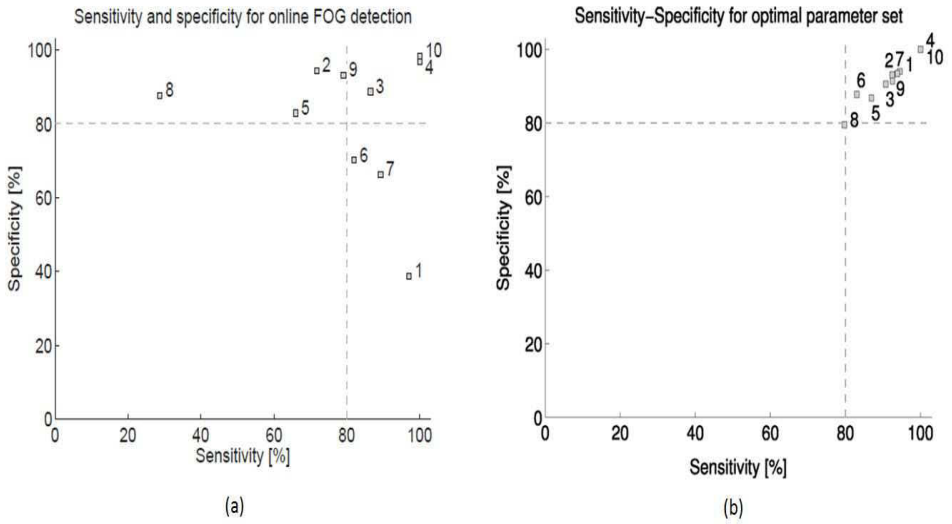

Figure 2.19: Sensitivity and specificity plots for the Bachlin *et al.* (2010)'s online detection device accuracy using (a) global parameter (b) subject-dependent parameter

3-point finite impulse response filter applied to time-delayed and time-advanced versions of the input. Eighty three percent sensitivity of the system from testing of 4 PWF and ninety seven percent specificity from testing of 2 healthy controls, was found.

In developing their wearable device for FOG detection based on the input data of 3 accelerometers and a smartphone as the computational unit, Mazilu *et al.* (2012) evaluated several supervised classifier algorithms based on the Weka Application Program Interface for Android: Random Forest, C4.5 Decision Trees, Naive Bayes, multilayer perceptron, boasting and bagging methods. Machine learning (compared with manual thresholds) deal better with the high dimensionality features of FOG, as did an automatically built patient specific FOG detection model. The proposed system was tested on the off-line data output of three 3D-accelerometers attached to the lower back, the thigh and the shank of 10 PWF.

The performance and detection latency of the system optimized by a combination of chosen machine learning algorithm, sensor location and window size of sample data. They found that the ensemble methods obtained better results, when compared with the single classifier. The AdaBoost showed the highest sensitivity and specificity, 98.35% and 99.72%, respectively, in case of window lengths of 1 s and user dependent experiments.

However, the C4.5 and Random Forest classifier was chosen for use based on its advantages in providing the shortest latency (0.24 s and 0.35 s, respectively). For the 1 s window user independent experiment using Random Forest classifier, the system obtained 62.05% sensitivity and 95.15% specificity. The large variability in motor performance among subjects was seen as a main factor for these comparatively lower results for user-independent FOG detection. A single sensor was found to provide sufficient data for FOG detection. In the latest development (Mazilu *et al.*, 2014), this group developed the GaitAssist which provides 2 functionalities, FOG detection and training support using FI as its feature and the C4.5 as its classifier system (Fig. 2.20).

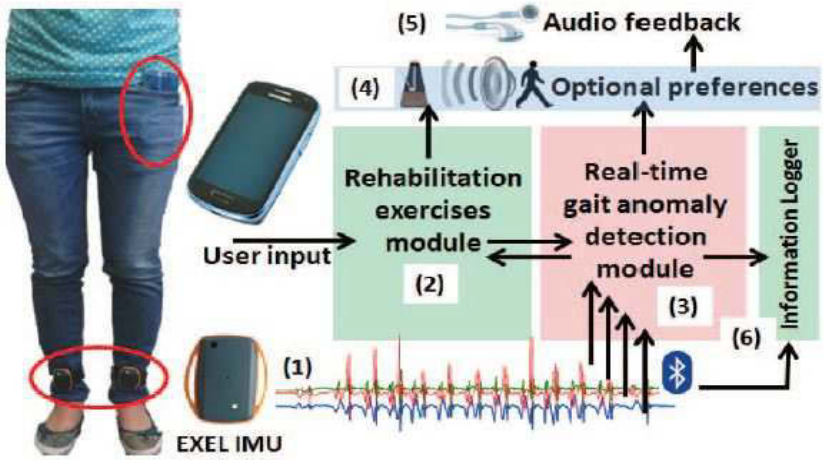

Figure 2.20: The GaitAssist system for a PD patient daily-life assistant with inertial measurement unit sensors (1), 2 functionalities for training support and FOG detection (2 and 3), preferences setting (4), audio feedback (5) and logging module (6) (Mazilu *et al.*, 2014).

Tripoliti *et al.* (2013) proposed similar methods in their FOG detection experiments using 4 classification algorithms: Random Tree, Random Forest, Decision Trees, and Naive Bayes. Using 6 accelerometers and 2 gyroscopes in the study of 5 PWF, 6 PWoF and 5 healthy control, the entropy was extracted using a sliding window with 1 s duration and 0.5 s overlapping. Their result was in agreement with Mazilu *et al.* (2012), with the ensemble methods having a better performance (compared with the selected single classifier). The Random Forest classifier was proposed as giving the best result, with sensitivity, specificity and accuracy of 81.94%, 98.74% and 96.11%, respectively.

2.4 Discussion and the Proposed Strategy for FOG Detection

Most studies in FOG detection have been based on the measurement of the patient's movement using on-body acceleration sensors. While the results appear promising, with some recent research claiming over 95% sensitivity, specificity and accuracy, this method has limitations.

First, the results showed the system's ability to detect a freezing condition after it has happened. The physical changes monitored using various sensors (the accelerometer, gyroscope, goniometers, force sensitive resistors and magnometer) were compared under 2 conditions: normal and freezing. However, the failures to start or continue movement do not happen suddenly, and can be seen as the disruption of a series of motor planning and execution. Thus, there is a possibility to detect the freezing episode while it is still in transition and before it appears as a gait disturbance, which the physician recognizes as freezing.

Second, as has been discussed by Mazilu *et al.* (2012), acceleration sensor measurement is prone to personal walking style, and so it cannot always provide good measurement in user-independent FOG detection system. In their system, for 1 s window experiments, a user-independent system achieved 62.05% sensitivity and 95.15% specificity compared to 97.76% and 99.75% in an user-dependent system using Random Forest as the classifier. The comparison of the results of each patient provides further insights on using this method, when the system detected a FOG event up to 98.19% sensitivity in one patient (patient 09) but failed to detect FOG in another patient (patient 01) where it achieved only 20.53% sensitivity.

Third, Niazmand *et al.* (2011b) acknowledged that the system deployed -in common with other acceleration sensor based FOG detection systems could not identify the akinesia type of freezing and could not classify stillness. This limitation may be due to the different gait mechanism of akinesia especially in the start hesitation (freezing when trying to take the initial step) compared with gait disturbance during normal walking with trembling legs in place or shuffling forward with small steps. However, because there is no significant change of acceleration in the change of gait which can be used to measure this type of

freezing, a different approach is needed for its detection.

Electroencephalogram (EEG) appears as a novel approach in FOG detection which may offer a more effective technique in the study and treatment of FOG, compared with the current methods. First, the novel approach using EEG has the ability to measure dynamic physiological change in the brain before movement disturbances occur. Using EEG, both cortical and subcortical activity can be studied through the time-varying changes in certain spectral bands, which also allow insights into the mechanism of FOG. With its high temporal resolution, EEG is well suited to capture electro-neurophysiological processes related to freezing of gait, including motor, cognitive and emotional processes. Moreover, the portability and relative ease of use of EEG make it far more useful for the mobile collection of brain activity data compared to fMRI or Voxel-Based Morphometry (VBM).

Second, the advantage of using the EEG for the detection of FOG compared with using sensors which measure body or gait movement, is that EEG is independent of an individual's movement style. Thus, it provides a better user-independent FOG detection. The analysis of the brain dynamic also presents the opportunity for detecting start hesitation, which cannot be measured using gait/body movement based sensor. Combined with the visual and auditory cues given on-demand, the system's detection of the freezing at the earliest time, allows it to be used to unfreeze at an earlier time than other methods.

Third, the EEG signal is actually multi-dimensional, measuring time, frequency, space, power (the strength of activity) and phase (the timing position of activity along the sine wave), although mostly presented as two-dimensional data of voltage changes over time and space only (represented by different electrodes). This multi-dimensionality provides many possibilities for characterization and conceptualization of freezing episodes as an enormous complex biological system as well as the possibility of linking previous findings related to various biophysical models of neural activity which may be related to this debilitating symptom (Cohen, 2011).

The 4-channel EEG system used in this thesis, makes possible the analysis of the movement signals propagated within the neural network of the brain. The analysis provides

a better understanding of the FOG mechanism by analyzing the interaction and cross-talk among the EEG electrodes and the correlation between various regions in the brain represented by the electrodes. Further, as part of brain effective connectivity analysis, the multichannel data will be used to measure the direction of coupling between two locations of the EEG electrodes.

Computational intelligence based on multilayer perceptron neural networks (MLP-NN) will be discussed, utilized and developed in this project. It will be used to draw a boundary between different condition classes and to label the testing data based on the training data. MLP-NN was chosen because of its good results in classification of EEG signals (Lotte *et al.*, 2007). Bayesian regularization will be used for training to optimize the classification system. Therefore, the outcome of this research will contribute to a better understanding on FOG, "the mysterious clinical phenomenon", as well as aid the development of the monitoring and detection of this debilitating symptom of PD.

Chapter 3

Electroencephalography-Based Detection of Freezing of Gait Using Artificial Neural Networks

"I have a form of Parkinson's disease, which I don't like. My legs don't move when my brain tells them to. It's very frustrating."
-George H. W. Bush

3.1 Introduction

Freezing of Gait (FOG) affects approximately half of the patients in the advanced stages of the Parkinson's disease (PD) (Giladi *et al.*, 2001). It is characterized by a sudden inability to initiate or continue walking, making it the most dangerous symptom of PD. Besides, it is resistant to treatment and its pathophysiology still largely unknown (Nutt *et al.*, 2011a). Therefore, this study of brain signals activity of PD patients using EEG has two main goals: to give insight into this largely unknown symptom including searching for indicators of FOG, and using the extracted indicators of EEG signals for detection of FOG. The goal of this chapter is to assess the feasibility of developing a FOG detection system using the time-frequency and power features of brain signals and multilayer

perceptron neural networks (MLP-NN). Section 3.2 provides an overview of the system. Section 3.3 discusses data acquisition and signal pre-processing. Section 3.4 explains features extraction both linear and non-linear, focusing on the univariate analysis. Section 3.5 discusses the features selection using statistical analysis and section 3.6 presents the Artificial Neural Networks. Section 3.7 presents the feature extraction and classification results. The discussion and conclusion follows in section 3.8.

3.2 System Overview

An overview of the proposed system is illustrated in Fig. 3.1. Brain signal data was acquired using the University of Technology, Sydney built 4-channel wireless EEG system. After the raw EEG data was preprocessed, a feature extraction was applied on the data set which was categorized into two conditions: normal walking and transition 5 s before freezing. The third condition, FOG, was analyzed for further investigation on the pathophysiology of FOG. The spectral and temporal pattern were examined using the non parametric Wilcoxon Sum Rank test to investigate the alteration of power spectral/wavelet energy and centroid frequency/scale caused by FOG. Several features were selected based on their statistical significant in differentiating those two conditions using MLP-NN.

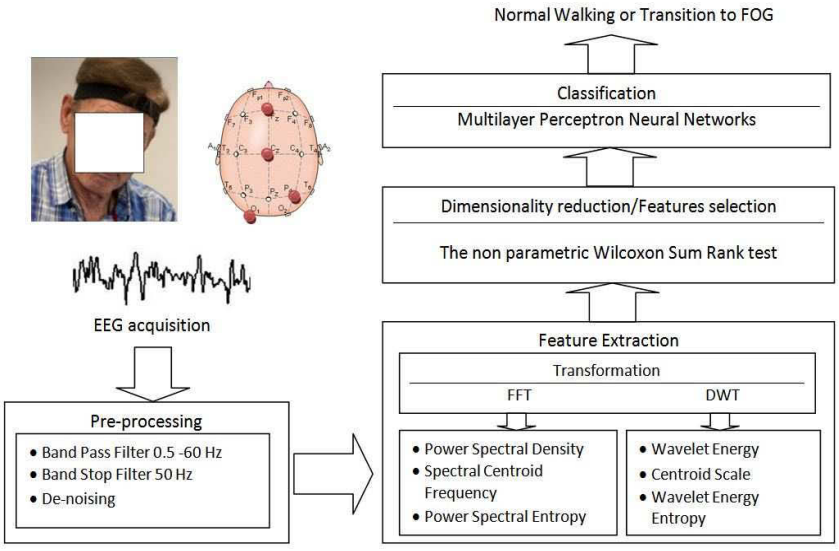

Figure 3.1: Signal processing flows for detecting FOG from the EEG data

3.3 Data Acquisition

3.3.1 Participants

Sixteen patients ranging in age from 62 to 85 years (mean: 70.88 years, std: 6.92 years) with idiopathic PD and significant FOG were recruited from the Parkinson's Disease Research Clinic at the Brain and Mind Research Institute, University of Sydney. All of them had a FOG history with different severity and frequency. The research protocol was approved by The Human Research and Ethics Committee from the University of Sydney and by the University of Technology, Sydney. All the patients provided written informed consent to participate as subjects for the study. The data collection was conducted at the Parkinson's Disease Research Clinic at the Brain and Mind Research Institute, University of Sydney over a one week period.

All patients satisfied the inclusion criterion under the United Kingdom Parkinson's Disease Study Brain Bank (Gibb & Lees, 1988) and were deemed unlikely to have dementia according to the Movement Disorder Society Task force guidelines (Dubois *et al.*, 2007) or major depression under the Diagnostic and Statistical Manual of Mental Disorder, Fourth Edition (DSM-IV) criteria of consensus rating of a Neurologist and a Neuropsychologist. All patients underwent a neurological assessment to determine the stage of the disease and the relative level of disability, applying the Unified Parkinsons Disease Rating Scale (UPDRS), Hoehn and Yahr stage (H&Y), and Freezing Of Gait-Questionnaire (FOGQ). In addition, a Mini Mental State Examination (MMSE) was performed to estimate cognitive impairment. Demographic information about the participants is shown in Table 3.1

3.3.2 Procedure

The EEG was recorded with a custom-made 4-channel wireless EEG system. The gold cup electrodes were placed on 4 scalp locations based on their roles in perceptual and control movement (Fig.3.2): O1-visual, P4-sensorimotor affordance, Cz-motor execution and Fz-motor planning. Bipolar EEG leads were used to acquire data from central zero

Table 3.1: Patient's demographics, neurological, cognitive and freezing characteristics

Number	ID	Age (years)	DD (years)	HY	UPDRS III	MMSE	NFOG-Q 2 and 3	Frequency of FOG	Percentage of time FOG
1	JM	65	4	4	65	29	20	31	75.7
2	PJ	67	11	2.5	22	27	4	9	9.3
3	JB	76	11	3	43	30	26	63	38.3
4	JM	65	4	2.5	36	28	18	16	7.9
5	AM	65	14	2.5	28	29	20	4	1.2
6	PD	77	3	2	31	25	24	40	56.5
7	HB	75	16	3	72	29	21	37	70.6
8	BD	66	14	2.5	50	30	20	7	1.6
9	MC	64	7	2.5	46	29	18	10	1.3
10	FS	77	6	3	49	28	19	13	61.9
11	BH	62	10	2	19	28	17	35	24.0
12	DK	67	2	3	43	28	24	12	31.4
13	GW	69	26	4	47	28	25	9	56.2
14	GP	85	2	3	44	30	18	24	62.8
15	DR	76	6	2.5	52	23	22	21	5.8
16	WC	81	2	2	33	25	16	47	9.9
Mean		70.88	8.63	2.75	42.50	27.69	19.69	23.63	32.15
$\pm$ STD		6.92	6.58	0.61	14.25	2.02	5.23	16.96	27.83

DD: Disease Duration, HY: Hoehn and Yahr scale, UPDRS: Unified Parkinson's Disease Rating Scale
MMSE: Mini Mental State Examination, NFOG-Q: New Freezing of Gait Questionnaire

(Cz) and frontal zero (Fz) with the reference electrode placed at FCz, and from occipital one (O1) and parietal four (P4) with the reference electrode at T4 and T3, respectively. Henceforward, in this study, the measurements of EEG signal reported as taken from channel Cz are referred to Cz-FCz, channel Fz are referred to Fz-FCz, channel O1 are referred to O1-T4, and channel P4 are referred to P4-T3.

The EEG signals were amplified with the common-mode rejection ratio $>$95 dB, sampled at a rate of 500 Hz, and band-pass filtered between 0.15 and 100 Hz using an analogue electronic band-pass filter. Several studies have shown that information on EEG signals relating to mental tasks or the physiological condition can be tracked using only a few points of measurement (Wikström *et al.*, 2012), (Picot *et al.*, 2012). Clearly, fewer channels promotes patient ease, and limits noise and artifacts. Moreover, it reduces the cost in signal processing, feature extraction and classification processes; and makes the setting up of the system much easier and faster.

Patients were asked to perform a series of Timed "Up-and-Go" tasks on a standardized course and were video recorded for evaluation as can be seen in Fig 3.3. The pathway

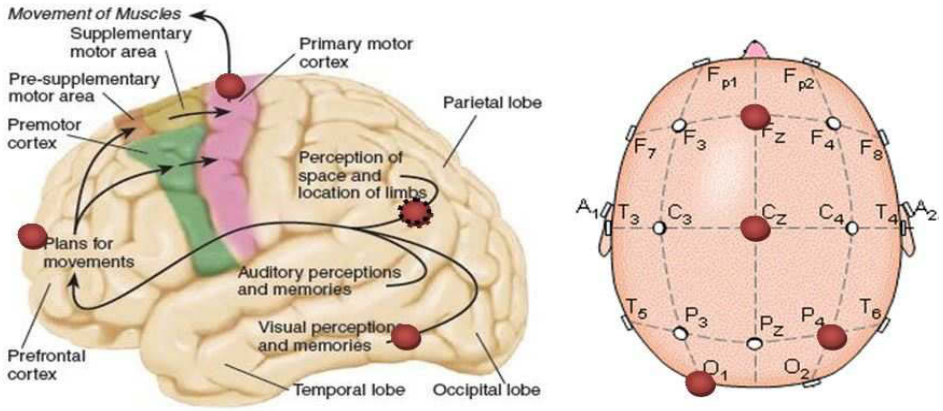

Figure 3.2: Location of four electrodes related to cortical control of movement (Carlson, 2013).

of the experiment was created to provoke different types of freezing episodes: turn hesitations, runway freezes, freezing during narrow gaps, target hesitations, and start hesitations. Starting from a sitting position, the patients walked approximately five meters to a target 0.6 m X 0.6 m box marked on the floor and performs different turning movements: (1) a standard turn within the box, (2) two revolutions within the box, (3) a walk around the outside of the box, and (4) pass a narrow gap of $<$1 m as the patients return to the chair, with turns to the patient's left and right. An additional experiment based on the effect of complex cognitive action in increasing freezing episodes was utilized by asking the patients to vocalize the months of the year forwards and backwards whilst walking. Patients also underwent the 10 m walk test in which they walked in a straight-line to evaluate start hesitations, runway freezes and turn hesitations.

Two clinicians specializing in movement disorders reviewed the video recording and labeled the time of onset and offset of the freezing episodes. Only the freezing episodes which have been logged by both of the raters were included as freezing episodes in the further process and time synchronized with EEG data. This provided 5.5 hours of data comprising 404 FOG episodes of duration between 1 s and 220 s. Two other episodes were determined based on this period: transition episodes which cover a period between 5 s to 1 s before freezing and normal walking, defined as a period after freezing to 5 s before the next freezing period. The variability of 16 patients conditions can be seen in Table 3.1 where 4 patients were affected by less than 10 freezing episodes during testing

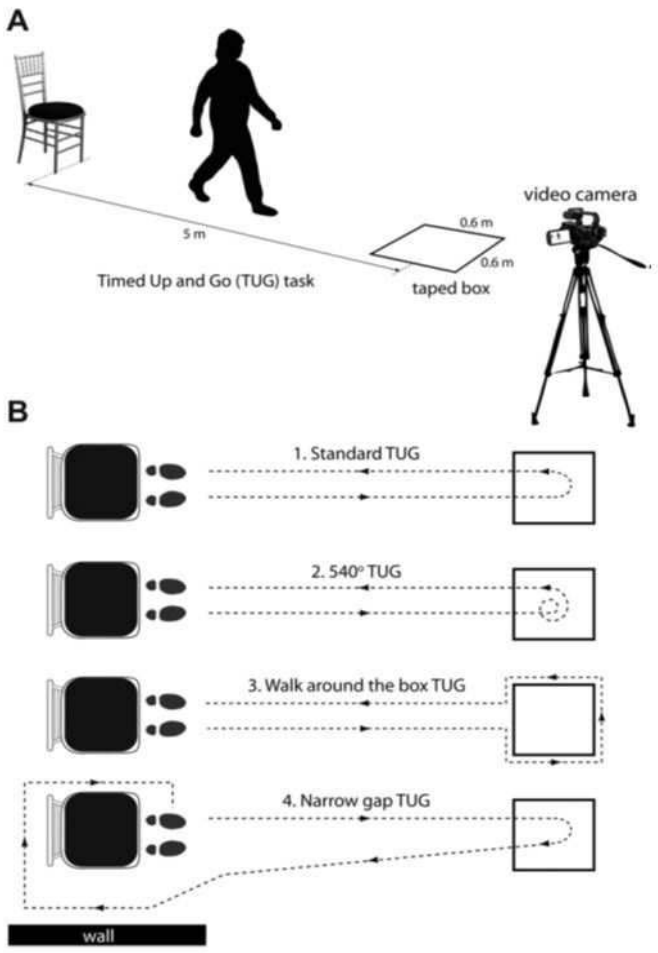

Figure 3.3: (A) The timed up and go (TUG) task for FOG assessment. (B) Four different trials with different additional tasks to trigger a freezing condition during walking from a chair to a taped box on the floor and back to chair (Shine *et al.*, 2012).

and 7 patients were affected by FOG episodes for less than 10 % of the total test duration.

After manual inspection to remove epoch with bad and artifact-ridden data, a total of 1902 one s duration samples of 3 episodes (normal walking, transition, FOG), with each episode contributed evenly (634 samples), were included in the analysis. Data from 11 patients were randomly chosen for training and testing (1386 samples, 462 in each class). Another set of testing data files, not selected previously for the training process, was taken from 5 other patients (516 samples, 172 in each class) to examine the robustness of the system in classifying the EEG signals from out-group patients.

3.3.3 Signal Preprocessing

All data was passed through band-pass (0.5-60 Hz) and band-stop (50 Hz) Butterworth infinite impulse response filters, in order to eliminate low frequency noise, high frequency noise and 50 Hz line frequency noise as can be seen in Fig 3.4 and Fig. 3.5. Ocular and muscular artifacts were removed using Stein's unbiased risk estimate thresholding based on wavelet transforms with the mother wavelet resembling the shape of the eye movement, Coiflet (Coif5) wavelet (Geetha & Geethalakshmi, 2011), level 6. Since the effect of ocular artifacts were expected to be dominant in the frontal and frontopolar area and limited within the range of 0 to 16 Hz, this algorithm was applied only to EEG data from Fz-FCz in the lower frequency band (delta, theta, alpha). Muscle artifacts correction was made using the same methods with a different mother wavelet, Daubechies (dB5) level 3 in all electrode locations and sub frequencies (Xizheng *et al.*, 2010).

3.4 Feature Extraction

Features are variable constructs of data representation from the original input. Finding the appropriate set of features is crucial step in achieving good prediction of class membership for distinguishing the data. Moreover, in this study related to system neurophysiology, the relevant features may give insight to the pathophysiological mechanisms underlying the studied symptoms or diseases. In this chapter, the classical methods of power spectral

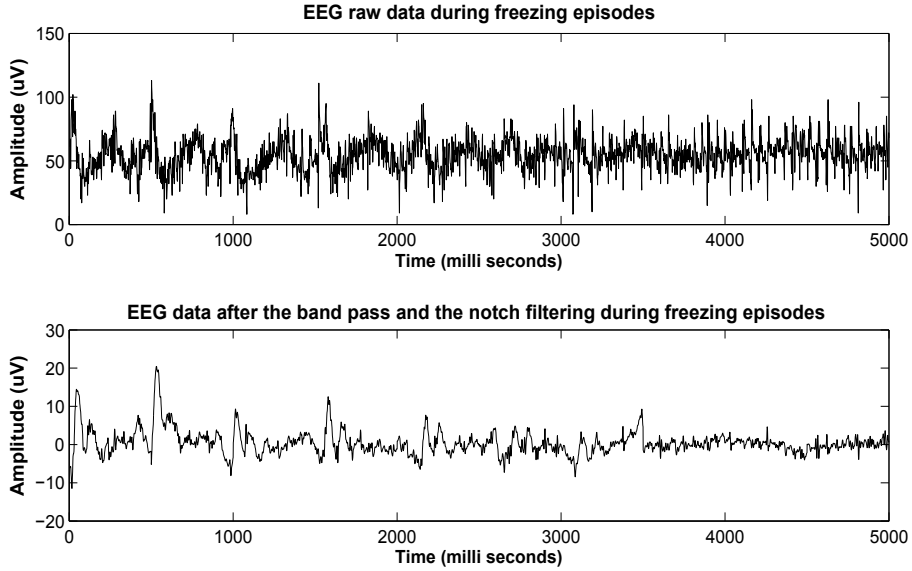

Figure 3.4: The sample of EEG signal before and after the band-pass and the band-stop filtering during freezing episodes in the time domain

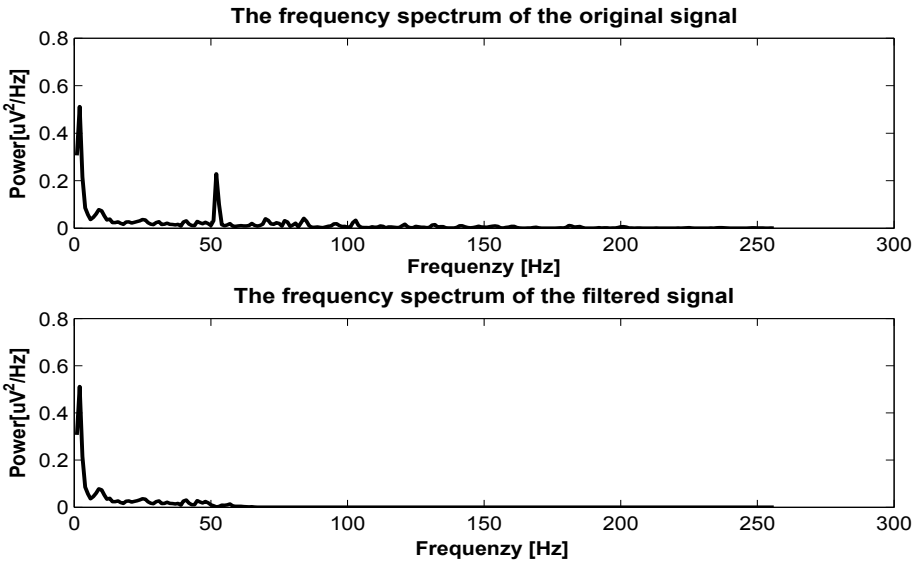

Figure 3.5: Frequency distribution of the EEG signal before and after filtering stage

analysis as well as its paired, wavelet energy (WE) analysis, were investigated to observe their alteration during transition to freezing and freezing episodes. The shift of the center of gravity of frequency band, spectral centroid frequency and its paired, WE centroid scale, derived from the same analysis as other investigated features. These linear features were compared to the non-linear features based on the information theory, which measures the regularity of the signal, entropy.

3.4.1 Power Spectral Density

EEG signals are captured in the time domain and can be described as a sequence of numbers:

$$x(t) = [x(1), x(2), x(3), ...x(N)] \tag{3.1}$$

Power spectral density (PSD), widely used and successfully applied to characterize signals in a system, shows the strength of energy as a function of frequency. It is based on the Fourier transform which represents a time series in the frequency domain. It can be defined as the average signal power over the interval [0,T] or as the Fourier transform of the autocorrelation function $r_{xx}(t)$ and in continuous and discrete notation are given by (Semmlow, 2011)

$$P(f) = \int_0^T r_{xx}(\tau) e^{-j2\pi f\tau} d\tau \tag{3.2}$$

$$P(f) = \sum_{n-0}^{N-1} r_{xx}(n) e^{-j2\pi f_T T_s} \tag{3.3}$$

The direct approach based on Parseval's theorem led to the fast Fourier transform, which relates the energy of an analog signal, $x(t)$, to the magnitude of the signal squared, integrated over time

$$E = \int_{-\infty}^{\infty} |x_t|^2 dt = \int_{-\infty}^{\infty} |X_T(f)|^2 df \tag{3.4}$$

The power spectral density in the direct approach is then given by

$$P(f) = \frac{|X_T(f)|^2}{T} \tag{3.5}$$

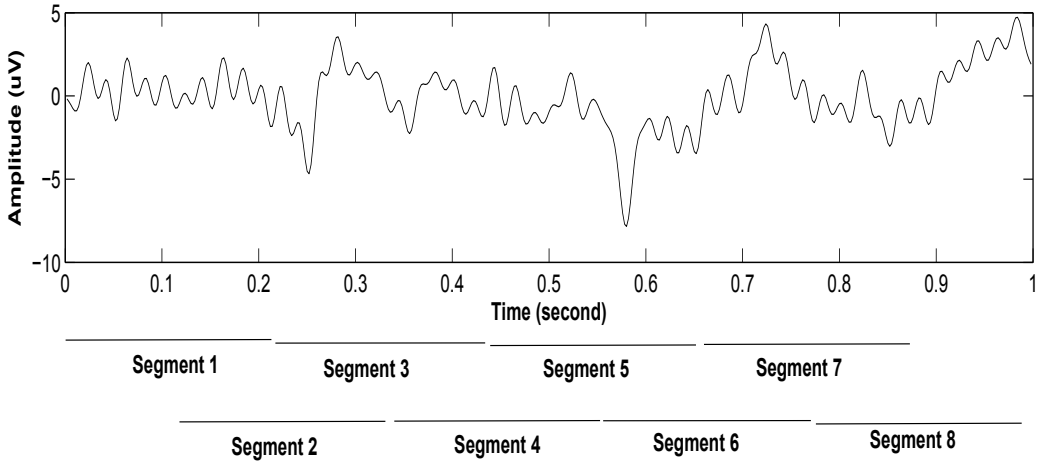

Figure 3.6: The EEG signal is divided into 8 segments with a 50 % overlap between each segment in the Welch method of spectral analysis. The output is the averaged data of the 8 transforms which are calculated separately.

Fourier transform implies stationary process during the time window. While EEG signals are known as a non-stationary signal with non-linear behavior (Sanei & Chambers, 2008), fragments of EEG with length up to 290 ms can be treated as stationary (Schack & Krause, 1995). In this study, the spectra are calculated using the Welchs method (Welch, 1967). This method uses overlapping segments and applies a window to each segment (Fig. 3.6). The segmented and averaged data produce a periodogram which is significantly smoother, thus reducing the noise of the data. This study used a 516 point Fast Fourier Transform (FFT) and periodic Hamming windows with an overlap of 50 %. The duration of the stationary fragments is assumed to be 220 ms with the sampling frequency 500Hz.

To eliminate inter-individual and inter-electrode variance in absolute measurements, power spectra were normalized using z-score normalization:

$$x_{new} = \frac{x_{old} - \mu}{\sigma} \tag{3.6}$$

where x_{old} is the original value, x_{new} is the new value, and μ and σ are the mean and standard deviation of the original data range, respectively. The normalized power spectrum in the transition period tends to increase significantly in the lower frequency band (see Fig.3.7).

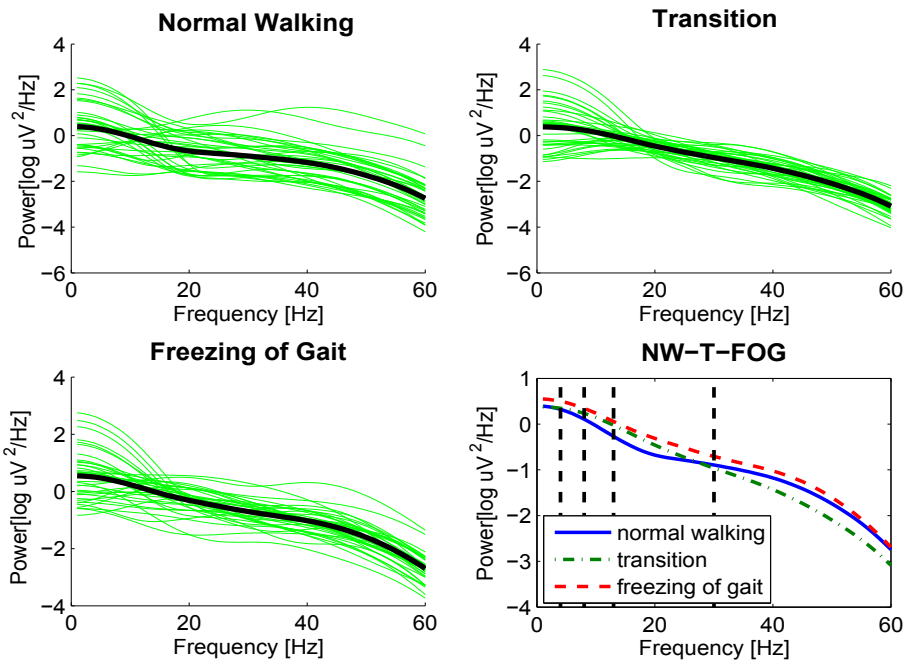

Figure 3.7: Sample PSD from subject 7 channel P4; the mean of the PSD indicates the significant increase of power during transition to FOG in alpha and beta frequencies

3.4.2 Centroid Frequency

The shift of the centre of gravity of the frequency band based on this normalized power spectrum, Centroid Frequency (CF), has been reported to have the capability to classify different types of EEG in various health conditions (Nguyen *et al.*, 2012) (Staudinger & Polikar, 2011) and is defined as:

$$CF = \frac{\sum_i f_i * P(f)}{\sum_i P(f)} \tag{3.7}$$

3.4.3 Power Spectral Entropy

Brain signals have been known as the output of a nonlinear system. Consequently, various measures which characterize the nonlinear behavior of EEG signals have also been developed. Based on the concept of information theory, Shannon introduced entropy as an index of signal complexity or irregularity (Shannon, 1948). This theory defines the power spectral entropy (PSE) of EEG signal x as:

$$PSE(x) = -\sum_{i=f_l}^{f_h} P_i log P_i \tag{3.8}$$

where P_i is the normalized power density from the signal's spectrum so that $\sum P_n = 1$ while f_l and f_h are the frequency band of of interest. The higher the entropy, the greater complexity of the signal.

3.4.4 Wavelet Energy

Over the past few decades, wavelet analysis has been developed as an alternative and improvement on Fourier analysis. Its main advantage in analyzing the physiological systems is its capability to detect and analyze non-stationarity in signals and their related aspects such as trends, breakdown points, and discontinuity. Unlike Fourier transform which is limited to a scaled single sinusoidal function, wavelet transform uses "mother wavelets" which were created by multiplying a sine wave and a Gaussian window, so that they become stationary only during the period in which the wavelet looks like a sine wave in the centre/peak frequency areas.

Wavelets are well localized in both time and frequency domain based on the Heisenberg uncertainty principle. A wavelet in the high frequency signal (small-scale) has fine time resolution but is poorly localized in frequency. On the other hand, a wavelet in the low frequency signal (large-scale) has fine frequency resolution but lower time resolution. This ability to contracting the wave-like scalable function to adapt the analysis to the depth of focus of interest enabled it to perform a multi-scale inspection of data from macro resolution (low-frequency) to micro resolution (high-frequency).

Unlike the Fourier transform which is limited to a scaled single sinusoidal function, wavelet transform generates a 2 parameter family of wavelet function $\psi_{a,b}(t)$ by scaling (a) and shifting (b) the function. The correlation called continuous wavelet transform (CWT) is given by (Semmlow, 2011).

$$CWT(a,b) = \int_{-\infty}^{\infty} x(t) \frac{1}{\sqrt{|a|}} \psi^*(\frac{t-b}{a}) dt \tag{3.9}$$

with $^{(*)}$ denotes the complex conjugation.

The development of wavelet-based signal compression algorithm led to the invention of the fast discrete wavelet transforms (DWT) which removes redundancy in the signals and simplifies the numerical calculations. In the DWT time-scaled parameters (b,a) are sampled on a dyadic grid with scales $a = 2^j$ (reciprocal of frequency) and positions $b = 2^j k$ (time localization), so that DWT is defined as,

$$DWT(j,k) = \frac{1}{\sqrt{|2^j|}} \sum_{t=-\infty}^{\infty} x(t)\psi(\frac{t-2^j k}{2^j}). \tag{3.10}$$

In the multi resolution analysis, signal $x(t)$ with maximum cut-off frequency f_m is split into 2 components using a low-pass filter and a high-pass filter, and is down sampled by 2 to provide the approximation signals A_j and the detail signals D_j with a lower cut-off frequency band $[0 : f_m/2]$ and upper cut-off frequency band $[f_m/2 : f_m]$, respectively (Mallat, 1999). Based on the Nyquist criterion, the maximum cut-off frequency is determined by f_m=$f_s/2^{(l+1)}$ where f_s is the sampling frequency of the original signal and l is the level of decomposition. The approximation is subsequently decomposed and this process is continued until the target level is achieved (Fig. 3.8).

The wavelet decomposition for a given EEG signal $x(t)$ at scales j=1,2,..., J and time point k then could be written as

$$x(t) = \sum_k c_{J,k}\varphi_{J,k}(t) + \sum_k \sum_{j \le J} d_{j,k}\psi_{j,k}(t) \tag{3.11}$$

where $c_{J,k}$, $d_{j,k}$, $\varphi_{j,k}(t)$ and $\psi_{j,k}(t)$ are the approximation coefficients, the detail coefficients, scaling function and wavelet functions, respectively. The Daubechies (db4) wavelet that has been found as properly representing EEG signals and spikes (Subasi, 2007) was selected as wavelet function.

With the EEG sampled at 500 Hz, a good match to the standard clinical EEG subbands can be achieved using a 6 level decomposition (Table 3.2). Reconstruction of these signals which are decomposed into 5 constituent EEG subbands is depicted in Fig. 3.9.

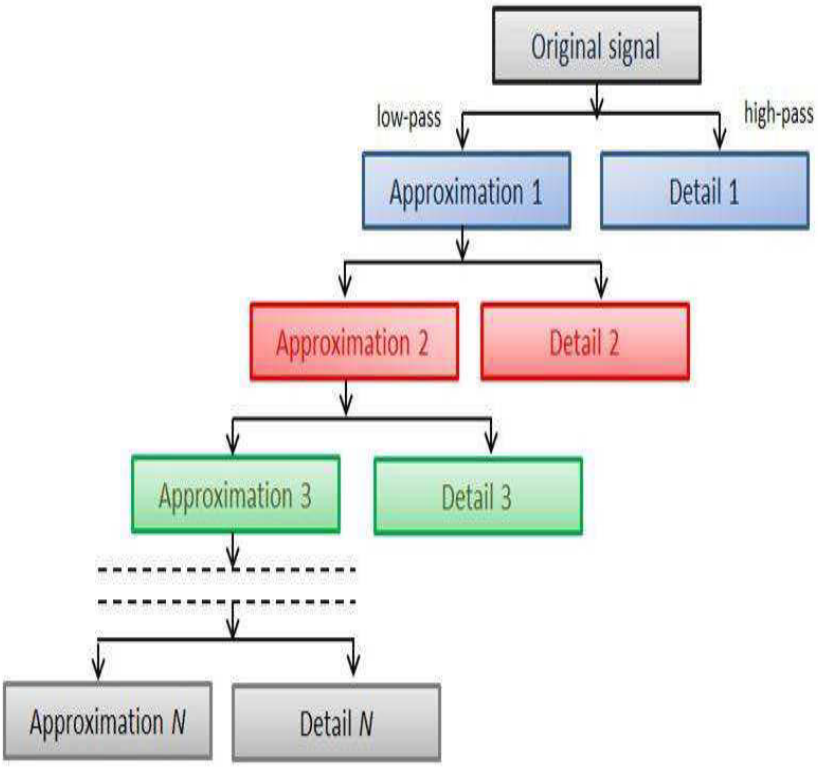

Figure 3.8: Multi-Resolution Analysis

Table 3.2: Frequency bands corresponding to different decomposition levels

Decomposed signals	Frequency bands (Hz)	Decomposition Level
D1	125-250	1 (noises)
D2	62.5-125	2 (noises)
D3	31.3-62.5	3 (γ)
D4	15.6-31.3	4 (β)
D5	7.8-15.6	5 (α)
D6	3.9-7.8	6 (θ)
A6	0-3.9	6 (δ)

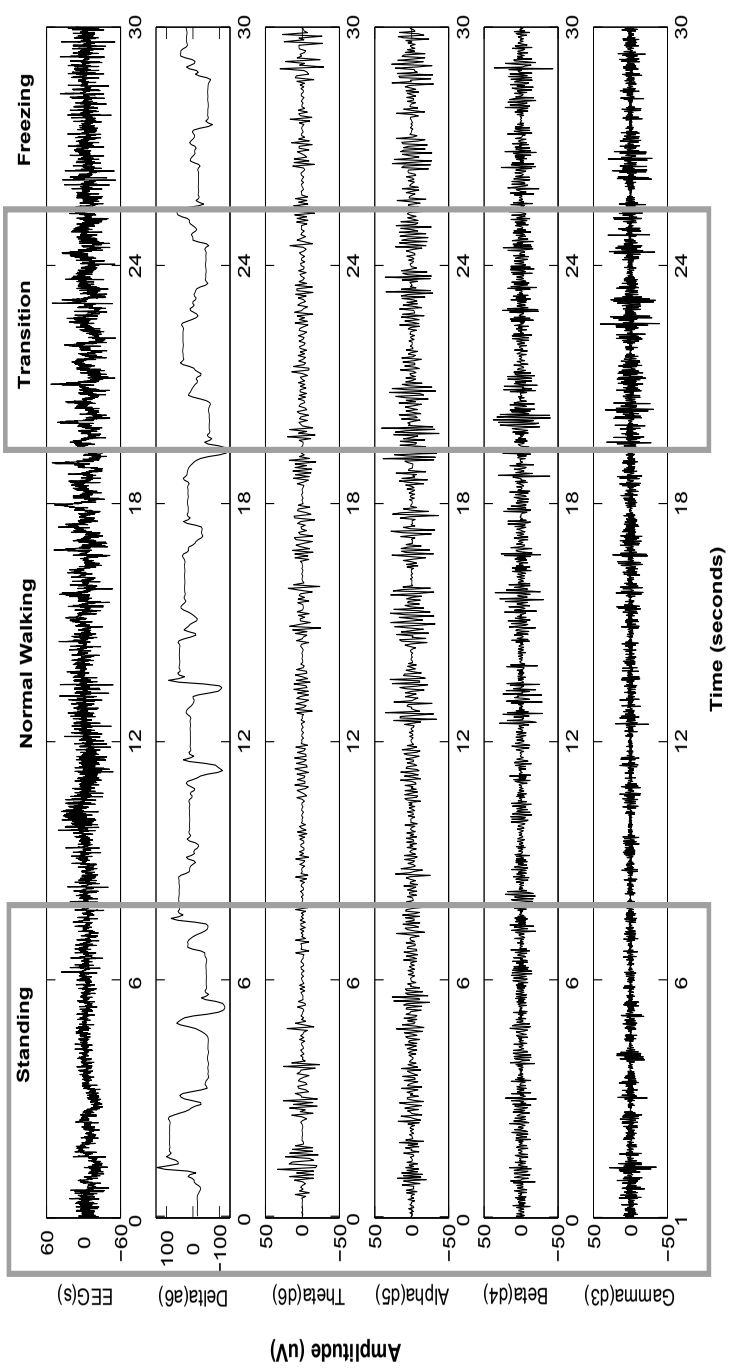

Figure 3.9: Decomposition of EEG into detail (d1-d5) signals related to five standard clinical EEG subbands by db4 wavelet taken from electrode P4 in subject 6 shows the amplitude and frequency alterations preceding and during freezing episode.

According to Parseval's Theorem, in wavelet analysis, the energy of signals which correspond to PSD, WE can be partitioned at different levels of wavelet decomposition ($j = 1, ...l$) and is expressed as a function of the scaling and wavelet coefficient (Burrus *et al.*, 1998):

$$E_T = \int |f(t)|^2 dt = \sum_k |c_{J,k}|^2 + \sum_k \sum_{j \leq J} |d_{j,k}|^2. \tag{3.12}$$

The analysis of each detail of decomposed signals also captured the temporal dynamics of the signals in each electrode and frequency band through the calculation of the mean, minimum and maximum values of signals.

3.4.5 Centroid Scale

Corresponding to CF, we also calculated Centroid Scale (CS) based on the CWT scalogram to show the shift of the center of gravity of frequency band. The CWT was chosen since it has a better frequency (scale) representation compared to the DWT. We used the complex Morlet wavelet due to its narrow spectral band and its having an extended time domain made it more suitable for extracting information in frequency domain (Misiti *et al.*, 2007). It is equivalent to a complex sinusoid with a Gaussian envelope and can be written as (Addison, 2010)

$$\psi_0(t) = \frac{1}{\sqrt[4]{\pi}} e^{j2\pi f t} e^{-\frac{t^2}{2}}. \tag{3.13}$$

3.4.6 Wavelet Energy Entropy

The wavelet energy entropy (WEE) is found using a similar formula to PSE, with

$$P_i = \frac{E_j}{E_T} \tag{3.14}$$

where E_j refers to the energy of signals at j^{th} frequency band of decomposition and E_T refers to the energy of all frequency bands of decomposition.

3.5 Feature Selection

Feature extractions processes often yield a large number of candidates, including many that are irrelevant to the target of the classification problem. The selection of a subset of features aims to find the most informative and compact set of features, that are rich in discriminatory information between different conditions. This is a crucial step to improve classifier performance and the efficiency of data processing by avoiding an excessive number of features used for classification, often known as the curse of dimensionality problem. In other words, it aims to find the most informative and compact set of features.

There are 3 paradigms of evaluation strategies in the selection process: the filter, the wrapper and the embedded methods (Guyon *et al.*, 2008). First, filter methods which rank each feature according to some univariate metric (the score of significance test based on correlation, information gain, and area under curve of the receiver operating characteristic), the scoring of each feature reflecting its discriminative power. Under this method, only some of the highest ranking features are taken as input for the classification system. Thus, it is very efficient and fast. However it may miss features that are not useful by themselves but can be very useful when combined with other features.

Second, wrapper methods which assess the quality of a set of features using an induction algorithm together with an internal cross validation. It is therefore classifier dependent. While they usually provide the best performing feature set for the related model, they involve an exhaustive search and are computationally intensive. Third, embedded methods, in which feature selection becomes part of the model building, such as in a decision tree.

Having regards to the computational complexity and the chance of an over fitting, the probability of which are higher in the wrapper and the embedded methods, the filter method is chosen as the feature selection method. Since the distribution of the features of the experiment data cannot be assumed Gaussian, the Wilcoxon Sum Rank Test, a non-parametric statistical analysis, was used. Only the most relevant features with significant statistical differences between groups, that is of normal walking and transition to freezing data (p-value <0.05), were chosen for further process and classification.

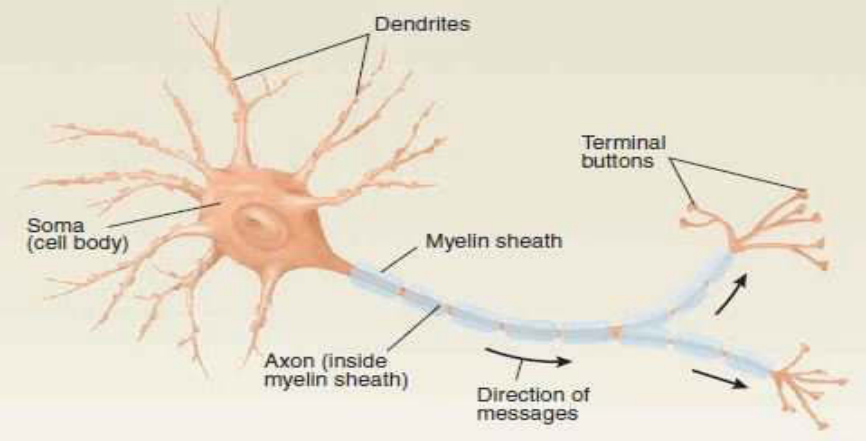

Figure 3.10: Biological neuron (Carlson, 2013).

3.6 Artificial Neural Networks Classification Algorithm

An accurate model of the data has to be built to detect their hidden patterns of classification. Such a model can be very helpful also for the prediction and the description necessary to extract knowledge of the process underlying the data. Where the process of learning is unsupervised, input data is without any indicator/labels; where supervised, the set of input representation data with their labels enables learning or the prediction a class of new data representation sets.

Artificial Neural networks (ANN) are computational models of learning that taking their inspiration from the biology of the human brain. Originally proposed by McCulloch and Pitts (1943), they are built from artificial neurons, grouped in layers. Like a biological neuron (Fig. 3.10), an artificial neuron called the perceptron by the psychologist Frank Rosenblatt, Cornell University (Fig. 3.11), receives signals from the environments or the outputs of other artificial neuron. This multiple input represents the dendrites in a biological model. When fired, perceptron transmits a signal to the connected artificial neuron, and simulates the axon which carries impulses away from the cell body of the biological neurons. The perceptron collects all incoming signals and computes a net input signal as a function of the respective connection or synaptic weights. The activation function controls the firing and the strength of the exiting signals, usually [0,1] or [-1,1], based on this net input.

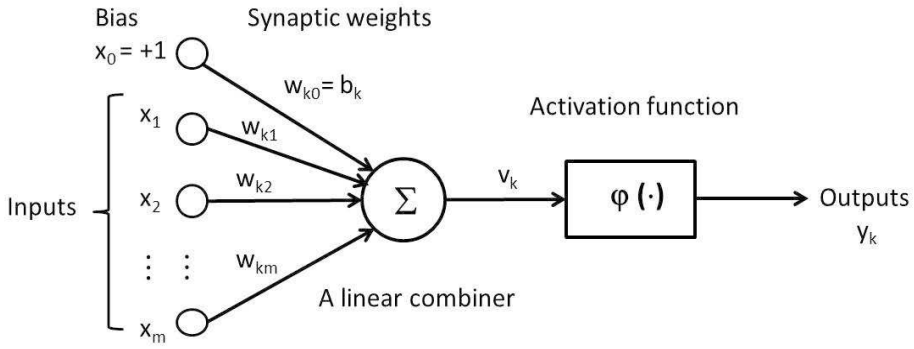

Figure 3.11: Perceptron, a model of a neuron.

3.6.1 Architecture

In its mathematical model, a relationship between the input and the output of a perceptron can be described as the pair of equations

$$v = \sum_{j=1}^{m} w_j x_j + w_0 \tag{3.15}$$

and

$$y = \varphi(v) \tag{3.16}$$

where v is the linear combination output of the input signals x_j, w_j is a connection weight, w_0 is the weight coming from an extra bias unit b_k, y is an output of the perceptron, and $\varphi(.)$ is the activation function. When m=1, the first equation can be seen as an equation of a line with the slope w_1 and the intercept w_0. The line becomes a hyper plane when the perceptron has more than one input, and can be used to separate two classes based on the output of the perceptron. The 3-layer Multilayer Perceptron (MLP) ANN model (Fig. 3.12) is selected for this study with an input-output relationship mapping is calculated as follows:

$$y = \varphi_{output}\left(\sum_{j=1}^{J} w_j \varphi_{hidden}\left(\sum_{i=1}^{I} w_{ij} x_i + b_0\right) + w_0\right) \tag{3.17}$$

where J is the number of hidden nodes, I is the number of inputs, w_{ij} is the weight of link between input i and hidden nodes j, w_j is the weight of link between hidden nodes j and output nodes, b_0 and w_0 are the biases for hidden and output nodes, and x_i is the i-th input variable.

In this study, hyperbolic tangent transfer function, tansig, which accelerates the convergence of the MLP (Vogl *et al.*, 1988), is chosen as an activation function:

$$\varphi(v) = tansig(n) = \frac{2}{1+e^{-2n}} - 1. \tag{3.18}$$

3.6.2 Learning of Artificial Neural Networks

A learning process in the ANN, which shows its intelligence, can be seen as the process of finding the optimum network architecture and connection weights based on the representatives' examples from available training patterns, to efficiently perform a specific task. The supervised learning paradigm is used in this study, based on the error correction learning principle. In the following section, two ANN-training algorithms, the Back-propagation and the Levenberg-Macquardt algorithms, are discussed further.

The Back-Propagation Algorithm of ANN

The Back-propagation (BP) algorithm is a generalization of the least mean squared algorithm. It modifies networks weights to minimize the mean square error between the

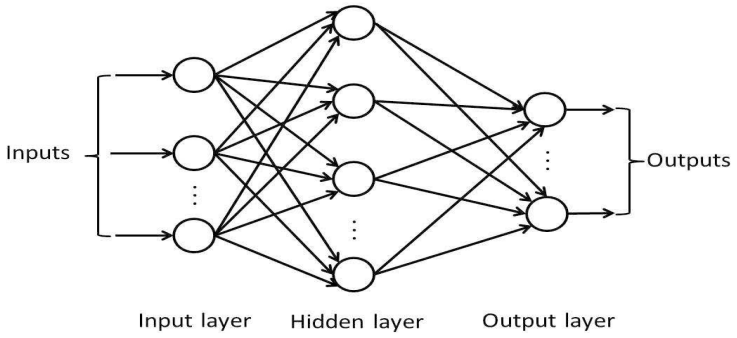

Figure 3.12: Feedforward networks with 1 hidden layer and 1 output layer.

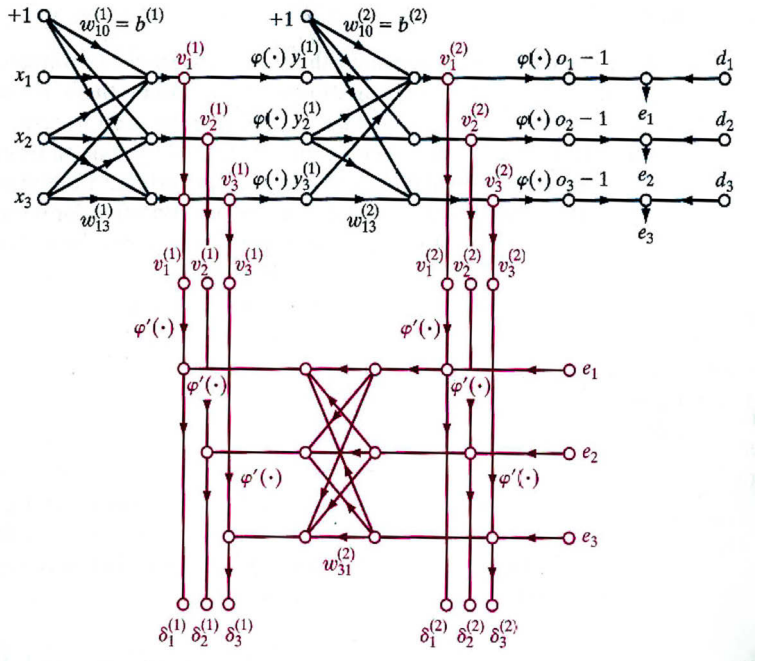

Figure 3.13: A summary flow graphs of back-propagation learning with the forward pass on the top part of the graph and backward pass on the bottom part of the graph (Haykin, 2009).

desired and actual outputs of the networks. Backward path of BP propagates error signal δ_i through the network in the backward direction. During this phase, using data for which inputs as well as desired output are known, adjustments are applied to the weight matrices of the network, so that the error values decreases. Once trained, the network weights are stored and can be used to compute output values for new input samples.

The procedure for BP algorithm is illustrated in Fig. 3.13 and can be summarized as follows (Haykin, 2009):

1. *Initialization*. Set synaptic weights w to small random numbers; set learning rate η and momentum α.

2. *Forward computation*. Propagate the signal input pattern x_n forward through the network, layer by layer, and calculate the outputs y from all nodes using the activation function, which is in our study is tansig:

$$y = \frac{2}{1 + e^{-2\varphi(\Sigma_{i=1}^{I} w_{ij})}} - 1 \tag{3.19}$$

Compute the error signal

$$e_j(n) = d_j(n) - o_j(n) \tag{3.20}$$

where d_j is the jth element of the desired response vector $d(n)$ and o_j is the output signal of neuron j.

3. *Backward computation*. Compute local gradients of the output layer and hidden layer networks, δs:

$$\delta_j^{(L)}(n) = (d_j(n) - o_j(n))\varphi_j'(v_j^{(L)}(n)) \text{ for neuron } j \text{ in output layer } L \tag{3.21}$$

and

$$\delta_j^{(l)}(n) = \varphi_j' v_j^{(l)}(n) \sum_k \delta_k^{(l+1)}(n) w_{kj}^{(l+1)}(n) \text{ for neuron } j \text{ in hidden layer } l \tag{3.22}$$

where φ_j's is the differentiation with respect to the argument.

Update all the weights of the networks in layer l according to the generalized delta rule:

$$w_{ji}^{(1)}(n+1) = w_{ji}^{(l)}(n) + \alpha[w_{ji}^{(l)}(n-1)] + \eta \delta_j^{(l)}(n) y_i^{(l-1)}(n) \tag{3.23}$$

where η is the learning constant, α is a momentum term which is used to speed up convergence and prevent the network from getting stuck in some local minimum.

4. *Iteration*. The learning process under point 2 and 3 is repeated until fulfill the stopping condition.

During training, the progress is constantly updated and observed. Some common criterions are applied in this study for early stopping to avoid overfitting,:

1. Terminate when a maximum number of iterations, 1000, has been exceeded
2. Terminate when a maximum training time, has been exceeded
3. Terminate when it reaches minimum performance value (0.01), usually using the mean square error (MSE) on the training set

$$E_c = \frac{1}{IJ} \sqrt{\sum_{i=1}^{I} \sum_{j=1}^{J} (d_{ij} - o_{ij})^2} \tag{3.24}$$

where E_c is the cycle error, d_{ij} is the desired output, and o_{ij} is the actual output.

4. Terminate when the validation error fails to increase after number of times (6 to 10), indicating that the training data is being memorized.

The Levernberg Marquardt Algorithm of ANN

Levernberg Marquardt algorithm is chosen as a training method for its speed and stability (Übeyli, 2009). Known as a combination of the Gauss-Newton technique and the steepest descent method, the Levernberg-Marquardt algorithm is essentially an iterative technique that located the minimum of an objective error function:

$$E(w) = \sum_{i=1}^{m} e_i^2(w) = \|f(w)\|^2 \tag{3.25}$$

where $e_i^2(w) = (y_{di} - y_i)^2$ is an individual error (the difference between the desired value of output neuron y_{di} and the actual output of that neuron, y_i) and w is the weight vector. The Levenberg-Marquardt algorithm is used to find the new weight vector w_{k+1} needed to reach the optimum performance of the system:

$$w_{k+1} = w_k - (J_k^T f(w_k))(J_k^T J_k + \lambda I)^{-1} \tag{3.26}$$

where J_k is the Jacobian of function $f(.)$ at w_k, λ is the learning rate and I is the identity matrix.

Performance Evaluation of ANN

Classification data sampled using selected features was based on 3 layers MLP (Fig. 3.12) with 56%, 25% and 19% of the data, randomly split, used for training, validation and testing, respectively (Fig. 3.12). Validation set was used as a stopping criterion to avoid over fitting and error goal 0.01. The number of neurons comprising in input layer is varied corresponding with selected extracted features from EEG signals. The output layer contains only 1 output node which indicates the condition of normal walking or transition to FOG. The number of hidden nodes is varied from 2 to 12, corresponding to 11 different networks architecture. The best architecture was selected based on trial and error, starts from small number (2). Each feature was trained and tested 50 times based on the repeated random sub-sampling and the mean result was recorded. The performance of the proposed features was determined using following statistical measures:

$$1) Sensitivity = \frac{TP}{TP + FN} \tag{3.27}$$

$$2) Specivificity = \frac{TN}{FP + TN} \tag{3.28}$$

$$3) Accuracy = \frac{TP + TN}{TP + FN + FP + TN} \tag{3.29}$$

where

- *TP* (true positive) is the number of inputs which correspond to transition to FOG classified as transition to FOG.
- *TN* (true negative) is the number of inputs which correspond to normal walking classified as transition to FOG.
- *FP* (false positive) is the number of inputs which correspond to normal walking classified as normal walking.
- *FN* (false negative) is the number of inputs which correspond to transition to FOG classified as normal walking.

3.7 Experimental Results

In the statistical analysis of PSD and WE for differentiation of 2 EEG conditions, normal walking and transition to FOG, from 16 PD patients with FOG, the discriminative value (p-value <0.05) is found in almost all frequency bands as can be seen in Table 3.3. However, when effect size is taken into account, the alpha frequency band in parietal appears as the most important feature signified with the decreasing of normalized PSD and WE during transition to FOG compared to normal walking (PSD, z = 7.98 p <0.0001, r = 0.40; WE, z = 8.36, p <0.05, r = 0.42). In addition, there are significant increases in beta power in occipital (PSD, z = 7.98, p <0.0001, r = 0.40; WE, z = 9.57, p <0.0001, r = 0.48), parietal (PSD, z = 7.98, p <0.0001, r = 0.40; WE, z = 8.87, p <0.0001, r = 0.45) and central leads (PSD, z = 7.98, p <0.0001, r = 0.40; WE, z = 2.63, p = 0.0087, r = 0.13), along with theta activity in central (PSD, z =-12.80, p <0.0001, r = 0.62; WE, z = -5.27, p <0.0001, r = 0.27).

Table 3.3: Correlation analysis of normalized PSD and normalized WE between normal walking (N), transition to FOG (T), and FOG (F). The result of the statistical analysis shows the separability of EEG signals using power based features.

		Power Spectral Density					Wavelet Energy				
Elect.	Freq.	N	T	F	N vs T	N vs F	N	T	F	N vs T	N vs F
O1	δ	0.087 ± 0.060	0.082 ± 0.074	0.070 ± 0.047	$*$	$*$	0.005 ± 0.009	0.008 ± 0.037	0.009 ± 0.004	$*$	$*$
	θ	0.087 ± 0.057	0.081 ± 0.072	0.072 ± 0.045	$*$	$*$	0.001 ± 0.001	0.000 ± 0.001	0.000 ± 0.001	$*$	
	α	0.064 ± 0.036	0.058 ± 0.046	0.056 ± 0.031	$*$	$*$	0.001 ± 0.002	0.000 ± 0.003	0.000 ± 0.002	$**$	
	β	0.069 ± 0.038	0.043 ± 0.025	0.061 ± 0.039	$***$	$*$	0.001 ± 0.002	0.000 ± 0.003	0.001 ± 0.001	$***$	$*$
	γ	0.042 ± 0.033	0.016 ± 0.016	0.034 ± 0.038	$**$		0.000 ± 0.001	0.001 ± 0.008	0.002 ± 0.017	$***$	$*$
P4	δ	0.144 ± 0.084	0.092 ± 0.065	0.115 ± 0.071	$**$	$*$	0.013 ± 0.054	0.007 ± 0.033	0.006 ± 0.027	$**$	$**$
	θ	0.146 ± 0.077	0.095 ± 0.063	0.121 ± 0.066	$**$	$*$	0.001 ± 0.002	0.000 ± 0.001	0.000 ± 0.001	$*$	$*$
	α	0.110 ± 0.044	0.075 ± 0.045	0.099 ± 0.043	$***$		0.001 ± 0.003	0.001 ± 0.004	0.001 ± 0.001	$***$	$***$
	β	0.143 ± 0.071	0.101 ± 0.074	0.151 ± 0.082	$***$	$*$	0.001 ± 0.004	0.001 ± 0.003	0.001 ± 0.003	$***$	$***$
	γ	0.103 ± 0.083	0.066 ± 0.067	0.108 ± 0.072	$*$	$*$	0.001 ± 0.003	0.001 ± 0.004	0.001 ± 0.005	$**$	$***$
Cz	δ	0.044 ± 0.055	0.147 ± 0.107	0.060 ± 0.068	$***$	$*$	0.001 ± 0.002	0.005 ± 0.012	0.002 ± 0.008	$*$	$*$
	θ	0.044 ± 0.054	0.144 ± 0.105	0.060 ± 0.067	$***$	$*$	0.000 ± 0.001	0.001 ± 0.001	0.001 ± 0.001	$*$	
	α	0.030 ± 0.035	0.097 ± 0.070	0.044 ± 0.047	$***$	$*$	0.000 ± 0.000	0.000 ± 0.001	0.000 ± 0.001		
	β	0.020 ± 0.016	0.047 ± 0.033	0.026 ± 0.025	$***$	$*$	0.000 ± 0.000	0.000 ± 0.000	0.000 ± 0.000	$*$	$*$
	γ	0.002 ± 0.002	0.004 ± 0.006	0.002 ± 0.003			0.000 ± 0.000	0.000 ± 0.001	0.000 ± 0.001		$*$
Fz	δ	0.002 ± 0.002	0.004 ± 0.009	0.004 ± 0.009			0.000 ± 0.000	0.000 ± 0.002	0.000 ± 0.000	$*$	$*$
	θ	0.002 ± 0.002	0.004 ± 0.009	0.004 ± 0.008			0.000 ± 0.000	0.000 ± 0.000	0.000 ± 0.000		
	α	0.001 ± 0.001	0.003 ± 0.005	0.002 ± 0.005	$*$		0.000 ± 0.000	0.000 ± 0.000	0.000 ± 0.000	$*$	
	β	0.000 ± 0.000	0.001 ± 0.002	0.001 ± 0.001	$*$	$*$	0.000 ± 0.000	0.000 ± 0.000	0.000 ± 0.000	$*$	$*$
	γ	0.000 ± 0.000	0.000 ± 0.001	0.000 ± 0.001	$*$	$*$	0.000 ± 0.000	0.000 ± 0.000	0.000 ± 0.000	$*$	$*$

Elect. = Electrodes; Freq. = Subband Frequency

$* = p \leq 0.05$ and $r < 0.3$

$** = p \leq 0.05$ and $0.3 \leq r < 0.4$

$*** = p \leq 0.05$ and $r \geq 0.4$

Common patterns shared by the Fourier transform based features and the wavelet transform based features appear clearly in the shifting centroid frequency, in the beta, alpha and theta frequency band during the transition and freezing episodes. The beta frequency band stands out as the most affected frequency band in transition to freezing with the most significant shift happening in the central lead (CF, $z = 11.04$, $p < 0.05$, $r = 0.56$; CS, $z = -8.33$, $p < 0.05$, $r = 0.42$) (Fig. 3.14) while the frontocentral cortical region is more affected than the parietooccipital region. When compared to the walking period, episodes of freezing are associated with significant shifting in the theta frequency band with the largest shift of centroid frequency in the frontal leads (CF, $z = -4.11$, $p < 0.05$, $r = 0.21$; CS, $z = 4.55$, $p < 0.05$, $r = 0.23$)(Fig. 3.15).

The results of entropy analysis show a decrease of entropy in most of the frequency bands and electrodes during FOG. The most significant change during transition to freezing is detected in the beta frequency band both at central (PSE, $z = 11.01$, $p < 0.05$, $r = 0.56$) and frontal (PSE, $z = 8.23$, $p < 0.05$, $r = 0.42$) (Fig.3.16). This trend continues in the onset of freezing with lower effect size (Central: PSE, $z = 4.35$, $p < 0.05$, $r = 0.22$; Frontal: PSE, $z = -5.44$, $p < 0.05$, $r = 0.28$).

The entropy analysis on WE which measures the temporal regularity of energy in each frequency band also reveals the loss of complexity during transition in most of the frequency bands and electrodes with the beta band appearing as the most affected frequency band (Fig.3.17). There is a significant decreased regularity of gamma activity in the central (WEE, $z = 11.04$, $p < 0.05$, $r = 0.56$) during the transition, along with a decrease in the beta band (WEE, $z = 11.04$, $p < 0.05$, $r = 0.56$). While entropy is then increased at the onset of the freezing period, it is still significantly lower compared to walking, unlike the diminishing of all irregularity at the occipital and parietal leads.

The performance of the classifier using an ANN depends on different parameters: the number of neurons in the hidden layer, the learning rate and the momentum. These have different levels of importance, and must be decided upon in the design of the structure (Haykin, 2009). The number of hidden neurons determines the effectiveness and efficiency of the neural networks. Generalization of the system is reduced in a system with too many hidden neurons as it becomes over specified. Moreover, the process will be

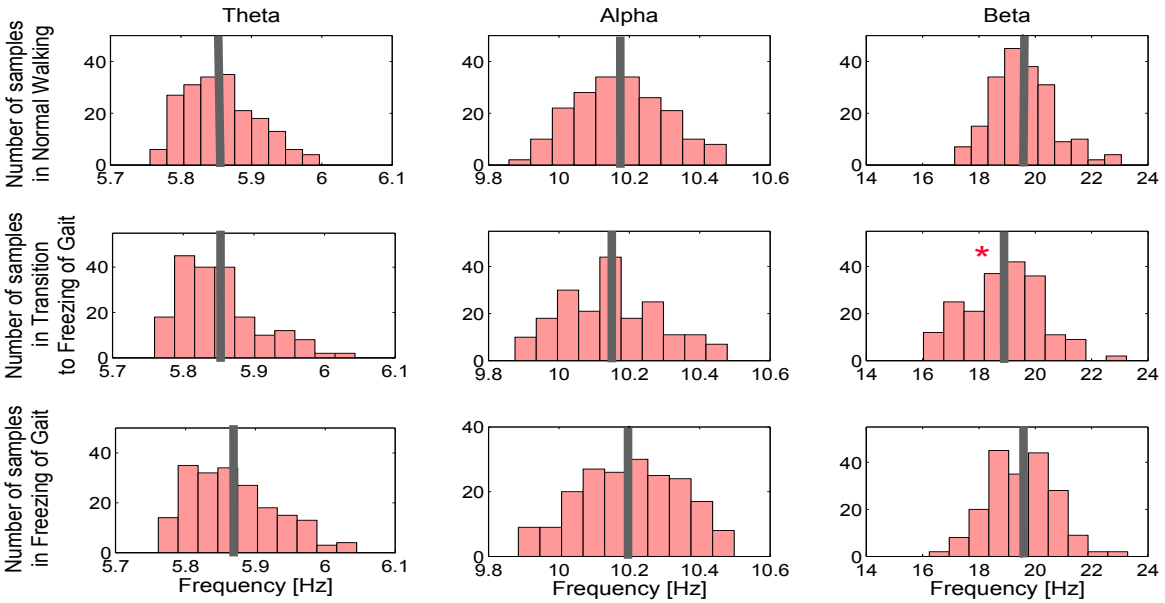

Figure 3.14: Shift of CF in electrode Cz in 3 mid-range frequencies band. Decreasing of centroid frequency in beta frequency band of normal walking signifies transition to freezing episode.

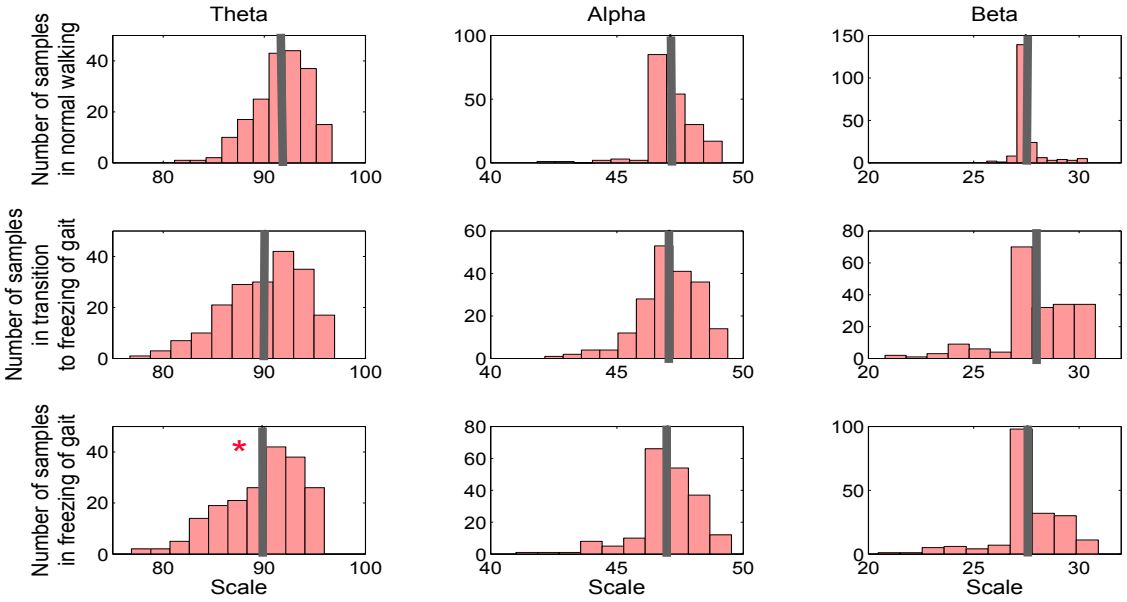

Figure 3.15: Shift of CS in electrode Fz in 3 mid-range frequency bands. Decreasing of centroid frequency in theta frequency band of normal walking signifies freezing episodes.

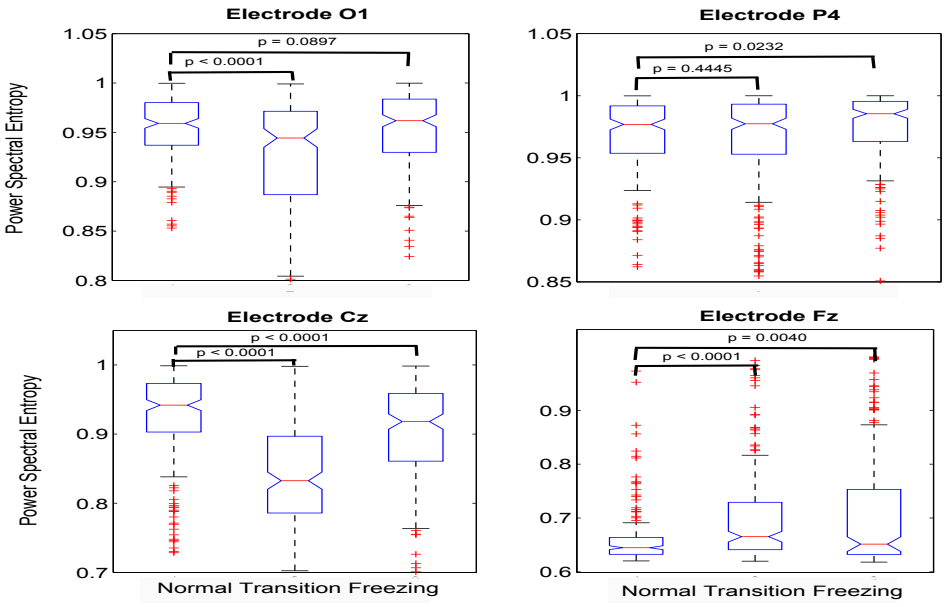

Figure 3.16: Boxplot of PSE of 3 different conditions and 4 EEG electrodes in beta frequency band.

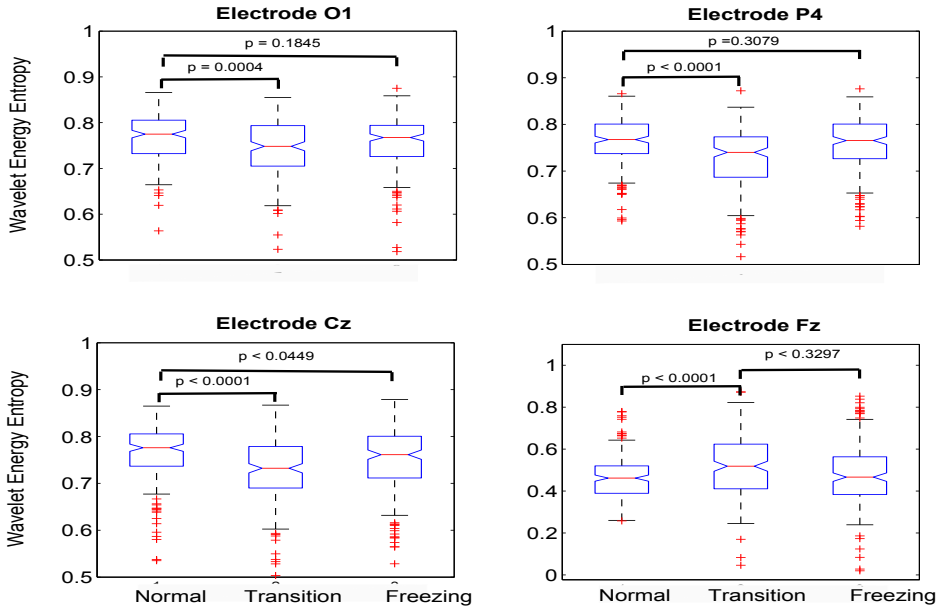

Figure 3.17: Boxplot of WEE of 3 different conditions and 4 EEG electrodes in beta frequency band.

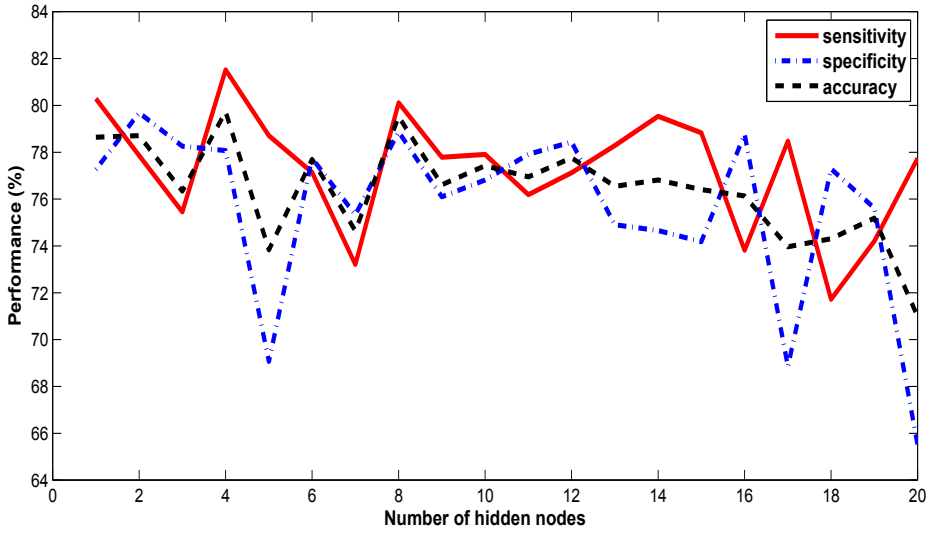

Figure 3.18: Testing result of using CF at centroid zero as input for the MLP-NN with different number of hidden nodes.

more time consuming. On the other hand, the system will not be properly fitting with the input data in a system with too few hidden neurons, and therefore will be less robust. The optimal number of hidden nodes is determined empirically through trial and error.

Figure 3.18 presents the average testing results of the classification system analysis over 50 runs using CF at centroid zero as an input parameter. It shows that accuracy improved, as the number of hidden nodes increases from 1 to 4, when it reaches the best accuracy of 79.73%. The accuracy is oscillated in the classifier system with 5 to 12 hidden nodes. It steadily decreases as the number of hidden nodes increases from 12 to 20. Four hidden nodes are chosen as it gives the best accuracy and highest sensitivity. The same process is used to determine the number of hidden nodes in each ANN architecture with different input features for classification. The optimum number of hidden nodes was found to be between 2 and 12.

The strength of the alteration of EEG signals parameters differ from one location on the scalp to another. This study evaluates the best indicator of freezing between 4 locations of electrodes by comparing the performance of the classification system using data from 1 channel only. The combination of the extracted features from the related location data was observed to determine the best combination of location in detecting freezing.

Table 3.4 shows that central zero (Cz) provides the best indicator of freezing in all extracted Fourier transform based parameters, where the spectral centroid frequency (SCF) and the power spectral entropy (PSE), obtained comparable result, both at around 79% accuracy of testing of in-group and out-group, respectively. Not only do these locations provide a better indication of freezing than other locations, the extracted data taken only from these locations also lead to better performance of the classifier.

The strength of Cz in providing an indication of freezing in the frequency domain is equally clear from the centroid scale (CS), with in-group results at 81.12%, 77.41% and 79.34% of sensitivity, specificity, and accuracy, respectively; and out-group results at 77.40%, 64.58% and 75.99% sensitivity, specificity, and accuracy, respectively (Table 3.5). This result is better than the classifier using CS from other channels, or with any combination of 4 channels. However, when using WE, combined data from the 4 channels provided better results than similar features extracted from single channel only with sensitivity, specificity, and accuracy in in-group at 86.00%, 74.43%, and 80.20%, respectively. The performance was decreased when testing in out-group, with results at 73.19%, 80.16%, and 76.67% of sensitivity, specificity, and accuracy, respectively.

The result of the experiment shows that the Fourier analysis provided better result compared to wavelet analysis in the extraction of the features related to centroid frequency and entropy. However, the changes in the WE were found to be the best indicators of transition to FOG.

Table 3.4: Classification results of proposed Fourier Transform based features using MLP-NN in detecting transition 5 s before freezing from normal walking.

Elec.	Feat	In-group (11 patients)									Out-group (5 patients)		
		Training			Validation			Testing			Testing		
		Se %	Sp%	Ac %	Se %	Sp %	Ac %	Se %	Sp %	Ac %	Se %	Sp %	Ac %
1	PSD	74.53	76.47	75.46	73.14	75.37	74.31	72.56	73.79	73.12	71.51	55.38	63.40
	CF	56.11	73.12	59.65	55.46	72.09	59.59	55.67	71.91	58.43	52.37	54.58	58.48
	PSE	49.42	71.22	60.48	47.41	70.97	60.88	46.04	69.57	57.53	49.09	56.00	57.55
2	PSD	65.27	77.25	70.14	65.70	74.18	70.00	60.75	73.74	67.59	66.19	76.00	71.09
	CF	71.19	49.18	58.20	71.29	48.09	59.05	71.21	47.85	55.90	71.14	42.62	55.45
	PSE	74.64	43.25	59.41	74.38	42.33	58.11	73.09	41.89	56.33	75.42	43.14	59.28
3	PSD	66.74	84.66	77.35	67.03	84.41	77.17	62.62	83.46	77.38	63.65	80.72	75.19*
	CF	78.68	80.23	80.37	78.72	76.51	79.32	76.69	74.05	79.54	75.21	80.65	79.91*
	PSE	82.51	77.33	80.91	80.72	77.26	79.12	76.99	77.43	79.66	81.40	74.91	78.65*
4	PSD	59.01	71.21	59.86	57.22	70.15	58.11	55.71	70.87	58.19	51.44	67.02	54.73
	CF	50.27	78.17	64.18	49.05	77.27	63.39	48.89	76.53	62.74	48.89	57.88	55.29
	PSE	51.69	79.57	65.82	50.54	78.89	64.83	47.91	78.16	62.99	56.42	56.33	56.37
2,3	PSD	72.01	81.69	76.82	71.25	79.06	75.53	70.01	76.31	73.16	72.47	73.53	73.01
3,4	CF	83.36	81.21	81.15	79.56	78.77	80.71	77.71	77.20	77.38	74.28	87.26	75.77
1,3	PSE	79.56	82.98	81.30	77.66	81.74	79.73	76.98	79.72	78.30	84.86	74.86	79.86
1,2,3	PSD	80.43	81.12	80.71	77.27	80.21	79.25	77.40	77.66	77.49	78.53	71.09	74.81
1,3,4	CF	80.38	81.66	81.01	79.15	80.63	80.03	76.40	77.46	76.88	74.72	80.58	77.65
1,3,4	PSE	78.67	84.58	81.55	78.84	79.17	79.22	78.20	79.07	76.62	83.60	72.42	78.01
1,2,3,4	PSD	84.81	84.89	84.83	80.04	82.84	81.59	79.69	77.98	78.68	75.86	65.37	70.62
1,2,3,4	CF	85.12	82.29	83.67	83.58	81.27	82.44	81.00	78.96	80.00	68.51	83.65	76.08
1,2,3,4	PSE	83.46	82.54	83.00	82.72	80.23	82.58	79.45	76.94	78.10	70.63	77.86	74.24

Elect: Electrodes; Feat: Features; Se: Sensitivity; Sp: Specificity; Ac: Accuracy
Electrode 1: O1, Electrode 2: P4, Electrode 3: Cz, Electrode 4: Fz
PSD: Power Spectral Density; CF: Centroid Frequency ; PSE: Power Spectral Entropy

Table 3.5: Classification results of proposed Wavelet Transform based features using MLP-NN in detecting transition 5 s before freezing from normal walking.

Elec.	Feat	In-group (11 patients) Training			Validation			Testing			Out-group (5 patients) Testing		
		Se %	Sp%	Ac %	Se %	Sp %	Ac	Se %	Sp %	Ac %	Se %	Sp %	Ac %
1	WE	82.49	68.31	75.26	82.01	68.20	76.05	81.23	67.76	74.21	76.44	67.35	56.90
	CS	60.45	67.37	63.95	59.99	67.30	63.55	57.25	67.26	62.03	63.30	61.93	62.62
	WEE	47.44	66.94	57.23	47.55	66.56	56.87	47.91	66.40	56.34	68.51	56.05	52.28
2	WE	80.56	55.05	67.40	80.45	55.20	67.32	80.08	55.39	67.76	64.02	57.40	65.71
	CS	52.10	57.43	54.86	51.02	55.65	52.33	50.90	52.63	50.21	45.95	70.95	58.45
	WEE	63.93	60.58	62.18	62.50	59.97	61.45	61.09	58.51	59.62	65.05	57.53	61.29
3	WE	80.49	71.09	75.71	80.05	70.67	75.44	78.96	69.80	74.24	77.88	64.51	66.20
	CS	83.81	80.92	82.37	82.29	79.82	80.78	81.12	77.41	79.34	77.40	64.58	75.99 *
	WEE	69.27	62.02	65.54	65.98	61.45	64.33	64.92	59.20	61.48	71.44	66.73	64.19
4	WE	73.44	59.19	66.24	73.22	59.04	65.74	73.10	59.75	65.00	62.91	66.40	54.65
	CS	67.78	80.30	74.13	67.12	78.49	73.27	63.42	77.08	70.34	69.33	61.51	60.42
	WEE	70.39	60.79	65.58	69.35	60.03	64.78	67.84	59.40	63.43	64.71	62.60	64.71
2,3	WE	85.58	73.73	79.54	82.88	72.41	78.42	82.56	69.07	75.79	70.19	76.12	73.15
3,4	CS	85.93	83.64	84.76	80.31	81.25	80.90	79.36	79.91	79.76	71.86	72.86	72.36
1,3	WEE	74.01	68.65	71.18	69.18	67.74	70.79	70.13	66.76	68.76	69.19	71.67	70.43
1,2,3	WE	83.34	78.49	80.94	83.23	73.75	78.31	82.52	71.71	77.93	71.34	77.21	74.29
1,3,4	CS	85.50	79.84	82.61	81.14	76.04	78.84	80.13	75.04	77.38	71.47	74.84	73.15
1,3,4	WEE	73.73	79.62	76.56	70.38	75.67	72.09	67.63	71.09	69.38	64.91	75.21	70.06
1,2,3,4	WE	89.28	78.21	83.75	86.58	74.80	80.11	86.00	74.43	80.20	73.19	80.16	76.67 *
1,2,3,4	CS	85.82	80.82	83.29	83.55	74.11	79.98	79.35	73.81	76.47	68.77	76.98	72.87
1,2,3,4	WEE	77.51	73.19	75.29	74.59	68.88	71.47	75.09	67.00	69.32	71.53	67.05	71.07 *

Elect: Electrodes; Feat: Features; Se: Sensitivity; Sp: Specificity; Ac: Accuracy
Electrode 1: O1, Electrode 2: P4, Electrode 3: Cz, Electrode 4: Fz
WE: Wavelet Energy P; CS: Centroid Scale ; WEE: Wavelet Energy Entropy

3.8 Discussion and Conclusion

This study compares several Fourier analysis based features with their wavelet analysis counterpart, and explores their roles in neural dynamics related to FOG in PD. The observation on the power spectral density (Table 3.3) reveals that beta power changes significantly in all locations of interest, when in transition to FOG. Previous research found that worse motor severity in PD is associated with increase in beta activity, which implies temporal impairment takes place during the freezing episode in the motor regions of the cortex (Silberstein *et al.*, 2005). This is in line with our finding of increasing beta power in all locations of interest except at occipital.

The finding that the theta oscillations in the human cortex increases during the transition to freezing, and remain high during freezing in the central region, is consistent with previous studies which suggest that there is a relationship between FOG, and specific deficits in cognition and impairment in the motor planning mechanism (Suchan *et al.*, 2003)-(Knobl *et al.*, 2011).

The entropy analysis of the frequency domain based on the changing of the power spectral shows increased regularity on nearly all frequency bands and most electrodes during transition and that this continues in the freezing period. Therefore it can be inferred that brain activity is "less complex" when patients undergo change from their normal walking state to FOG.

The alteration in information processing during this stage is possibly due to an inactivation of previously active neural networks, which resulted from the impairment of the more "executive" functions of the brain. This finding is in line with the general "loss of complexity" behavior in other diseases and states of the brain including epilepsy (Rosso, 2007), Alzheimer's (Abásolo *et al.*, 2008), and autism (Catarino *et al.*, 2011).

In most extracted features, Cz provides the most statistically significant indicator of FOG. This finding is supported by the result of the study on the classification system using single electrode and combination of electrodes. In FFT-based features, the classification performance in the testing set both in-group and out-group shows that information extracted

from this site are generally stronger than other sites, even when combined.

The comparison between PSE based on the signals dynamic in the frequency domain and WEE based on the signals dynamic in the time domain and their related statistics features, revealed that information of EEG signals are coded in the frequency domain rather than in the time domain. Along with the results of classification using CF and CS, it shows that Fourier analysis provides better features in frequency domain compared to wavelet analysis. This precision on frequency, following the Heisenberg Uncertainty Principle, is at the cost of zero information about the temporal dynamic of the signal.

Optimization of classifier was done mainly by setting the number of the hidden nodes which provided a better result. Interestingly, optimum result was achieved with less hidden nodes, between 4 to 12, even when the number of input was increased significantly. Accuracy in classification was taken as the main indicator of the strength of the feature in providing distinctive information related to the condition. In the detection of FOG, the ability to correctly identify the transition to FOG episode, sensitivity, also significant in giving indication of FOG and its treatment to unfreeze the episode.

The best accuracy of the FOG detection was achieved using CF as input of the classifier extracted from channel Cz. The neural networks based classifier with this input obtains 79.54% and 79.91% accuracy when tested in in-group and out-group testing data set, respectively. The accuracy of the system when using WE extracted from all four electrodes locations as inputs is comparably the same at 80.20% and 76.67%, when tested using in-group and out-group testing data set, respectively. A FOG detection system using WE from all four channels also provides the highest sensitivity when tested using in-group testing data set at 86.00%. The best sensitivity when tested using out-group testing data set is 84.86% , obtained using PSE extracted from channel O1 and Cz as inputs for the system.

This study demonstrated the potential use of the EEG features extracted using both the Fourier and wavelet analysis to give increased insights into the pathophysiology of FOG in PD. The results show the advantages of using wavelet analysis in extracting EEG basic feature, energy, compared to Fourier analysis, providing a better indicator in classification

system. This finding may be due to its representation of signals in 3 dimensions (amplitude, frequency and time) compared to Fourier (amplitude and frequency), which is more convenient for non-stationary EEG signals.

Chapter 4

Detection of FOG Using Brain Signal Spectral Coherence

"One cannot think of their taking place in any other way than through an infinitely complex and involved interaction and cooperation of numerous elementary activities [...] We are dealing with a physiological process extending widely over the whole cortical surface and not a localized function within a specific region."
-Korbinian Brodmann, 1909

Early detection of FOG episodes was developed using features based on the Fourier transform (including power spectral density, spectral centroid frequency and power spectral entropy). The study of the strength of each feature from each channel showed better information did not result from using an increased number of features or number of channels. Using only channel Cz gave the best classification of motor execution: 76.69% sensitivity, 74.05% specificity, and 79.54% accuracy applying spectral centroid frequency to the in-group patients and 75.21%, 80.65%, and 79.91% when applied to the out-group patients. Compared to their paired measurement extracted using wavelet transform, the combination of wavelet energies from 4 channels provided the best indicator of freezing with the sensitivity, specificity and accuracy were up to 86.00% accuracy, 74.43% sensitivity and 80.20% specificity in the in-group patients and 73.19%, 80.16% and 76.67% in the out-group patients.

In this chapter, we explore the strength of 3 functional integration based features when used as an input for classifier to detect FOG: cross power spectral, spectral coherence and phase synchronization.

4.1 Introduction

4.1.1 Limitations of Segregated Spectral Analysis in EEG-Based FOG Detection

Chapter 3 examined brain functions exclusively as an intrinsic feature of isolated network nodes. The EEG features were extracted and computed separately on each EEG channel, identifying a particular brain region with a specific function following German physician Franz Joseph Gall's ideas of phrenology in 1796 (Friston, 2011). While functional localization brain mapping such as Brodmann Areas (1909) (Fig. 4.1) made great contribution to neuroscientific and clinical brain research, it was realized early on that localization which discounted interaction integration among different brain areas was insufficient to explain the cortical organization (Friston, 2011). This popular segregation method does not provide information of the interrelation between signals reflecting neural activity at locations of interest, because it is based on measuring each single channel and assumes the brain as a "set of segregated tissues with static specialized functions" (Sameshima & Baccalá, 1999).

4.1.2 Advantages of Functional Integration Features

More recently, a new mathematical approach based on a more holistic paradigm of analysis of connectivity in neuronal networks, gained significant prominence in the neuroscience community. This emerging network science also impacted real-world observation in social, technological, biological and other domains. In the last 20 years, driven by the emergence of neuroimaging as the predominant technique in systems neuroscience systems, the emphasis of study by the neuroscience community shifted from functional localization to functional integration in segregated brain areas (Friston, 2011). Functional segregation analysis has been used to study neurological conditions and disorders,

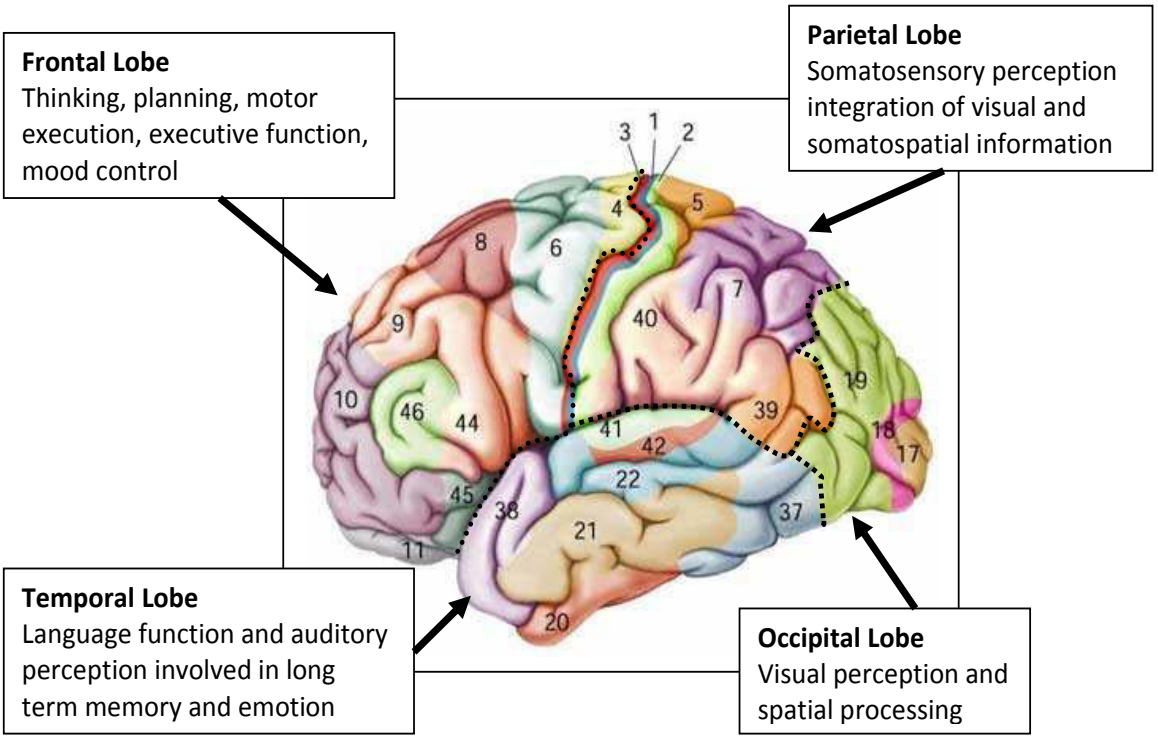

Figure 4.1: Brodman area functional atlas.

such as autism (Belmonte *et al.*, 2004), Alzheimer's disease (Supekar *et al.*, 2008), and schizophrenia (Skudlarski *et al.*, 2010). A search of the U.S National Library of Medicine shows that annually, from 2010, the number of publications on "connectivity" surpassed publications on "activation" (Fig. 4.2).

Observation of the interaction between EEG channels based on the concept of synchronization beyond the simple mapping of the activity of each measured cortical location is important for several reasons (Quian Quiroga, 2009). First, in the assessment of synchronization, the similarity between 2 areas, time lag/delay and phase, reveals the level of functional connectivity between the locations of interest. The analysis provides fundamental insights into the integrative functions of the brain, and its complex and irreducible dynamic network patterns (Sporns, 2011). For example, empirical evidence shows that repeated synchronous oscillation strengthened the functional connections between neurons in the study of neuronal plasticity in the cortex of adult monkeys (Ahissar *et al.*, 1992).

Second, synchronization change can be used as a bio-marker for pathology or different brain states activities, which are less (or non) observable with amplitude comparisons

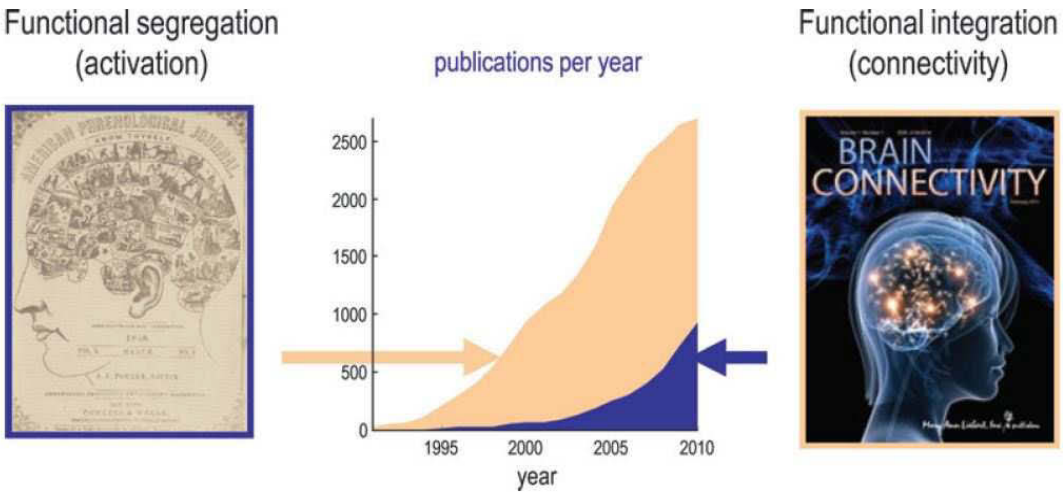

Figure 4.2: Publications search rates recorded by PubMed.gov. U.S. National Library of Medicine shows an increase in the number of studies looking for information on functional segregation (activation) and functional integration (connectivity) (Friston, 2011).

(Blinowska & Zygierewicz, 2011). Using EEG measurement in intelligence prediction, Thatcher *et al.* (2005) found the EEG network properties (coherence and phase delay) to have (a) a stronger correlation to intelligence quotient (IQ) than power measures of EEG, and (b) a decreased coherence positively correlated with IQ as spatial differentiation and complexity of the brain increase. The Coben *et al.* (2008) study on an autistic spectrum disorder found coherence to decrease across inter-electrode, and across the frontal, temporal, and posterior regions. This pattern of under-connectivity in autistic is more pronounced than the group differences in power.

Third, synchronization measures may reveal the operational principles of neurons and neuronal system in the transmission information between different brain locations. Tas *et al.* (2015) found lower interhemispheric alpha coherence in unipolar and bipolar depression. This suggests that the cognitive processes create an excessive increase of information transfer by primary signals, leading to bipolar (rather than unipolar) depression.

Fourth, synchronization measures provide meaningful information and useful characterization of subject conditions as inputs for detection of various physiological conditions. Using cross correlation and phase-locking synchrony to extract the spatio-temporal pattern of EEG synchronization in 15 epilepsy patients, Mirowski *et al.* (2009) predicted

seizure with 71% sensitivity and without false alarms. Lee & Hsieh (2014) classified different emotional states of 40 young participants. They used 3 connectivity indicators, correlation, coherence and phase synchronization, as inputs for Quadratic Discriminant Analysis, to estimate the dynamic coupling between EEG channels associated with emotion. The classification accuracy was 0.61 % for correlation, 0.62 % for coherence, and 0.82 % for phase synchronization. These results are superior to classification accuracy at 0.53 % using features extracted, based on EEG power.

This chapter considers the advantages of the functional integration features, and the EEG functional connectivity of PD patients, for detecting FOG. The temporal dynamic couplings were estimated using the 3 connectivity indicators correlation, coherence, and phase locking, and show statistical dependencies of different measurements among remote neurophysiological events.

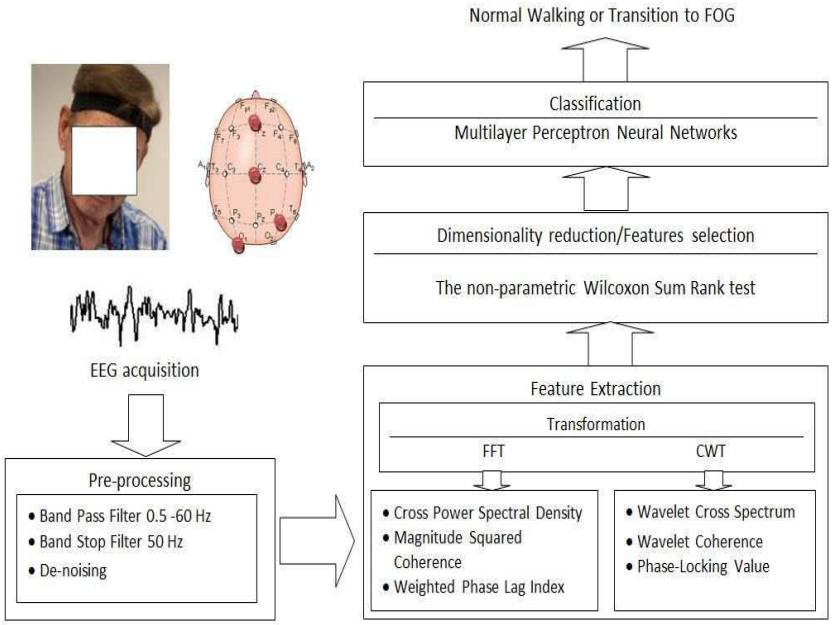

Figure 4.3: System overview of FOG detection using functional integration features of EEG data

4.2 System Overview

Fig. 4.3 presents an overview of the system, using functional integration features. A 4 channel wireless EEG system was used to collect brain signal data from 16 PD patients with FOG. Low frequency noise, high frequency noise, and 50 Hz line frequency noise were eliminated using a Band Pass Filter (0.5-60 Hz) and a Band Stop Filter (50 Hz). The classification system labelled the data set according to 2 conditions: normal walking, or the 5 s transition before FOG. The pathophysiology of the FOG condition was analysed; functional integration measures were calculated between pairs of electrodes and their strength investigated in differentiating normal walking and the 5 s transition, applying the non parametric Wilcoxon Sum Rank test. Selected features components were used as input for the MLP-NN classifier, for individual features, and also in combination with other features (including the single channel based measures discussed in chapter 3).

4.3 Synchronization of the Cortical Activity Measurements

There is a growing interest in studying nervous system, particularly the (dynamic) organization of communication within the nervous system, which may be related to FOG. Their focus includes its diverse functions such as motor activity (Press *et al.*, 2011; Weiss *et al.*, 2015), attention (Loo & Makeig, 2012; Gruzelier *et al.*, 2014), memory (Morison *et al.*, 2012) and emotion (Frølich *et al.*, 2015). The signals from multiple channels were joined to detect the alteration of the connectivity in the brain, related to different brain conditions.

4.3.1 Magnitude-Squared Coherence

Cross-correlation is a classical interdependence measurement between 2 simultaneously measured EEG signals (Pereda *et al.*, 2005). The linear correlation between 2 signals variables x and y is measured as a function of their time delay (τ) which may reflect a causal relationship between those 2 signals. It has values between -1 (complete linear inverse correlation) and +1 (complete linear direct correlation)and is defined as (Van Drongelen,

2006)

$$R_{xy}(\tau) = E\{x(t)y(t+\tau)\} \tag{4.1}$$

where $x(t)$ and $y(t+\tau)$ are 2 joint signals, τ is the number of time units that the signal $y(t+\tau)$ is lagged in regards to $x(t)$, and $E\{.\}$ is the expectation operator.

The cross-correlation integral can be denoted as

$$s_{xy}(t) = \int_{-\infty}^{\infty} x(\tau)y(t+\tau)d\tau. \tag{4.2}$$

The Fourier transform of $s(t)$, the cross correlation in the frequency domain, is given by

$$S_{xy}(\omega) = \int_{-\infty}^{\infty} s_{xy}(t)e^{-j\omega t}dt = \int_{-\infty}^{\infty}[\int_{-\infty}^{\infty} x(\tau)y(t+\tau)d\tau]e^{-j\omega t}dt. \tag{4.3}$$

By changing the order of integration, we get

$$S_{xy}(\omega) = \int_{-\infty}^{\infty} x(\tau)\Big[\int_{-\infty}^{\infty} y(t+\tau)e^{-j\omega t}dt\Big]d\tau. \tag{4.4}$$

Substitution of the term in the brackets into the Fourier transform of function Y gives

$$S_{xy}(\omega) = \int_{-\infty}^{\infty} x(\tau)Y(\omega)e^{-j\omega t}d\tau = Y(\omega)\int_{-\infty}^{\infty} x(\tau)e^{-j\omega t}d\tau. \tag{4.5}$$

With complex conjugates $\int_{-\infty}^{\infty} x(\tau)e^{j\omega t}d\tau = X^*(\omega)$, the final equation of cross-correlation S in the frequency domain, cross power spectral density (CPSD), can be seen as

$$S_{xy}(\omega) = Y(\omega)X^*(\omega). \tag{4.6}$$

The ratio of CPSD to the product of the related auto power spectral densities (APSD), a generalization of correlation in the frequency domain, shows the coherency, which is a measurement of amplitude and phase coupling, and is defined as

$$C_{xy}(\omega) = \frac{|S_{xy}(\omega)|^2}{S_{xx}(\omega)S_{yy}(\omega)} \tag{4.7}$$

with

$$S_{xx}(\omega) = X(\omega)X^*(\omega) \tag{4.8}$$

$$S_{yy}(\omega) = Y(\omega)Y^*(\omega). \tag{4.9}$$

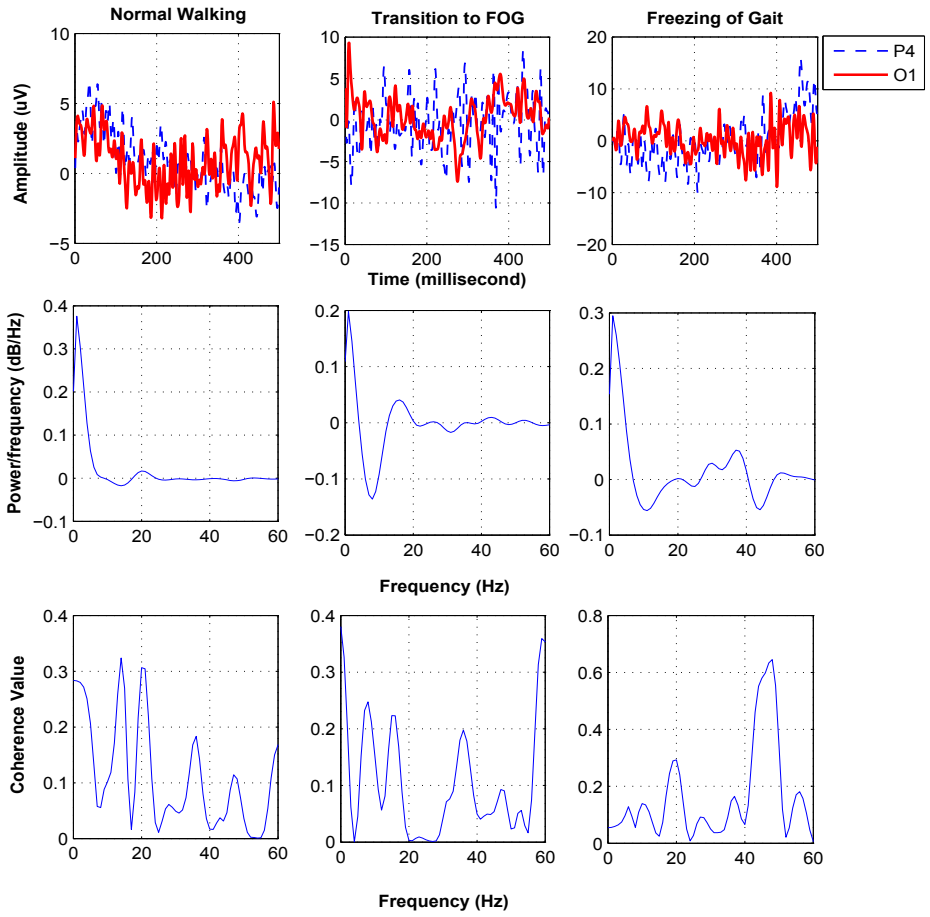

Figure 4.4: Subject 1 - samples extracted from electrodes P4 and O1 of cross power spectral density and magnitude-squared coherence under 3 conditions.

In practice, both the CPSD and the coherency value are estimated by approximation in which the finite time series x and y are divided into N overlapping segments in the same way as the Welch method for power spectra calculation, x_j and y_j, where $j = 1, ..., N$. The CPSD are estimated by averaging the coefficients C_j over the N segments:

$$S_{xy}(\omega) \approx \tilde{S}_{XY}(\omega) = \frac{1}{N}\sum_{j=1}^{N} C_j(\omega) = \frac{1}{N}\sum_{j=1}^{N} X_j(\omega).Y_j^*(\omega). \tag{4.10}$$

The APSD is calculated with the same approximation:

$$\tilde{S}_{xx}(\omega) = \frac{1}{N}\sum_{j=1}^{N} X_j(\omega).X_j^*(\omega). \tag{4.11}$$

$$\tilde{S}_{yy}(\omega) = \frac{1}{N}\sum_{j=1}^{N} Y_j(\omega).Y_j'^{*}(\omega). \tag{4.12}$$

The magnitude squared coherence (MSC)is defined as the modulus of the coherency. It is determined by averaging both CPSD and APSD over n epochs, indicated by $\langle ... \rangle_n$

$$C_{xy}(\omega) = \frac{|\langle S_{xy}(\omega)\rangle_n|^2}{\langle S_{xx}(\omega)\rangle_n \langle S_{yy}(\omega)\rangle_n} \tag{4.13}$$

Coherency function is a function of frequency. It can be used to analyse which frequency of 2 sets of time series data is coherent. While cross correlation emphasizes the similarity of waveform between 2 signals, and gives information on their time coupling, coherency measures the stability of that similarity with respect to power asymmetry and phase relationship (Guevara & Corsi-Cabrera, 1996).

Correlation is sensitive to polarity, and has values from -1 to +1. Squaring the signal in the calculation of coherence omits the polarity information, and produces values from 0 (no relationship) to 1 (maximal synchronous change). Coherence, also called the magnitude squared coherence (MSC), is defined as the modulus of the coherency. This measure is analogous to the squared Pearson correlation, r^2, describing the proportion of variance of channel X at frequency f accounted for by a linear transformation of the complex spectral coefficient derived from channel Y (Nunez & Srinivasan, 2006).

In the present study, the cross spectrum coefficient is estimated in the same way of the Welch method for power spectra calculation using the Hamming window as a weighting function, with the duration of the stationary fragment assumed to be 220ms with 50% overlap.

4.3.2 Wavelet Coherence

Methods based on the simple Fourier analysis are inadequate in estimating the non-stationary signals because they cannot provide the temporal structure information of signals (Lachaux *et al.*, 2002). Therefore, wavelet analysis is used as an alternative in estimating the time varying coherence among non-stationary signals, including neural signals. A real wavelet function is used to detect peaks and discontinuities, while a complex wavelet function is more suitable for extracting information about phase difference. Moreover, a complex wavelet function works better in capturing oscillatory behaviour. This study uses a complex Morlet wavelet, proven to provide the best time frequency resolution in the EEG analysis compared to other wavelet functions (Sitnikova *et al.*, 2009), and is defined by Teolis (1998) as:

$$\Psi(t) = \frac{1}{\sqrt{\pi f_b}} e^{2i\pi f_c t} e^{\frac{t^2}{f_b}} \tag{4.14}$$

where $\Psi(x)$ can be seen as a sinusoidal wave, centred at frequency f_c which is windowed by the Gaussian envelope with the variance $\sigma = \sqrt{\frac{f_b}{2}}$ at time t. Morlet wavelet has 2 parameters. The first parameter, f_b, represents a bandwidth parameter. The second parameter, f_0, is a central frequency. It determines the number of oscillations of the Morlet wavelet and requires a minimum value of $2\pi f_0$=6 to provide a good balance between time and frequency localization (Farge, 1992). This frequency can be interpreted as a localized Fourier frequency, $f = f_0/a$ with a as the scale parameters of continuous wavelet transform in (3.8) (Priestley, 1996).

Corresponding to a similar concept in the Fourier analysis, the autocorrelation function of the wavelet transformation produces a wavelet power spectrum (WPS) which describes the power of the signals $x(t)$ at a certain time t_i on a scale s:

$$WPS_i(s) = W_i(s)W_i(s)^* \tag{4.15}$$

where $W_i(s)^*$ is the complex conjugate of wavelet transform W_i.

The extension of the univariate WPS to a comparison of 2 time series x and y at time shift index i and scale s with their wavelet transform coefficients W_{x_i} and W_{y_i}, the wavelet cross

correlation spectrum $WCS_i(s)$, is defined as

$$WCS_{xy_i}(s) = S(W_{x_i}(s)W_{y_i}^{*T}(s)) \tag{4.16}$$

where S is a smoothing operator in both time and scale. These filters are designed according to the wavelet used. For the Morlet wavelet a suitable smoothing operators is (Grinsted *et al.*, 2004)

$$S_{time}(W)|_s = \left(W_i(s) * c_1^{\frac{-t^2}{2s^2}}\right) \tag{4.17}$$

and

$$S_{scale}(W)|_s = (W_i(s) * c_2\Pi(0.6s))|_i, \tag{4.18}$$

where c_1 and c_2 are normalization constants and Π is the rectangle function.

The interaction between signals x and y at the given frequency is measured by the product of 2 spectra expressed by wavelet coefficients of the time scale representation of EEG sub-bands. Since the Morlet function includes both a real and an imaginary part, the WCS is complex valued. The average amplitude of this local WCS over time samples t ($|\overline{WCS^i_{xy}(t,s)}\ |$) shows the global WCS at related EEG sub-bands (see Fig.4.5). Total wavelet cross spectrum of EEG sub-bands is obtained by calculating the sum of the global wavelet spectrum over scale (frequency) sub-bands and is taken as features.

Analogous to the Fourier-based coherence, wavelet coherence (WCO) is defined as the amplitude of the WCS normalized to the 2 single WPS:

$$WCO_{xy_i}(s) = \frac{S(WCS_{xy_i}(s))}{\sqrt{S(|WPS_{xx_i}(s)|^2)}\sqrt{S\left|WPS_{yy_i}(s)\right|^2}} \tag{4.19}$$

where S is a smoothing operator. WCO_{xy_i} has values between 0 (no coherence) and 1 (maximum coherence).

4.3.3 Weighted Phase Lag Index

Analysis of the stability of phase shift over the specified time interval also provides measurement of phase difference between 2 signals. If phase difference between 2 signals, $\Delta\phi$, is constant, the signals are in phase synchrony. Rosenblum *et al.* (1996) introduced

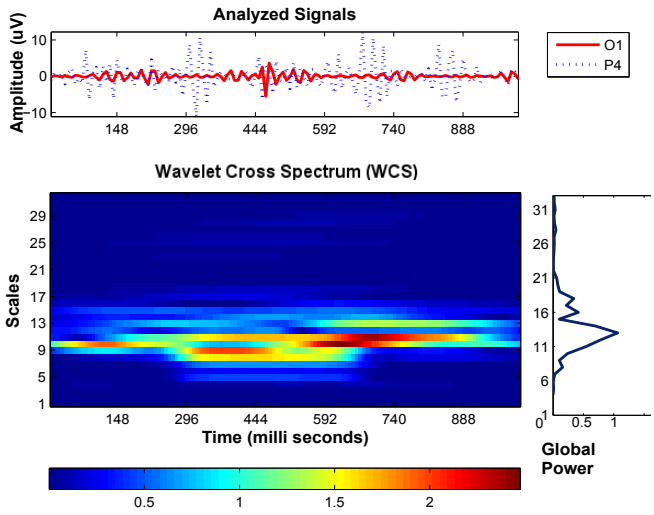

Figure 4.5: Wavelet cross spectrum for transition of freezing at gamma sub-band. The upper panels shows EEG signals from electrode pairs O1 and P4. The right panel presents the global wavelet spectrum obtained by averaging over time samples.

the weaker version of phase synchrony in noisy system, phase entrainment, which is defined as:

$$|\Delta\phi_{n,m}| = |n\phi_1 - m\phi_2| < const \tag{4.20}$$

where $\Delta\phi_{n,m}$ is the phase difference, ϕ_1 and ϕ_2 are the phases of 2 oscillators, and n and m are some integers.

Detecting this phase-locking when the phase difference is constant using correlation and coherence can pose a problem since they are affected by the amplitude component which can be noisy or uncorrelated. Furthermore, it is also susceptible to a transmission of electric field from a source activity through biological tissue towards the EEG sensors.

Nolte *et al.* (2004) proposed to use the imaginary component of the coherence (ImC), defined as $\Im\{C\}$, as an index of phase synchronization to solve these problems. The rationale is that the linear mixing of uncorrelated sources (volume conduction) produces the real component of the cross-spectrum $E\{\Re\{X\}\} \neq 0$, corresponding to a spurious coherence. However, it does not have impact on the imaginary component of the cross-spectrum, $E\{\Im\{X\}\}$. The imaginary component of the coherence $\Im\{C\}$ is zero follows from $E\{\Im\{X\}\} = 0$ in the case where all sources are uncorrelated, so that it reflects true interaction of the sources of signals of interests.

Stam *et al.* (2007) identified that the magnitude of phase delay and the amplitude of signals strongly influence on ImC. Thus, to find the consistent, nonzero phase lag from a single source that is not caused by volume conduction, Stam *et al.* (2007) discarded the phase differences that center around 0 mod π by applying an asymmetry index for the distribution of phase difference of 2 times series, $\Delta\phi$. The phase delay captured using this estimation showed that axonal transmission properties may have accounted for communication between brain regions.

Stam *et al.* (2007) proposed the Phase Lag Index (PLI), defined as

$$PLI \equiv |\langle sgn[\Delta\phi(t_k)]\rangle| = |E\{sgn(\Im\{X\})\}| \tag{4.21}$$

where $\Im\{X\}$ is the imaginary component of the cross spectrum.

Vinck *et al.* (2011) proposed the Weighted Phase Lag Index (WPLI) as a further improvement of PLI in phase-synchronization measurement since the PLI was limited by the discontinuity of its estimation between zero and infinitesimally small non-zero phase lags. The WPLI demonstrated reduced sensitivity to noise, increased capacity to detect changes in phase synchronization and was not affected by volume-conducting correlated sources of interest. It outperformed coherence, imaginary coherence, and the PLI with real local field potential data (Vinck *et al.*, 2011). Furthermore, the WPLI has been used to detect complex and variable EEG activity patterns during human movement (Lau *et al.*, 2012) and during the resting state in children (Ortiz *et al.*, 2012).

The WPLI limits the effect of cross spectrum elements around a real axis by weighting the cross spectrum to the magnitude of the imaginary component of the cross spectrum:

$$\Phi \equiv \frac{|E\{\Im\{X\}\}|}{E\{|\Im\{X\}|\}} = \frac{|E\{|\Im\{X\}|sgn(\Im\{X\})\}|}{E\{|\Im\{X\}|\}}. \tag{4.22}$$

4.3.4 Phase-Locking Value

The Phase Locking Value (PLV), also known as mean phase coherence (Mormann *et al.*, 2000), is the index of phase synchronization. Lachaux *et al.* (1999) used the PLV to measure phase synchrony based on the wavelet transform. The phase of signal $x(t)$ and signal

$y(t)$ is determined by the convolution of the respective signals with a mother wavelet Ψ:

$$W_x(t) = (\Psi \circ x)(t) = \int |\Psi(t^{'})x(t-t^{'})|dt^{'} = A_x^W(t)e^{i\phi_x^W(t)}. \tag{4.23}$$

$$W_y(t) = (\Psi \circ y)(t) = \int |\Psi(t^{'})x(t-t^{'})|dt^{'} = A_y^W(t)e^{i\phi_y^W(t)}. \tag{4.24}$$

The phases are defined as

$$\phi_x^W(t) = arctan\frac{ImW_x(t)}{ReW_x(t)}. \tag{4.25}$$

$$\phi_y^W(t) = arctan\frac{ImW_y(t)}{ReW_y(t)}. \tag{4.26}$$

The PLV is obtained by calculating the absolute value of the mean difference between 2 signals (Mormann *et al.*, 2000)

$$PLV_t = \frac{1}{N}\left|\sum_{n=1}^{N} Ne^{i|\theta_x(t_j)-\phi_y(t_j)|}\right|. \tag{4.27}$$

As in the WPLI, the value of the PLV is always in the interval [0,1]. The maximum value of 1 signifies perfect phase synchronization, in which 1 signal perfectly follows another. The minimum value of 0 corresponds to no phase synchronization.

4.4 Feature Selection and Artificial Neural Networks Classification

The abnormal functional connectivity patterns during freezing can be represented by features which indicate the highly discriminating functional connections. In a classifier system. these features are good indicators for the prediction of the target labels y for new data input x (Guyon *et al.*, 2008). The selection of the most predictive features will lead to the improvement of performance prediction and data understanding, and reducing computational and data storage requirements. In the evaluation of a single feature, simple feature is ranked based on the strength of correlation between 2 conditions of interest: normal walking and transition to freezing. A non-parametric statistical analysis - the Wilcoxon Sum Rank Test, with the significant statistic difference threshold p-value <0.05, is used. Only the most relevant features with significant statistical differences between groups are chosen as input for the classifier.

A combination of features is investigated using forward selection to make the best use of the data acquired through different features. The performance of the individual features is used to rank their discriminative power in the features in the classification system. Further feature selection is done by constructing combinations of features, starting from the most distinctive feature, and progressively adding the less powerful features (Guyon *et al.*, 2007).

Classification data sampled using selected features based on 3 layers MLP-NN with 56%, 25% and 19% of the data, randomly split, are used in training, validation and testing, respectively. The number of of the input layer, corresponding with the number of selected extracted features from the EEG signals, therefore varies. The output layer in the FOG detection classifier has 1 output node which indicates the condition of normal walking or transition to FOG. The number of hidden layers ranging from 4 to 12 neurons is applied randomly and selected based on performance.

Early stopping base on cross-validation using validation set and error goal 0.01, decreased generalization error and overfitting (see 3.6.2). The Levernberg Marquardt algorithm is applied to each feature for training and tested 50 times based on the repeated random sub-sampling, and the result is recorded. The performance of the classifier is measured by calculating the sensitivity, specificity, and accuracy of classification system.

4.5 Experimental Results

Generally, the transition to FOG condition had greater CPSD and WCS value on the 3 mid-range frequency bands in all pairwise channels (Table 4.1). The estimation of power cross correlation tended to remain high during FOG. Correlation analysis on the CPSD and WCS showed a strong statistical significance difference in both features, between normal walking and transition to freezing, and between normal walking and freezing. Pairwise correlation based on wavelet transform, the WCS, appeared to be more promising for use as inputs than pairwise correlation based on the FFT (CPSD) for FOG detection with $p \leq 0.05$ and $r \geq 0.4$ in all pairs of electrodes between normal walking and transition to FOG except for the Cz-Fz at beta frequency band.

Table 4.1: Correlation analysis of CPSD and WCS between normal walking (N), transition to FOG (T), and FOG (F) in 3 mid-range frequency bands

Electrode Pairs		Normal Walking	Transition to FOG	Freezing of Gait	N vs T	N vs F
	O1-P4	0.0363 ± 0.0473	0.0424 ± 0.0569	0.0488 ± 0.0691		
	O1-Cz	0.0147 ± 0.0279	0.0610 ± 0.1110	0.0404 ± 0.0902	***	*
CPSD	O1-Fz	0.0182 ± 0.0051	0.0096 ± 0.0261	0.0075 ± 0.0230	***	**
Theta	P4-Cz	0.0205 ± 0.0422	0.0772 ± 0.1067	0.0483 ± 0.0985	***	***
	P4-Fz	0.0023 ± 0.0056	0.0111 ± 0.0194	0.0096 ± 0.0261		***
	Cz-Fz	0.0022 ± 0.0095	0.0195 ± 0.0412	0.0151 ± 0.0508	***	***
	O1-P4	0.0172 ± 0.0229	0.0243 ± 0.0356	0.0263 ± 0.0354	**	***
	O1-Cz	0.0057 ± 0.0088	0.0185 ± 0.0286	0.0150 ± 0.0254	***	***
CPSD	O1-Fz	0.0005 ± 0.0015	0.0031 ± 0.0092	0.0027 ± 0.0078	***	***
Alpha	P4-Cz	0.0097 ± 0.0188	0.0245 ± 0.0326	0.0174 ± 0.0247	***	***
	P4-Fz	0.0006 ± 0.0016	0.0028 ± 0.0062	0.0031 ± 0.0092	**	***
	Cz-Fz	0.0003 ± 0.0014	0.0040 ± 0.0119	0.0040 ± 0.0182	***	***
	O1-P4	0.0242 ± 0.0356	0.0354 ± 0.0549	0.0365 ± 0.0503	**	***
	O1-Cz	0.0055 ± 0.0060	0.0162 ± 0.0263	0.0140 ± 0.0213	***	***
CPSD	O1-Fz	0.0003 ± 0.0008	0.0026 ± 0.0085	0.0024 ± 0.0101	***	***
Beta	P4-Cz	0.0014 ± 0.0021	0.0027 ± 0.0038	0.0022 ± 0.0038	***	**
	P4-Fz	0.0005 ± 0.0015	0.0028 ± 0.0073	0.0026 ± 0.0085	***	***
	Cz-Fz	0.0002 ± 0.0005	0.0022 ± 0.0076	0.0018 ± 0.0054	***	***
	O1-P4	0.0449 ± 0.0850	0.0571 ± 0.0857	0.0387 ± 0.0616	***	***
	O1-Cz	0.0163 ± 0.0198	0.0138 ± 0.0188	0.0629 ± 0.0116	***	***
WCS	O1-Fz	0.0161 ± 0.0190	0.0731 ± 0.0135	0.0592 ± 0.0161	***	***
Theta	P4-Cz	0.0184 ± 0.0231	0.0105 ± 0.0176	0.0044 ± 0.0078	***	***
	P4-Fz	0.0214 ± 0.0257	0.0463 ± 0.0885	0.0385 ± 0.0808	***	***
	Cz-Fz	0.0090 ± 0.0135	0.0955 ± 0.0161	0.0560 ± 0.0131	***	***
	O1-P4	0.0507 ± 0.0644	0.0333 ± 0.0337	0.0440 ± 0.0967	***	***
	O1-Cz	0.0234 ± 0.0307	0.0596 ± 0.0775	0.0834 ± 0.0209	***	***
WCS	O1-Fz	0.0028 ± 0.0029	0.0193 ± 0.0395	0.0548 ± 0.0177	***	**
Alpha	P4-Cz	0.0306 ± 0.0451	0.0511 ± 0.0645	0.0619 ± 0.1382	***	***
	P4-Fz	0.0029 ± 0.0025	0.0154 ± 0.0335	0.0310 ± 0.0106	***	**
	Cz-Fz	0.0013 ± 0.0015	0.0252 ± 0.0626	0.0670 ± 0.0217	***	**
	O1-P4	0.3625 ± 0.5374	0.1154 ± 0.1527	0.1347 ± 0.2022	***	***
	O1-Cz	0.1643 ± 0.1784	0.1236 ± 0.1681	0.1029 ± 0.2292	***	***
WCS	O1-Fz	0.0002 ± 0.0002	0.0025 ± 0.0084	0.0049 ± 0.0017	***	**
Beta	P4-Cz	0.1285 ± 0.1103	0.1848 ± 0.2360	0.1819 ± 0.3196	***	***
	P4-Fz	0.0003 ± 0.0004	0.0027 ± 0.0083	0.0051 ± 0.0016	***	**
	Cz-Fz	0.0001 ± 0.0002	0.0034 ± 0.0134	0.0041 ± 0.0014	**	**

CPSD: Cross Power Spectral Density; WCS: Wavelet Cross Spectrum

$* = p \leq 0.05$ and $r < 0.3$

$** = p \leq 0.05$ and $0.3 \leq r < 0.4$

$*** = p \leq 0.05$ and $r \geq 0.4$

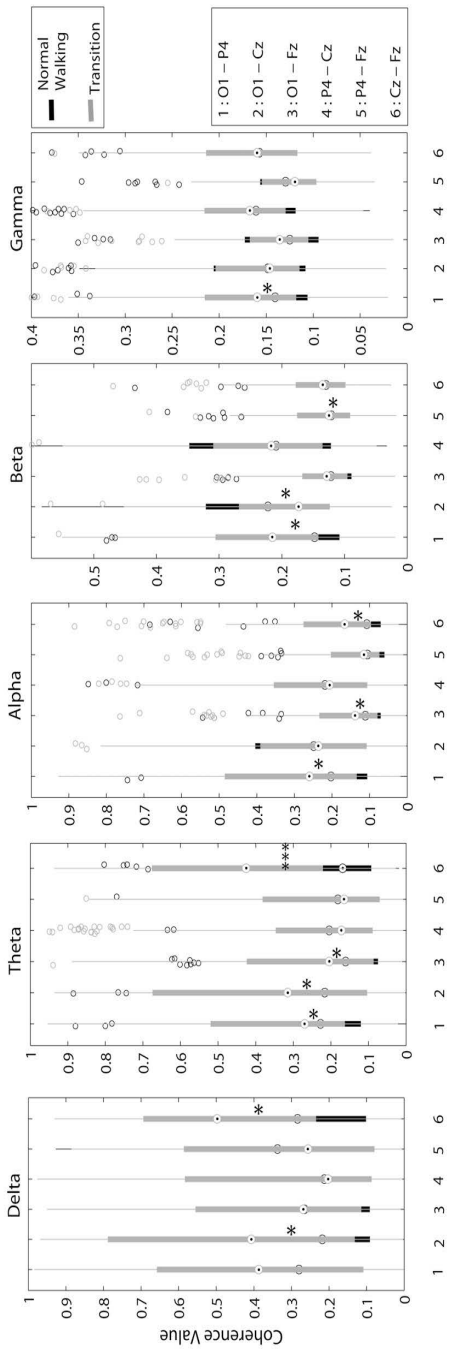

Figure 4.6: Boxplot of MSC of EEG signals during normal walking and transition to FOG (frequency band 5, used electrode 4) with number 1, 2, 3, 4, 5 and 6 in the x-axes referring to O1-P4, O1-Cz, O1-Fz, P4-Cz, P4-Fz and Cz-Fz respectively. The asterisk indicates p-value <0.05. A higher number of the asterisk refers to a higher r-value.

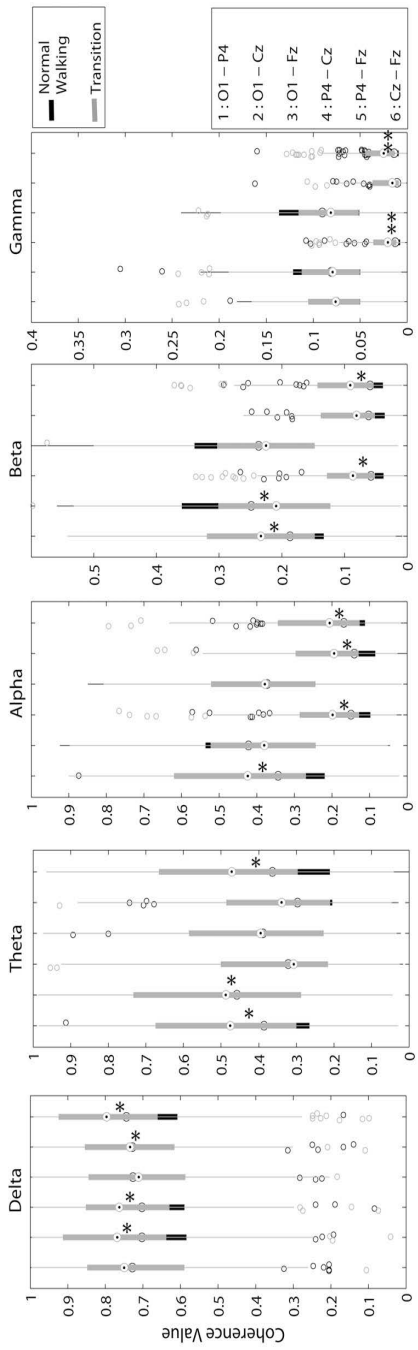

Figure 4.7: Boxplot of wavelet coherence of EEG signals during normal walking and transition to freezing of gait (frequency band 5, used electrode 4) with number 1, 2, 3, 4, 5 and 6 in x-axes refer to O1-P4, O1-Cz, O1-Fz, P4-Cz, P4-Fz and Cz-Fz respectively. The asterisk indicates p-value <0.05. A higher number of the asterisk refers to a higher r-value.

During transition to freezing, and during freezing, the EEG signal change in the beta frequency band measuring the CPSD and WCS, was strong. This finding is consistent with the previous finding in the single channel based power spectral measurement in Chapter 3. The increasing CPSD in the theta frequency band between normal walking and transition to FOG in the pairwise (which included central region (O1-Cz, P4-Cz, Cz-Fz)) also reflects the power spectral measurement in the single channel.

In the coherency analysis, both the MSC and WCO indicated a significant different coherency during transition to freezing in parieto occipital pairwise of electrodes, in the theta, alpha and beta frequency bands as illustrated in Fig. 4.6 and Fig. 4.7. There was no significant change of coherency in parietal-central and parietal-frontal cortices connection.

Pairwise fronto-central showed alteration of coherence in all frequency bands detected using WCO and in the 3 lowest band frequencies using MSC. The most significant of all the changes observed was in the theta frequency band at this pairwise of electrode (PSD: $z = -8.11$, $p < 0.05$, $r = 0.41$; WE: $z = -5.05$, $p < 0.05$, $r = 0.26$).

Fig. 4.9 and Fig. 4.8 show the results from the phase synchrony analysis obtained from electrodes pairs during 3 conditions: normal walking, transition to freezing and FOG. According to the WPLI analysis, the occipital frontal, parietal frontal and central frontal cortices connections in the beta and gamma frequency bands were strongly synchronized in phase. When the PLV analysis was applied, a strong synchronization was measured in theta frequency band in all pairwise of electrode except the parietal central. A stronger synchronization was also indicated in the phase synchronization measured using the PLI except in occipital-parietal.

Based on those statistical results, the functional integration features at all 4 channels were selected as inputs for classification. Table 4.2 and Table 4.3 show the comparison of classifier performance when using different features as inputs. Not all features extracted from available pairwise electrodes were of sufficient statistically significance enough to be used as input for classifier. No significant phase synchronization (the WPLI) was extracted from P4-Cz and P4-Fz, and coherence (MSC and WCO) of P4-Cz.

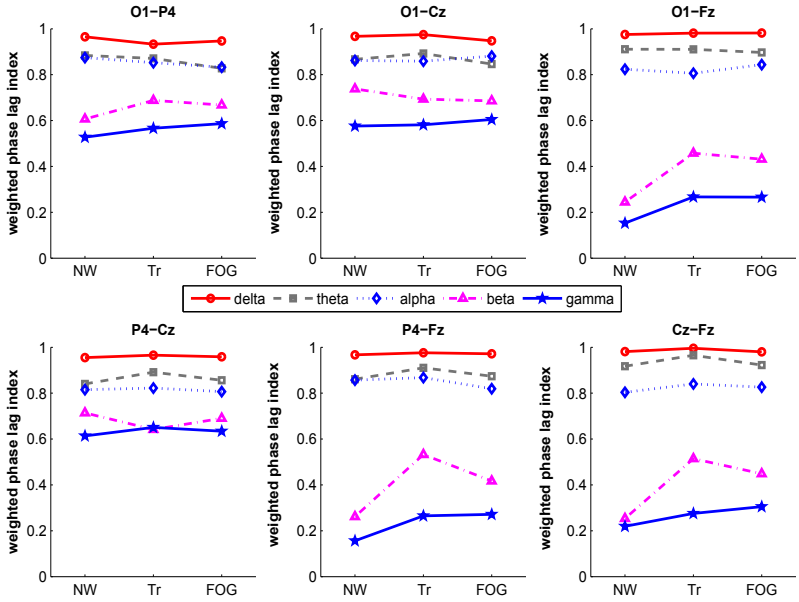

Figure 4.8: Phase synchronization measured using the WPLI.

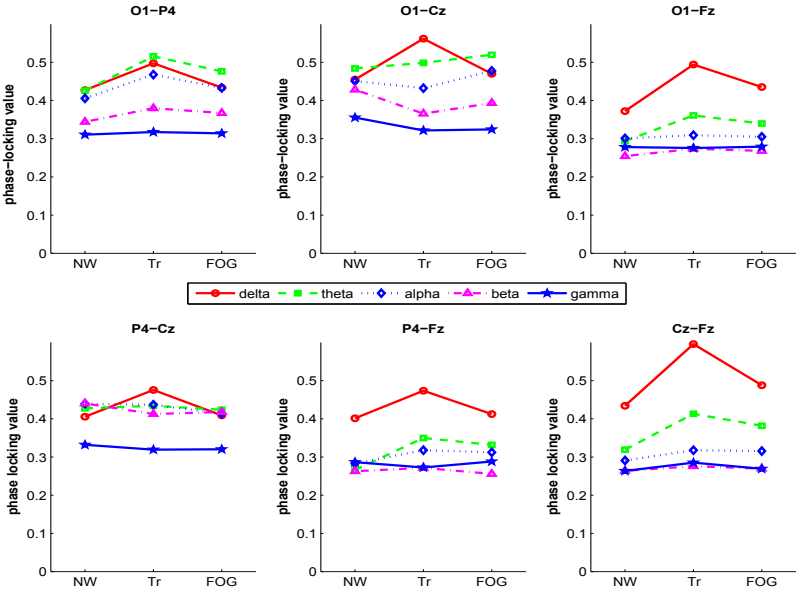

Figure 4.9: Phase synchronization measured using the PLV.

Table 4.2: Classification results of proposed Fourier transform based features using MLP-NN to detect the 5 s transition before freezing from normal walking

Elect.	Feat.	In-group (11 patients)						Out-group (5 patients)		
		Training			Testing			Testing		
		Se %	Sp%	Ac %	Se %	Sp %	Ac %	Se %	Sp %	Ac %
1	CPSD	47.18	57.05	52.48	44.18	54.34	46.95	44.18	54.34	49.26
	MSC	50.87	54.83	52.55	46.01	53.18	48.53	60.78	53.99	57.38
	WPLI	45.35	59.35	52.34	41.04	57.06	47.23	45.62	37.95	41.78
2	CPSD	69.8	77.10	73.55	65.23	74.29	69.38	86.82	60.19	73.51
	MSC	64.09	60.05	61.90	62.00	59.79	61.07	62.75	42.13	52.44
3	CPSD	63.23	72.93	68.06	62.96	74.18	68.19	71.05	52.25	61.65
	MSC	40.62	68.52	54.47	48.13	67.41	51.81	54.42	63.6	59.01
	WPLI	42.06	77.96	60.00	40.34	77.78	58.98	32.98	82.25	57.62
4	CPSD	64.76	63.07	63.86	62.88	57.65	60.06	64.27	62.43	63.35
	WPLI	45.39	56.07	50.85	42.51	53.15	46.95	47.21	52.79	50.00
5	CPSD	54.93	69.16	61.75	57.11	68.74	62.94	65.27	49.27	47.15
	MSC	59.75	44.53	52.68	57.56	43.27	47.34	58.18	43.33	50.76
6	CPSD	59.47	72.33	65.82	59.60	70.20	64.75	68.91	67.48	68.20
	MSC	48.07	72.18	60.07	50.21	69.92	59.66	56.63	72.25	64.44
	WPLI	54.68	70.52	62.59	54.89	70.21	62.43	49.42	78.68	54.05
2,6	CPSD	76.46	74.87	75.62	74.70	73.33	73.84	87.40	56.94	72.17
6,2	MSC	69.05	62.79	66.03	68.14	58.77	63.16	77.71	53.10	65.41
3,6	WPLI	55.02	80.08	67.63	51.64	70.43	65.03	41.9	72.21	57.05
2,6,3	CPSD	72.04	78.42	75.11	68.90	77.28	73.05	82.48	62.60	72.54
6,2,3	MSC	69.54	66.97	68.24	65.17	60.76	62.99	72.91	56.98	64.94
3,6,4	WPLI	53.88	79.59	66.73	50.49	78.77	63.95	49.11	73.57	56.34
2,6,3,4	CPSD	77.26	78.03	77.55	71.96	76.86	74.58	79.88	69.11	74.58 *
6,2,3,1	MSC	72.91	59.96	66.45	69.87	54.39	61.75	77.25	50.93	64.09
3,6,4,1	WPLI	63.70	80.43	72.10	64.20	81.22	72.88	54.88	87.09	70.99 *
2,6,3,4,5	CPSD	79.30	73.34	76.25	77.33	67.57	72.09	82.13	61.94	72.03
6,2,3,1,5	MSC	71.92	77.14	74.58	70.75	71.73	70.75	66.16	72.88	68.42 *
2,6,3,4,5,1	CPSD	81.31	81.49	81.71	74.88	74.76	74.88	68.40	68.77	68.56

Elect.: Electrodes Pairs; Feat.: Features; Se: Sensitivity; Sp: Specificity; Ac: Accuracy
Elect. 1: O1-P4, Elect. 2: O1-Cz, Elect. 3: O1-Fz, Elect. 4: P4-Cz, Elect. 5: P4-Fz, Elect. 6: Cz-Fz
CPSD: Cross Power Spectral Density; MSC: Magnitude-Squared Coherence ; WPLI: Weighted Phase Lag Index

The best performance accuracy using only single pairwise electrodes in FFT based functional integration features, was achieved when using the CPSD in O1-Cz pairs with testing in-group results at 65.23%, 74.29% and 69.38% of sensitivity, specificity, and accuracy, respectively; and testing out-group results at 86.82%, 60.19% and 73.51%. When using more than 1 pair of channels, the best results were obtained using combined CPSD extracted from 4 pairwise channels: O1-Cz, Cz-Fz, O1-Fz, and P4-Cz. It achieved 71.96%, 76.86% and 74.58% of sensitivity, specificity, and accuracy, respectively, in the testing of the in-group; and 79.88%, 69.11% and 74.58% in the testing of the out-group.

The Wavelet Transform based functional integration features had a better performance compared to the FFT based functional integration features. The classifier achieved the

Table 4.3: Classification results of proposed wavelet transform based features using MLP-NN to detect the 5 s transition before freezing from normal walking

Elect.	Feat.	In-group (11 patients)						Out-group (5 patients)		
		Training			Testing			Testing		
		Se %	Sp%	Ac %	Se %	Sp %	Ac %	Se %	Sp %	Ac %
1	WCS	75.66	68.38	71.89	71.88	65.19	68.19	80.7	48.91	64.81
	WCO	43.44	73.65	58.64	43.3	70.5	56.44	45.78	58.84	47.31
	PLV	45.93	72.06	59.03	41.99	68.2	53.22	52.29	51.01	51.65
2	WCS	73.78	81.5	77.78	68.67	78.93	73.16	81.32	71.63	76.47
	WCO	53.17	69.84	61.41	51.92	66.64	59.04	46.94	59.42	53.18
	PLV	45.03	81.97	63.5	44.86	78.25	61.24	47.29	68.49	57.89
3	WCS	69.72	87.58	78.71	66.81	84.74	75.59	77.87	57.71	62.7
	WCO	64.57	77.95	71.25	59.19	77.96	68.64	53.06	61.05	57.05 *
	PLV	44.98	69.77	57.29	45.02	70.27	57.34	49.03	65.66	52.34
4	WCS	69.3	81.77	75.55	70.77	81.11	76.05	73.14	82.98	78.06
	PLV	61.83	59.88	60.71	60.18	59.68	59.49	47.44	41.36	44.4
5	WCS	59.68	85.61	72.63	59.71	84.85	71.64	52.91	80	66.45
	WCO	49.69	68.26	58.86	48.42	65.45	56.1	46.94	57.17	52.05
6	WCS	72.43	84.63	78.52	77.43	83.9	78.87	74.53	77.79	76.16
	WCO	48.58	87.68	68.14	48.56	85.62	66.55	48.56	65.27	52.62
	PLV	45.7	75.96	60.64	43.61	73.25	58.42	53.37	55.47	54.42
6,4	WCS	73.76	86.82	80.2	73.18	85.49	79.77	71.55	83.22	77.38 *
3,6	WCO	62.02	81.85	72.02	55.58	79.69	67.34	52.79	54.84	53.82
2,6	PLV	59.07	76.89	68.03	53.88	72.31	62.43	69.96	43.1	56.53 *
6,4,2	WCS	74.61	87.01	80.81	72.93	84.01	78.42	67.95	85.78	76.86
3,6,2	WCO	69.03	75.26	72.02	62.47	72.66	67.46	56.78	49.22	53.00
2,6,3	PLV	59.77	74.86	67.32	52.16	71.33	61.92	65.97	47.44	56.71
6,4,2,3	WCS	78.18	85.94	81.95	73.07	82.19	77.85	69.61	82.91	76.26
3,6,2,5	WCO	62.92	81.76	72.16	55.25	75.92	65.71	49.5	55.85	52.67
2,6,3,1	PLV	56.52	81.95	69.35	56.52	76.41	61.41	61.32	52.36	56.84
6,4,2,3,5	WCS	77.21	88.15	83.04	77.19	86.07	78.31	68.41	86.01	77.21
3,6,2,5,1	WCO	75.66	78.88	78.67	66.33	67.71	69.42	57.51	53.72	52.16
2,6,3,1,4	PLV	70.02	74.15	72.07	60.80	66.13	62.47	73.07	54.42	52.13
6,4,2,3,5,1	WCS	78.73	87.22	83	72.76	82.89	77.42	69.93	85.16	77.55

Elect.: Electrodes Pairs; Feat.: Features; Se: Sensitivity; Sp: Specificity; Ac: Accuracy
Elect. 1: O1-P4, Elect. 2: O1-Cz, Elect. 3: O1-Fz, Elect. 4: P4-Cz, Elect. 5: P4-Fz, Elect. 6: Cz-Fz
WCS: Wavelet Cross Spectral; WCO: Wavelet Coherence; PLV: Phase-Locking Value

Table 4.4: Features Rank based on the average of the classification accuracy

Features			Accuracy			Group
			Ingroup	Outgroup	Mean	rank
FFT based	Segregated	PSD	77.38	75.19	76.28	3
		CF	79.54	79.91	79.73	1
		PSE	79.66	78.65	79.16	2
	Integrated	CPSD	74.58	74.58	74.58	4
		MSC	70.75	68.42	69.59	6
		WPLI	72.88	70.99	71.94	5
Wavelet Transform based	Segregated	WE	80.2	76.67	78.44	2
		CS	79.34	75.99	77.66	3
		WEE	69.32	71.07	70.19	4
	Integrated	WCS	79.77	77.38	78.57	1
		WCO	68.64	57.05	62.84	5
		PLV	62.43	56.53	59.48	6

PSD: Power Spectral Density; CF: Centroid Frequency ; PSE: Power Spectral Entropy
CPSD: Cross Power Spectral Density; MSC: Magnitude-Squared Coherence ; WPLI: Weighted Phase Lag Index
WE: Wavelet Energy; CS: Centroid Scale ; WEE: Wavelet Energy Entropy
WCS: Wavelet Cross Spectral; WCO: Wavelet Coherence; PLV: Phase-Locking Value

Table 4.5: Classification results of combination features using MLP-NN in detecting transition 5 s before freezing from normal walking

Features	Training - Ingroup			Testing-Ingroup			Testing-Outgroup			Mean
	Sens	Spec	Acc	Sens	Spec	Acc	Sens	Spec	Acc	Acc
CF	78.68	80.23	79.37	76.69	74.05	79.54	75.21	80.65	79.91	79.73
CF, PSE	83.36	78.96	81.18	80.10	74.56	77.18	83.57	72.44	78.00	77.59
CF, PSE, PSD	79.42	79.35	79.35	78.31	74.86	76.61	80.43	77.71	79.07	77.84
CF, PSE, PSD, CPSD	81.02	86.23	83.59	75.98	81.47	78.76	79.69	82.44	81.07	79.92 *
WCS	73.76	86.82	80.20	73.18	85.49	79.77	71.55	83.22	77.38	78.58
WCS, WE	86.82	92.69	89.78	83.22	91.50	87.06	72.36	81.78	77.07	82.07 *
WCS, WE, CS	90.68	89.84	90.26	85.30	86.06	85.48	68.80	86.78	77.79	81.64
WCS, WE, CS, WEE	90.31	90.97	90.65	80.55	84.12	83.32	68.64	81.59	75.12	79.22

PSD: Power Spectral Density; CF: Centroid Frequency ; PSE: Power Spectral Entropy
CPSD: Cross Power Spectral Density; MSC: Magnitude-Squared Coherence ; WPLI: Weighted Phase Lag Index
WE: Wavelet Energy; CS: Centroid Scale ; WEE: Wavelet Energy Entropy
WCS: Wavelet Cross Spectral; WCO: Wavelet Coherence; PLV: Phase-Locking Value

best performance when using the WCS from pairwise Cz-Fz and P4-Cz, with testing in-group resulted at 73.18%, 85.49% and 79.77% of sensitivity, specificity, and accuracy, respectively; and testing out-group resulted at 71.55%, 83.22% and 77.38%. These results showed the significance of the central area in the alteration of connectivity related with FOG.

Generally, the performance of features extracted from the single channel based measurement of its activation (Chapter 3) was stronger than pair channels based measurement of their connectivity. The exception was the WCS which provides slightly better accuracy than its single channel based measurement, WE. Both the sub-band power spectrum and the sub-band wavelet energy features gave better results compared to their pairwise mode, cross power spectrum and wavelet cross spectrum. The coherence based features performed poorly when applied to out-group patients. It may indicate that connectivity based features are less robust against the inter individual variability, compared to single channel activation based features.

When both measures were combined as inputs of artificial neural networks, the performance of the classifier increased significantly in the in-group patients when using wavelet transform based features. The best results were achieved when correlation information between channel Cz-Fz and P4-Cz were used as inputs, combined with the wavelet energy extracted from all 4 channels, with sensitivity, specificity and accuracy were up to 83.22%, 91.50%, and 87.06% on average, respectively.These features produced better classification than either class of features alone, increased nearly 10%, 6%, and 8% of sensitivity, specificity, and accuracy, respectively (see Table 4.4. and Table 4.5.). These classifier performance improvements implied that WCS based features contain information that is different from that contained in the WE in transition to FOG episodes.

4.6 Discussion and Conclusion

While there are clear differences in the result of phase synchrony calculation using the WPLI and the PLV, both showed an increase of beta synchronization during transition to FOG in any pairwise related to frontal area. This result is aligned with the work of E.

Heinrichs-Graham et al. (Heinrichs-Graham *et al.*, 2013) who used magnetoencephalography (MEG) and found beta desynchronisation before and during movement onset as well as increased gamma activity in PD patients. The analysis of the primary motor cortex arm area by Hemptinne et al. (de Hemptinne *et al.*, 2013) found exaggerated coupling between the beta-phase and gamma amplitude in those areas in PD patients. This coupling has been reported in relation to movement preparation and control of different cognitive functions including memory and attention. Interestingly, we also noticed the significant coherence in the gamma frequency band at pairwise O1-Cz and Cz-Fz, was detected using wavelet coherence.

This study demonstrates the potential of the EEG synchronization-based features, extracted using both the Fourier and wavelet analysis to give greater insights into the pathophysiology of FOG in PD. Results in Chapter 3 show the advantage of using wavelet analysis in extracting EEG basic feature, energy, compared to Fourier analysis, providing a better indicator in classification system. This finding may be due to its representation of signals in three dimensions (amplitude, frequency and time) compared to Fourier (amplitude and frequency), which is more convenient for non-stationary EEG signals. The synchronization measure from two pairwise channel based on correlation of power also shows the advantage of features extraction using wavelet transform (WCS) over Fourier transform (CPSD), as it provides a better performance when it is applied as input of classifier.

Different aspects of the EEG signal, when combined, provide more significant information, and lead to a better classification of the signal. The classification results of combination features show that using features measure from a single channel and pairwise channel as inputs for the classifier, improve the performance of the system. In the FFT based features, the accuracy of detection of the FOG system is decreased when SCF is used as input with PSE and PSD. However, when they are used as input with CPSD, the pairwise based measurement, the accuracy of the system improves slightly. Detection of FOG using WCS, measured from pairwise Cz-Fz and P4-Cz, and WE measured from all 4 channels as inputs provides the best result with accuracy of 87.06% and 77.07% when tested in in-group and out-group testing data sets.

Chapter 5

Advanced FOG Detection Using Independent Component Analysis and Brain Effective Connectivity

"Far from being able to accept the idea of the individuality and independence of each nerve element, I have never had reason, up to now, to give up the concept which I have always stressed, that nerve cells, instead of working individually, act together [. . .]. However opposed it may seem to the popular tendency to individualize the elements, I cannot abandon the idea of a unitary action of the nervous system [. . .]"
-Camillo Golgi, 1906

The strong negative impact on patient quality of life from frequent falls, related injuries and resultant loss of independence in PD patients with FOG, call for novel therapies that can predict the freeze and hence prevent falls. The feasibility of developing devices that can detect FOG preceding the symptom, using brain parameters as inputs of the computational detecting methodology, was demonstrated in previous chapters. Chapter 4 reported that the ability to provide information to distinguish between normal walking and transition to FOG improved, when combined with additional spatial information based on cross correlation, coherence and phase synchronization. When information of correlation

between channels Cz-Fz and P4-Cz was used as inputs combined with wavelet energy extracted from O1, P4, Cz, and Fz, the classification results of FOG detection was enhanced with sensitivity, specificity and accuracy up to 83.22%, 91.50%, and 87.06% on average, respectively. Against the background of growing interest amongst neuroscientists in integration and interaction of networks analysis, functional connectivity also opened the way to a better understanding of several important aspects of the pathophysiological mechanism underlying FOG, beyond the brain's localized function in segregation.

This chapter applies an advanced brain signal connectivity analysis to detect FOG, and aims to enhance the performance of the developed neural networks based classifier in predicting the FOG episode. The study uses the brain effective connectivity (BEC) measure: generalized partial directed coherence (sGPDC). It is compared to directed direct transfer function (dDTF) and its original forms, partial directed coherence (PDC) and directed transfer function (DTF). The optimization of algorithm is achieved by applying independent component analysis as part of preprocessing signals, and by using Bayesian regularization instead of early stopping to prevent over fitting.

5.1 Introduction

Different methods have been used to study the information processing in the brain to get a better understanding of neuronal disorder and diseases, including PD. Estimation of power spectra, obtains by FFT, appears to be the most used methods of single channel analysis. Chapter 3 showed that changes in EEG spectral characteristics are proven to be useful markers in FOG.

Signal power measured in one channel can come from superposition of the activity of coherent sources. This interdependence between EEG signals, often seen as synchronization between EEG signals, can be found by a cross correlation or coherence (presented in Chapter 4). The analysis of the influences that one system can exert over others, leads to the development of the concept of causality.

In his 1956 study of feedback system, mathematician Norbert Wiener (1956) proposed

the earliest formulation of causality, asserting that a time series X causes another time series Y, if the past of X has a strictly positive influence on the quality of prediction of Y. In his paper, neuroscience was already given as example:

"...in the study of brain waves we may be able to obtain electroencephalograms more or less corresponding to electrical activity in different parts of the brain. Here the study of coefficients of causality running both ways and of their analogues for sets of more than two functions f may be useful in determining what part of the brain is driving what other part of the brain in its normal activity."

The Nobel Prize winning economist Clive Granger adapted Wiener's definition of causality, emphasizing a measurement of statistical dependence between the past of a process and the present of another. In 2 time-series X and Y, Y_t would "Granger cause" X_{t+1} if Y_t :(a) occurs before X_{t+1}; and (b) contains information useful in forecasting X_{t+1} that is not found in a group of other appropriate variables. The current activity process X can be predicted based on the past activity process Y, if Y causes X. This "Granger cause" is different from causation in the classical philosophical sense. But because "correlation does not imply causation" (Wright, 1921), it provides estimation of causation above simple contemporaneity correlated by chance (Geweke, 1982).

The search for a better understanding of the human brain function leads to further development of generative models of coupling or directed causal influence among observed brain regions based on Granger causality. As Granger causality is not reciprocal, it can therefore be used to determine the direction of information flow between hypothetical models built and tested using this connectivity measurement on the study of brain diseases or states, such as autism (Deshpande *et al.*, 2013), schizophrenia (Mutlu & Aviyente, 2009), and general anaesthesia (Nicolaou *et al.*, 2012). Furthermore, measures of neuronal signal causality have been applied in some research on PD.

In the PD study of the EEG recorded simultaneously with subcortical oscillation measured using the local field potential from the pedunculopontine nucleus (PPN), the alpha

sub-band synchronization was reported to have been promoted by the administration of levodopa (Androulidakis *et al.*, 2008). The directed transfer function (DTF) was used to investigate the causal connectivity between the cortex area (FPz) and the PPN area. This result suggests that medication impacts on the motor related attentional process.

Study of the causal interaction on control and PD patients with FOG using re-normalized partial directed coherence (PDC) was conducted by Velu *et al.* (2013). Increasing information flow was found in the beta range from visual area (O1) to motor region (Cz) and integrating sensory region (P4) before and after visual cuing during the walking task. The results suggest that alteration of visual feedback is related to the cortical neural process. With only 2 PD patients and 6 control patients involved in the study, further validation is needed in larger cohorts of subjects.

Compared to synchronized estimates using pairwise analysis cross correlation and coherence, the causal connection estimation has 3 advantages.

1. Coherence has been used to give insight to the underlying anatomical structures of brain connectivity related with certain condition such as epilepsy (Mormann *et al.*, 2000), autism (Catarino *et al.*, 2013), and obsessive-compulsive disorder (Olbrich *et al.*, 2013). While this structural connectivity generates behavior, many neurobiological processes are modulated also by the dynamical process operating on that structure (Sporns *et al.*, 2004). Spectral causality analyzes this brain dynamic and provides a causal description to give new insights to complex brain networks (Seth, 2005).

2. Pair-wise analysis of bivariate signals is prone to mistakenly finding correlation between 2 responses, because of the difference in the delays information is received from a common driver component, even when the signals are independent of each others (Kus *et al.*, 2004) (see Fig. 5.1). Multivariate estimate reveals all covariance structure information of the full data to avoid this type of error.

3. The multi-channel causal estimate can be used to differentiate between direct and indirect interactions. For example, a simple pairwise analysis would be unable to distinguish the 2 connectivity patterns in Figure 5.2. A multichannel analysis

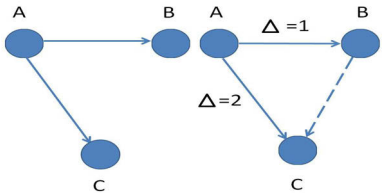

Figure 5.1: False flow (dotted arrows) of signal from B to C can be found as the result of the different delays (Δ_1 and Δ_2) of the propagation of signals (blue arrow) from A to B and A to C

amongst groups of 3 simultaneously recorded signals recognizes direct interactions between channel A and C beyond those signals mediated by B. This more accurate description of the connectivity can be very useful in building a pathophysiological model of FOG as well as in capturing the alteration of brain signals during transition to FOG.

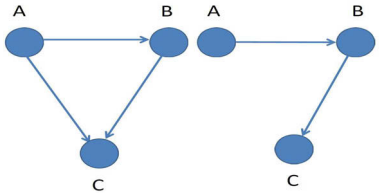

Figure 5.2: 2 different patterns of connectivity amongst 3 channels. In the left networks, there is a direct pathway from A to C, while in the right networks there is 1 indirect pathway from A to C only

5.2 System Overview

Fig. 5.3 shows an overview of an advanced FOG detection strategy system using BEC. A 4-channel wireless EEG system was used to collect brain signal data from 16 PD patients with FOG (reported in Chapter 3). Noise and artifact handling followed. Independent sources embedded in these filtered signals is de-mixed using fastICA to maximize separation between independent components (ICs). The direct causal influence in brain networks is then estimated using square Generalized PDC (sGPDC) among channels of ROIs. The non parametric Wilcoxon Sum Rank test is used to select features (mean, minimum and maximum of sGPDC from 5 frequency sub-bands). Based on these selected features as input, using multilayer perceptron artificial neural networks, brain signals are classified into 2 conditions: normal walking or transition to freezing.

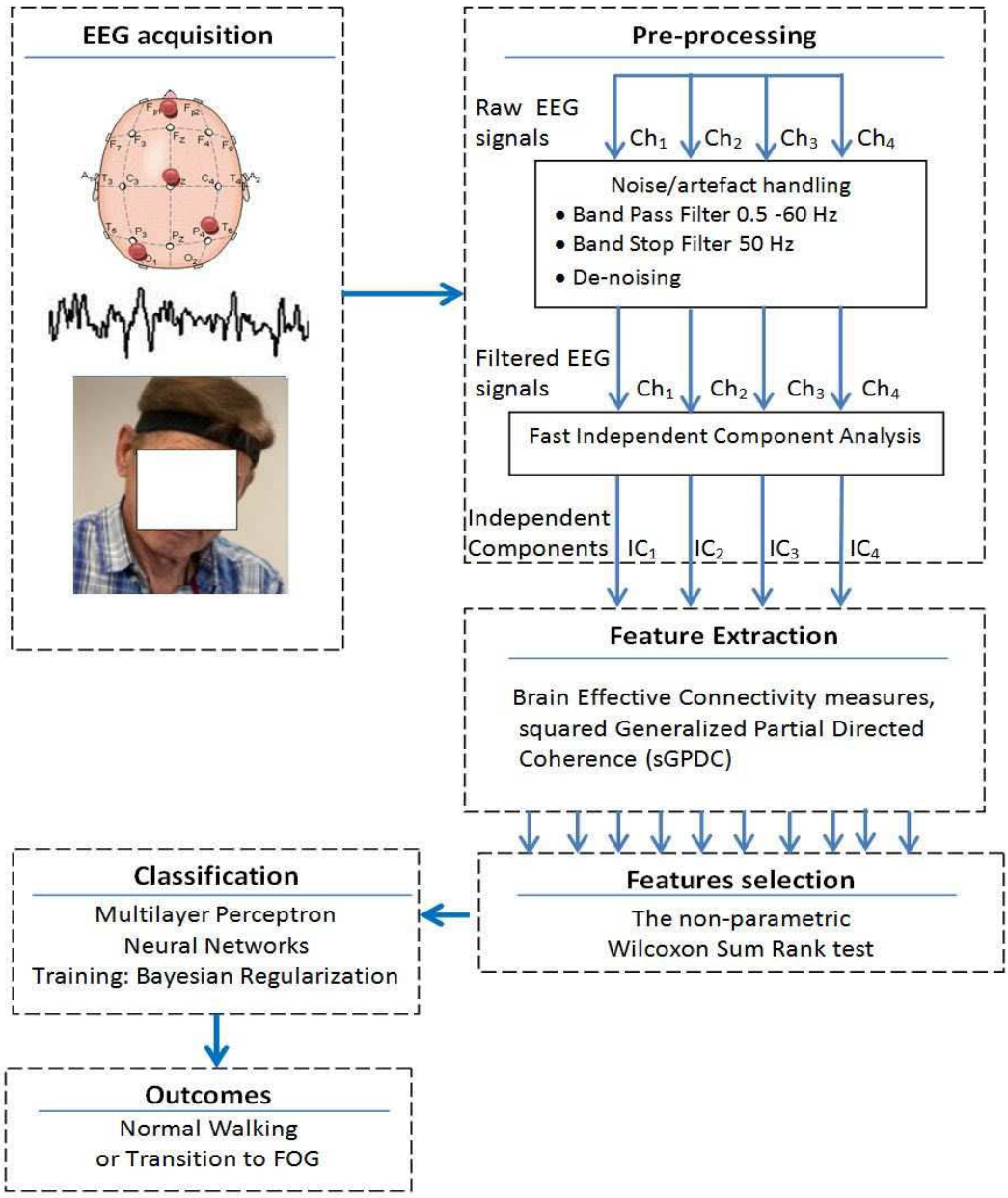

Figure 5.3: System overview for detecting FOG from the EEG data using BEC features

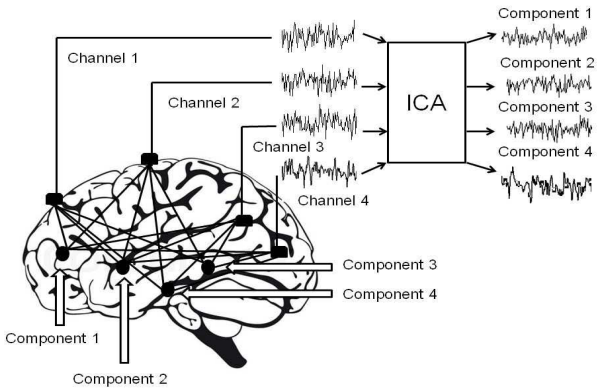

Figure 5.4: Mixing and blind separation of the EEG signals using ICA

5.3 Data Preprocessing: Maximization of Non-Gaussianity of the EEG Feature Set Using FastICA

Claude Shannon established the information theory in his classic paper which addressed the need to design efficient and reliable communication systems (Shannon, 1948). His theory provides a benchmark to compute the optimal representation and transmission of information bearing signals. Optimization of the mutual information between certain variables of the system by minimizing the statistical dependence between the components of the output vector Y from the input vector X with the equal dimensionality, leads to the development of the Independent Component Analysis (ICA).

ICA also can be seen as an extension of the principal-components analysis (PCA). PCA is based on second-order statistics (variances), where data fit Gaussian distribution yields orthogonal vectors, thus minimizing the covariance of the data and de-correlating a multivariate signal. ICA minimizes higher-order statistics such as skew and kurtosis by demixing independent sources for non-Gaussian signals. This is equivalent to minimizing the mutual information between the components of the output (Comon, 1994). Since the EEG and its derived statistical measurement rarely have a Gaussian probability distribution, ICA can be said to be more appropriate for use in EEG signal processing than PCA.

ICA was originally developed to solve the *blind source separating problem* (BSS), also called the *cocktail-party problem*. The EEG data records from many different locations

on the scalp, measure the electrical potential generated by mixing some underlying component of brain activity. It presents a situation similar to the cocktail-party problem with different speakers involved in it. Based only on the observation of input vector X at the recoding channels, BSS estimates the independent source signals S in the output vector Y as illustrated in Fig.5.4.

A noise-free linear BSS model is expressed as

$$X = AS \tag{5.1}$$

where $X = [X_1, X_2, ..., X_n]^T$ denotes observed linear mixtures of n independent elements, $S = [S_1, S_2, ..., S_n]^T$ is the random vector represents n source signals, and A denotes an m x m full-rank mixing matrix. The objective of ICA is to estimate the un-mixing matrix $W = A^{-1}$ that recover the sources S:

$$Y = WX \cong S \tag{5.2}$$

where Y is independent component (IC).

The statistical IC estimations in the ICA algorithm are based mainly on the minimization of mutual information or on the maximization of non-Gaussianity (Langlois *et al.*, 2010). In this present study, fastICA is used for its fast convergence and robustness (Hyvarinen, 1999).

A quantitative measure of non-Gaussianity in fastICA estimation is defined by *negentropy*. This is based on the information-theoretic quantity of differential entropy which found that *a Gaussian random variable has the largest entropy among all other random variables of equal variance* (Hyvärinen & Oja, 2000). Negentropy measures a distance from normality and is defined as

$$N(X) = H(X_{Gaussian}) - H(X) \tag{5.3}$$

where $H(X)$ is the entropy of X and $X_{Gaussian}$ is a Gaussian random variable whose covariance matrix is equal to that of X.

Statistically, negentropy appears as the optimal estimator of non-Gaussianity. However, it is highly demanding in computational term. Hyvärinen & Oja (2000) have proposed the approximation of negentropy to solve this problem:

$$N(Y) \propto [EG(Y) - EG(\nu)]^2 \tag{5.4}$$

where Y is a non-Gaussian random variable (assumed to be of zero mean and unit variance), ν is a standardized Gaussian variable, and G is a non-quadratic function. The stepwise implementation of the fastICA algorithm can be seen in Algorithm 1 [(Hyvärinen *et al.*, 2004)].

Algorithm 1 A fastICA algorithm

1: **procedure** FASTICA(*MatrixInput*)
2: $x \leftarrow x - x_m, x_m = Ex$ ▷ center the data x to make its mean zero
3: $z = \vee\Lambda^{1/2}V^T x, \vee\Lambda V^T = E\{xx^{\{T\}}\}$ ▷ whiten x by linearly transforming the data to uncorrelated the components
4: $\|w\| =$ random vector of length N ▷ choose an initial random vector, w
5: **while** not converge **do** ▷ update w, maximally non-Gaussian direction
6: $w = E\{z * g(w^T\} - E\{g'(w^T z)\}w,$
7: $g(y) = \tanh(a_1 y), 1 < a_1 < 2$
8: $w\frac{w}{\|w\|}$
9: $s = [w_1 w_2 ... w_n]x$ ▷ obtained the independence component

5.4 Causality Measures of Brain Signals for Detecting FOG Episodes

Friston (1994) proposed 3 aspects of connectivity when applied to the brain: structural connectivity, functional connectivity and effective connectivity. Structural connectivity refers to physical pattern of connections between sets of neurons or neuronal elements. Functional connectivity corresponds to the measurement of statistical dependencies (correlation, coherence, and phase locking) between distributed neuronal units. Effective connectivity can be seen as the union of structural and functional connectivity, presenting networks of causal influences of one neural element over another. This type of connectivity can be estimated by building a model related to anatomical pathways between brain regions and their directional interaction (Friston *et al.*, 2003). Another way to estimate effective connectivity is by using time-series analysis. This study uses sGPDC to analyze directed connectivity, based on frequency domain Granger causality of multivariate autoregressive models of time series modeling causality measures Granger causality on the

frequency domain.

5.4.1 Multivariate Autoregressive Process

Time series modeling of neuroscience data, has two main goals: prediction and characterization of the "dynamic brain" from the observed time series data (Ozaki, 2012). The one-variable model, for instance, will give a prediction error ε_t from the prediction of a value $x(t)$ using p previous values of time series x.

$$x(t) = \sum_{n=1}^{p} a_n x_{t-n} + \varepsilon_t. \tag{5.5}$$

Extending the model into two-variable models, with x_t and y_t representing the temporal dynamic of 2 time series, shows Granger causality, and can be characterized as:

$$\begin{aligned} x(t) &= \sum_{n=1}^{p} a_n x_{t-n} + \sum_{n=1}^{k} b_n y_{t-n} + \varepsilon_{xyt}, \\ y(t) &= \sum_{n=1}^{p} c_n y_{t-n} + \sum_{n=1}^{k} d_n x_{t-n} + \varepsilon_{yxt} \end{aligned} \tag{5.6}$$

where a_n, b_n, c_n, d_n are the model parameters, t is time points, k is the model order, and ε_{xyt} and ε_{yxt} represent an error residual associated with the bivariate model. In the sense of Granger causality, y can be said to cause x if the variance prediction error ε_{xyt} is reduced after including series y to the prediction of series x. Those equations also show that the influence of x on y, as is indicated by coefficient vector d, can be distinct from the influence of y on x, as is expressed by b.

Given a set of cortical waveform $x(t) = x_1(t), x_2(t), ..., x_N(t)$ that are simultaneously observed from several cortical ROIs where t refers to time and N is the number of channels,

the data set can be described using MVAR process with order p as (Blinowska & Zygierewicz, 2011):

$$\begin{bmatrix} x_1(t) \\ \cdots \\ \cdots \\ \cdots \\ x_N(t) \end{bmatrix} = \sum_{r=1}^{p} A_r \begin{bmatrix} x_1(t-r) \\ \cdots \\ \cdots \\ \cdots \\ x_N(t-r) \end{bmatrix} + \begin{bmatrix} w_1(t) \\ \cdots \\ \cdots \\ \cdots \\ w_N(t) \end{bmatrix} \tag{5.7}$$

where $x(t)$ is the data vector in time t, A_r are the model coefficients, and $w(t)$ represents the vector of independent Gaussian white noise.

In this study, because of its robustness, Schwarz-Bayes Criterion (SBC) is used to determine the model order p (Porcaro *et al.*, 2009), by means of ARfit algorithm (Schneider & Neumaier, 2001). SBC involves estimating the model order p so that it minimizes the estimated residual variance $\hat{\mathbf{V}}$ and a number of freely estimated parameters (Blinowska & Zygierewicz, 2011):

$$SBC(p) = \log[\det(\hat{\mathbf{V}}] + \log(N)\frac{pk^2}{N}, \tag{5.8}$$

where k is the number of channels, and N is number of data points. The selected model will model the data accurately without too many parameters. With model order p, an estimate of the remaining MVAR model parameters for each Hamming windowed signals is computed by means of the Nuttall Strand algorithm (multivariate Burg) implemented in the Biosig toolbox (Schlögl, 2006).

5.4.2 Squared Generalized Partial Directed Coherence

The signals collected from more than 2 channels can be related directly or indirectly through other channels. Coherence obtained by pair-wise analysis in Chapter 4 cannot determine this directionality. In their study to get a better understanding of cerebral information processing by means of multivariate statistical time series analysis, Walter & Adey (1965) developed a basic concept of partial coherence (PCoh) which is analogous

to partial correlation, "*to determine the degree of relationship between 2 chosen traces, if both were to be freed of the effects of all other traces*".

Referring to this idea, in their research to identify the site of epileptic focus using simultaneous examination of brain data collected from three electrodes, Gersch & Goddard (1970) proposed "Gersch causality" in their partial coherence based driver identification approach "*one channel is said to drive the other channels if the first channel explains or accounts for the linear relation between the other two*". Since the above, various neurobiological data including EEG signals have been analyzed using PCoh to identify the pattern of neural circuits underlying the studied physiological condition (Saito & Harashima, 1981; Cohen *et al.*, 1995; Waser *et al.*, 2013).

The PCoh can be seen as a measurement of the level of synchronization between 2 signals in the multi channel data set when the shared influence from all other signals has been removed. For signals X, Y, and Z, this direct interrelation is obtained by calculating the partial cross-spectrum (PCS) by subtracting all linear influences from other processes (Blinowska & Zygierewicz, 2011):

$$P_{xy|z}(f) = P_{xy}(f) - P_{xz}(f)P_{zz}^{-1}(f)P_{zy}(f) \tag{5.9}$$

so that three channels partial coherence is defined as normalized PCS:

$$PCoh_{xy|z}(f) = \frac{|P_{xy|z}(f)|}{\sqrt{P_{xx|z}(f)P_{yy|z}(f)}}. \tag{5.10}$$

For n number of channels, PCoh can be defined as:

$$PCoh_{ij}(f) = \frac{M_{ij}(f)}{\sqrt{M_{ii}(f)M_{jj}(f)}} \tag{5.11}$$

and $M_{ij}(f)$ is a minor obtained by removing ith row and jth column from the cross-spectral power density matrix $P(f)$. Unlike ordinary coherence, PCoh is non zero only for direct relations between channels. The PCoh of any signal in a given channel which appeared as a result of indirect relations between channels will be low.

The concept of partial coherence inspired Baccalá & Sameshima (2001) to propose the partial directed coherence (PDC). PDC is a frequency version of the concept of Granger

causality in a full multivariate spectral measure. PDC estimates only direct flows between channels and has values at the interval [0,1] where higher values reflect stronger inflow of signals from channel j to i. PDC is normalized to the total outflow of information from channel j. The PDC from channel j to i could be calculated as

$$PDC_{j\to i}(f) = \frac{A_{ij}(f)}{\sqrt{\sum_{k=1}^{N} A_{kj}(f)A_{kj}^{*}(f)}}, \tag{5.12}$$

where $A_{i,j}$ is the i,jth element of $A(f)$, $(.)^{*}$ denotes complex conjugation, and $A_{kj}(f)$ is the Fourier transformation of the coefficient matrices $A_{kj,r}$.

Baccald & de Medicina (2007) improved PDC in their further proposal, the squared Generalized Partial Directed Coherence (sGPDC). This connectivity estimate addresses the problem of dependency of PDC on a signal's dynamic ranges, the need to shift the emphasis from the sinks to the sources following the interest in neurophysiological applications, and increase sensitivity. It is defined by:

$$sGPDC_{j\to i}(f) = \frac{(\frac{1}{\sigma_i}\left|A_{ij}(f)\right|)}{\sqrt{\sum_{k=1}^{N} \frac{1}{\sigma_k^2}A_{kj}(f)A_{kj}^{*}(f)}}. \tag{5.13}$$

Analysis of connectivity on frequency and time to investigate the dynamical change of signal propagation leads to the development of short time PDC. It has already been applied in the motor task experiment (Kuś *et al.*, 2005) and in the analysis of EEG data from a newly born (Omidvarnia *et al.*, 2011).

In this study, the MVAR model of EEG signals obtained by 4 EEG electrodes is fitted to short data windows. A window size of 128 points length (256 ms) is shifted by 32 points (64 ms) consecutively. The 4 methods, DTFs, dDTFs, PDCs, and sGPDCs for each window time are computed over 1-60 Hz frequency range, and the causal connectivity of 5 clinical EEG frequency bands, delta, theta, alpha, beta and gamma are extracted.

To construct a specific threshold for discriminating between deterministic measurement of data connectivity and noise induced randomness, a surrogate data method based on

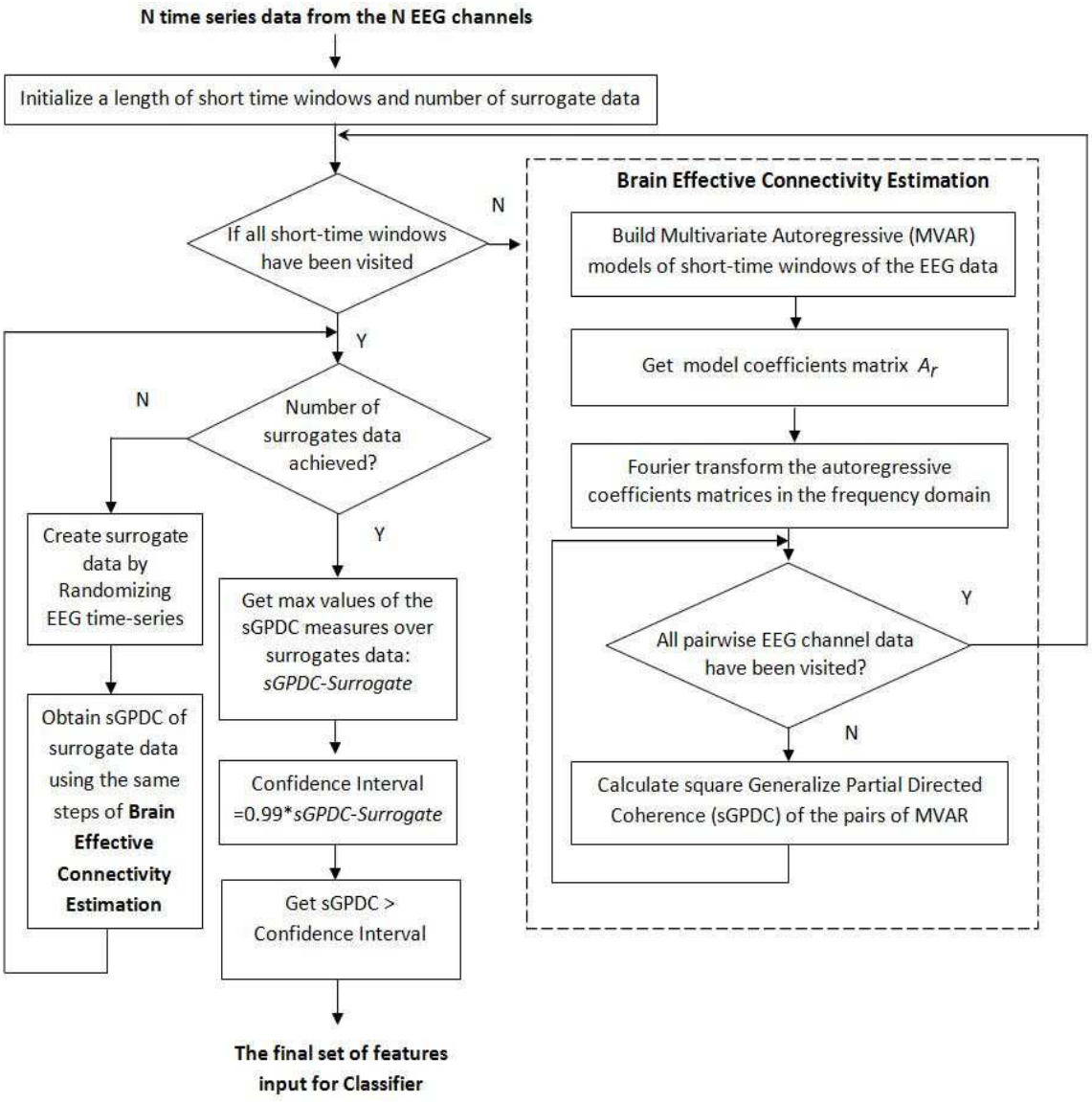

Figure 5.5: sGPDC Flowchart

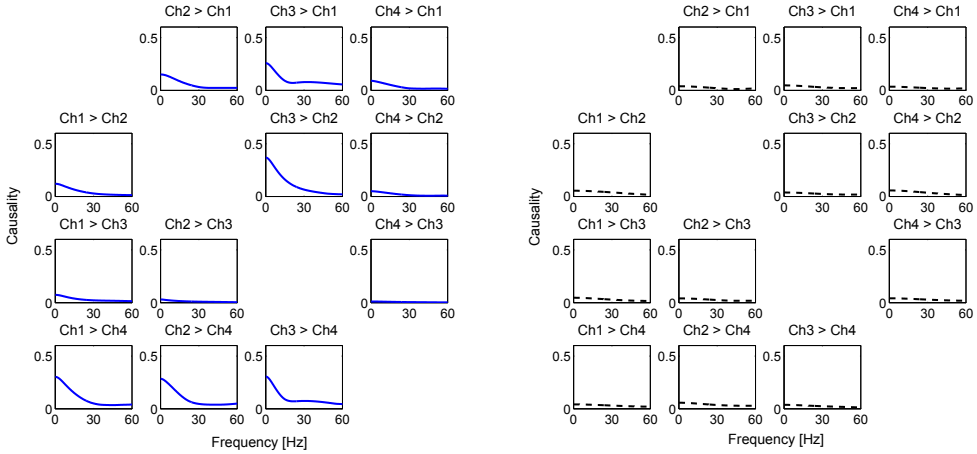

(a) Experimental data

(b) Surrogate data

Figure 5.6: sGPDC functions calculated for experimental data and surrogate data of subject 7. The results of surrogate data show the "leak flows" between channels, which determine the thresholds for considering the significant flows.

Theiler algorithm was used (Theiler *et al.*, 1992). The connectivity measured using surrogate data reflects the presence of correlations in the noise ("leak flows"), which always present even in the uncorrelated signals. The objective of this method is to compare the measured topological properties of an ensemble of random nondeterministic surrogate data sets to the measured topological properties of the experimental time series of data.

This algorithm estimates levels of confidence for causality measurement by constructing the FFT of the experimental time series data. Then, it applies a set of randomized phases to the FFT data. Finally, the surrogate data are obtained by constructing the invert FFT from the randomized data. This process destroys nonlinear-phase relations while maintaining the spectral properties of the original data sample (the same mean, variance and Fourier power spectrum). This process is repeated many times to estimate the thresholds for the function values. Only a directed causal influence which passed a test at the 99% level of significance based on these threshold values, indicating a less than 1% probability of occurrence by chance, are taken to the next process (Kus *et al.*, 2004).

The individual trial DTF, dDTF, PDC and sGPDC spectrograms are averaged within each subject and then averaged across all subjects within each group, for all directions of connectivity between pairs of electrode regions. These measures represent the strength and the number of causal interactions originating at each electrode, and provide a measure of

the source activity arising from each node in a network. Figure 5.6a shows sGPDC for the EEG data of subject 7 linearly transformed and their corresponding average of 20 sets of surrogate data (Fig. 5.6b) which was used to determine the significance of the data.

5.5 Feature Selection and Artificial Neural Networks Classification

In this study, the detection of FOG was based on the recognition of the brain connectivity alteration in EEG signals during the transition to freezing compared to normal waking. These changes were signified by the statistical properties of directed connectivity measures (the mean, the maximum and the minimum values of the 4 methods, DTF, dDTF, PDC and sGPDC) for each pairs of electrodes (without ICA) or components (with ICA). The characterization of brain connectivity patterns were then fed to the classifier to test whether the patterns differentiate between EEG signals of transition to FOG from those typical normal walking. Only features with a p-value <0.05 and r-value >0.2 tested using the non parametric Wilcoxon Sum Rank Test were chosen as input for the classifier.

For classification, MLP-NN was used because of its superior results in the classification of EEG signals (Lotte *et al.*, 2007). A 3-layer Back Propagation Neural Networks with 4 to 12 hidden nodes was built, corresponding to the architecture of 8 different networks. The best architecture was selected based on trial and error, starting from the smallest number. Early stopping was used to avoid over fitting (see 3.6.2), in which the training stopped mostly when the mean squared error reached the minimum performance value (0.01) or otherwise when the validation error failed to increase after 6 to 10 times. The performance of the proposed features in differentiating brain signals collected during normal walking from those collected during transition to FOG, was measured using sensitivity, specificity and accuracy. The average and standard deviation of 50 training and testing were recorded for further analysis.

5.5.1 Improving the Generalization Using Bayesian Regularization

ANNs are one of the most popular classifiers used with EEG signals, selected because of their highly non-linear characteristic, and do not require any relationship to the data (Lotte *et al.*, 2007). As a multilayer ANN can be highly prone to over fitting during the training period, it will not generalize well. Cross validated early stopping appears to be the most popular method of avoiding this over training problem. Yet, it has some drawbacks in the need to divide the data set into 3 subsets (training, validation and testing sets), thus restricting its use in systems with limited data.

Probabilistic interpretation of network training in the Bayesian regularization method provides a solution for this problem because it does not need a validation set. It modifies the objective function of the networks such as the sum of squared error (MSE)

$$F = E_d = \frac{1}{I}\sqrt{\sum_{i=1}^{I}(d_i - o_i)^2} \tag{5.14}$$

where E_d is the MSE, d_i is the desired output, and o_i is the actual output.

The regularization improves the model's generalization by adding the sum of squared weights, E_w, to the objective function component:

$$F = \beta E_d + \alpha E_W \tag{5.15}$$

where β and α are 2 Bayesian hyperparameters which indicate minimal error, and minimal weights to seek in the learning process. MacKay (1992) proposed the finding of the best generalization by optimizing these parameters in the Bayesian framework. To improve the efficiency of the optimization, Foresee & Hagan (1997) proposed to add the Bayesian regularization to the Levenberg-Marquardt and to use the Gauss-Newton approximation to the Hessian matrix, available in this optimization algorithm for learning. In this study, the Bayesian regularization was used to improve generalization, with 80% of the data trained by the Levenberg Marquardt algorithm and 20% of the data being used for testing.

5.6 Experimental Results

Estimate of BEC is based on the spectral analysis of the autoregressive (AR) model parameters, fitted to the EEG data. The MVAR model characterizes interregional dependence between data. Therefore, analysis of this model creates advanced measures of relations between signals of multichannel set, including an investigation of the influence between signals (causality). One important problem in the model parameters estimate is finding the optimal model order. Too low, the model is less fit, whilst a higher model order is prone to creating false signal components. In this study, SBC was used to select the model order for each data epoch separately, with orders range from 1 to 20. The minimum value of the criterion (Eq. (5.8)) indicates related model order is the optimal one (see Fig. 5.7). Model order varied between 2 to 6 in this study.

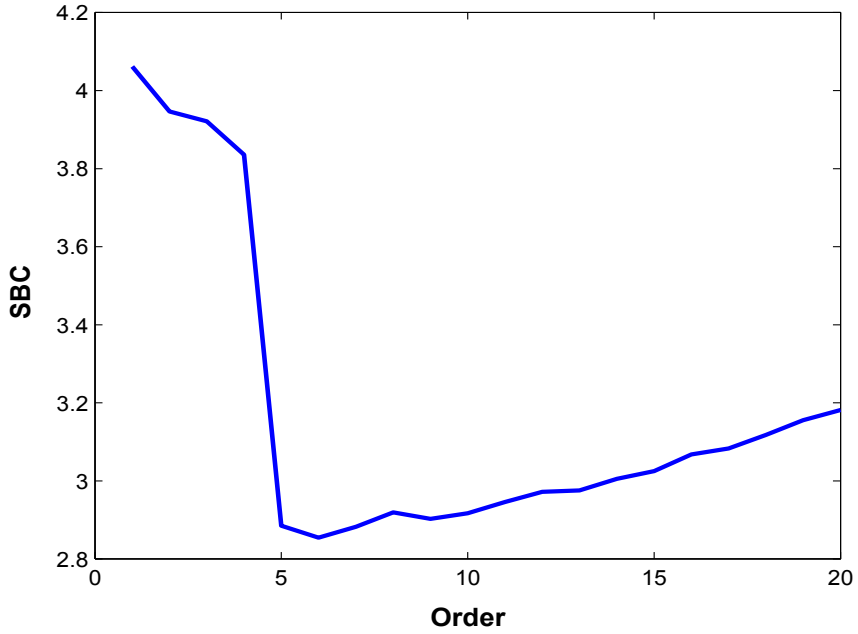

Figure 5.7: Optimal model order selection using SBC on the study data sample of transition condition in subject 1. The minimum value, 6, is the optimal model order.

Table 5.1 shows the result of the extraction of BEC using dDTF and sGPDC from all in group patients (11 patients) under 3 conditions in whole frequency band of interests (0-60 Hz). There was an agreement between the 2 methods in the significant alteration of information flow related to the central area during transition to FOG (O1 $\rightarrow$ Cz, P4 $\rightarrow$ Cz, Fz $\rightarrow$ Cz, Cz $\rightarrow$ O1, Cz $\rightarrow$ P4, Cz $\rightarrow$ Fz). Observation of the connectivity dynamic strength

indicated that during the transition to FOG, there was a relatively increase of information flow from central to frontal, occipital, and parietal. On the other hand, information flow to central from other locations of interest decreased.

Information transmission strength was subdued when patients experienced FOG, yet remaining significant in some connectivity (O1 $\rightarrow$ Cz, P4 $\rightarrow$ Cz, Fz $\rightarrow$ Cz, Cz $\rightarrow$ O1, Cz $\rightarrow$ P4). These dynamics are inline with the previous results in Chapters 3 and 4, where change of the signals during transition to FOG, is more significant than during FOG itself. The correlation analysis results offer further support to the central area as the best indicator of FOG neurophysiological processing.

Table 5.1: Correlation analysis of effective connectivity in 0.5-60 Hz frequency band between normal walking, transition to FOG, and FOG estimated by dDTF and sGPDC

	Source $\rightarrow$ Sink	Normal Walking	Transition to FOG	Freezing of Gait	N vs Tr	N vs FOG
	O1 $\rightarrow$ P4	0.0043 $\pm$ 0.0027	0.0046 $\pm$ 0.0036	0.0043 $\pm$ 0.0025		
	O1 $\rightarrow$ Cz	0.0052 $\pm$ 0.0033	0.0037 $\pm$ 0.0036	0.0043 $\pm$ 0.0034	**	*
	O1 $\rightarrow$ Fz	0.0045 $\pm$ 0.0027	0.0051 $\pm$ 0.0039	0.0042 $\pm$ 0.0030		
	P4 $\rightarrow$ O1	0.0052 $\pm$ 0.0027	0.0039 $\pm$ 0.0025	0.0043 $\pm$ 0.0026	**	*
	P4 $\rightarrow$ Cz	0.0060 $\pm$ 0.0049	0.0040 $\pm$ 0.0052	0.0052 $\pm$ 0.0061	**	*
dDTF	P4 $\rightarrow$ Fz	0.0053 $\pm$ 0.0033	0.0052 $\pm$ 0.0041	0.0054 $\pm$ 0.0035		
	Cz $\rightarrow$ O1	0.0048 $\pm$ 0.0025	0.0075 $\pm$ 0.0039	0.0059 $\pm$ 0.0031	**	*
	Cz $\rightarrow$ P4	0.0046 $\pm$ 0.0026	0.0078 $\pm$ 0.0037	0.0055 $\pm$ 0.0030	***	*
	Cz $\rightarrow$ Fz	0.0050 $\pm$ 0.0031	0.0078 $\pm$ 0.0039	0.0055 $\pm$ 0.0032	**	
	Fz $\rightarrow$ O1	0.0038 $\pm$ 0.0021	0.0033 $\pm$ 0.0022	0.0037 $\pm$ 0.0026	*	
	Fz $\rightarrow$ P4	0.0037 $\pm$ 0.0019	0.0034 $\pm$ 0.0021	0.0039 $\pm$ 0.0024		
	Fz $\rightarrow$ Cz	0.0036 $\pm$ 0.0020	0.0031 $\pm$ 0.0021	0.0032 $\pm$ 0.0021	*	*
	O1 $\rightarrow$ P4	0.0756 $\pm$ 0.0670	0.0988 $\pm$ 0.0852	0.0844 $\pm$ 0.0692	*	
	O1 $\rightarrow$ Cz	0.1139 $\pm$ 0.0962	0.0588 $\pm$ 0.0779	0.0865 $\pm$ 0.0838	**	*
	O1 $\rightarrow$ Fz	0.1027 $\pm$ 0.0704	0.1456 $\pm$ 0.1191	0.0983 $\pm$ 0.0818	*	
	P4 $\rightarrow$ O1	0.0955 $\pm$ 0.0698	0.0975 $\pm$ 0.0819	0.0915 $\pm$ 0.0735		
	P4 $\rightarrow$ Cz	0.1283 $\pm$ 0.1157	0.0752 $\pm$ 0.1105	0.1103 $\pm$ 0.1372	**	*
sGPDC	P4 $\rightarrow$ Fz	0.1112 $\pm$ 0.0744	0.1545 $\pm$ 0.1183	0.1233 $\pm$ 0.0840	*	
	Cz $\rightarrow$ O1	0.0845 $\pm$ 0.0654	0.1397 $\pm$ 0.1040	0.1100 $\pm$ 0.0853	**	*
	Cz $\rightarrow$ P4	0.0669 $\pm$ 0.0619	0.1324 $\pm$ 0.0917	0.0887 $\pm$ 0.0760	***	*
	Cz $\rightarrow$ Fz	0.1069 $\pm$ 0.0841	0.1681 $\pm$ 0.1004	0.1055 $\pm$ 0.0774	**	
	Fz $\rightarrow$ O1	0.0748 $\pm$ 0.0584	0.0837 $\pm$ 0.0814	0.0830 $\pm$ 0.0755		
	Fz $\rightarrow$ P4	0.0638 $\pm$ 0.0502	0.0776 $\pm$ 0.0743	0.0748 $\pm$ 0.0693		
	Fz $\rightarrow$ Cz	0.0712 $\pm$ 0.0527	0.0409 $\pm$ 0.0407	0.0541 $\pm$ 0.0487	**	*

$* = p \leq 0.05$ and $r < 0.2$
$** = p \leq 0.05$ and $0.2 \leq r < 0.4$
$*** = p \leq 0.05$ and $r \geq 0.4$

Figure 5.8 presents examples of sGPDC results from the EEG data in matrix layout plots and diagrams for patient 8. It depicts the causal influences of EEG signals from each channel location to the other channel locations. It shows the interaction of signals between

those 4 locations from four locations of interest from which EEG data were collected.

The causality measures obtained from surrogate data which reflecting the "leak flows" caused by noise between channels, were relatively small. This indicates that sGPDC was insensitive to artifact or noise which have no causal relationship with the signals. Interestingly, for this patient, while channel Cz has substantial influence over other channel locations and appears as the main source of activity during transition to FOG, it was relatively free of direct influence from other channels locations. The inflows to channel Cz during transition to FOG were below the threshold, as determined by surrogate data.

In the mapping the causality measures between signals in Fig. 5.8 (left column), the propagation of the low frequency bands signals was stronger than those of the high frequency bands. This indicates that the information flows between locations of interest during normal walking and transition to FOG were practically occur in the delta, theta, alpha and beta frequency band. There was no significant differences between flows for higher frequency band, except during transition to FOG, when here were strong information flows from Cz to other channel locations, in all frequency bands.

Before FOG, comparison of the connectivity between normal walking and transition to FOG, showed a significant increased of outflows from Cz to the other channel locations. On the other hand, inflows to Cz from other channel locations were decreased. There was a drop of activity in outflows to Fz from O1 and P4, but not from Cz. During transition to FOG, the reducing number of significant connectivity between channels indicated loss of connections between several locations of interest, anticipating the freezing episode.

Observation of the connectivity estimate in the overall data on more specific frequency band theta (4 - 8 Hz) also underlines the significant effective connectivity from central zero to the remaining of the location of interest (O1, P4, Fz), especially during the transition to freezing episode (Fig. 5.9, Fig. 5.10). This alteration of effective connectivity, shown in both dDTF and sGPDC (Fig. 5.11), may signify the overload of cognitive resources as a consequence of a loss of automaticity which shifted neural activation from the subcortical (basal ganglia) to more cortical areas (Shine *et al.*, 2011). The alteration of this connectivity appears to be the strongest indication of the freezing episode, whilst

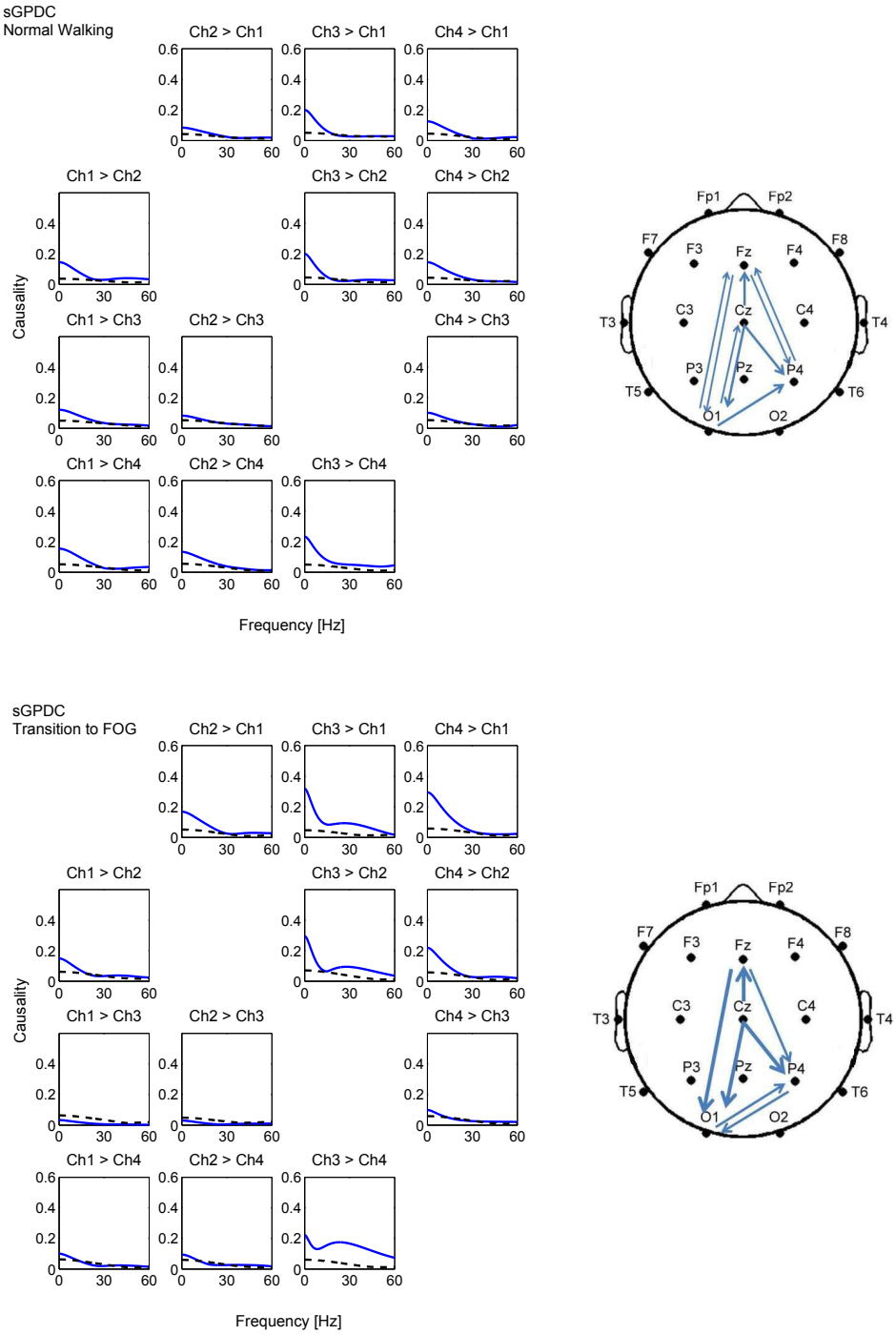

Figure 5.8: Information flow between locations of interest during normal walking and transition to FOG, estimated with the sGPDC function for 0.5-60 Hz frequency band in patient 8. The arrow width in the diagram (right column) depicts the connectivity strength between locations of interest.

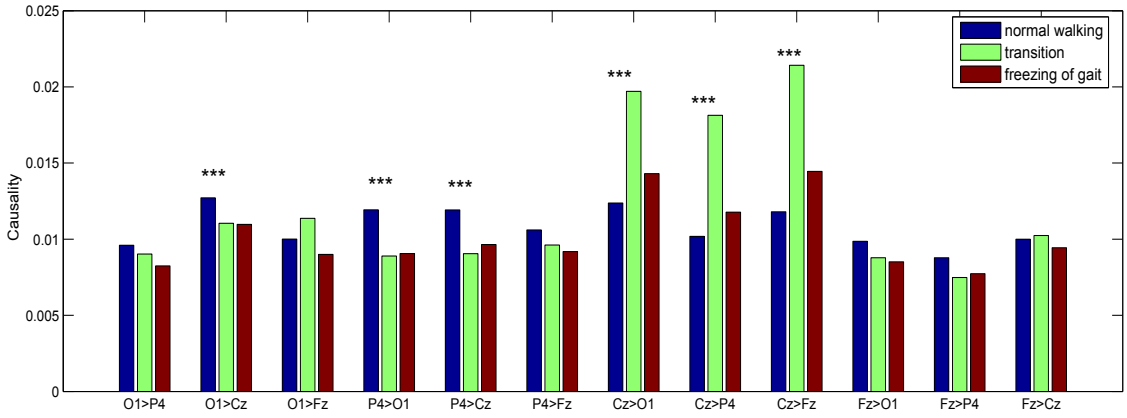

Figure 5.9: Causality values in the theta frequency bands of the overall population of subjects extracted using dDTF. The asterisk symbol indicates significant difference between normal waking and transition to freezing in the locations pair (p-value <0.05; r-value >0.2).

the change of effective connectivity at P4 $\rightarrow$ Cz, which also inline with earlier finding of the alteration of power spectral density at Cz during transition to freezing (Table 3.3).

The alteration of causal connectivity in electrode pairs involving Cz during transition to FOG in theta band frequency is in line with the results in the study of coherence in Chapter 4 (Figure 4.6, Figure. 4.7) where pair-wise O1-P4, O1-Cz and Cz-Fz appeared to change significantly during transition to FOG. The difference in this study is the ability of the BEC analysis to determine the direction of causality between the location pairs.

The application of ICA in data preprocessing aims to minimize the mutual information between signals. It is done by minimizing the statistical dependence between the components of the output vector Y from the input vector X to increase the separation between signal ICs. Consequently, instead of measuring the causal connectivity between locations of interests, this optimization provides analysis of causal connectivity between ICs.

Table 5.2 shows that this approach increases the level of significant difference between connectivity measurements. The dDTF and sGPDC algorithms extracted 6 strong connectivity alterations in the frequency range 0.5-60 Hz, which then were taken as inputs for the classifier.

Fig. 5.12 presents the comparisons of the BEC measured using dDTF and sGPDC with and without ICA. Effect size measures based on the Pearson correlation coefficient (r) is

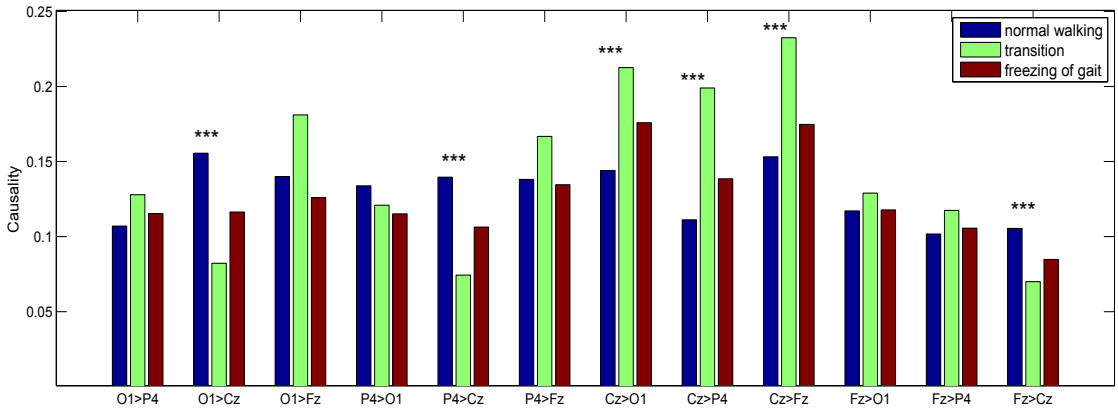

Figure 5.10: Causality values in the theta frequency bands of the overall population of subjects extracted using sGPDC. The asterisk symbol indicates significant difference between normal waking and transition to freezing in the locations pair (p-value <0.05; r-value >0.2).

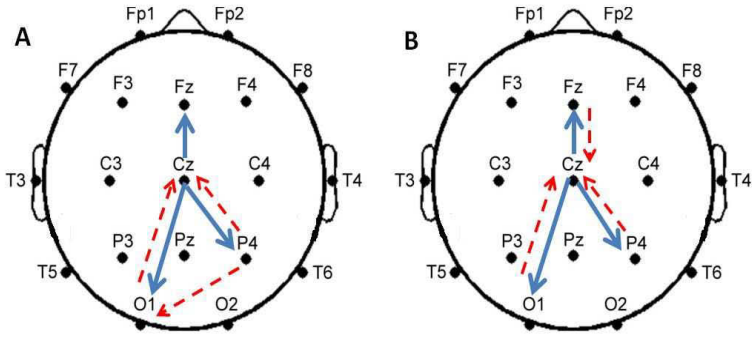

Figure 5.11: The schematic alteration interaction between 4 locations of EEG electrodes during normal walking and transition to FOG estimated using (A) dDTF and (B) sGPDC at theta band frequency. The solid line arrow represents the significant increase in connectivity strength and the dash line arrow indicates the significant decrease in connectivity strength.

Table 5.2: Correlation analysis of Effective Connectivity in the 0.5-60 Hz frequency band between normal walking, transition to FOG, and FOG estimated using dDTF and sGPDC with ICA

	Source → Sink	Normal Walking	Transition to FOG	Freezing of Gait	N vs Tr	N vs FOG
	IC1 → IC2	0.0080 ± 0.0029	0.0053 ± 0.0022	0.0064 ± 0.0025	***	*
	IC1 → IC3	0.0082 ± 0.0030	0.0058 ± 0.0024	0.0063 ± 0.0026	***	**
	IC1 → IC4	0.0078 ± 0.0027	0.0057 ± 0.0024	0.0067 ± 0.0026	***	*
	IC2 → IC1	0.0066 ± 0.0025	0.0096 ± 0.0030	0.0077 ± 0.0025	***	*
	IC2 → IC3	0.0066 ± 0.0025	0.0095 ± 0.0030	0.0077 ± 0.0026	***	*
dDTF	IC2 → IC4	0.0067 ± 0.0025	0.0100 ± 0.0032	0.0079 ± 0.0026	***	*
	IC3 → IC1	0.0069 ± 0.0025	0.0065 ± 0.0026	0.0087 ± 0.0030		
	IC3 → IC2	0.0067 ± 0.0024	0.0057 ± 0.0024	0.0090 ± 0.0031	*	**
	IC3 → IC4	0.0067 ± 0.0024	0.0060 ± 0.0024	0.0089 ± 0.0032	*	**
	IC4 → IC1	0.0066 ± 0.0025	0.0068 ± 0.0026	0.0067 ± 0.0025		**
	IC4 → IC2	0.0067 ± 0.0025	0.0063 ± 0.0027	0.0066 ± 0.0025		
	IC4 → IC3	0.0066 ± 0.002	0.0065 ± 0.0025	0.0064 ± 0.0025		
	IC1 → IC2	0.2121 ± 0.0951	0.1281 ± 0.0834	0.1904 ± 0.0924	***	*
	IC1 → IC3	0.2189 ± 0.0992	0.2193 ± 0.1064	0.1628 ± 0.0920		*
	IC1 → IC4	0.2055 ± 0.0958	0.2053 ± 0.1070	0.2327 ± 0.0958		*
	IC2 → IC1	0.1676 ± 0.0852	0.2525 ± 0.1069	0.2185 ± 0.0925	***	*
	IC2 → IC3	0.2159 ± 0.0920	0.2267 ± 0.1082	0.1643 ± 0.0939		*
sGPDC	IC2 → IC4	0.2123 ± 0.0960	0.2058 ± 0.1077	0.2310 ± 0.1004		*
	IC3 → IC1	0.1699 ± 0.0928	0.2524 ± 0.1054	0.2166 ± 0.0892	***	*
	IC3 → IC2	0.2127 ± 0.0986	0.1309 ± 0.0837	0.1922 ± 0.0900	***	*
	IC3 → IC4	0.2106 ± 0.0974	0.2060 ± 0.1053	0.2278 ± 0.1008		
	IC4 → IC1	0.1682 ± 0.0927	0.2525 ± 0.1054	0.2138 ± 0.0895	***	*
	IC4 → IC2	0.2130 ± 0.0965	0.1294 ± 0.0842	0.1973 ± 0.0928	***	
	IC4 → IC3	0.2157 ± 0.09703	0.2211 ± 0.1012	0.1688 ± 0.0942		*

$* = p \leq 0.05$ and r < 0.2
$** = p \leq 0.05$ and $0.2 \leq$ r < 0.4
$*** = p \leq 0.05$ and r ≥ 0.4

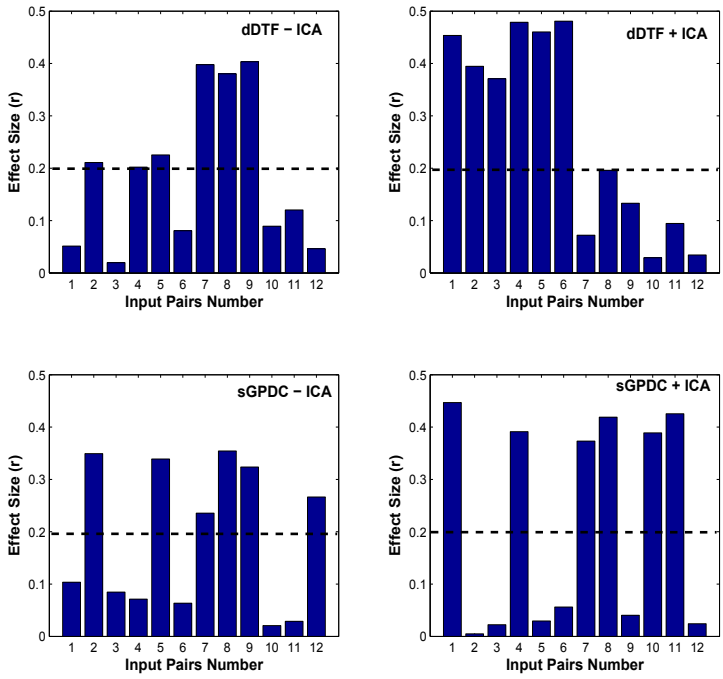

Figure 5.12: Comparison of the levels of separation of BEC features extracted from EEG data during normal walking and transition to FOG using dDTF (top row) and sGPDC (bottom row), without ICA (left column) and with ICA (right column) measured with Pearson's correlation coefficient *r*.

a quantitative measure of the strength and direction of relationship between 2 variables (Ellis, 2010). A larger value of absolute effect size indicates a stronger difference between 2 different groups (Sullivan & Feinn, 2012). It is clear that applying ICA as data preprocessing increased separation of signals of normal walking and those of transition to FOG, reflected by larger *r*-value in data preprocessed using ICA (right column). In the case of dDTF, the increasing separation also increased the number of connectivity measures which fulfill the threshold (p-value <0.05 and r-value >0.2) and were taken as input for the classifier.

A neural network structure of N inputs nodes, comprising 4 to 12 hidden nodes, and 1 output node was developed as the classification unit for detection of FOG. The N input varied for each of the 4 methods, DTF, dDTF, PDC, and sGPDC. It was determined by the number of extracted features which display significant differentiation between the transition to FOG and the normal walking conditions. Table 5.3 presents the results of the

analysis of the neural networks based classification system using sGPDC preprocessed by ICA as a input parameter, and trained using Bayesian regularization. It presents the mean values which were calculated by averaging over 50 runs. It shows that as the number of hidden nodes was increased from 1 to 12, accuracy increased, and at 12 nodes, it attained the best accuracy of 90.15% in in-group data testing and 89.52% in out-group data testing. No significant statistical enhancement occurred when the number of hidden nodes was increased further. Thus, the final neural networks structure of 12 hidden nodes was derived.

Table 5.3: Comparison between classification performance of the neural network structure of 1 to 20 hidden nodes with input sGPDC+ICA+BR

Number of	Testing: in-group			Testing: out-group		
hidden nodes	Sen. (%)	Spe. (%)	Acc. (%)	Sen. (%)	Spe. (%)	Acc. (%)
1	88.48	87.74	88.11	84.30	88.89	86.67
2	90.32	86.39	88.36	87.42	88.52	87.79
3	90.37	86.72	88.54	86.20	87.83	86.91
4	89.23	89.60	89.41	84.23	90.49	87.59
5	86.04	89.27	89.34	86.83	91.73	89.22
6	89.37	88.67	89.02	86.03	90.33	88.20
7	89.27	88.81	89.04	85.57	90.63	88.16
8	89.74	87.72	88.73	87.04	89.61	88.27
9	88.79	89.72	89.25	85.88	90.90	88.37
10	89.39	89.79	89.59	86.17	90.91	88.50
11	89.53	89.46	89.50	86.87	90.18	88.54
12	**89.11**	**91.20**	**90.16**	**86.47**	**92.75**	**89.52**
13	88.86	90.72	89.79	86.94	91.06	88.84
14	89.00	90.11	89.55	85.92	90.53	88.20
15	89.11	90.74	89.93	85.08	91.70	88.27
16	88.90	90.67	89.79	86.25	92.05	89.11
17	88.95	91.41	90.18	85.12	92.98	88.98
18	89.11	90.86	89.98	84.83	92.67	88.74
19	89.41	90.25	89.83	86.02	90.26	88.03
20	88.86	90.34	89.60	85.50	92.90	89.15

Four classifier algorithms were used: (1) non-ICA preprocess data as input with early stopping training, (2) non-ICA preprocess data as input with Bayesian regulation training, (3) ICA preprocess data as input with early stopping training, and (4) ICA preprocess data as input with Bayesian regularization.

Table 5.4 presents classification results of the first algorithm. It shows the feasibility of

Table 5.4: Classification results of the neural network with BEC as feature, using early stopping in training, to detect the 5 s transition before freezing in normal walking

			DTF	dDTF	PDC	sGPDC
In-group (11 patients)	Training	Sen. (%)	78.40	79.17	79.43	79.45
		Spe. (%)	77.89	79.71	76.82	74.38
		Acc. (%)	77.97	79.34	78.05	76.94
	Validation	Sen. (%)	67.31	69.25	71.00	70.63
		Spe. (%)	65.08	69.70	68.21	65.30
		Acc. (%)	66.68	70.35	69.84	68.03
	Testing	Sen. (%)	64.67	67.84	69.40	68.80
		Spe. (%)	64.90	67.38	65.91	62.79
		Acc. (%)	64.32	67.33	67.53	65.71
Out-group (5 patients)	Testing	Sen. (%)	64.95	73.67	59.14	65.44
		Spe. (%)	57.44	64.26	61.09	60.98
		Acc. (%)	61.20	68.97	60.12	63.21

BEC feature in distinguishing the transition to FOG episode from the normal walking episode. The improvement of methods in dDTF from DTF and sGPDC from PDC also resulted in the improvement of their strength when they were used as features to detect FOG especially when the classifier system was tested with out-group data. The best result in generalization was achieved when using dDTF as feature with sensitivity and accuracy are 73.67% and 68.97%, respectively.

Table 5.5 presents the results of the optimization strategy using (a) Bayesian regularization in training to improve generalization, and (b) ICA in preprocessing data to increase the separation between signals. There was a significant performance improvement of the classifier system using the ICA in preprocessing data. It offered a marked increase of sensitivity, specificity and accuracy compared with using Bayesian regularization. While the performance of system using dDTF and sGPDC was comparable when optimized using Bayesian Regularization in training, the classifier system using the sGPDC measure as input provided the best performance in testing, in both the in-group patients and the out-group patients, with 85.43% and 85.08% accuracy, and 84.28% and 80.60% specificity, respectively.

Additional significant performance improvement was achieved when both types of optimization were combined and used together in the classification. Table 5.6 (compared to

Table 5.5: Classification results of the neural network using BEC as the features, optimized by using Bayesian regularization in training or ICA data preprocessing

				DTF	dDTF	PDC	sGPDC
Bayesian Regularization training	In-group (11 patients)	Training	Sen. (%)	82.14	81.33	89.68	88.91
			Spe. (%)	82.00	84.45	85.78	85.55
			Acc. (%)	82.07	82.91	87.73	87.25
		Validation	Sen. (%)	na	na	na	na
			Spe. (%)	na	na	na	na
			Acc. (%)	na	na	na	na
		Testing	Sen. (%)	72.68	79.53	77.13	73.84
			Spe. (%)	71.12	74.26	69.92	72.1
			Acc. (%)	71.75	74.65	73.22	71.69
	Out-group (5 patients)	Testing	Sen. (%)	72.09	68.61	65.12	71.76
			Spe. (%)	56.59	69.77	62.33	68.49
			Acc. (%)	64.34	71.3	63.72	71.16
ICA preprocessing data	In-group (11 patients)	Training	Sen. (%)	94.48	94.98	92.89	96.25
			Spe. (%)	97.20	96.14	91.28	97.67
			Acc. (%)	95.83	95.52	92.07	96.93
		Validation	Sen. (%)	83.85	85.56	81.15	87.08
			Spe. (%)	88.54	87.97	79.39	88.30
			Acc. (%)	86.41	86.84	80.24	87.84
		Testing	Sen. (%)	82.3	84.69	78.48	84.28
			Spe. (%)	85.51	85.74	75.33	86.66
			Acc. (%)	83.71	85.08	76.86	85.43
	Out-group (5 patients)	Testing	Sen. (%)	84.09	81.33	81.37	80.60
			Spe. (%)	82.21	82.40	73.05	89.56
			Acc. (%)	83.15	81.86	77.21	85.08

Table 5.4) shows the application of ICA and Bayesian regularization results in a significant increase of 68.80% to 89.11% in sensitivity, and an increase of 65.71% to 86.47% in accuracy, when using sGPDC as a feature input in the testing of the in-group patients. When the classifier system was tested in the out-group patients, there was an increasing of 65.44% to 90.16% in sensitivity, and 63.21% to 89.52% in accuracy. These results, with approximately 1% difference in accuracy, indicates the method improved generalization. Lastly, using sGPDC as input, provided stronger signals of FOG compared to using PDC, but it was only slightly better, compared to DTF and dDTF. However it has the advantage of faster processing because it does not use the inversion of matrix A as required to calculate DTF and dDTF.

Table 5.6: Classification results of the neural network using BEC as the features, optimized by using Bayesian regularization in training and ICA data preprocessing at a time.

			DTF	dDTF	PDC	sGPDC
In-group (11 patients)	Training	Sen. (%)	90.59	90.63	87.84	88.98
		Spe. (%)	95.40	95.99	91.97	95.93
		Acc. (%)	93.02	93.31	89.92	92.49
	Validation	Sen. (%)	na	na	na	na
		Spe. (%)	na	na	na	na
		Acc. (%)	na	na	na	na
	Testing	Sen. (%)	85.26	85.67	85.97	89.11
		Spe. (%)	92.12	94.70	86.88	91.20
		Acc. (%)	88.47	90.11	85.45	90.16
Out-group (5 patients)	Testing	Sen. (%)	84.46	85.89	79.46	86.47
		Spe. (%)	93.72	91.12	84.92	92.75
		Acc. (%)	89.09	88.51	82.99	89.52

5.7 Discussion and Conclusion

The primary objective of the study in this chapter is to increase the performance of detection of FOG using brain signal dynamics, by means of effective connectivity and ICA in Parkinson's disease patients. Using BEC as a feature allows the extraction of dynamic brain information which integrates spatial, spectral and temporal information. Applying ICA to the EEG signals opened a way to analyze ICs related with FOG in order to develop a better model for the symptom. It has already been successfully applied in previous studies investigating other conditions (Ding & Lee, 2013), (Demirci *et al.*, 2009).

More recent BEC analysis methods (dDTF, PDC, sGPDC) which were introduced as an improvement of the previous method (DTF) generally achieved better classification results (Table 5.3). However, when using ICA, the results of this study show a different trend. Classifier results acquired with DTF as a feature were relatively better than PDC, and were comparable to dDTF and sGPDC. These results indicate that by providing ICs as an input for BEC instead of the original "mixed" EEG signal captured in regions of interest, ICA may enhance the analysis of the direct flows between components as well as reduce the influence of noise.

ICA has been used previously for identifying and removing artefacts. It has been reported to improve the classification performance during preprocessing when compared to systems without ICA (Melissant *et al.*, 2005; Molavi & Bin Yunus, 2012). This study demonstrates the benefit of decomposing multivariate EEG signals into their additive non-gaussian subcomponents which maximized separation between ICs before extracting the effective connectivity for classification. The performance of the classifier increased in all the parameters that are used, obtaining significantly higher sensitivity, specificity and accuracy.

Furthermore, used together with Bayesian regularization in classifier training, there was marked improvement in the classification performance of both in-group and out-group patients. Chapter 3 (Table 3.4) reported that using centroid frequency as the input feature in the mean classification of 50 running times, in the in-group testing data set, obtained 76.69% sensitivity and 79.54% accuracy. With the out-group testing data set, the MLP classifier obtained 75.21% sensitivity and 79.91% accuracy. Chapter 4 (Table 4.5) presented that the inclusion of spatial brain dynamic information through spectral coherence analysis improved the performance of the classifier algorithm. Simultaneous use of wavelet cross correlation and wavelet energy as input classifiers resulted in 82.33% sensitivity and 87.06% accuracy in the in-group testing data set. The MLP classifier obtained 81.78% sensitivity and 82.07% accuracy when it is tested in the out-group testing set.

The proposed FOG detection method using BEC optimized with ICA and Bayesian regularization provides significant improvement of the system. Using sGPDC to extract the strength of causality values between inputs signals, the system provided 89.11% sensitivity and 90.16% accuracy in the in-group testing data set, and 86.47% sensitivity and 89.52% accuracy in the out-group testing data set. This supports the proposed BEC+ICA+Bayesian regularization strategy as an effective enhancement in the performance of the classifier. There was no significant difference in the classifier performance between in-group and out-group testing data. This support the optimization of information separation using ICA and generalization of training using Bayesian regularization eliminate the variability of EEG signals in patients.

Lastly, the brain connectivity analysis in Chapter 4 and this Chapter 5 proposes further insight into the pathophysiology underlying the freezing phenomenon (Shine *et al.*, 2014). In particular, the large increase in theta activity in the Cz electrode, located above the Motor cortex (Table 3.3), spreads to the Fz electrode when the patient experiences difficulty in starting or continuing the movement (Figure 4.6 and 5.8). This may reflect increased theta activity in the pre-supplementary motor area (pSMA) which controls stability during walking, coordinates sequences of movements, prepares and executes voluntary movements as well as linking cognition to action (Penfield & Welch, 1951; Nachev *et al.*, 2008; Arai *et al.*, 2012). The association of freezing behavior in PD with a paroxysmal increase in 5-7 Hz (i.e. theta) oscillation has been reported in many clinical studies (Gatev *et al.*, 2006), (Follett & Torres-Russotto, 2012). Figure 5.13 proposes that the predicted mechanism underlying FOG.

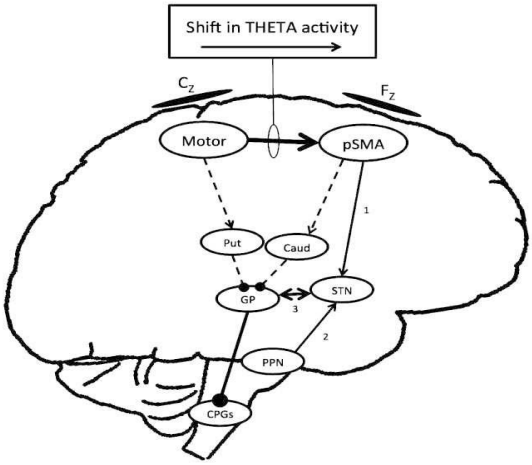

Figure 5.13: Graphical depiction of the predicted mechanism underlying FOG (Shine *et al.*, 2014).

Motor blocking in freezing may appear as a result of the dysfunctional caudate (a "sensory" component of the basal ganglia which integrates sensory information from visual, somatosensory, and auditory inputs), with freezing-related decreases of glucose and fluro-L-dopa uptake in the right anterior parietal cortex is indicated (Bartels *et al.*, 2006). The increase of connectivity strength between central to parietal during transition to FOG (Fig. 5.11) suggests that FOG is related to this sensory over-load in environments with complex visual stimuli leads to FOG (Moreau *et al.*, 2007).

Chapter 6

Discussion and Future Work

"The most important thing is to bring people with Parkinson's into our world and for the public to have a real understanding of it, as they're beginning to have with autism".
-Helen Mirren

6.1 Discussion

As people live longer and many countries have an ageing population because of the improvements in nutrition, public health and medicine, more individuals will be affected by PD, and consequently, FOG.

FOG is a common gait deficit in persons with advanced PD. During FOG, abruptly, patients would lose their ability to initiate or continue gait. Often it is experienced as if the feet are glued to the floor (Nutt *et al.*, 2011b). Found in a majority of advanced PD patients, it presents in up to 53% of the population after 5 years of illness, especially in those with Hoehn Yahr stages 3 and 4 (Okuma, 2006; Niewboer *et al.*, 2004). However, a study shows that up to 26% of patients experienced FOG in the early stages of PD (Moore *et al.*, 2008).

Inability to move forward disturbs balance and is connected with an increased number in falls for PD patients, resulting in injuries and creating a loss of independence for these patients. These physical and psychosocial consequences in turn reduce the quality of life

for patients with PD, making FOG a highly important symptom to study (Moore *et al.*, 2007).

Investigating FOG is difficult due to its paroxysmal and unpredictable nature (Giladi & Niewboer, 2008). Important aspects of the underlying pathophysiology of FOG (for example, the important role of temporal information processing between neural circuits associated with freezing), remain unclear (Shine *et al.*, 2013a). Treatment options offer limited benefit (for example, non invasive treatments and cueing strategies only offer limited relieve to the patients and often lose their effect over time). Furthermore, currently, no device or mechanism can detect FOG effectively before it occurs, to allow time for a sufferer to avert a freezing episode.

The likelihood of an increased proportion of the population experiencing PD and FOG which diminish patient quality of life, the current lack of complete therapeutic or other relief, calls for novel therapies that can predict the freeze and prevent falls. This thesis has chosen to investigate the effectiveness of brain signal dynamics to predict the onset of freezing at the earliest possible time because of their ability to measure dynamic physiological change in the brain before movement disturbances occur.

The objective of this thesis is to develop new methodologies to detect FOG through the automatic interpretation of brain data associated with FOG in PD patients. The investigation addresses 2 main concerns: (a) finding indicators in EEG signals which signify transition from normal walking to FOG; (b) detecting FOG using classifier system that applies the representation of the time, frequency, and space domain characteristics of EEG signals. The investigation finds using neural network algorithm and brain effective connectivity measures, optimized by ICA, provides an advanced non-invasive detection method, with high accuracy in FOG prediction.

The investigation detected significant brain activity change in the brain's central area relates to FOG. Investigation over the power spectral of 4 locations of interest reveals the significant alteration of power spectral density and spectral centroid frequency shifting in this area. The performance of classifier using PSD, SCF and PSE from centroid zero channel only, supports this finding.

The coherence analysis uncovers the frontocentral functional connectivity alteration during transition to FOG. The significant increase of information flows from central to the other location of the brain shown in the brain effective connectivity analysis, supports this finding. It points to the area for further investigation and for development of the mechanism to predict underlying FOG followed through this thesis.

A neural network-based classifier is used as a computational algorithm to predict FOG by detecting the transition to FOG episode. Input classifier which characterized FOG from the basic power spectral density to the advanced power measurement application in autoregressive model of EEG to analyze effective connectivity between locations of interest are explored. The strength of those EEG characteristic in differentiate normal walking from transition to FOG is investigated. The best experiment results of the detection of FOG in each proposed methods are presented in Table 6.1.

Table 6.1: Best performance of proposed methods in detecting transition 5 s before freezing from normal walking

Features - Classifier		Sensitivity (%)	Specificity (%)	Accuracy (%)
CF + ANN	Training	78.68	80.23	79.37
	Validation	78.72	76.51	79.32
	Testing - Ingroup	76.69	74.05	79.54
	Testing - Outgroup	75.21	80.65	79.91
WCS,WE + ANN	Training	86.82	92.69	89.78
	Validation	83.87	91.74	87.85
	Testing - Ingroup	83.22	91.50	87.06
	Testing - Outgroup	72.36	81.78	77.07
ICA + sGPDC + ANN(BR)	Training	88.98	95.93	92.49
	Testing - Ingroup	89.11	91.20	90.16
	Testing - Outgroup	86.47	92.75	89.52

CF: Centroid Frequency; ANN: Artificial Neural Networks;
WCS: Wavelet Cross Spectral; WE: Wavelet Energy;
ICA: Independent Component Analysis; sGPDC: squared Generalized Partial Directed Coherence; BR: Bayesian Regularization

Power spectral density is one of the most popular features for extracting information of the brain condition. It shows distribution of energy over the frequency. This measure has been proven to be effective in detecting transients in many different signals. The proposed methodology for FOG detection using EEG signals and neural networks classifier were shown to produce acceptable classification results when using power spectral density extracted from 4 channels (O1, P4, Cz and Fz) as input. It is obtained classification performance of 78.68 % and 70.62 % accuracy when tested in in-group and out-group

testing data set, respectively.

The performance of the neural networks-based classifier, trained by Levernberg-Marquardt, provides better accuracy of the FOG detection when using CF as input of the classifier extracted from channel Cz. It is obtained classification performance of 79.54% and 79.91% accuracy when tested in in-group and out-group testing data set, respectively. Using more recent method in transforming time series signals to frequency domain, wavelet transformation, a FOG detection system provides a significant improvement in term of sensitivity. Using WE from all four channels as feature inputs, the neural networks based classifier provides the highest sensitivity of 86.00% when tested using in-group testing data set, with specificity of 74.43%.

The segregated spectral features characterize signals based on the information extracted in time and frequency domain. Brain functions are examined exclusively as an intrinsic feature of isolated network nodes as EEG features are extracted by computed on each EEG channel separately. Thus, this method does not provide information of the interrelations between signals reflecting neural activity which may indicate a pathophysiology of FOG. In order to extract the information regarding the synchronization between signals, to improve the performance of the FOG detection, more advanced feature extraction techniques named cross spectral, coherence and phase synchrony are explored. These connectivity measures are based on the application of cross power spectral in pairwise of channel to reveal the interdependency strength between two simultaneously measures EEG signals. By utilizing advantage of synchronization measures in extracting information in spatial domain and capturing interdependency between signals, the neural networks based classifier is shown to increase significantly the classification performance. When information of correlation between channel Cz-Fz and P4-Cz are used as input combined with wavelet energy extracted from all four channels, the classification result are 83.22% sensitivity and 87.06% accuracy on the in-group testing data set, and 72.36% sensitivity and 77.07% accuracy on the out-group testing data set.

In order to further enhance the performance of FOG detection and overcome the inability of ordinary coherence analysis in capturing the dynamical process operating on the anatomical structure beyond the correlation, a brain effective connectivity based on partial

coherence strategy is applied in this thesis. Unlike ordinary coherence, partial coherence is non zero only for direct relations between channels, while any signal which appeared as a result of indirect relations between channels will be low. The squared generalized partial directed coherence (sGPDC) applies the concept of Granger causality in full multivariate spectral measure to capture the transmission of information strength between different channel locations. This effective connectivity is used as input for the FOG detection.

FastICA is applied in this thesis to improve input recognisability through maximizing the separation between the component of the classifier input, leading to increasing classifier system performance. It uses *negentropy* to maximizing non-Gaussianity of the extracted independent components from the original EEG data. This pre-processing data allows source separation from a multivariate signals which reveals hidden factors underlying signals in extracted additive subcomponents. The effective connectivity analysis on the more precise sources signals enhances the identifiability of transition to FOG in the neural networks-based classifier. To further enhance the performance of the classifier, Bayesian regularization is used in the training process of the Levenberg-Marquardt. Unlike early stopping, it does not need validation set, so that it optimized the uses of all collected data.

6.2 Conclusion

This thesis has presented the contributions to FOG detection technology. Several EEG parameters appear as the indicators of FOG has been investigated into a better understanding of FOG. A model of pathophysiological underlying FOG has been proposed based on this study. It emphases the alteration of information flow in theta frequency band, related to motor cortex and pre-supplementary motor area (pSMA), which controls stability during walking, coordinates sequences of movements, prepares and executes voluntary movements as well as linking cognition to action.

A final advanced FOG detection algorithm using ICA and brain effective connectivity is proposed. With the data from 16 PD patients who participated in the FOG study, the neural networks based classifier using sGPDC of EEG data preprocessed by fast ICA, trained by the Levenberg-Marquardt and applying Bayesian regularization is shown to achieve

significant improvement of classification performance. This method provides 89.11% sensitivity and 90.16% accuracy on the in-group testing data set, and 86.47% sensitivity and 89.52% accuracy on the out-group testing data set. These results demonstrate that the proposed BEC+ICA+Bayesian regularization strategy is an effective method for detecting FOG using EEG data.

6.3 Future Directions

The FOG detections in this thesis have focused on episodes of freezing that had mixed provocation factors. The future works should extend the study into 5 subtypes FOG based on their trigger factors: starting, turning, walking in narrow quarters, upon reaching destination and stressful situations such as mental overload (Giladi & Niewboer, 2008). Different mechanisms responsible for different subtypes of FOG and might reflected different pathophysiologies. Thus, they are correlated with different brain activity patterns. FOG study by Fling *et al.* (2013) found the general trend of the reduced connectivity in the right hemisphere's locomotor networks of the patient with FOG involving frontal and prefrontal cortical areas. However, they also presented different characteristic of brain connectivity for two different tasks related to FOG, the Stroop conflict task and the Flanker's congruent task. Schaafsma *et al.* (2003) also shows different FOG subtypes response differently to levodopa medication during a walking task, highlighting the need to find more precise characterization of EEG signals for each subtype of FOG. This expanded approach to include 5 different subtypes of FOG rather than 1 general type of FOG will add complexity of the classification system, yet it will lead to a further improvement of the classifier's performance. Our group has started this further step by studying turning freeze (Handojoseno *et al.*, 2015b).

The study on the EEG signals related to FOG provides an insight into effective features that can be used to characterize FOG. Feature extraction greatly affects the accuracy of the detection system. The better extracted features, the higher the performance of classification methods. The advanced FOG detection based on the effective connectivity required the using of all proposed four channels (O1, P4, Cz, Fz). The using of ICA to find the

independent components from these channels before quantifying the time varying interaction in the frequency domain using sGPDC, are proved to provide strong features as inputs of the classification algorithm. In the future, the application of PCA for dimension reduction and the using of fewer channels which might provide higher portability, computational efficiency and complexity, noise resilience, and performance of the system, can be explored. In addition, the exploration and the integration of different aspects of brain dynamics which significantly marking the FOG episode may also contribute to further improvement of the FOG detection system.

Standard ANN with Bayesian regularization for training has been employed as a classifier. With current inputs based on the extraction of brain effective connectivity on the independent components of the EEG processed by ICA, the FOG detection yields satisfactory performance. This shows the strength of ANN as a classifier in the detection of FOG in PD patients as well as ICA as a preprocessing signals and brain effective connectivity as features. The development of more advanced classifier could be further explored to improve the performance of the FOG detection system. It can be done by applying different methods of regularization in training, by applying various advanced Neural Networks such as deep neural networks and spiking neural network, or by combining ANN with other computational intelligence such as fuzzy logic, evolutionary computation and swarm intelligence.

Mechanism responsible for the FOG is still unclear. All proposed models (Table 2.1) are likely to play a role in the occurrence of FOG (Nieuwboer & Giladi, 2013b). While our study has obtained several finding on the characterization of FOG which are in line with previous studies of FOG, more rigorous evaluations and descriptions of some EEG patterns with respect to the normal condition are needed.

Improving efficiency of the methods in balance to the high level of accuracy and sensitivity is one of the main tasks for the future. Further validation involving a larger number of patients is also required, before the translation of the methods studied in this thesis into a practical FOG detection system.

Appendix A Research Ethics Clearance

Appendix A. Research Ethics Clearance

HREC RESPONSE 141125

HREC – 2014/255

NHMRC APP1062319 LEWIS

Dear Applicant

[External Ratification: University of Sydney HREC - 2014/255 - 23/04/2014-23/04/2018]

The UTS Human Research Ethics Expedited Review Committee reviewed your application titled, "Understanding and predicting freezing of gait in Parkinson's Disease", and agreed that the application meets the requirements of the NHMRC National Statement on Ethical Conduct In Human Research (2007). I am pleased to inform you that your external ethics approval has been ratified.

Your approval number is UTS HREC REF NO. 2014000723

Please note that the ethical conduct of research is an on-going process. The National Statement on Ethical Conduct in Research Involving Humans requires us to obtain a report about the progress of the research, and in particular about any changes to the research which may have ethical implications. This report form must be completed at least annually, and at the end of the project (if it takes more than a year). The Ethics Secretariat will contact you when it is time to complete your first report.

I also refer you to the AVCC guidelines relating to the storage of data, which require that data be kept for a minimum of 5 years after publication of research. However, in NSW, longer retention requirements are required for research on human subjects with potential long-term effects, research with long-term environmental effects, or research considered of national or international significance, importance, or controversy. If the data from this research project falls into one of these categories, contact University Records for advice on long-term retention.

You should consider this your official letter of approval. If you require a hardcopy please contact Research.Ethics@uts.edu.au.

To access this application, please follow the URLs below:
* if accessing within the UTS network:
http://rmprod.itd.uts.edu.au/RMENet/HOM001N.aspx
* if accessing outside of UTS network:
https://remote.uts.edu.au , and click on "RMENet -

Appendix A. Research Ethics Clearance

ResearchMaster Enterprise" after logging in.

We value your feedback on the online ethics process. If you would like to provide feedback please go to:
http://surveys.uts.edu.au/surveys/onlineethics/index.cfm

If you have any queries about your ethics approval, or require any amendments to your research in the future, please do not hesitate to contact Research.Ethics@uts.edu.au.

Yours sincerely,

Professor Marion Haas
Chairperson
UTS Human Research Ethics Committee
C/- Research & Innovation Office
University of Technology, Sydney
T: (02) 9514 9645
F: (02) 9514 1244
E: Research.Ethics@uts.edu.au
I:
http://www.research.uts.edu.au/policies/restricted/ethics.html
P: PO Box 123, BROADWAY NSW 2007
[Level 14, Building 1, Broadway Campus]
CB01.14.08.04

E:13

Appendix B Publications

Analysis and Prediction of the Freezing of Gait using EEG Brain Dynamics

A. M. Ardi Handojoseno, *Student Member, IEEE*, James M. Shine, Tuan N. Nguyen, *Member, IEEE*, Yvonne Tran, Simon J. G. Lewis, Hung T. Nguyen, *Senior Member, IEEE*

***Abstract*—Freezing of Gait (FOG) is a common symptom in the advanced stages of Parkinson's disease (PD), which significantly affects patients' quality of life. Treatment options offer limited benefit and there are currently no mechanisms able to effectively detect FOG before it occurs, allowing time for a sufferer to avert a freezing episode. Electroencephalography (EEG) offers a novel technique that may be able to address this problem. In this paper, we investigated the univariate and multivariate EEG features determined by both Fourier and wavelet analysis in the confirmation and prediction of FOG. The EEG power measures and network properties from 16 patients with PD and FOG were extracted and analyzed. It was found that both power spectral density and wavelet energy could potentially act as biomarkers during FOG. Information in the frequency domain of the EEG was found to provide better discrimination of EEG signals during transition to freezing than information coded in the time domain. The performance of the FOG prediction systems improved when the information from both domains was used. This combination resulted in a sensitivity of 86.0%, specificity of 74.4%, and accuracy of 80.2% when predicting episodes of freezing, outperforming current accelerometry-based tools for the prediction of FOG.**

***Index Terms*—biomedical signal processing, electroencephalogram, freeing of gait, movement disorders, parkinson's disease.**

I. Introduction

FREEZING of Gait (FOG) is a highly disabling symptom that affects approximately one quarter of patients with Parkinson's disease (PD) in the early stages and over two thirds in the advanced stages of the disease[1]. Clinically, FOG is defined as a *"brief, episodic absence or marked reduction of forward progression of the feet despite the intension to walk"* [2]. Balance impairment and falls due to sudden FOG often develop into one of the chief complaints among patients with PD and also often lead to falls, which are associated with a high morbidity and mortality in PD [3].

Manuscript received April 07, 2014; revised September 13, 2014 and November 03, 2014; accepted November 23, 2014. Date of publication ; date of current version September 07, 2014.

A. M. Ardi Handojoseno, Tuan N. Nguyen and Hung T. Nguyen are with Faculty of Engineering and Information Technology, University of Technology, Sydney, Broadway, NSW 2007, Australia. (Aluysius-MariaArdi.Handojoseno@student.uts.edu.au, TuanNghia.Nguyen@uts.edu.au, Hung.Nguyen@uts.edu.au).

James M. Shine and Simon J. G. Lewis are with Parkinson's Disease Research Clinic, Brain and Mind Research Institute, University of Sydney, Level 4, Building F, 94 Mallet Street, Camperdown, NSW, 2050, Australia. (mac.shine@sydney.edu.au, simonl@med.usyd.edu.au).

Yvonne Tran is with the Centre for Health Technologies, University of Technology, Sydney, and also with the Rehabilitation Studies Unit, University of Sydney, Australia. (Yvonne.Tran@uts.edu.au).

Digital Object Identifier 10.1109/TNSRE.2014.

The manifestation of FOG is intimately related to the external environment of the individual. Several specific scenarios have been found to initiate FOG, including dual tasking, passing through doorways or crowded areas, as well as stress and anxiety. Together, the multifactorial nature of these triggers indicates a multisystem deficit in FOG, in which impaired information processing across cognitive, affective, and motor domains leads to overwhelming inhibition over the brainstem structures that control gait [4], [5]. This proposal has been supported by the results of functional neuroimaging [6]-[8].

Since dopaminergic replacement therapy only partially alleviates FOG, different strategies have been developed to trigger alternative neural circuits in behavioral control. Somatosensory cues have been found to improve walking, -with visual cues offering the strongest influence, followed by tactile, emotional and auditory cues [9]. A recent investigation on the effect of visual cues using laser on 7 PD patients with FOG showed that on-demand cueing (only given when FOG episodes were observed) is more efficient for reducing the duration of FOG periods than continuous cueing [10], which indicates the importance of a FOG detection system.

While various methods have been investigated to detect the onset of freezing, none of these techniques seem able to reliably detect FOG [11]-[15]. To predict the onset of freezing at the earliest time before the actual FOG episodes, as oppose to detection, we have used EEG due to its ability to measure dynamic physiological change in the brain prior to the occurrence of movement disturbances. Using EEG, both cortical and subcortical activity can be studied through the time-varying changes in certain spectral bands, which also allow insights into the mechanism of FOG. Finally, the portability and relative ease of use of EEG make it far more useful for the mobile collection of brain activity data.

Wavelet decomposition based features have been developed and show the potential of EEG signals as a bio-marker for detecting FOG [16]. In this study, we attempted to find highly discriminating features by investigating the performance of Fourier based features and their counterpart in the wavelet domain, and the performance of univariate and bivariate EEG measurements in detecting FOG in PD patients. Two inter-related categories of EEG measurement were examined: power or amplitude measures and EEG network properties, - which may also disclose critical aspects of the functional connectivity of neural networks during a freezing episode. Some classic features such as power spectrum, centroid frequency and statistical parameters were also computed, as well as more recently developed features such as entropy, cross correlation,

coherence, phase-locking value and weighted phase lag index. Multilayer perceptron neural networks (MLP-NN) classifier was employed for FOG detection, concentrating on the transition period between normal walking and an overt FOG episode.

II. Methods

The study included sixteen patients ranging in age from 56 to 78 years (mean: 64 years, std: 7.25 years) with the mean Hoehn and Yahr stage when "off" medications over night was 2.34 $\pm$ 0.73 and the mean of the Unified Parkinson's Disease Rating Scale III stage when "off" was 40.10 $\pm$ 12.21. All of them had a FOG history with different severity and frequency. The research protocol was approved by The Human Research and Ethics Committee from the University of Sydney before data collection began. The experiment took place in the Parkinson's Disease Research Clinic at the Brain and Mind Research Institute, University of Sydney during a one week period. A series of a standardized timed up-and-go tasks were performed and all trials were video recorded for scoring.

Several researchers have shown that information on EEG signals relating to mental tasks or the physiological condition can be tracked using only a minimum points of measurement [17], [18]. Fewer channels are clearly preferred for patient ease and to limit noise and artifacts. Moreover, it reduces the cost in signal processing, feature extraction and classification process; and makes the setting up of the system much easier and faster.

In this study, the EEG was recorded using a 4-channel wireless EEG system with gold cup electrodes which were placed on 4 scalps locations based on their roles in perceptual and control movement (O1-visual, P4-sensorimotor affordance, Cz-motor execution and Fz-motor planning). Bipolar EEG leads were used to acquire data from central zero (Cz) and frontal zero (Fz) with the reference electrode placed at FCz, and from occipital one (O1) and parietal four (P4) with the reference electrode at T4 and T3, respectively. The EEG signals were amplified with common rejection ratio >95 dB, sampled at a rate of 500 Hz, and band-pass filtered between 0.15 and 100 Hz.

Overall 5.5 hours of data were collected from the standardized timed up-and-go test and 404 FOG episodes, with a duration between 1 sec and 220 sec, were labeled by two clinicians specializing in movement disorders. Two other episodes were determined based on this period: transition episodes which cover a period between 5 to 1 seconds before freezing, and normal walking which refers to a period of 1 second after freezing to 5 seconds before the next freezing period. The distribution of FOG among the patients were not equal: 3 patients had between 6 and 10 episodes during testing and the remaining 13 patients experienced more than 10 events. A total of 1902 one second duration samples of three episodes (normal walking, transition, FOG) from all patients were included with each episode contributed evenly (634 samples). Data from eleven patients were randomly chosen for training and testing (consisting of 1386 samples, 462 in each class). Another set of testing data files, which have never been used in the training process, were also taken from the other five patients (516 samples, 172 in each class) to examine the robustness of the system in classifying the EEG signals from out-group patients. Low frequency noise, high frequency noise and 50 Hz line frequency noise were eliminated using band-pass (0.5-60 Hz) and band-stop (50 Hz) Butterworth IIR filters. Ocular and muscular artifacts were removed using Stein's unbiased risk estimate thresholding based on wavelet transforms.

III. Feature Extraction

A. EEG Linear Univariate Measurements

Power spectral density (PSD), which is widely used and successfully applied to characterize signals in a system, shows the strength of the energy as a function of frequency. It implies stationary process during the time window. While EEG signals are known as non-stationary signals with non-linear behaviour [19], fragments of EEG with length up to 290 ms can be treated as stationary [20].

In this study, the spectra are calculated via Welchs method using a 516 point Fast Fourier Transform (FFT) and periodic Hamming windows with an overlap of 50 %. The duration of the stationary fragments is assumed to be 110 ms with the sampling frequency 500Hz. To eliminate inter-individual and inter-electrode variance in absolute measurements, the power spectrum was normalized by expressing each power spectral as a percentage of total power in a frequency window of 0.5Hz-60HZ and in all electrodes. EEG bands of interest were delta (1-4 Hz), theta (4-8 Hz), alpha (8-13 Hz), beta (13-30 Hz), and gamma (30-60 Hz).

Furthermore, we calculate the shift of the center of gravity of frequency band based on this normalized power spectrum, Spectral Centroid Frequency (SCF). It has been reported to be capable of classifying different types of EEG in various health conditions [21] [22] and is defined as:

$$SCF = \frac{\sum_i f_i * P(f)}{\sum_i P(f)}. \quad (1)$$

Over the past few decades, wavelet analysis has been developed as an alternative and improvement on Fourier analysis. Its main advantage in analyzing physiological systems is its capability to detect and analyze non-stationarity in signals and its related aspect like trends, breakdown points, and discontinuity, since wavelets are well localized in both time and frequency domain. Unlike Fourier transform which is limited to a scaled single sinusoidal function, wavelet transform generates a two-parameter family of wavelet function $\psi_{a,b}(t)$ by scaling (a) and shifting (b) the function, so that the correlation called continuous wavelet transform (CWT) is given by [23].

$$CWT(a,b) = \int_{-\infty}^{\infty} x(t) \frac{1}{\sqrt{|a|}} \psi^*(\frac{t-b}{a}) dt \quad (2)$$

with $^{(*)}$ denotes the complex conjugation.

The development of wavelet-based signal compression algorithm led to the invention of the fast discrete wavelet transforms (DWT) which removes redundancy in the signals and simplify the numerical calculations. In DWT time-scaled

parameters (b, a) are sampled on a dyadic grid with scales $a = 2^j$ (reciprocal of frequency) and positions $b = 2^j k$ (time localization), so that DWT is defined as,

$$DWT(j,k) = \frac{1}{\sqrt{|2^j|}} \sum_{t=-\infty}^{\infty} x(t)\psi(\frac{t-2^j k}{2^j}). \quad (3)$$

In the multi resolution analysis, signal $x(t)$ with maximum cut-off frequency f_m is split into two components using low pass filter and high pass filter and is down sampled by 2 to provide the approximation signals A_j and the detail signals D_j with lower cut-off frequency band $[0 : f_m/2]$ and upper cut-off frequency band $[f_m/2 : f_m]$, respectively [24]. Based on the Nyquist criterion, maximum cut-off frequency is determined by f_m=$f_s/2^{(l+1)}$ where f_s is the sampling frequency of the original signal and l is the level of decomposition. The approximation is subsequently decomposed and this process is continued until the target level is achieved.

The wavelet decomposition for a given EEG signal $x(t)$ at scales *j*=1,2,..., *J* and time point *k* then could be written as

$$x(t) = \sum_k c_{J,k}\varphi_{J,k}(t) + \sum_k \sum_{j \le J} d_{j,k}\psi_{j,k}(t) \quad (4)$$

where $c_{J,k}$, $d_{j,k}$, $\varphi_{j,k}(t)$ and $\psi_{j,k}(t)$ are the approximation coefficients, the detail coefficients, scaling function and wavelet functions, respectively. Daubechies (db4) wavelet that has been found as properly representing EEG signals and spikes [25] was selected as wavelet function.

With the EEG sampled at 500 Hz, a good match to the standard clinical EEG subbands can be achieved using a six level decomposition as can be seen in Table 1. Reconstruction of these signals which are decomposed into five constituent EEG subbands is depicted in Fig.1.

TABLE I
FREQUENCY BANDS CORRESPONDING TO DIFFERENT DECOMPOSITION LEVELS

Decomposed signals	Frequency bands (Hz)	Decomposition Level
D1	125-250	1 (noises)
D2	62.5-125	2 (noises)
D3	31.3-62.5	3 (γ)
D4	15.6-31.3	4 (β)
D5	7.8-15.6	5 (α)
D6	3.9-7.8	6 (θ)
A6	0-3.9	6 (δ)

In wavelet analysis, the energy of signals which correspond to PSD, wavelet energy (WE), can be partitioned at different levels of wavelet decomposition ($j = 1, ...l$) according to Parseval's Theorem, and is expressed as a function of the scaling and wavelet coefficient [26]:

$$E_T = \int |f(t)|^2 dt = \sum_k |c_{J,k}|^2 + \sum_k \sum_{j \le J} |d_{j,k}|^2. \quad (5)$$

Corresponding to SCF, we also calculated Centroid Scale (CS) based on the CWT scalogram to show the shift of the center of gravity of frequency band. The CWT was chosen since it has a better frequency (scale) representation compared to the DWT. We used the complex Morlet wavelet due to its narrow spectral band and an extended time domain made it more suitable for extracting information in frequency domain [27]. It is equivalent to a complex sinusoid with Gaussian envelope and can be written as [28]

$$\psi_0(t) = \frac{1}{\sqrt[4]{\pi}} e^{j2\pi f t} e^{-\frac{t^2}{2}}. \quad (6)$$

B. EEG Non-Linear Univariate Measurements

Brain signals have been known as the output of a nonlinear system. Consequently, various measures which characterize the nonlinear behaviour of EEG signals have also been developed. In this study, entropy was used as an index of EEG complexity or irregularity based on Shannon's Information Theory. The power spectral entropy (PSE) of EEG signal x is defined as:

$$PSE(x) = -\sum_{i=f_l}^{f_h} P_i log P_i \quad (7)$$

where P_i is the normalized power density from the signal's spectrum so that $\sum P_n = 1$ while f_l and f_h are the frequency band of interest. Larger entropy values suggest a greater complexity. The wavelet energy entropy (WEE) were found using similar formula, with

$$P_i = \frac{E_j}{E_T} \quad (8)$$

in which E_j refers to the energy of signals at j^{th} frequency band of decomposition and E_T refers to the energy of all frequency bands of decomposition.

C. EEG Bivariate Measurements

There is a growing interest in the study of oscillatory rhythms and their synchronization related to the dynamic organization of communication in the nervous system. They have been associated with diverse functions such as motor activity, attention, memory and emotion. This was obtained by joining signals from multiple channels to detect the alteration of the functional connectivity in the brain related to different brain conditions.

In this study, quantification of neural correlation was done based on the cross-correlation function, defined as [30]

$$R_{xy}(k) = E[x(n)y(n+k)] \quad (9)$$

where *x(n)* and *y(n+k)* are two joint signals, k is the number of time units that the signal *y(n)* is lagged in regards to *x(n)*, and *E[.]* is the expectation operator.

Cross Power Spectral Density(CPSD) as the distribution of power per unit frequency is defined as

$$P_{xy}(f) = \sum_{k=-\infty}^{\infty} R_{xy}(k) e^{-j2\pi f k T}. \quad (10)$$

Ratio of CPSD to the product of the related auto-power spectral densities (APSD) shows the coherency, a measurement of amplitude and phase coupling, and is defined as

$$C_{xy}(f) = \frac{|P_{xy}(f)|}{\sqrt{P_{xx}(f)P_{yy}(f)}}. \quad (11)$$

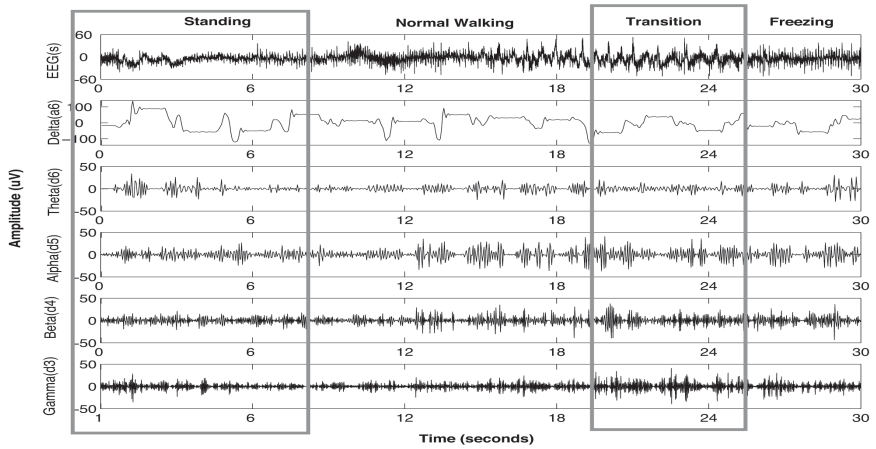

Fig. 1. Decomposition of EEG into detail (d1-d5) signals related to five standard clinical EEG subbands by db4 wavelet in subject 6 shows the amplitude and frequency alterations preceding and during freezing episode. Movement amplitude is increased preceding the freezing episode.

Coherency function is a function of frequency and can be used to analyse which frequency of two sets of time series data are coherent. While correlation emphasizes the similarity of waveform between two signals and gives the information on their time coupling, coherency measures the stability of that similarity [31]. Coherence is defined as the modulus of the coherency, also called the magnitude squared coherence (MSC) and typically estimated by averaging over several epochs.

Analysis on the stability of phase shift over the specified time interval also provides measurement of phase difference between two signals. Detecting this phase-locking when the phase difference is constant using correlation and coherence can be problematic since they are affected by the amplitude component which can be noisy or uncorrelated.

Weighted Phase Lag Index (WPLI) was calculated to measure this phase-synchronization. Proposed by Vinck et al [32], it has been demonstrated as reduced sensitivity to noise, increased capacity to detect changes in phase synchronization and is not affected by volume-conducting correlated sources of interest. WPLI is defined as

$$\Phi \equiv \frac{|P\{\Im\{X\}\}|}{P\{|\Im\{X\}|\}} = \frac{|P\{|\Im\{X\}|\, sgn(\Im\{X\})\}|}{P\{|\Im\{X\}|\}}. \quad (12)$$

Wavelet analysis has been proposed in estimating the time varying coherence among non-stationary signals including neural signals since FFT is incapable of providing temporal structure information of signals. While a real wavelet function has been used for detecting peaks and discontinuities, information about the difference of phase can only be extracted using a complex wavelet function. Moreover, it is a better method for capturing oscillatory behaviour. In this study, we used a complex Morlet wavelet which has been proved provided the best time-frequency resolution in the EEG analysis compared to other wavelet functions [33].

Corresponding to a similar concept in Fourier analysis, the autocorrelation function of the wavelet transformation produces a wavelet power spectrum (WPS) which describes the power of the signals $x(t)$ at a certain time t_i on a scale s:

$$WPS_i(s) = W_i(s)W_i(s)^*. \quad (13)$$

The extension of the univariate WPS to a comparison of two time series x and y at time shift index i and scale s with their wavelet transform coefficients W_{x_i} and W_{y_i}, the wavelet cross spectrum $WCS_i(s)$, is defined as

$$WCS_{xy_i}(s) = S(W_{x_i}(s)W_{y_i}^{*T}(s)) \quad (14)$$

where S is a smoothing operator. The interaction between signals x and y at the given frequency is measured by the product of two spectra expressed by wavelet coefficients of the time scale representation of EEG sub-bands.

Analogous to Fourier-based coherence, wavelet coherence is defined as the amplitude of the WCS normalized to the two single WPS:

$$WCO_{xy_i}(s) = \frac{WCS_{xy_i}(s)}{\sqrt{S(|WPS_{xx_i}(s)|^2)}\sqrt{S\,|WPS_{yy_i}(s)|^2}}. \quad (15)$$

To measure phase synchrony based on wavelet transform, Phase Locking Value (PLV) proposed by Lachaux et al. [34], which has been also called as mean phase coherence [35], was used in this study, defined as

$$PLV_t = \frac{1}{N}\left|\sum_{n=1}^{N} N e^{j\theta(t,n)}\right| \quad (16)$$

where $\theta(t,n)$ is the phase difference between the signals which can be derived from the angles of their wavelet-coefficients $\theta_1(t,n) - \theta_2(t,n)$. Just like WPLI, the value of PLV is always

TABLE II
CORRELATION ANALYSIS OF NORMALIZED POWER SPECTRAL DENSITY AND NORMALIZED WAVELET ENERGY BETWEEN NORMAL WALKING (NW) AND TRANSITION TO A FREEZING OF GAIT (TR)

		Power Spectral Density			Wavelet Energy		
Lead	Frequency	NW	TR	NW vs TR	NW	TR	NW vs TR
O1	δ	0.0868 ± 0.0595	0.0816 ± 0.0743	$*$	0.0051 ± 0.0094	0.0082 ± 0.0373	$*$
	θ	0.0872 ± 0.0565	0.0814 ± 0.0716	$*$	0.0005 ± 0.0012	0.0003 ± 0.0007	$*$
	α	0.0643 ± 0.0361	0.0575 ± 0.0459	$*$	0.0007 ± 0.0018	0.0004 ± 0.0029	$**$
	β	0.0691 ± 0.0375	0.0426 ± 0.0252	$***$	0.0005 ± 0.0017	0.0004 ± 0.0032	$***$
	γ	0.0415 ± 0.0330	0.0160 ± 0.0159	$**$	0.0003 ± 0.0012	0.0007 ± 0.0081	$***$
P4	δ	0.1436 ± 0.0837	0.0920 ± 0.0652	$**$	0.0133 ± 0.0536	0.0068 ± 0.0333	$**$
	θ	0.1456 ± 0.0770	0.0949 ± 0.0632	$**$	0.0007 ± 0.0019	0.0003 ± 0.0009	$*$
	α	0.1104 ± 0.0444	0.0750 ± 0.0445	$***$	0.0013 ± 0.0030	0.0006 ± 0.0041	$***$
	β	0.1428 ± 0.0711	0.1013 ± 0.0744	$***$	0.0013 ± 0.0040	0.0005 ± 0.0030	$***$
	γ	0.1033 ± 0.0827	0.0663 ± 0.0668	$*$	0.0011 ± 0.0025	0.0006 ± 0.0039	$**$
Cz	δ	0.0439 ± 0.0552	0.1466 ± 0.1070	$***$	0.0014 ± 0.0023	0.0052 ± 0.0120	$*$
	θ	0.0435 ± 0.0536	0.1443 ± 0.1048	$***$	0.0002 ± 0.0006	0.0008 ± 0.0015	$*$
	α	0.0301 ± 0.0349	0.0972 ± 0.0699	$***$	0.0002 ± 0.0004	0.0003 ± 0.0006	
	β	0.0200 ± 0.0158	0.0473 ± 0.0326	$***$	0.0001 ± 0.0001	0.0001 ± 0.0002	$*$
	γ	0.0024 ± 0.0022	0.0039 ± 0.0055		0.0000 ± 0.0000	0.0001 ± 0.0009	
Fz	δ	0.0021 ± 0.0025	0.0042 ± 0.0094		0.0001 ± 0.0002	0.0003 ± 0.0016	$*$
	θ	0.0019 ± 0.0023	0.0040 ± 0.0089		0.0000 ± 0.0000	0.0000 ± 0.0002	
	α	0.0012 ± 0.0014	0.0025 ± 0.0054	$*$	0.0000 ± 0.0000	0.0000 ± 0.0001	$*$
	β	0.0003 ± 0.0004	0.0009 ± 0.0017	$*$	0.0000 ± 0.0000	0.0000 ± 0.0000	$*$
	γ	0.0000 ± 0.0000	0.0001 ± 0.0006	$*$	0.0000 ± 0.0000	0.0000 ± 0.0001	$*$

$* = p \leq 0.05$ and r < 0.3
$** = p \leq 0.05$ and $0.3 \leq$ r < 0.4
$*** = p \leq 0.05$ and r ≥ 0.4

between 0 and 1 with a value of 1 signifying perfect synchrony in which one signal perfectly follows the other.

D. Statistical Test and Classification

In order to build a faster and better classification system, we selected the most relevant univariate features using non-parametric statistical analysis - the Wilcoxon Sum Rank Test. Only features with significant statistical differences between those groups of data (p-value <0.05) were chosen for further process.

Classification data sampled using selected features were based on three layers MLP-NN with 56%, 25% and 19% of the data, randomly split, used for training, validation and testing, respectively. Levernberg Marquardt algorithm was chosen as a training method for its speed and stability [38]. Known as a combination of the Gauss-Newton technique and the steepest descent method, the Levernberg-Marquardt algorithm essentially is an iterative technique that located the minimum of an objective error function:

$$E(w) = \sum_{i=1}^{m} e_i^2(w) = \|f(w)\|^2 \tag{17}$$

where $e_i^2(w) = (y_{di} - y_i)^2$ is an individual error, the difference between the desired value of output neuron y_{di} and the actual output of that neuron, y_i, and w is the weight vector. The Levenberg-Marquardt algorithm is used to find the new weight vector w_{k+1} to reach the optimum performance of the system:

$$w_{k+1} = w_k - (J_k^T f(w_k))(J_k^T J_k + \lambda I)^{-1} \tag{18}$$

where J_k is the Jacobian of function $f(.)$ at w_k, λ is the learning rate and I is the identity matrix.

Validation set was used as a stopping criterion to avoid overfitting as well as error goal 0.01 in single MLP-NN with 4 to 12 hidden layer neurons. Each feature was trained and tested fifty times based on the repeated random sub-sampling and the mean result was recorded. The sensitivity, specificity, accuracy and area under the Receiver Operating Characteristic curve of classification system were calculated to measure the performance of the features.

IV. RESULTS

A. EEG Linear Univariate Measurements

In the statistical analysis of PSD and WE for differentiation of two EEG conditions, normal walking and transition to FOG, the discriminative value (p-value <0.05) was found in almost all frequency bands as can be seen in Table 2. However, when effect size was taken into account, the alpha frequency band in parietal appeared as the most important feature signified with the decreasing of normalized PSD and WE during transition to FOG compared to normal walking (PSD, z = 7.98 p <0.05, r = 0.40; WE, z = 8.36, p <0.05, r = 0.42). In addition, there were significant increases in beta power in occipital (PSD, z = 7.98 p <0.05, r = 0.40; WE, z = 9.57, p <0.05, r = 0.48), parietal (PSD, z = 7.98 p <0.05, r = 0.40; WE, z = 8.87, p <0.05, r = 0.45) and central leads (PSD, z = 7.98 p <0.05, r = 0.40; WE, z = 2.63, p <0.05, r = 0.13), along with theta activity in central (PSD, z =-12.80 p <0.05, r = 0.92; WE, z = -5.27, p <0.05, r = 0.27).

Common patterns shared by Fourier transform based features and wavelet transform based features clearly showed in the shifting centroid frequency in the beta, alpha and theta frequency band during transition and freezing episodes. The beta frequency band stands out as the most affected frequency band in transition to freezing with the most significant shift happening in the central lead (SCF, z = 11.04 p <0.05, r = 0.56; CS, z = -8.33, p <0.05, r = 0.42) while the

fronto-central cortical region has been more affected than the parieto-occipital region. When compared to the walking period, episodes of freezing were associated with significant shifting in the theta frequency band with the largest shift of centroid frequency in the frontal leads (SCF, z = -4.11 p <0.05, r = 0.21; CS, z = 4.55, p <0.05, r = 0.23).

B. EEG Non-Linear Univariate Measurements

The result of entropy analysis shows a decrease of entropy in most frequency bands and electrodes during freezing of gait. The most significant change during transition to freezing was detected in the beta frequency band both at central (PSE, z = 11.01, p <0.05, r = 0.56) and frontal (PSE, z = 8.23, p <0.05, r = 0.42). This trend was continued in the onset of freezing with lower effect size (Central: PSE, z = 4.35, p <0.05, r = 0.22 ; Frontal: PSE, z = -5.44, p <0.05, r = 0.28).

The entropy analysis on wavelet energy which measures the temporal regularity of energy in each frequency band also revealed the loss of complexity during transition in most of all the frequency bands and electrodes with the beta band appearing as the most affected frequency band. There was a significant decreased regularity of gamma activity in the central (WEE, z = 11.04, p <0.05, r = 0.56) during the transition, along with a decrease in the beta band (WEE, z = 11.04, p <0.05, r = 0.56). While these entropy were then increased at the onset of the freezing period, they were still significantly lower compared to walking, unlike the diminishing of all irregularity at the occipital and parietal leads.

C. EEG Bivariate Measurements

Fig. 2 shows the results from the phase synchrony analysis obtained from electrodes pairs in three mid-high frequency bands during freezing of gait. Both parietal-frontal and occipital-frontal cortices connections in the beta and gamma frequency band are strongly synchronized in phase according to WPLI analysis. In contrast, when PLV analysis was applied, phase synchronization decreased significantly in the gamma frequency band in both pairs of electrodes location.

In the coherency analysis, both MSC and WCO indicated a significantly different coherency during transition to freezing in parieto-occipital pairwise of electrodes in the theta, alpha and beta frequency band as illustrated in Fig. 3 and Fig. 4. We observed no significant change of coherency in parietal-central cortices connection. Pairwise fronto-central shows alteration of coherence in all frequency bands detected using WCO and in three lowest band frequency using MSC. Amongst all the changes, the most significant one is in the theta frequency band at this pairwise of electrode (MSC, z = -8.11 p <0.05, r = 0.41; WCO, z = -5.05, p <0.05, r = 0.26).

D. Statistical Test and Classification

The performance of features extracted through univariate analysis is generally stronger than bivariate analysis based features. Both sub-band power spectrum and sub-band wavelet energy features gave better results compared to their bivariate mode, cross power spectrum and wavelet cross spectrum.

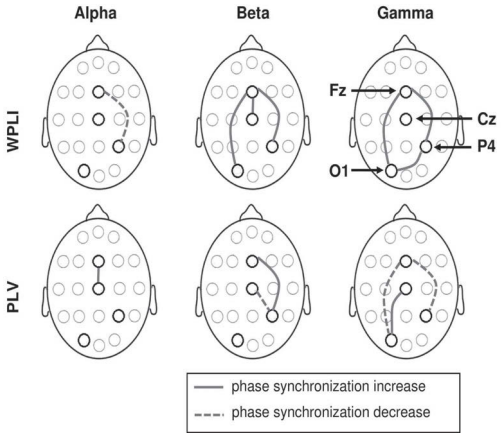

Fig. 2. Phase synchronization alterations during freezing of gait measured using Weighted-Phase Lag Index and Phase Locking Value show the functional link between motor and visual in the high frequency EEG.

While our interest is more in the result of in-group testing, since the translation of this method into a real device will be customized for each user due to variation FOG characteristics across patients, it is interesting to point out that the coherence based features poorly performed when it was applied to out-group patients. It shows that multivariate based features are less robust against the inter-individual variability compared to univariate based features.

The result of the experiment also shows that Fourier analysis provided better result compared to wavelet analysis in the extraction of the features related to frequency, entropy, and phase synchrony. However, the changes in the wavelet energy were found to be the best indicators of transition to FOG, with sensitivity and accuracy of testing obtained in the experiment involving in-group patients at 86% and 80.2%, respectively. The using of wavelet cross spectrum also resulted in a better accuracy compared to cross power spectrum in the experiment related to in-group subjects and has been proven as to be more robust when tested against out-group patients, maintaining the accuracy at 77%.

V. Discussion

The present study compared several Fourier analysis based features with their wavelet analysis counter-part and explored their role in neural dynamics related to freezing of gait in PD. Our finding that theta oscillations in human cortex increase during transition to freezing and remain high during freezing in the central region (see Table II-Power Spectral Density)is consistent with multiple studies suggesting that there is a relationship between FOG, specific deficits in cognition and impairment in the motor planning mechanism [39]-[43]. The analysis of the frequency shift and coherency based on MSC and WCO provided more support to the importance of frontocentral activity in FOG (see Fig. 3 - Fig. 4 in which the

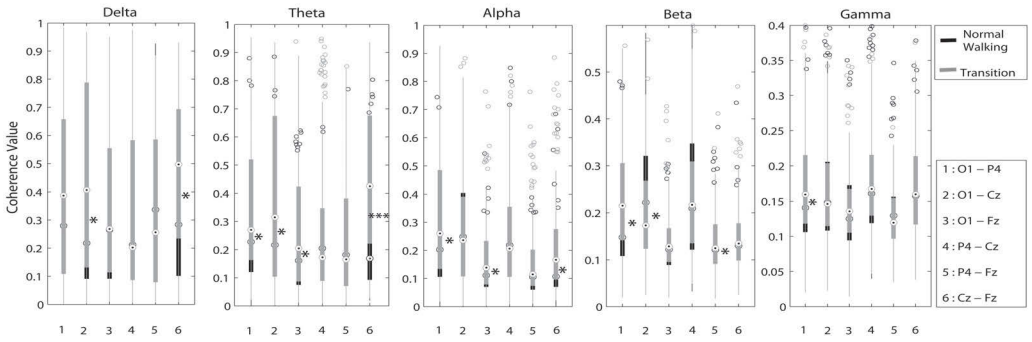

Fig. 3. Boxplot of Magnitude-Squared Coherence of EEG signals during normal walking and transition to freezing of gait (frequency band 5, used electrode 4). The Asterisk symbol indicates that the boxplot at its left is significant (p-value <0.05). The higher number of the asterisk symbol refers to the higher r-value.

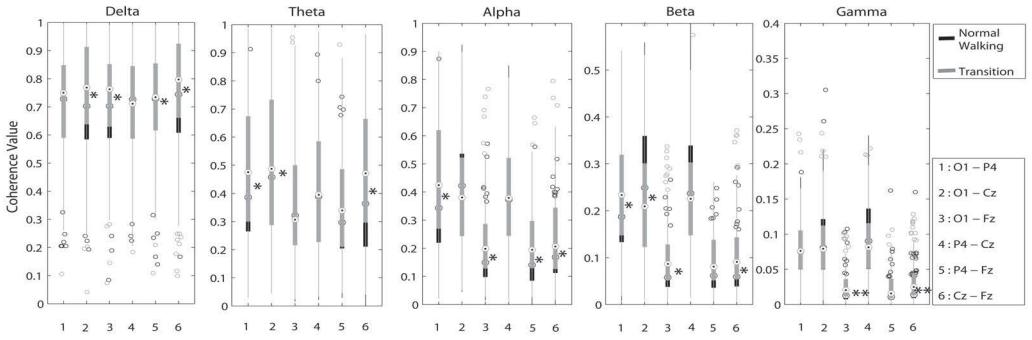

Fig. 4. Boxplot of Wavelet Coherence of EEG signals during normal walking and transition to freezing of gait (frequency band 5, used electrode 4). The Asterisk symbol indicates that the boxplot at its left is significant (p-value <0.05). The higher number of the asterisk symbol refers to the higher r-value.

TABLE III
CLASSIFICATION RESULTS OF PROPOSED FEATURES USING MLP-NN IN DETECTING TRANSITION 5 SECOND BEFORE FREEZING FROM NORMAL WALKING

Features	In-group (11 patients)								Out-group (5 patients)			
	Training				Testing				Testing			
	Se %	Sp %	Ac %	Au %	Se %	Sp %	Ac %	Au %	Se %	Sp %	Ac %	Au %
F1	84.81	84.89	84.83	85.61	79.69	77.98	78.68	79.14	75.86	65.37	70.62	71.52
F2	85.12	82.29	83.67	84.12	81.00	78.96	80.00	79.40	68.51	83.65	76.08	74.53
F3	83.46	82.54	83.00	81.95	79.45	76.94	78.10	79.31	73.02	79.53	76.28	74.30
F4	81.31	81.49	81.71	81.44	74.88	74.76	74.88	75.88	68.40	68.77	68.56	67.42
F5	71.92	77.14	74.58	74.86	70.75	71.73	70.75	69.41	66.16	72.88	68.42	67.23
F6	63.70	80.43	72.10	71.06	64.20	81.22	72.88	71.18	54.88	87.09	70.99	69.04
F7	89.28	78.21	83.75	83.55	86.00	74.43	80.20	79.73	73.19	80.16	76.67	75.88
F8	85.82	80.82	83.29	83.54	79.35	73.81	76.47	75.75	68.77	76.98	72.87	71.27
F9	77.51	73.19	75.29	75.46	71.53	67.00	69.32	70.10	75.09	67.05	71.07	70.14
F10	78.73	87.22	83.00	84.66	72.76	82.89	77.42	77.20	69.93	85.16	77.55	77.80
F11	75.66	78.88	78.67	77.54	66.33	67.71	69.42	68.51	57.51	53.72	52.16	52.37
F12	70.02	74.15	72.07	72.31	60.80	66.13	62.47	61.41	73.07	54.42	52.13	52.52

Se: Sensitivity; Sp: Specificity; Ac: Accuracy; Au: Area under the Receiver Operating Characteristic curve
F1: Power Spectral Density (PSD); F2: Spectral Centroid Frequency (SCF); F3: Power Spectral Entropy (PSE)
F4: Cross Power Spectral Density (CPSD); F5: Magnitude-Squared Coherence (MSC)
F6: Weighted Phase Lag Index (WPLI); F7: Wavelet Energy (WE)
F8: Centroid Scale (CS); F9: Wavelet Energy Entropy (WEE)
F10: Wavelet Cross Spectrum (WCS); F11: Wavelet Coherence (WCO); F12: Phase-Locking Value (PLV)

frontocentral pairwise is significant in most of all frequency bands).

The entropy analysis of the frequency domain based on the changing of power spectral shows an increase of regularity on nearly all frequency bands and most electrodes during transition and this continued in the freezing period. Therefore we can infer that brain activity is "less complex" when patients undergo change from their normal walking state to freezing of gait. The alteration in the information processing during this stage is possibly due to an inactivation of previously active neural networks as a result of the impairment of the more "executive" functions of the brain. This result is also aligned with the general "loss of complexity" behaviour in other diseases and states of the brain including epilepsy [44], Alzheimer's [45], and autism [46].

While there are clear differences in the result of phase synchrony calculation using WPLI and PLV, both are in agreement with the increase of beta synchronization. This result is aligned with the work of E. Heinrichs-Graham et al. [47] who used magnetoencephalography (MEG) and found beta desynchronization prior to and during movement onset as well as increased gamma activity in Parkinson's disease. The analysis on the primary motor cortex arm area by Hemptinne et al. [48] also found the exaggerated coupling between beta-phase and gamma amplitude in those areas in PD patients. This coupling has been reported in relation to movement preparation and control of different cognitive functions including memory and attention. Interestingly, we also noticed the significant coherence in the gamma frequency band at pairwise O1-Cz and Cz-Fz, detected using wavelet coherence.

The comparison between power spectral entropy based on the signals dynamic in the frequency domain and wavelet energy entropy based on the signals dynamic in the time domain revealed that information of EEG signals are coded in the frequency domain rather than in the time domain. Along with the results of classification using centroid frequency and centroid scale, it shows that Fourier analysis provides better features in frequency domain compared to wavelet analysis. This precision on frequency, following the Heisenberg Uncertainty Principle, is at the cost of zero information about the temporal dynamic of the signal.

The wavelet analysis provides information on time localization which has increased the performance of the classification system as is shown in the result of wavelet energy. However, in the time-space correlation and coherence, the performance of features extracted using the windowed Fourier transform and the wavelet transform were comparable, with the computation time taken by CWT found to be significantly longer than the windowed Fourier transform. This limits the practical uses of CWT in practical application.

Wearable systems for the detection of FOG episodes have been developed using accelerometers as the main sensor with the sensitivity exceeding 80% [14] [15] [49] [50]. However, unlike the detection system with EEG, those results were acquired in identifying the onset once FOG appeared. Moreover, due to dependency to the physical movement of the body, accelerometers could not differentiate between freezing and voluntarily stopping [51]. EEG has the potential to be an effective means for the prediction of FOG in our study, with sensitivity and accuracy around 80% using power spectral or wavelet energy as a single feature. Besides, there is a possibility to increase the transition period to provide enough window time for signal processing as well as a follow up treatment.

VI. Conclusion

This study demonstrated the potential of the EEG features extracted using both Fourier and wavelet analysis in giving more insights into the pathophysiology of Freezing of Gait in PD. Results also show the advantage of using wavelet analysis in extracting EEG basic feature, energy, compared to Fourier analysis, providing a better indicator in classification system. This finding may be due to its representation of signals in three dimensions (amplitude, frequency and time) compared to Fourier (amplitude and frequency), which is more convenient for non-stationary EEG signals. However, it was less differentiated in coherency and phase synchrony, when computation of the Fourier coefficients were done in a short time window shifting through the time line, capturing the entire time-frequency of the signals.

Different aspects of the EEG signal, when combined, may provide more significant information, leading to a better classification of the signal. Future work will include dimension reduction of the features highlighted, further exploration regarding the location of electrodes, and investigating different classification methods for better performance of the system. It is hoped that such approaches may lead to clinical translation with device capable of sufficient computational cost and time processing.

References

[1] D. M. Tan, J. L. McGinley, M. E. Danoudis, R. Iansek, and M. E. Morris, "Freezing of gait and activity limitations in people with Parkinson's disease," *Arch. Physic. Med. Rehab.*, vol. 92, no. 7, pp. 1159-1165, 2011.

[2] J. G. Nutt, B. R. Bloem, N. Giladi, M. Hallett, F. B. Horak, and A. Nieuwboer, "Freezing of gait: moving forward on a mysterious clinical phenomenon," *The Lancet Neurology*, vol. 10, no. 8, pp. 734-744, 2011.

[3] B. R. Bloem, J. M. Hausdorff, J. E. Visser, N. Giladi, "Falls and freezing of gait in Parkinson's disease: a review of two interconnected, episodic phenomena," *Mov. Disord.*, vol. 19, no. 8, pp. 871-884, 2004

[4] J. M. Shine, S. L. Naismith, and S. J. G. Lewis, "The differential contributions of motor, cognitive and affective disturbance to freezing of gait in Parkinsons Disease," *Clin. Neurol. Neurosurg.*, vol. 115, no.5, pp. 542-545, 2013.

[5] A. Nieuwboer, and N. Giladi, "Characterizing freezing of gait in Parkinson's disease: Models of an episodic phenomenon," *Mov. Disord.*, vol. 28, no. 11, pp. 1509-1519, 2013.

[6] A. L. Bartels and K. L. Leenders, "Parkinson's disease: The syndrome, the pathogenesis and pathophysiology," *Cortex* vol. 45, no. 8, pp. 915-921, 2009.

[7] J. M. Shine, A. M. A. Handojoseno, T. N. Nguyen, Y. Tran, S. L. Naismith, H. Nguyen, and S. J. G. Lewis, "Abnormal patterns of theta frequency oscillations during the temporal evolution of freezing of gait in Parkinsons disease," *Clin. Neurophysiol.*, vol. 125, no. 3, pp. 569-576, 2014.

[8] Q. J. Almeida and C. A. Lebold, "Freezing of gait in Parkinson's disease: a perceptual cause for a motor impairment?" *J. Neurol. Neurosurg. Psychi.*, vol. 81, no. 5, pp. 513-518, 2010.

[9] S. Rahman, H. J. Griffin, N. P. Quinn, and M. Jahanshahi, "The factors that induce or overcome freezing of gait in Parkinson's disease," *Behav. Neurol.* vol. 19, no. 3, pp. 127-136, 2008.

Appendix B. Publications

[10] R. Velik, U. Hoffmann, H. Zabaleta, J. F. M. Masso, and T. Keller, The effect of visual cues on the number and duration of freezing episodes in parkinsons patients, in *Proc. 34th Annu. Int. Conf. IEEE Eng. Med. Biol. Soc.*, pp. 4656-4659, 2012.

[11] S. T. Moore, H. G. MacDougall, and W. G. Ondo, Ambulatory monitoring of freezing of gait in Parkinson's disease, *J. Neurosci. Methods*, vol. 167, no. 2, pp. 340-348, 2008.

[12] M. B. Popovic, M. D. Jovicic, S. Radovanovic, I. Petrovic, and V. Kostic, "A simple method to assess freezing of gait in PD patients", *Braz. J. Med. Biol. Res.*, vol. 43, no. 9, pp. 883-889, Sep. 2010.

[13] A. Delval, A. H. Snijders, V. Weerdesteyn, J. E. Duysens, L. Defebvre, N. Giladi, and B. R. Bloem, "Objective detection of subtle freezing of gait episodes in Parkinson's disease," *Mov. Disord.*, vol. 25, no. 11, pp. 1684-1693, 2010.

[14] M. Bachlin, M. Plotnik, D. Roggen, D. Maidan, J. M. Hausdorff, N. Giladi, and G. Troster, "Wearable Assistant for Parkinsons Disease Patients with the Freezing of Gait Symptom," *IEEE Trans. Inf. Technol. Biomed.*, vol. 14, no. 2, pp. 436-446, Mar. 2010.

[15] S. Mazilu, M. Hardegger, Z. Zhu, D. Roggen, G. Troster, M. Plotnik, and J. M. Hausdorff, "Online detection of freezing of gait with smartphones and machine learning techniques," in *Proc. 6th Int. Conf. Perv. Comput. Tech. Health.*, pp. 123-130, 2012.

[16] A. M. A. Handojoseno, J. M. Shine, T. N. Nguyen, Y. Tran, S. J. G. Lewis, and H. T. Nguyen, "The detection of Freezing of Gait in Parkinson's disease patients using EEG signals based on wavelet decomposition," in *Proc. 34th Annu. Int. Conf. IEEE Eng. Med. Biol. Soc.*, 2012, pp. 69-72.

[17] S. Wikstrom, I. H. Pupp, I. Rosen, E. Norman, V. Fellman, D. Ley, and L. Hellstrom-Westas, "Early single-channel aEEG/EEG predicts outcome in very preterm infants," *Acta Paediatrica* vol. 101, no.7, pp. 719-726, 2012.

[18] A. Picot, S. Charbonnier, and A. Caplier, "On-line detection of drowsiness using brain and visual information," *IEEE Trans. Syst. Man Cybern. A., Syst. Humans*, vol. 42, no. 3, pp. 764-775, Jun. 2012.

[19] S. Sanei and J. A. Chambers, *EEG signal processing*, West Sussex, UK: John Wiley & Sons, 2008.

[20] B. Schack and W. Krause, "Dynamic power and coherence analysis of ultra short-term cognitive processesA methodical study," *Brain topography*, vol. 8, no. 2, pp. 127-136, 1995.

[21] L. B. Nguyen, A. V. Nguyen, S. H. Ling, and H. T. Nguyen, "An adaptive strategy of classification for detecting hypoglycemia using only two EEG channels," in *Proc. 34th Annu. Int. Conf. IEEE Eng. Med. Biol. Soc.*, 2012, pp. 3515-3518.

[22] T. Staudinger and R. Polikar, "Analysis of complexity based EEG features for the diagnosis of Alzheimer's disease," in *Proc. 33th Annu. Int. Conf. IEEE Eng. Med. Biol. Soc.*, 2011, pp. 2033-2036.

[23] J. L. Semmlow, *Biosignal and biomedical image processing: MATLAB-based applications*, Vol. 22, CRC press, 2004.

[24] S. Mallat, *A wavelet tour of signal processing*, London, UK: Academic Press, 1999.

[25] A. Subasi, "EEG signal classification using wavelet feature extraction and a mixture of expert model," *Expert Syst. Appl.*, vol. 32, no. 4, pp. 1084-1093, 2007.

[26] C. S. Burrus, R. A. Gopinath, and H. Guo, *Introduction to wavelets and wavelet transforms: a primer*, New Jersey, USA: Prentice-Hall, Inc., 1998.

[27] Y. Misiti, G. Oppenheim, and J.M. Poggi, *Wavelets and their Applications*, Vol. 330, ISTE, 2007.

[28] P. S. Addison, *The illustrated wavelet transform handbook: introductory theory and applications in science, engineering, medicine and finance*, Bristol, UK: Institute of Physics Publishing, 2002.

[29] C. Torrence, and G. P. Compo, "A practical guide to wavelet analysis," *Bull. the American Meteorol. Soc.*, vol. 79, no. 1, pp. 61-78, 1998.

[30] R. Shiavi, *Introduction to applied statistical signal analysis: Guide to biomedical and electrical engineering applications*, London, UK: Academic Press, 2010.

[31] M. A. Guevara, and M. C. Cabrera, "EEG coherence or EEG correlation?" *Int. J. Psychophysiol.*, vol. 23, no. 3, pp. 145-153, 1996.

[32] M. Vinck, R. Oostenveld, M. Wingerden, F. Battaglia, and C. Pennartz. "An improved index of phase-synchronization for electrophysiological data in the presence of volume-conduction, noise and sample-size bias," *Neuroimage*, vol. 55, no. 4, pp. 1548-1565, 2011.

[33] E. Sitnikova, A. E. Hramov, A. A. Koronovsky, and G. van Luijtelaar, "Sleep spindles and spikewave discharges in EEG: Their generic features, similarities and distinctions disclosed with Fourier transform and continuous wavelet analysis," *J. Neurosci. methods*, vol. 180, no. 2, pp. 304-316, 2009.

[34] J. P. Lachaux, E. Rodriguez, J. Martinerie, and F. J. Varela, "Measuring phase synchrony in brain signals," *Hum. Brain Mapp.*, vol. 8, no. 4, pp. 194-208, 1999.

[35] F. Mormann, K. Lehnertz, P. David, and C. E. Elger, "Mean phase coherence as a measure for phase synchronization and its application to the EEG of epilepsy patients," *Physica D: Nonlinear Phenomena*, vol. 144, no. 3, pp. 358-369, 2000.

[36] H. M. Hurtado, L. L. Rubchinsky, K. A. Sigvardt, V. L. Wheelock, and C. T. Pappas, "Temporal evolution of oscillations and synchrony in GPi/muscle pairs in Parkinson's disease," *J. Neurophysiol.*, vol. 93, no.3, pp. 1569-1584, 2005.

[37] M. G. Knyazeva, M. Jalili, A. Brioschi, I. Bourquin, E. Fornari, M. Hasler, R. Meuli, P. Maeder, and J. Ghika, "Topography of EEG multivariate phase synchronization in early Alzheimer's disease," *Neurobiol. Aging* vol. 31, no. 7, pp. 1132-1144, 2010

[38] E. D. Ubeyli, "Combined neural network model employing wavelet coefficients for EEG signals classification," *Digital Signal Process.*, vol. 19, no. 2, pp. 297-308, 2009.

[39] B. Suchan, D. Zoppelt, and I. Daum, "Frontocentral negativity in electroencephalogram reflects motor response evaluation in humans on correct trials," *Neurosci. Lett.*, vol. 350, no. 2, pp. 101-104, 2003.

[40] N. Giladi and J. M. Hausdorff, "The role of mental function in the pathogenesis of freezing of gait in Parkinson's disease," *J. Neurol. Sci.*, vol. 248, no.1, pp. 173-176, 2006.

[41] G. Yogev-Seligmann, J. M. Hausdorff, and N. Giladi, "The role of executive function and attention in gait," *Mov. Disord.*, vol. 23, no. 3, pp. 329-342, 2008.

[42] J. M. Shine, A. A. Moustafa, E. Matar, M. J. Frank, and S. J. Lewis, "The role of frontostriatal impairment in freezing of gait in Parkinson's disease," *Front. Syst. Neurosci.*, vol. 7, 2013.

[43] P. Knobl, L. Kielstra, and Q. Almeida, "The relationship between motor planning and freezing of gait in Parkinson's disease," *J. Neurol. Neurosurg. Psych.*, vol. 83, no. 1, pp. 98-101, 2012.

[44] O. A. Rosso, "Entropy changes in brain function," *Int. J. Psychophysiol.*, vol. 64, no. 1, pp. 75-80, 2007.

[45] D. Abasolo, J. Escudero, R. Hornero, C. Gomez, and P. Espino, "Approximate entropy and auto mutual information analysis of the electroencephalogram in Alzheimers disease patients," *Med.& Biol. Eng. & Comput.*, vol. 46, no. 10 pp. 1019-1028, 2008.

[46] A. Catarino, O. Churches, S. Baron-Cohen, A. Andrade, and H. Ring, "Atypical EEG complexity in autism spectrum conditions: a multiscale entropy analysis," *Clin. Neurophysiol.*, vol. 122, no. 12, pp. 2375-2383, 2011.

[47] E. Heinrichs-Graham, T. W. Wilson, P. M. Santamaria, S. K. Heithoff, D. Torres-Russotto, J. A. Hutter-Saunders, and H. E. Gendelman, "Neuromagnetic Evidence of Abnormal Movement-Related Beta Desynchronization in Parkinson's Disease," *Cerebral Cortex*, 2013.

[48] C. de Hemptinne, E. S. Ryapolova-Webb, E. L. Air, P. A. Garcia, K. J. Miller, J. G. Ojemann, J. L. Ostrem, N. B. Galifianakis, and P. A. Starr, "Exaggerated phaseamplitude coupling in the primary motor cortex in Parkinson disease," *Proc. of the Nat. Acad. of Scienc.*, vol. 110, no. 12, pp. 4780-4785, 2013.

[49] Y. Zhao, K. Tonn, K. Niazmand, U. M. Fietzek, L. T. D'Angelo, A. Ceballos-Baumann, and T.C. Lueth, "Online FOG Identification in Parkinson's disease with a time-frequency combined Algorithm," in *IEEE-EMBS Int. Conf. on Biom. and Health Inf.*, 2012, pp. 192-195.

[50] E. E. Tripoliti, A. T. Tzallas, M. G. Tsipouras, G. Rigas, P. Bougia, M. Leontiou, S. Konitsiotis, M. Chondrogiorgi, S. Tsouli, and D. I. Fotiadis, "Automatic detection of freezing of gait events in patients with Parkinson's disease," *Comput. Meth. Prog. in bio.*, vol. 110, no. 1, pp. 12-26, 2013.

[51] K. Niazmand, K. Tonn, Y. Zhao, U. M. Fietzek, F. Schroeteler, K. Ziegler, A. O. C. Baumann, and T. C. Lueth, "Freezing of gait detection in parkinson's disease using accelerometer based smart clothes," in *Proc. IEEE Bio. Circ. and Syst. Conf.*, 2011, pp. 201-204.

Appendix B. Publications

A.M. Ardi Handojoseno SJ received the M.Eng. degree in electrical engineering from the University of Technology, Sydney, Australia, where he has been working toward the Ph.D. degree in electrical engineering in the Centre for Health Technologies, since August 2011. His current research interests include biomedical signal processing with specialisation in neurosignal processing and machine learning. He is a student member of the Institute of Electrical and Electronics Engineers (IEEE).

Yvonne Tran received her BSc (Hons) in Biomedical Science in 1997 and Ph.D. degree in Psychophysiology in 2001 both from the University of Technology, Sydney, (UTS) Australia. In 2001, she joined the Centre of Health Technology, UTS. In 2007, she joined the Rehabilitation Studies Unit, University of Sydney.

James 'Mac' Shine is a NHMRC CJ Martin Fellow currently working at Stanford University. Despite being early in his career, Mac has already made key contributions to the understanding of the pathophysiological mechanisms underlying common, yet poorly understood, symptoms of Parkinsons disease. By using a combination of neuropsychological tasks with advanced analysis of functional brain imaging data, Dr Shine has published over 40 papers in peer reviewed journals, including many in high-impact international journals. In addition, his work has been highlighted multiple times by the Faculty of 1000. He has over 450 citations and an H-index of 14.

Simon J.G. Lewis is an NHMRC Practitioner Fellow who works as a Consultant Neurologist at the Royal Prince Alfred Hospital and is Associate Professor in Cognitive Neuroscience at the University of Sydney. He is the Director of the Parkinson's Disease Research Clinic at the Brain & Mind Research Institute and heads the NSW Movement Disorders Brain Donor program. He has published over 100 peer review papers exploring various aspects of disease heterogeneity, gait, cognition, sleep and neuropsychiatry.

Tuan N. Nguyen received his PhD in Engineering from the University of Technology, Sydney (UTS) in 2010. He was awarded as a recipient of the Chancellor's List in recognition of exceptional scholarly achievement in PhD research in 2010. Currently, he is a Chancellors Postdoctoral Research Fellow in the Centre for Health Technologies, Faculty of Engineering at the UTS. His current research interests include biomedical engineering, advanced control and artificial intelligence for health technologies. He is also a member of the Institute of Electrical and Electronics Engineers (IEEE) and the Institution of Engineers, Australia (IEAust).

Hung T. Nguyen is Assistant Deputy Vice-Chancellor (Innovation) at the University of Technology, Sydney (UTS). He is also Director of the Centre for Health Technologies and Professor of Electrical Engineering. He received his PhD in 1980 from the University of Newcastle, Australia. His research interests include biomedical engineering, artificial intelligence and image processing, and neurosciences. He has developed biomedical devices for diabetes, neurological disorders, and cardiovascular diseases. Prof Hung T Nguyen is a senior member of the Institute of Electrical and Electronic Engineers; and a Fellow of the Institution of Engineers, Australia, the British Computer Society and the Australian Computer Society.

J. M. Shine, A. M. A. Handojoseno, T. N. Nguyen, Y. Tran, S. L. Naismith, H. Nguyen, and S. J. G. Lewis, 2014, “Abnormal patterns of theta frequency oscillations during the temporal evolution of freezing of gait in Parkinson’s disease”, *Clinical Neurophysiology*, vol. 125, pp. 569-576.

Note: Fulltext not included due to copyright restrictions.

An EEG Study of Turning Freeze in Parkinson's Disease Patients: The Alteration of Brain Dynamic on the Motor and Visual Cortex

A.M. Ardi Handojoseno[1], *Student Member, IEEE*, Moran Gilat[2], Quynh Tran Ly[1], Hayat Chamtie[2], James M. Shine[3], Tuan N. Nguyen[1], *Member IEEE*, Yvonne Tran[1,4], Simon J.G. Lewis[2,*], Hung T. Nguyen[1,*], *Senior Member, IEEE*

***Abstract*— Freezing of gait is a very debilitating symptom affecting many patients with Parkinson's disease, leading to a reduced mobility and increased risk for falls. Turning is known to be the most provocative trigger for freezing of gait. However, the underlying brain dynamic changes associated with a turning freeze remain unknown. This study therefore used ambulatory EEG to investigate the brain dynamic changes associated with freezing of gait during turning. In addition, this study aimed to determine the most suitable EEG sensor location to detect freezing of gait during turning using our classification system. Data from four Parkinson's disease patients with freezing of gait was analysed using power spectral density and brain effective connectivity, comparing periods of successful turning with freezing of gait during turning. Results showed that freezing of gait during turning is associated with significant alterations in the high beta and theta power spectral densities across the occipital and parietal areas. Furthermore, brain effective connectivity showed that freezing during turning was associated with increased connectivity towards the visual area, which also had the highest accuracy to detect freezing episodes in the O1 regions by using power spectral density in our classification analyses. This is the first study to show cortical dynamic changes associated with freezing of gait during turning, providing valuable information to enhance the performance of future freezing of gait detection systems.**

I. INTRODUCTION

Freezing of Gait (FOG) is a common gait deficit in persons with advanced Parkinson's disease (PD), often described by patients as a feeling of "being glued to the floor" [1]. This absence of forward progression disturbs balance and has been interconnected with an increase number in falls for PD patients resulting in injuries and creating a loss of independence for these patients. These physical and psychosocial consequences in turn reduce the quality of life for patients with PD, making FOG a highly important symptom to study [2]. This calls for the need for novel therapies that can aid in predicting a freeze and preventing falls.

Whilst many triggers of FOG have been described, the most precipitant is turning. In controlled timed-up-and-go (TUG) experiments, turning accounts for 48.4% of all witnessed FOG [3]. Turning is a complex motor task requiring both motor and cognitive processing to enable the correct selection, timing and scaling of movement. In addition, in PD patients with FOG the symptom can be exacerbated by emotion, attention and dopaminergic therapy, suggesting the existence of a complex pathophysiological process that not only involves the locomotor networks but also differing cortical areas and the basal ganglia system [3],[4],[5]. Despite advances in our understanding of FOG from recent neuroimaging work [6], the neurobiology specifically associated with turn provoked FOG remains unknown.

One method to advance our understanding of FOG would be through using surface ambulatory EEG techniques. Unlike neuroimaging studies this approach allows the potential to identify and detect FOG episodes during walking due to its ability to track the dynamic physiological changes throughout the brain in real time. The use of this portable measuring system allows the replication of an actual freezing event, allowing the patient to execute movements with timing and scaling as they would usually do outside of the testing environment. Being able to reflect actual gait planning whilst turning through the use of this system is a much more effective measurement of freezing which could allow for the prediction of FOG in a future treatment device.

Our group has developed a detection algorithm for recognizing FOG by analyzing energy power, entropy, correlation and brain effective connectivity (BEC) of EEG signals, providing valuable insights into the underlying brain mechanism [3],[7],[8]. However, these previous studies have focused on episodes of freezing that had mixed provocation factors. The current paper sought to analyse the EEG specifically associated with successful turning and turning associated with FOG.

As we have demonstrated from our previous studies, "classical" Power Spectral Density (PSD) and BEC are powerful methods for feature extraction from surface EEG recordings [7],[8]. Whilst we have established the role of PSD in analyzing FOG previously, BEC is a more recent and advanced approach, which might provide valuable insights into a better

[1]A.M. Ardi Handojoseno, Quynh Tran Ly, Tuan N. Nguyen and Hung T. Nguyen are with Faculty of Engineering and Information Technology, University of Technology, Sydney, Broadway, NSW 2007, Australia. (AluysiusMariaArdi.Handojoseno@student.uts.edu.au, Quynh.T.Ly@student.uts.edu.au, TuanNghia.Nguyen@uts.edu.au, Hung.Nguyen@uts.edu.au)

[2]Moran Gilat, Hayat Chamtie and Simon J.G. Lewis are with Parkinson's Disease Research Clinic, Brain and Mind Research Institute, University of Sydney, Level 4, Building F, 94 Mallet Street, Camperdown, NSW, 2050, Australia. (moran.gilat@sydney.edu.au, hcha1732@uni.sydney.edu.au, simonl@med.usyd.edu.au)

[3]James M. Shine is with Department of Psychology, Stanford University, CA, USA. (mac.shine@sydney.edu.au).

[4]Yvonne Tran is with the Key University Research Centre for Health Technologies, University of Technology, Sydney and the Rehabilitation Studies Unit, University of Sydney, Australia. (Yvonne.Tran@uts.edu.au)

*Dual senior authorship

understanding of the complex physiological mechanisms of freezing in the brain. We hypothesized that there would be a distinct signal change (PSD and BCE) detectable by EEG comparing freezing whilst turning to successful turning with a loss of functional connectivity across the fronto-parietal networks processing visual information [9].

II. METHODS

A. Subjects and Task

Four patients diagnosed with idiopathic PD with significant FOG were recruited from the Parkinson's Disease Research Clinic at the Brain and Mind Research Institute, University of Sydney. The study was approved by The Human Research and Ethics Committee from the University of Sydney and all subjects read and signed written informed consent. They were assessed in the practically-defined "off" state following overnight withdrawal of dopaminergic therapy.

The EEG were recorded from 32 Ag/AgCl scalp electrodes of Biosemi ActiveTwo system, band-passed filtered from 0.15 to 400 Hz, segmented to 1-s durations and digitized at 512 Hz. Only 8 location of interest were used based on previous finding of the affected location of the brain by FOG in a study using fMRI [10]: F3, Fz, F4 (motor planning and working memory), Cz (motor execution), P3, P4 (sensory integration), and O1, O2 (visual area). References was taken by averaging 2 EXG electrodes placed on the ear lobes.

The protocol consisted of several video-recorded TUG tasks that required subjects to walk 5 meters between a chair and a 0.6 x 0.6 m square target defined by a taped box on the floor. Subjects were asked to either make a right or a left turn (180 degrees or and 540 degrees) inside the taped box before returning to the chair. The video footage was labelled by two physicians specialized in movement disorders for the start and end of a turn and for periods of freezing of gait, defined as an absolute cessation or marked reduction of forward progression of the feet despite the intention to walk [1]. EEG data was extracted for periods of freezing of gait during turning (FT) and for periods of normal turning (NT), during which the subject was able to turn effectively inside the box during the TUG tasks. No distinctions were made between either left or right and 180 or 540 degrees turns to improve the power of the analyses.

B. Feature extraction

In this study, 341 selected samples data (117 NT and 224 FT) were filtered using a band-pass (0.5-60 Hz) and band-stop (50Hz) Butterworth IIR. To eliminate differences in source strength due to variance in absolute measurement between electrodes and individual subject, a Z-transformation was applied. Five frequency bands were analysed, namely: theta (4-8 Hz), alpha (8-13 Hz), low beta (13-21 Hz), high beta (21-38 Hz), and gamma (38-60 Hz) [Fig. 1]. The beta frequency band was divided into high and low, based on previous findings showing that specifically high beta frequencies correlate with FOG [11]. A Wilcoxon Sum Rank Test with an alpha of 0.05 was used to investigate the power

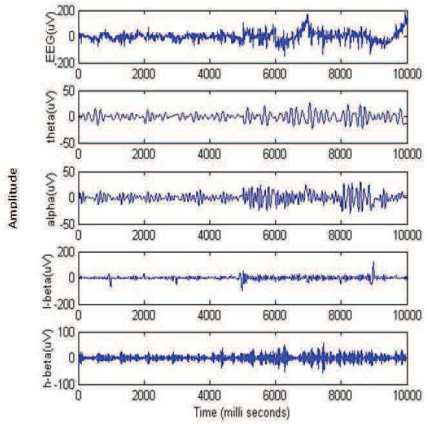

Fig. 1. Decomposition of EEG into four frequency bands in subject 1 shows the alteration of amplitude and frequency signals during a turning freeze (5001-1000 ms) as opposed to a normal turning (1-5000 ms)

spectral densities between periods of normal turning and periods of freezing turning. This feature was used as the main parameter for evaluating the significance of the electrode location during freezing turning.

Effective connectivity analysis was mapped between four brain regions (i.e. frontal, central, parietal, and occipital) by taking the mean of each related electrode in those regions and between electrode locations in subregions of interest, namely fronto-parietal regions (F3, Fz, F4, P3, P4) locations often associated with "executive-attention" and visual networks affected by in PD patients with FOG [12]. Squared generalized partial directed coherence (sGPDC) was used to describe the dynamics of the interactions between brain areas as it provides the best indication of FOG compare to several other methods [7].

Based on the concept of Granger causality, partial directed coherence (PDC) described the exclusive directional flow of information from the activity in the region of interest (ROIs) $s_j(n)$ to the activity in $s_i(n)$ [13]. The squared generalized PDC is a modification of PDC to increase its sensitivity, create an absolute strength of the coupling score, make it scale-invariant, emphasize the sources, and defined as [14]:

$$sGPDC_{j\to i}(f) = \frac{(\frac{1}{\sigma_i}\left|\bar{A}_{ij}(f)\right|)^2}{\sum_{k=1}^{N}\frac{1}{\sigma_k^2}\bar{A}_{kj}(f)\bar{A}_{kj}^*(f)}. \qquad (1)$$

This connectivity measures were obtained using the Nuttall Strand methods to estimate multivariate autoregressive models of time series, a frequency domain representation of the existing multivariate relationships between simultaneously analyzed time series. A short data sliding windows that tracts fast changes in the brain signals with a size of 128 points (256 ms) was consecutively shifted by 32 points (64 ms) to calculate a cross-spectral power density matrix, which allowed us to translate time domain into a frequency domain. Schwarz's Bayesian Criterion (SBC) was then used

to estimate the model order p, which was used due to its superiority over other methods [15].

The statistical significance of nonzero PDC values at each frequency domain was obtained using a bootstrap approach based on a Theiler algorithm to discriminate between noise induced randomness and as a deterministic measurement of data connectivity. The MVAR model coefficients were drawn from 20 different signal realizations, with a 99% level of significance being employed as the rule for rejecting a value that occurred by chance.

C. Statistical Test and Classification

The mean, maximum and minimum values of PSD from each electrode's location in each EEG frequency band were taken to evaluate their strength in detecting FOG. Only features with a p-value of <0.05, as computed by the non parametric Wilcoxon Sum Rank Test were chosen for this test. A three layer Back Propagation Neural Networks with 4 to 5 hidden nodes were used as a classifier with early stopping that helped prevent over-fitting and improved generalization. Using Levenberg Marquardt's algorithm, 59% of the data were trained, validated and tested by 25% and 19 % of the total data. The prediction of sensitivity, specificity and accuracy were measured based on mean squared prediction errors. The average and standard deviation of 20 training and testing data were recorded for further analysis.

III. RESULT AND DISCUSSION

Table 1 shows the power spectral density results between periods of normal turning and periods of freezing turning, with smaller p-values indicating stronger feature differences between the two conditions. The strongest significant differences between the two conditions were found in the beta bands of the occipital areas O1 and O2 ($p \leq 0.0001$). In addition, these results also showed that the parietal areas P3 and P4 were significantly affected by freezing in the theta, alpha, and high beta frequency bands ($p \leq 0.0005$).

This finding is supported by the inter-region BEC analysis [Fig. 2(A)], in which we found a significant increase of information flow toward the occipital areas from the three other areas (P $\rightarrow$ O, C $\rightarrow$ O, F $\rightarrow$ O). This indicates the freezers are 'over-relying' on visual information during a turning freeze. One can argue that patients adopt this strategy to compensate for a loss of kinaesthetic feedback [16], and especially during a FOG episode their feedback from the muscles and joints are a lot different than what they expected. Therefore freezers might need to use more of their visual system to gain information about what is happening so that Cz is able to come up with a motor plan again [16]. As an addition, the trouble of integrating visual information into a motor plan often associated with parietal regions, which were also significantly affected in all the frequency bands of interest except low beta [17]. Finally, the decreased information flow between the frontal regions (F3, Fz and F4) and right parietal regions P4 [Figs. 2(B) and 3] could indicate a loss of attention [18].

TABLE I
CORRELATION ANALYSIS OF NORMALIZED POWER SPECTRAL DENSITY BETWEEN NORMAL TURNING AND FREEZING TURNING

Lead	Freq.	Normal Turning	Freezing Turning	p-value
F3	θ	0.0324 $\pm$ 0.0183	0.0291 $\pm$ 0.0177	0.1029
	α	0.0231 $\pm$ 0.0124	0.0210 $\pm$ 0.0117	0.1036
	low β	0.0116 $\pm$ 0.0060	0.0108 $\pm$ 0.0051	0.2980
	high β	0.0044 $\pm$ 0.0060	0.0044 $\pm$ 0.0024	0.0010
Fz	θ	0.0296 $\pm$ 0.0129	0.0267 $\pm$ 0.0136	0.0349
	α	0.0214 $\pm$ 0.0092	0.0194 $\pm$ 0.0093	0.0366
	low β	0.0110 $\pm$ 0.0049	0.0102 $\pm$ 0.0043	0.1669
	high β	0.0035 $\pm$ 0.0019	0.0041 $\pm$ 0.0021	0.0131
F4	θ	0.0506 $\pm$ 0.0281	0.0462 $\pm$ 0.0303	0.0318
	α	0.0355 $\pm$ 0.0180	0.0328 $\pm$ 0.0199	0.0244
	low β	0.0169 $\pm$ 0.0071	0.0160 $\pm$ 0.0080	0.0397
	high β	0.0054 $\pm$ 0.0062	0.0052 $\pm$ 0.0028	0.0645
Cz	θ	0.0271 $\pm$ 0.0114	0.0230 $\pm$ 0.0110	0.0017
	α	0.0198 $\pm$ 0.0084	0.0169 $\pm$ 0.0075	0.0033
	low β	0.0105 $\pm$ 0.0047	0.0094 $\pm$ 0.0036	0.0779
	high β	0.0040 $\pm$ 0.0023	0.0048 $\pm$ 0.0024	0.0020
P3	θ	0.0330 $\pm$ 0.0152	0.0264 $\pm$ 0.0108	$\leq$0.0001
	α	0.0238 $\pm$ 0.0095	0.0200 $\pm$ 0.0070	0.0001
	low β	0.0125 $\pm$ 0.0041	0.0120 $\pm$ 0.0034	0.4643
	high β	0.0058 $\pm$ 0.0036	0.0082 $\pm$ 0.0044	$\leq$0.0001
P4	θ	0.0292 $\pm$ 0.0136	0.0234 $\pm$ 0.0106	0.0002
	α	0.0213 $\pm$ 0.0093	0.0176 $\pm$ 0.0070	0.0005
	low β	0.0116 $\pm$ 0.0046	0.0107 $\pm$ 0.0036	0.0967
	high β	0.0061 $\pm$ 0.0042	0.0079 $\pm$ 0.0042	$\leq$0.0001
O1	θ	0.0455 $\pm$ 0.0321	0.0492 $\pm$ 0.0318	0.1645
	α	0.0328 $\pm$ 0.0190	0.0381 $\pm$ 0.0193	0.0013
	low β	0.0200 $\pm$ 0.0080	0.0284 $\pm$ 0.0120	$\leq$0.0001
	high β	0.0217 $\pm$ 0.0192	0.0359 $\pm$ 0.0222	$\leq$0.0001
O2	θ	0.0455 $\pm$ 0.0240	0.0425 $\pm$ 0.0255	0.1391
	α	0.0330 $\pm$ 0.0139	0.0335 $\pm$ 0.0156	0.4778
	low β	0.0198 $\pm$ 0.0067	0.0255 $\pm$ 0.0110	$\leq$0.0001
	high β	0.0183 $\pm$ 0.0142	0.0302 $\pm$ 0.0190	$\leq$0.0001

Freq.: Frequency

In the classification analysis where we used input from one channel at a time [Table 2], the occipital channel appeared to be providing the best information for detecting a turning freeze with the sensitivity and accuracy of testing data being 74.61 % and 68.63 %, higher relatively to the classification result obtained from the other locations of interest. These results support the previous finding of the significant alteration of power spectral and information flow in the visual cortex.

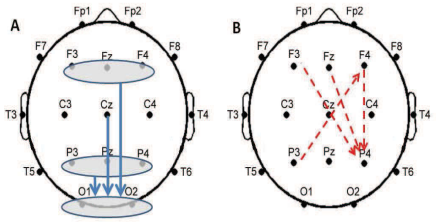

Fig. 2. The significant alteration of information flow during turning freezing (A) between region and (B) intra-frontoparietal region estimated using sGPDC causality. The regional analysis reveals an increase of information flow to occipital area while the fronto-parietal analysis shows a decrease of information flow affected right region of parietal and frontal.

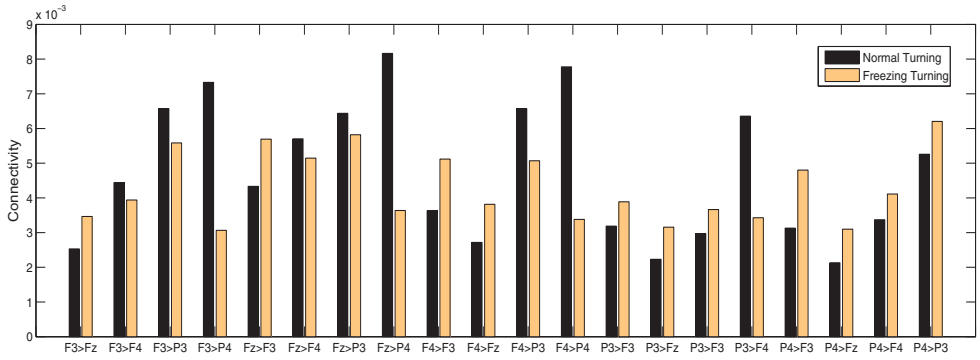

Fig. 3. Frontoparietal sGPDC causality.

TABLE II

CLASSIFICATION RESULTS OF PSD FEATURES USING MLP-NN IN DETECTING TURNING FREEZING

Lead	Training			Testing		
	Sens %	Spec %	Acc %	Sens %	Spec %	Acc %
F3	65.32	50.79	70.98	63.78	48.99	66.27
Fz	69.51	47.14	64.22	68.22	48.38	62.35
F4	71.00	44.99	69.02	67.74	43.65	65.39
Cz	66.79	57.65	69.80	60.40	47.72	60.00
P3	61.62	51.92	70.39	60.92	48.07	66.27
P4	68.90	53.75	70.00	69.98	44.20	69.22
O1	76.88	50.62	71.08	74.61	48.43	68.63
O2	66.27	53.84	66.37	64.61	50.56	62.35

Sens: Sensitivity; Spec: Specificity; Acc: Accuracy

IV. CONCLUSIONS

While frontoparietal processing is known to be associated with directing attention and integrating visual information into a motor plan, in this study we found that the occipital area was more affected during a turning freeze. The results of a classification system using data from one location only also suggests that this visual cortex region is the optimal reference location for the detection of a turning freeze, whilst also providing possible insights into the neural processes underlying freezing of gait during turning. Further studies using larger cohorts of patients are needed to further validate this finding. Using combination of input data from different locations instead of using a single channel can be expected to increase the performance of the system. Finally, the application of this novel observation in more advanced feature extraction and classifier systems will provide a better performance of the FOG detection system.

REFERENCES

[1] J. G. Nutt, B. R. Bloem, N. Giladi, M. Hallett, F. B. Horak, and A. Nieuwboer, Freezing of gait: moving forward on a mysterious clinical phenomenon, The Lancet Neurology, vol. 10, no. 8, pp. 734-744, 2011.

[2] O. Moore, C. Peretz, and N. Giladi, Freezing of gait affects quality of life of peoples with Parkinson's disease beyond its relationships with mobility and gait, Mov. Disord., vol. 22, no. 15, pp. 2192-2195, 2007.

[3] J. M. Shine, A. M. A. Handojoseno, T. N. Nguyen, Y. Tran, S. L. Naismith, H. Nguyen, and S. J. G. Lewis, Abnormal patterns of theta frequency oscillations during the temporal evolution of freezing of gait in Parkinson's disease, Clin. Neurophysiol., vol. 125, no. 3, pp. 569-576, Mar. 2014.

[4] A. Delval, C. Moreau, S. Bleuse, D. Guehl, E. Bestaven, E. Guillaud, and D. Devos, D, Gait and attentional performance in freezers under methylphenidate, Gait & posture, 2014.

[5] S. J. G. Lewis and R. A. Barker, A pathophysiological model of freezing of gait in Parkinson's disease, Parkinsonism & related disorders, vol. 15, no. 5, pp. 333-338, 2009.

[6] J. M. Shine, E. Matar, P. B. Ward, S. J. Bolitho, M. Gilat, M. Pearson, & S. J. Lewis, Exploring the cortical and subcortical functional magnetic resonance imaging changes associated with freezing in Parkinson's disease, Brain, vol. 136, no. 4, pp. 1204-1215, 2013.

[7] A. M. Handojoseno, J. M. Shine, M. Gilat, T. N. Nguyen, Y. Tran, S. J. G. Lewis, and H. T. Nguyen, Prediction of freezing of gait using analysis of brain effective connectivity, in Proc. 31th Annu. Int. Conf. IEEE Eng. Med. Biol. Soc., Chicago, 2014, pp. 4119-4122.

[8] A. M. A. Handojoseno, J. M. Shine, T. N. Nguyen, Y. Tran, S. J. Lewis, and H. T. Nguyen, Analysis and prediction of the freezing of gait using EEG brain dynamics, IEEE Trans. Neural Syst. Rehabil. Eng. 2014 Dec 18, Epub 2014 Dec 18.

[9] P.D. Velu, T. Mullen, E. Noh, M. C. Valdivia, H. Poizner, Y. Baram, and V. R. de Sa, Effect of visual feedback on the occipital-parietal-motor network in Parkinsons disease with freezing of gait, Frontiers in neurology, vol. 4, pp. 1-6, 2013.

[10] A.H. Snijders, Tackling freezing of gait in Parkinson's disease, PhD thesis, Radboud Univ., Nijmegen, the Netherlands, 2012.

[11] J.B. Toledo, J. Lpez-Azcrate, D. Garcia-Garcia, J. Guridi, M. Valencia, J. Artieda, J. Obeso, M. Alegre, and M. Rodriguez-Oroz, High beta activity in the subthalamic nucleus and freezing of gait in Parkinson's disease, Neurobiology of disease, vol. 64, pp. 60-65, 2014.

[12] A. Tessitore, M. Amboni, F. Esposito, A. Russo, M. Picillo, L. Marcuccio, M. T. Pellecchia et al, Resting-state brain connectivity in patients with Parkinson's disease and freezing of gait, Parkinsonism & related disorders, vol. 18, no. 6, pp. 781-787, 2012.

[13] L.A. Baccala and K. Sameshima, Partial directed coherence: a new concept in neural structure determination, Biol. Cyber., vol. 84, no. 6, pp. 463-474, 2001.

[14] E. Florin, J. Gross, J. Pfeifer, G.R. Fink, and L. Timmermann, Reliability of multivariate causality measures for neural data, J. Neurosci. Methods, vol. 198, no. 2, pp. 344-358, 2011.

[15] A. Schlogl, A comparison of multivariate autoregressive estimators, Signal processing, vol. 86, no. 9, pp. 2426-2429, 2006.

[16] K. A. E. Martens, F. Pieruccini-Faria, and Q. J. Almeida, Could sensory mechanisms be a core factor that underlies freezing of gait in Parkinsons disease?, PloS one, vol. 8, no. 5, e62602, 2013.

[17] M. Scolari, K. N. Seidl-Rathkopf, and S. Kastner, Functions of the human frontoparietal attention network: Evidence from neuroimaging, Current Opinion in Behavioral Sciences, vol. 1, pp. 32-39, 2005.

[18] J. M. Shine, E. Matar, P. B. Ward, M. J. Frank, A. A. Moustafa, M. Pearson, S. L. Naismith, and S.J.G. Lewis, Freezing of gait in Parkinson's disease is associated with functional decoupling between the cognitive control network and the basal ganglia, Brain, vol. 138, pp. 3671-3681, 2013.

Prediction of Freezing of Gait Using Analysis of Brain Effective Connectivity

A.M. Ardi Handojoseno[1], *Student Member, IEEE*, James M. Shine[2], Moran Gilat[2],
Tuan N. Nguyen[1], *Member IEEE*, Yvonne Tran[1,3],
Simon J.G. Lewis[2], Hung T. Nguyen[1], *Senior Member, IEEE*

***Abstract*— Freezing of gait (FOG) is a debilitating symptom of Parkinson's disease (PD), in which patients experience sudden difficulties in starting or continuing locomotion. It is described by patients as the sensation that their feet are suddenly glued to the ground. This, disturbs their balance, and hence often leads to falls. In this study, directed transfer function (DTF) and partial directed coherence (PDC) were used to calculate the effective connectivity of neural networks, as the input features for systems that can detect FOG based on a Multilayer Perceptron Neural Network, as well as means for assessing the causal relationships in neurophysiological neural networks during FOG episodes. The sensitivity, specificity and accuracy obtained in subject dependent analysis were 82%, 77%, and 78%, respectively. This is a significant improvement compared to previously used methods for detecting FOG, bringing this detection system one step closer to a final version that can be used by the patients to improve their symptoms.**

I. INTRODUCTION

Freezing of gait (FOG) is a common symptom affecting more than 70% of advance Parkinson disease (PD) patients [1]. It is characterized by an "episodic" incapability to start walking, suddenly failing to continue to move forward, a reduction of forward progression of the feet so that the patient "shuffles" forwards (the festination), or a complete absence of movement despite the intention to walk (akinesia) [2]. Even a brief FOG episode may lead to falls, affecting a patients' level of activity and reducing quality of life [3]. It is resistant to pharmacological treatment, especially in the advanced stages of the disease [4], making FOG prediction systems highly important.

Early detection of FOG episodes has already been developed by our group by analyzing energy, entropy and correlations of electroencephalography (EEG) signals. This system enabled to detect FOG with a sensitivity of 83%, however the specificity was only 58% and accuracy 70% [5]. Compared to motion sensors, such as accelerometers or EMG [6], EEG has an advantage in its ability to track the physiological process of freezing from the earliest stage throughout the analysis of brain dynamics, which also provides insights into possible pathophysiological mechanisms underlying neurological development and disease.

It is known that neural connectivity plays a crucial role in determining the functional properties of neurons and neuronal system. Therefore, the concept of brain connectivity is central for our understanding of organized behaviour of cortical regions beyond the simple mapping of their activity. It has been successfully used to study neurological conditions and disorders, such as Autism [7], Alzheimer's disease [8], and Schizophrenia [9]. In this paper, directed transfer function (DTF) and partial directed coherence (PDC) were used to investigate the connectivity pattern of PD patients' brain area's of interest during freezing episodes. DTF and PDC were used due to their reliability and robustness in neuronal directionality assessment, beyond correlational analyses [10]. The measures of DTF and PDC were taken as the input for the Multilayer Perceptron Neural Network (MLP-NN) to detect the transition of brain signals before freezing episodes.

II. METHODS

A. Data Collection and Preprocessing

The EEG data used in our study were collected from 10 patients (age 75.1 $\pm$6.3) with idiopathic Parkinson's disease and significant FOG as measured during a structured series of video-recorded timed up-and-go tasks (TUG). The patients were recruited from the Parkinson's Disease Research Clinic at the Brain and Mind Research Institute, University of Sydney. EEG data were acquired using a 4 channel wireless EEG system with gold cup electrodes. Based on their role in control movement, the electrodes were placed at the following bipolar EEG channels: O1-T4 (visual), P4-T3 (sensorimotor affordance), Cz-FCz (motor execution) and Fz-FCz (motor planning). The recordings were bandpass filtered between 0.15 and 100 Hz and were segmented to 1-s durations and digitized at 500 samples per second.

Two physicians specialized in movement disorders inspected and labeled the start and duration of the freezing episodes. Based on this analysis, two other groups were determined: normal walking data and transition data (5 seconds before freezing), as has been reported elsewhere [5]. After removing the EEG data segment that were affected by artifact using visual inspection, 843 selected samples data

[1]A.M. Ardi Handojoseno, Tuan N. Nguyen and Hung T. Nguyen are with Faculty of Engineering and Information Technology, University of Technology, Sydney, Broadway, NSW 2007, Australia. (AluysiusMariaArdi.Handojoseno@student.uts.edu.au,TuanNghia.Nguyen@uts.edu.au, Hung.Nguyen@uts.edu.au)

[2]James M. Shine, Moran Gilat and Simon J.G. Lewis are with Parkinson's Disease Research Clinic, Brain and Mind Research Institute, University of Sydney, Level 4, Building F, 94 Mallet Street, Camperdown, NSW, 2050, Australia. (mac.shine@sydney.edu.au, moran.gilat@sydney.edu.au, simonl@med.usyd.edu.au)

[3]Yvonne Tran is with the Key University Research Centre for Health Technologies, University of Technology, Sydney and the Rehabilitation Studies Unit, University of Sydney, Australia. (Yvonne.Tran@uts.edu.au)

were filtered from the low and high frequency noise and 50 Hz line frequency using band-pass (0.5-60 Hz) and bandstop (50Hz) Butterworth IIR with zero phase shift. The EEG data were normalized with a z-transformation to eliminated differences in source strength due to inter-individual and inter-electrode variance in absolute measurements.

B. Multivariate Autoregressive Process

DTF and PDC estimations are based on the application of the Granger causality into multivariate autoregressive (MVAR) models of time series. They are defined as a frequency domain representation of the existing multivariate relationships between simultaneously analyzed time series, which provide a linear measures of causality, indicating the direction and strength of the interactions between multiple coupled variables [11]. When considering a set of stationary EEG signals time series $X(t) = X_1, X_2, ..., X_N$ (N EEG signals simultaneously observed), then the MVAR model is defined as:

$$\begin{bmatrix} x_1(t) \\ \cdot \\ \cdot \\ \cdot \\ x_N(t) \end{bmatrix} = \sum_{r=1}^{p} A_r \begin{bmatrix} x_1(t-r) \\ \cdot \\ \cdot \\ \cdot \\ x_N(t-r) \end{bmatrix} + \begin{bmatrix} w_1(t) \\ \cdot \\ \cdot \\ \cdot \\ w_N(t) \end{bmatrix} \quad (1)$$

where A_r are the model coefficients, p is the model order, and $w_i(t)$ represents a random Gaussian white noise. The model order p was estimated by means of Schawarz's Bayesian Criterion (SBC) due to its robustness [12]. The Nuttall Strand method (multivariate Burg) which has been reported as superior to other methods was used to estimate the MVAR parameters [13].

The time domain representation was then translated to frequency domain by computing the cross-spectral power density matrix:

$$S(f) = H(f) \sum H^H(f) \quad (2)$$

where the superscript H indicates the Hermitian transpose and $H(f)$ is a transfer function matrix

$$H(f) = A^{-1}(f) = [I - A(f)]^{-1} \quad (3)$$

where

$$A(f) = I - \sum_{r=1}^{p} A_r e^{-2i\pi f r} \quad (4)$$

is the Fourier transform of the model coefficient matrix.

C. Directed Transfer Function

The directed transfer function (DTF) estimates the causal influence of the cortical waveform in the channel j on channel i at a certain frequency f, and normalized by dividing the inflow from channel j to channel i by all the inflows to channel i. It is defined as [14]

$$DTF^2_{j\to i}(f) = \frac{|H_{ij}(f)|^2}{\sqrt{\sum_{k=1}^{N} |H_{ik}(f)|^2}}. \quad (5)$$

This normalization resulted in the interval [0, 1] values, with 1 indicating that all of the signal in channel i is caused by the signal from channel j. The denominator of this ratio depends on the frequency, making it difficult when comparing the outflows at different frequencies. Besides, it does not distinguish between direct and cascade flows.

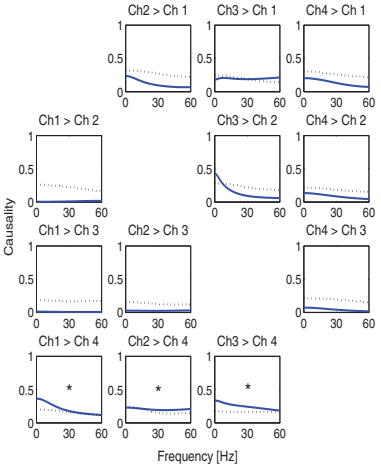

Fig. 1. Sample of estimated sGPDC values (solid lines) and their corresponding surrogates as a threshold of significance estimation (dotted lines), between O1 (channel 1), P4 (channel 2), Cz (channel 3) and P4 (channel 4) from patient 9 during transition preceding the FOG. Only values between 0 Hz and 60 Hz were shown due to physiological significance. An asterisk indicates channel pairs with significant sGPDC causality.

For estimation of direct connections, different normalization has been introduced as the full frequency Directed Transfer Function (ffDTF) [14]

$$ffDTF^2_{j\to i}(f) = \frac{|H_{ij}(f)|^2}{\sqrt{\sum_f \sum_{k=1}^{N} |H_{ik}(f)|^2}}. \quad (6)$$

When multiplied by the partial coherence, this modification of DTF results in the direct DTF (dDTF) [14]:

$$dDTF^2_{j\to i}(f) = ffDTFij(f) PCoh_{ij}(f) \quad (7)$$

where

$$PCoh^2_{ij}(f) = \frac{M^2_{ij}(f)}{M_{ii}(f) M_{jj}(f)} \quad (8)$$

and $M_{ij}(f)$ is the minor obtained by removing ith row and jth column from the spectral matrix S.

D. Partial Directed Coherence

The partial directed coherence (PDC) was introduced to improve and add more information to DTF by distinguishing direct from indirect flow between channels. It does not involve the inversion of matrix A, making it computationally more efficient and precise compared to DTF. With $\bar{A}_{i,j}$ being the i,jth element of $\bar{A}(f)$, the PDC from channel j to i could be calculated as [15]

$$PDC_{j\to i}(f) = \frac{\bar{A}_{ij}(f)}{\sqrt{\sum_{k=1}^{N} \bar{A}_{ki}(f)\bar{A}^*_{kj}(f)}}. \quad (9)$$

As in the DTF, the PDC has values between 0 and 1, with higher values indicating a higher strength of signals transmission from channel j to i at this frequency.

PDC emphasizes the sinks rather than the sources as it is normalized to show a ratio between the outflow from channel j to channel i to all the outflows from the source channel j. Normalization factor was modified in the squared generalized PDC to make PDC scale-invariant, has an absolute strength of the coupling, emphasizes the sources, and has a greater sensitivity[15] [10]:

$$sGPDC_{j\to i}(f) = \frac{(\frac{1}{\sigma_i}|\bar{A}_{ij}(f)|)^2}{\sum_{k=1}^{N} \frac{1}{\sigma_k^2}\bar{A}_{kj}(f)\bar{A}^*_{kj}(f)}. \quad (10)$$

Signals from four EEG electrodes were included in the MVAR model. The short-time DTF, and PDC method was used to measure the connectivity of the data due to its ability to tract fast changes in the brain signals [12]. A data epoch of one second was divided into short overlapping time windows, with a window length of 256 ms and a quarter overlap window. The DTF, dDTF, PDC, and sGPDC were computed in each window over the 1-60Hz frequency range, and were analyzed in five clinical EEG frequency bands: delta, theta, alpha, beta and gamma. A surrogate data method based on Theiler algorithm with 20 realizations was used to select only a directed causal influence, which has less than 1% probability occurring by chance [14]. Surrogates, which indicated the 'leak flows' between channels, were produced by randomizing the signal so that they maintained the spectral properties of the original data sample but destroyed nonlinear-phase relations. Fig.1 illustrates sGPDC measures of the EEG data of subject 9 during the transition to freezing.

For connectivity analysis, individual trial DTF, dDTF, PDC and sGPDC spectrograms were averaged within each subject and then averaged across all subjects within each group, for all directions of connectivity between pairs of electrode regions. These measures represent the strength and the number of causal interactions originating at each electrode, which provides a measure of the source activity arising from each node in a network.

E. Statistical Classification

The mean, the maximum and the minimum values of DTF, dDTF, PDC and sGPDC for each pair of electrodes in each EEG frequency band were taken from two conditions, normal walking and transition to freezing, as features for the prediction of FOG. The non parametric Wilcoxon Sum Rank Test was used to select the most significant feature to feed the classifier for each experiment. A p-value <0.05 and r-value >2.5 were chosen for further process.

For classification, MLP-NN was used due to its good results in classification of EEG signals [16]. A three layer Back Propagation Neural Networks with 4 to 5 hidden nodes was built. Bayesian regularization [17] was used to prevent over-fitting and to improve generalization, with 80% of the data trained by Levenberg Marquardt algorithm and 20% of the data being used for testing. Mean squared prediction error was used to measure the prediction of sensitivity, specificity and accuracy. The average and standard deviation of fifty training and testing were recorded for further analysis.

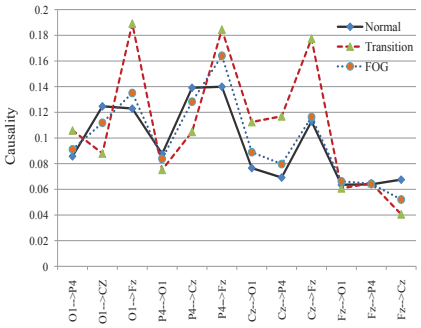

Fig. 2. The mean value of sGPDC from 10 patients which indicates the connection between four locations of EEG electrodes

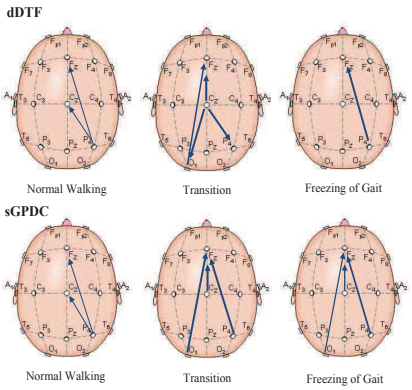

Fig. 3. The schematic interaction between four locations of EEG electrodes during normal walking and FOG estimated using dDTF and sGPDC at theta band frequency. The arrow line width shows the connectivity strength.

III. RESULT AND DISCUSSION

The first row of Fig. 1 indicates a lot of noise on the electrode which picks signals from the occipital one (channel 1), making the "leak inflows" from this electrode relatively high. When only directed causal influence which were higher than the threshold were taken, we noticed that FOG episodes were characterised by abnormal EEG hyperconnectivity involving the frontal region. It received stronger outflows connection from other regions (Fig. 2 and Fig. 3), especially in the lower frequency bands (the theta and alpha band). This suggests that the frontal region, which supports spatial attention, motor intention, cognitive and decision making processes is prominently involved in generating the hypersynchronization

TABLE I

CLASSIFICATION RESULTS OF PROPOSED FEATURES USING MLP-NN IN DETECTING TRANSITION 5 SECOND BEFORE FREEZING

Features	training			testing		
	Sens %	Spec %	Acc %	Sens %	Spec %	Acc %
DTF	70.62	75.49	73.09	65.80	69.52	67.40
dDTF	83.18	85.42	84.31	68.55	73.17	70.86
PDC	82.73	81.51	80.27	71.11	69.07	70.02
sGPDC	79.96	81.62	80.80	72.76	70.28	71.67

Sens: Sensitivity; Spec: Specificity; Acc: Accuracy

TABLE II

CLASSIFICATION RESULTS OF TESTING DATA USING SGPDC AS A FEATURE FOR INDIVIDUAL SUBJECT IN DETECTING TRANSITION 5 SECOND BEFORE FREEZING

Subj	Sens %	Spec %	Acc %	Subj	Sens %	Spec %	Acc %
1	85.93	70.24	77.50	6	85.28	74.10	75.33
2	93.24	88.41	91.00	7	96.53	95.27	94.80
3	74.37	70.64	70.00	8	83.54	87.98	86.17
4	86.80	73.71	78.57	9	60.40	63.67	59.33
5	74.50	73.73	70.67	10	81.77	75.40	77.00
Average: Sens: 82.24%, Spec: 77.32%, Acc: 78.04%							

Subj: Subject; Sens: Sensitivity; Spec: Specificity; Acc: Accuracy

underlaying FOG. This finding supports the hypotheses that attribute FOG to frontal executive dysfunction and visuo-spatial impairment in PD patients with FOG [18].

Both dDTF and sGPDC revealed significant connectivity of P4 >Fz and P4 >Cz in normal walking. They were also in agreement when indicating O1 >Fz and Cz >Fz connectivity during transition and a stronger P4 >Fz connectivity during freezing episodes. The dDTF analysis shows that the significant outflows from Cz to the other 3 electrode locations may signify the overload of cognitive resources as a consequence of a loss of automaticity which shifted neural activation from the subcortical (basal ganglia) to more cortical areas [19].

When used as features for the early detection of FOG, both dDTF and sGPDC show significant increases in performance of the prediction system compared to their original form, DTF and PDC. In addition, sGPDC appears to be the strongest indicator of the transition to freezing with an average sensitivity, specificity, and accuracy of 73%, 70 %, and 72%, respectively (see Table 1). In the subject-dependent analysis where training and testing data were taken from the related subject only, the performance of classification increased to 82%, 77%, and 78% of an average sensitivity, specificity, and accuracy, respectively, with the best results of all performance measures at around 90% obtained by 2 patients (see Table 2). However, the system achieved the performance of all measures at around 60% in 1 patient. This indicates the variability in brain connectivity among subjects.

IV. CONCLUSIONS

This study revealed that the information outflows from the central area during the transition to FOG and the information inflows to the frontal area during freezing episodes were enhanced. This estimation, based on DTF and PDC, also provides useful features for the prediction of FOG, especially in the customized system, with an accuracy of 94.80% obtained in one patient. The inclusion of more data from more patients, the additional feature selection procedure and the optimization of the algorithm on the brain connectivity estimation and classification will be our future work, to obtain a better performance of this potential approach.

REFERENCES

[1] I.C. Lopez, P.J.G. Ruiz, S.V.F. del Pozo, and V.S. Bernardos, "Motor complications in Parkinson's disease: Ten year follow-up study," *Mov. Disord.*, vol. 25, no. 16, pp. 2735-2739, 2010.

[2] J.D. Schaafsma, Y. Balash, T. Gurevich, A.L. Bartels, J.M. Hausdorff, and N. Giladi, "Characterization of freezing of gait subtypes and the response of each to levodopa in Parkinson's disease," *European J. Neurol.*, vol. 10, no. 4, pp. 391-398, 2003.

[3] D. Tan, M. Danoudis, J. McGinley, and M.E. Morris, "Relationships between motor aspects of gait impairments and activity limitations in people with Parkinson's disease: a systematic review," *Parkinsonism & Related Disord.*, vol. 18, no. 2, pp. 117-124, 2012.

[4] N. Giladi, "Medical treatment of freezing of gait," *Mov. Disord.*, vol 23, no. S2, pp. S482-S488, 2008.

[5] A.M. Handojoseno, J.M. Shine, T.N. Nguyen, Y. Tran, S.J.G. Lewis, and H.T. Nguyen, "Using EEG spatial correlation, cross frequency energy, and wavelet coefficients for the prediction of Freezing of Gait in Parkinson's Disease patients," in *Proc. 35th Annu. Int. Conf. IEEE Eng. Med. Biol. Soc.*, 2013, pp. 4263-4266.

[6] M. Bachlin, M. Plotnik, D. Roggen, D. Maidan, J.M. Hausdorff, N. Giladi, and G. Troster, "Wearable Assistant for Parkinsons Disease Patients with the Freezing of Gait Symptom," *IEEE Trans. Inform. Tech. Biomed.*, vol. 14, no. 2, pp. 436-446, 2010.

[7] M.K. Belmonte, G. Allen, A.B. Mitchener, L.M. Boulanger, R.A. Carper, and S.J. Webb, "Autism and abnormal development of brain connectivity," *J. Neurosci.*, vol. 24, no. 42, pp. 9228-9231, 2004.

[8] K. Supekar, V. Menon, D. Rubin, M. Musen, and M.D. Greicius, "Network analysis of intrinsic functional brain connectivity in Alzheimer's disease," *PLoS Computational Biology*, vol. 4, no. 6, pp.e1000100, 2008.

[9] P. Skudlarski, K. Jagannathan, K. Anderson, M.C. Stevens, V.D. Calhoun, B.A. Skudlarska, and G. Pearlson, "Brain connectivity is not only lower but different in schizophrenia: a combined anatomical and functional approach," *Biol. Psych.*, vol. 68, no. 1, pp. 61-69, 2010.

[10] E. Florin, J. Gross, J. Pfeifer, G.R. Fink, and L. Timmermann, "Reliability of multivariate causality measures for neural data," *J. Neurosci. Methods*, vol. 198, no. 2, pp. 344-358, 2011.

[11] L.A. Baccala and K. Sameshima, "Partial directed coherence: a new concept in neural structure determination," *Biol. Cyber.*, vol. 84, no. 6, pp. 463-474, 2001.

[12] C. Porcaro, F. Zappasodi, P.M. Rossini, and F. Tecchio, "Choice of multivariate autoregressive model order affecting real network functional connectivity estimate," *Clinic. Neurophysiol.*, vol. 120, no. 2, pp. 436-448, 2009.

[13] A. Schlogl, "A comparison of multivariate autoregressive estimators," *Signal processing* , vol. 86, no. 9, pp. 2426-2429, 2006.

[14] R. Kus, M. Kaminski, and K.J. Blinowska, "Determination of EEG activity propagation: pair-wise versus multichannel estimate," *Trans. Biomed. Eng.*, vol. 51, no. 9, pp. 1501-1510, 2004.

[15] B. Schelter, J. Timmer, and M. Eichler, "Assessing the strength of directed influences among neural signals using renormalized partial directed coherence," *J. Neurosci. Methods*, vol. 179, no. 1, pp. 121-130, 2009.

[16] F. Lotte, M. Congedo, A. Lecuyer, F. Lamarche, and B. Arnaldi. "A review of classification algorithms for EEG-based brain computer interfaces." *J. Neural Eng.*, vol. 4, pp. 1-24, 2007.

[17] F.D. Foresee and M.T. Hagan, "Gauss-Newton approximation to Bayesian learning," in *Proc. Int. Conf. Neural Netw.*, 1997, pp. 1930-1935.

[18] E. Heremans, A. Nieuwboer, and S. Vercruysse, "Freezing of gait in Parkinsons disease: where are we now?" *Current Neurol. Neurosci. Reports*, vol. 13, no. 6, pp. 1-9, 2013.

[19] J.M. Shine, S.L. Naismith, and S.J.G. Lewis, "The pathophysiological mechanisms underlying freezing of gait in Parkinsons disease," *J. Clinic. Neurosci.*, vol. 18, no. 9, pp. 1154-1157, 2011.

Using EEG Spatial Correlation, Cross Frequency Energy, and Wavelet Coefficients for the prediction of Freezing of Gait in Parkinson's disease patients

A.M. Ardi Handojoseno, James M. Shine, Tuan N. Nguyen, *Member, IEEE*,
Yvonne Tran, Simon J.G. Lewis, Hung T. Nguyen, *Senior Member, IEEE*

***Abstract*— Parkinson's Disease (PD) patients with Freezing of Gait (FOG) often experience sudden and unpredictable failure in their ability to start or continue walking, making it potentially a dangerous symptom. Emerging knowledge about brain connectivity is leading to new insights into the pathophysiology of FOG and has suggested that electroencephalogram (EEG) may offer a novel technique for understanding and predicting FOG. In this study we have integrated spatial, spectral, and temporal features of the EEG signals utilizing wavelet coefficients as our input for the Multilayer Perceptron Neural Network and k-Nearest Neighbor classifier. This approach allowed us to predict transition from walking to freezing with 87 % sensitivity and 73 % accuracy. This preliminary data affirms the functional breakdown between areas in the brain during FOG and suggests that EEG offers potential as a therapeutic strategy in advanced PD.**

I. INTRODUCTION

Freezing of gait (FOG) is common in advanced Parkinson's Disease (PD) affecting over half of all patients after 5 years of illness [1]. In addition, up to a quarter of patients can experience FOG in the early stages of disease [2]. Patients with FOG are paroxysmaly unable to initiate or continue walking, feeling as if their feet are "glued" or "magnetized" to the ground. This symptom causes both physical and psychological distress and is a common cause of fall, often leading to social withdrawal with only partial amelioration from current treatments [1].

Several techniques have been explored to detect FOG such as using electromyogram (EMG) [3], acceleration sensors [4], functional neuroimaging [1] and electroencephalogram (EEG) [5]. Amongst these approaches, EEG offers predictive capability due to its greater temporal resolution and ability to measure dynamic physiological change. Previous work from our group using sub-band wavelet energy and total wavelet entropy of EEG signals has shown the ability of EEG to identify the onset of FOG before it appeared, with average values of accuracy, sensitivity and specificity are 76 %, 74 %, and 78 %, respectively [5].

A pathophysiological model of FOG has been proposed highlighting breakdown in the integration of information from across neural networks related to motor, cognitive and limbic functions in various regions of the brain [6]. This is aligned with recent research exploring the brain as a network of coupled dynamic systems with functional interactions between areas across the brain [7]. Several studies also give insight into Cortico-Subcortical cross-talk (CSC-ct) indicated by the coupling between slow wave (SW) and fast wave (FW) activity related to behavioural inhibition, motivation, emotion and decision making [8]. This paper attempts to establish a link between such bio-markers for the onset of FOG. We propose that based on wavelet decomposition and statistical analysis of its coefficients, both EEG sub-band cross spatial correlation (by means cross spectral correlation) and SW/FW EEG ratio can serve as electrophysiological signatures of FOG. We improved the performance of our work using this method with 87 % classification sensitivity in predicting transition from walking to freezing.

II. METHODS

A. Experimental Setup and Data Acquisition

EEG signals were recorded in twenty-six PD patients with significant FOG (age 69.8 $\pm$ 8.41) during timed up-and-go tasks (TUG) using EEG videomonitoring for FOG assessment at the Parkinson's Disease Research Clinic, the Brain and Mind Research Institute, University of Sydney. EEG was digitally recorded at 4 different locations on the scalp relating to their roles in the general control movement (O1-primary visual receiving area, P4-navigational movement area, Cz-primary motor area and Fz-supplementary motor area). The bipolar electrodes O1-T4 and P4-T3, and monopolar electrodes Cz and Fz with CFz as a reference were used in this study. All data were sampled at 500 Hz. Three groups of data were analyzed: normal walking, transition of FOG (5 seconds before freezing) and FOG.

B. Data Preprocessing

For this study, the first 10 patients without significant artifacts were selected, and 400 samples, each of 1 second length, were taken from each group (i.e. 1200 samples). Low frequency noise, high frequency noise and 50 Hz line frequency noise were eliminated using band-pass (0.5-60 Hz)

A.M. Ardi Handojoseno, Tuan N. Nguyen and Hung T. Nguyen are with Faculty of Engineering and Information Technology, University of Technology, Sydney, Broadway, NSW 2007, Australia. (AluysiusMariaArdi.Handojoseno@student.uts.edu, TuanNghia.Nguyen@uts.edu.au, Hung.Nguyen@uts.edu.au)

James M. Shine and Simon J.G. Lewis are with Parkinson's Disease Research Clinic, Brain and Mind Research Institute, University of Sydney, Level 4, Building F, 94 Mallet Street, Camperdown, NSW, 2050, Australia. (mac.shine@sydney.edu.au, simonl@med.usyd.edu.au)

Yvonne Tran is with the Key University Research Centre for Health Technologies, University of Technology, Sydney and the Rehabilitation Studies Unit, University of Sydney, Australia. (Yvonne.Tran@uts.edu.au)

and band-stop (50 Hz) Butterworth IIR filters. Stein's unbiased risk estimate thresholding based on wavelet transforms is used to remove ocular and muscular artifacts.

C. Feature Extraction and Selection

Wavelet transform (WT) is chosen to extract the individual EEG data due to its strengths in time-scale (frequency) localization and multirate filtering [9]. It is defined as the convolution between the signal *f(t)* and the wavelet function $\psi_{u,s}(t)$ generated by dilations (contraction) and translation (shift) of mother wavelet $\psi(t)$

$$Wf(u,s) = f \star \bar{\psi}_s(u) = \int_{-\infty}^{+\infty} f(t)\frac{1}{\sqrt{s}}\psi^*(\frac{t-u}{s}) \qquad (1)$$

The discrete wavelet transforms (DWT) based on dyadic scales and position is used in which the EEG signal is decomposed into progressively finer details by means of multi-resolution analysis using complementary low and high pass filter, and is down sampled by 2. The scaling coefficients as the result of low pass filter are further decomposed into low-pass and high-pass coefficients of WT. Each EEG sample *x(t)* at scales *j*=1,2,..., *J* and time point *k* is then can be represented in terms of DWT as

$$x(t) = \sum_k c_{J,k}\varphi_{J,k}(t) + \sum_k \sum_{j \le J} d_{j,k}\psi_{j,k}(t) \qquad (2)$$

where $\varphi_{j,k}(t) = 2^{-j/2}\varphi(2^{-j}t-k)$, $\psi_{j,k}(t) = 2^{-j/2}\psi(2^{-j}t-k)$, $c_{J,k}$ is the approximation coefficient and $d_{j,k}$ is the detail coefficient. These wavelet coefficients under certain conditions completely represent the original signal and can be used for description, analysis, approximation and filtering.

After six levels of decomposition, the coefficients retained from EEG samples at 500 Hz are c_6 (0-3.9 Hz), d_6 (3.9-7.8 Hz), d_5 (7.8-15.6 Hz), d_4 (15.6-31.3 Hz), and d_3 (31.3-62.5 Hz). Noises d_2 (62.5-125 Hz) and d_1 (125-250 Hz) are discharged from further analysis as their magnitudes are negligible in a normal EEG. Daubechies wavelet of order 4 (db4) are used since its smoothing feature has been proved to work well in detecting changes of EEG signals [10]. Reconstruction of these five coefficients using the inverse wavelet transform approximately corresponding to the five physiological EEG sub-bands *delta*, *theta*, *alpha*, *beta*, and *gamma*, can be seen in Fig.1. The results of this filtering and decomposition are further processed to extract spatial, spectral and temporal parameters based on three feature extraction methods.

1) Wavelet Cross Spectrum : The brain can be seen as a complex network of interacting and coupled subsystems which determines its functions. Wavelet cross spectrum (WCS) based on the continuous WT is used to investigate changes among EEG signals being recorded at different locations on the scalp. It can be interpreted as an indicator of functional relationship between different brain regions.

We calculate the Morlet wavelet transform of EEG sub-band electrodes at 4 different positions as a function of both time *t* and frequency (scale) *s*, defined as [11]:

$$W_j^n(t,s) = \frac{1}{\sqrt{s}}\sum_{\tau}^{T} x_j^n(\tau)\psi^*[\frac{(\tau-t)}{s}] \qquad (3)$$

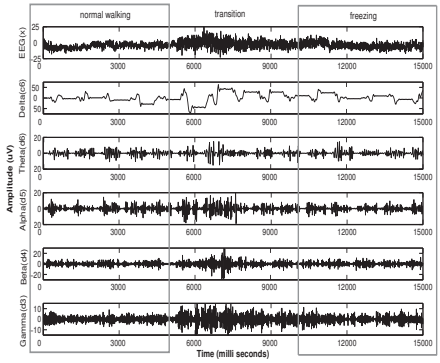

Fig. 1. Wavelet decomposition of EEG into five EEG sub-bands. It covers 3 conditions: normal walking, transition and freezing. Changing in wavelet energy between those three conditions are discernable.

where $\psi^*[]$ is the complex conjugate of the Morlet function. WCS measures the strength of a relationship between pairs of locations and can be defined as:

$$WCS_{jk}^n(t,s) = W_j^n(t,s)W_k^n(t,s)^* \qquad (4)$$

The product of two spectra expressed by wavelet coefficients of the time scale representation of EEG sub-bands is a local measure of the interaction between signals j and k at the given frequency. Since Morlet function includes both real and imaginary part, as a result the WCS is complex valued. The average amplitude of this local wavelet cross correlation spectrum over time samples *t* ($|\overline{WCS_{jk}^n(t,s)}|$) shows the global wavelet cross spectrum (GWCS) at related EEG sub-bands (see Fig.2). The first feature, total wavelet cross spectrum (TWCS) of EEG sub-bands, is obtained by calculating the sum of the global wavelet spectrum over scale (frequency) sub-bands. In addition, the centroid frequency wavelet cross spectrum (CFWCS) is calculated to show the center of gravity of each pair of signals at related EEG sub-bands and defined as follows [12]:

$$CF = \frac{\sum_i f_i * P(f)}{\sum_i P(f)} \qquad (5)$$

where f is a pseudo-frequency corresponding to the scale s, and $P(f)$ is the GWCS power.

2) Wavelet Cross Frequency Energy Ratios: The coupling between slow and fast frequency in the EEG spectrum has been studied as an indicator of cortico-subcortical cross-talk [8]. Studying the relations between the different frequency bandwidth could reveal some of the physiological dynamics of brain function related to different arousal systems. In PD research using quantitative EEG, some EEG electrode locations showed increased SW (*delta* and *theta*) and decreased FW (*alpha* and *beta*) which correlate with cognition decline in PD patients [13].

Wavelet energy is computed on each retained wavelet

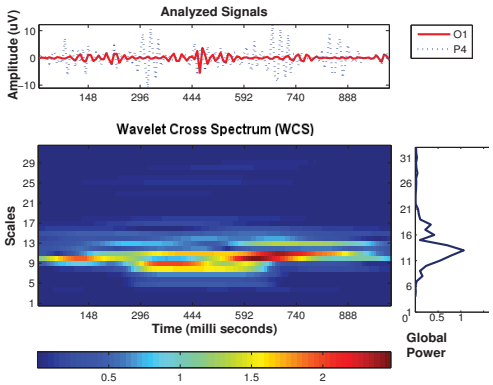

Fig. 2. Wavelet cross spectrum for transition of freezing at gamma sub-band. The upper panels shows EEG signals from electrode pairs O1 and P4. The right panel presents the global wavelet spectrum obtained by averaging over time samples.

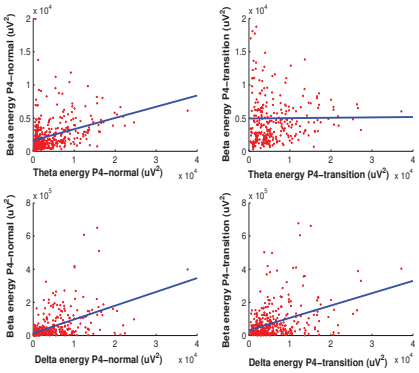

Fig. 3. Scatterplots of significant θ/β (electrode P4) correlation in the normal walking condition which is different with no significant correlation in the transition five seconds before freezing condition (upper panel). Two bottom scatterplots show a non-significant difference between δ/β (electrode P4) correlation in normal walking condition and the transition five seconds before freezing condition.

scale (c_6, d_6, d_5, d_4, d_3) by squaring and summing the wavelet coefficients of the decomposed level [5]. In this study, wavelet cross frequency energy ratios (ER) (δ/β) and (θ/β) were observed and selected as features since they are part of major frequency bands of oscillation in the basal ganglia which may have a functional role in movement [14].

3) Statistical Features: Various simple statistical properties of the EEG time series have already been used in preceding brain studies. It was proven to be effective for discriminating different brain conditions. In this study some popular methods were applied to extract information from wavelet coefficients of the EEG epoch *x(t)*: quantifying the central tendency (*mean*), degree of dispersion (*standard deviation*), asymmetry (*skewness*) and peakedness (*kurtosis, maximum, minimum*). They were used to represent the time frequency distribution of the EEG signals in each sub-band.

In view of the data having a non-normal distribution and to reduce false positives arising from the large dataset, non-parametric statistical analysis Wilcoxon sum rank test with continuity correction of 0.5 was implemented. Only features with significant statistical differences between those groups of data (p-value <0.05) were chosen for further processing.

D. Classification

Multilayer perceptron neural network (MLP) analysis was used to classify data samples based on selected features. The Levernberg Marquardt algorithm was chosen as a training method of a three layer MLP with 56%, 25% and 19% of the data used for training, validation and testing, respectively. The validation set was used as a stopping criterion to avoid overfitting as well as error goal 0.01 in single MLP with 8 to 12 hidden layer neurons. For comparison, the obtained features were also used to train and test using k-nearest neighbors (kNN) classifier with 15 to 40 nearest neighbors based on the Euclidian distance. Each feature and their combination were trained and tested for twenty times and the mean result was recorded.

III. RESULTS AND DISCUSSION

The selected spatial and spectral features with p-value <0.05 are presented in Table 1 from two of four features (CFWCS and ER). One can see that the freezing condition in PD patients significantly affected neural synchronization of different brain regions. Amongst four different regions under study, P4 and Cz appeared as the most important sites contributing in nine out of sixteen most important CFWCS features selected for their statistical significance during the transition of freezing (N-T). This result supports our view in the previous report that the freezing condition has a deep impact in the area that is responsible for integrating sensory information from various parts of the body [5].

The assessment of WCS between each EEG channel pair and CFWCS in each channel demonstrated an altered pattern of synchronisation in the *theta* sub-band during transition from walking to freezing and and in the freezing period. This finding is aligned with prior studies in FOG and PD in general, which suggests this activity is associated with motor-task changing [15]. In addition, since the freezing phenomenon has also been associated with non-motor features, the coupling of *delta* and *beta* oscillation during the transition and freezing periods may represent factors such as increased cognitive activity, a rise in anxiety levels or other perceptual processing [16]. Fig. 3 show the dynamics of sub-band wavelet energy as a result of transition from walking to freezing in electrodes P4 which have significant changing in θ /β but not in δ /β.

For classification, only features that were statistically significant (p-value <0.05) between two conditions were taken for input. We took 131 features representing the spatial spectral temporal characteristics of EEG signals based on spectral

TABLE I
SENSITIVITY OF CENTROID FREQUENCY WAVELET CROSS SPECTRUM AND WAVELET CROSS FREQUENCY ENERGY RATIOS FEATURES

Feature	N-T *p*-value	N-F *p*-value	Feature	N-T *p*-value	N-F *p*-value
CF-O1P4-β	0.0047	0.0659	CF-P4Cz-α	0.0005	0.1258
CF-O1Cz-γ	0.0001	0.0257	CF-P4Cz-θ	0.0001	0.2431
CF-O1Cz-β	0.0003	0.0037	CF-P4Fz-γ	$\leq$0.0001	$\leq$0.0001
CF-O1Cz-α	0.0001	0.0032	CF-P4Fz-β	0.0012	$\leq$0.0001
CF-O1Cz-θ	0.0139	0.4326	CF-P4Fz-α	0.0078	$\leq$0.0001
CF-O1Fz-θ	0.0001	0.0001	CF-P4Fz-θ	0.0060	$\leq$0.0001
CF-P4Cz-γ	$\leq$0.0001	0.0121	CF-CzFz-γ	0.0004	0.7581
CF-P4Cz-β	0.0031	0.0250	CF-CzFz-θ	0.0001	0.0001
δ /β O1	0.0079	0.5862	θ /β O1	$\leq$0.0001	0.0431
δ /β Cz	$\leq$0.0001	0.0288	θ /β P4	$\leq$0.0001	0.2335
δ /β Fz	$\leq$0.0001	$\leq$0.0001	θ /β Cz	$\leq$0.0001	$\leq$0.0001

N: normal walking; T: transient; F: freezing

cross correlation (magnitude and centroid frequency), cross frequency energy ratios and statistics of wavelet energies of EEG signals from 3 different conditions. The discriminant capability of each feature and their combination in differentiating normal walking and transition to freezing were then examined.

The performance of classification did not necessarily increase when different features were combined. As can be seen in Table 2, utilizing MLP, the highest result for sensitivity has been achieved using only WCS (83.37 % mean) whilst applying only the statistic features as the input of classifiers gave the best result for accuracy (73.47 % mean). Interestingly, WCS gave the best result for accuracy in differentiating normal walking and transition to freezing using kNN (72 % mean) while the combination of all features has increased sensitivity up to 87.25 %. However, both MLP and kNN consistently showed the strength of WCS in correctly detecting a transition condition, which presumably related to the combined information within this metric (spatial, spectral, and temporal). While stronger ability to correctly assess both conditions (accuracy) is still on the agenda, how good the test is at detecting freezing is determined by its sensitivity, as we are more concerned on correctly predicting transient/freezing than correctly predict normal walking. Our result suggest that -except for CFWCS- all other features (WCS, ER, and statistical information of wavelet coefficients) represent good candidates for further development.

TABLE II
CLASSIFICATION RESULTS OF PROPOSED FEATURES USING MLP-NN AND KNN CLASSIFIER IN DETECTING TRANSITION 5 SECOND BEFORE FREEZING FROM NORMAL WALKING

Inputs	MLP			kNN		
Features	Se %	Sp %	Acc %	Se %	Sp %	Acc %
WCS	83.37	57.63	69.9	83.50	60.50	72.00
CFWCS	63.51	62.6	62.73	64.25	61.50	62.87
ER	77.60	59.02	68.13	61.00	54.75	57.88
Stat	75.47	71.47	73.47	82.75	57.25	70.00
WCS,Stat	79.19	66.57	73.00	83.75	59.00	71.38
WCS,Stat,ER	74.28	69.89	72.18	87.00	52.00	69.50
All	76.27	67.29	71.75	87.25	52.75	70.00

Se: sensitivity; Sp: specificity; Acc: accuracy

IV. CONCLUSIONS AND FUTURE WORK

This study demonstrates that a novel approach combining the spatial, spectral and temporal features of surface EEG recording may prove effective for the prediction of FOG in PD. In addition, a greater understanding of these recordings will offer insight into the pathophysiological mechanisms underlying this devastating symptom. We propose that this higher sensitivity for event prediction has been achieved due to the integration of features measuring a dynamic pattern of space-time-frequency in EEG signals during transition to a freezing condition. The application of all four features proposed in this study has increased capacity to correctly detect a FOG attack. Therefore, they can serve as useful parameters in discriminating EEG signals. Future work will hone the use of these electrophysiological parameters, with dimensional reduction and classification methods that should hopefully improve the utility of this approach.

REFERENCES

[1] Y. Okuma, Freezing on gait in Parkinson's disease, J. Neurol, no. 253, Dec. 2006, pp. 27-32.

[2] S.T. Moore, H.G. MacDougall, and W.G. Ondo, Ambulatory monitoring of freezing of gait in Parkinson's disease, J Neuroscience Meth, vol. 167, no. 2, pp. 340-348, 2008.

[3] M.B. Popovic, M.D. Jovicic, S. Radovanovic, I. Petrovic, and V. Kostic, A simple method to assess freezing of gait in PD patients, Braz J Med Biol Res, vol. 43, no. 9, pp. 883-889, Sep. 2010.

[4] S. Mazilu, M. Hardegger, Z. Zhu, D. Roggen, G. Troster, M. Plotnik, and J.M. Hausdorff, Online detection of freezing of gait with smartphones and machine learning techniques, in Proc. 6th Int. Conf. Pervasive Computing Technologies for Healthcare, 2012, pp. 123-130.

[5] A.M. Handojoseno, J.M. Shine, T.N. Nguyen, Y. Tran, S.J.G. Lewis, and H.T. Nguyen, The detection of Freezing of Gait in Parkinson's disease patients using EEG signals based on Wavelet decomposition, in Proc. 34th Annu. Int. Conf. IEEE EMBC, 2012, pp. 69-72.

[6] S.J.G. Lewis and R. A. Barker, A pathophysiological model of freezing of gait in PD,in Park. Relat. Disord. vol. 15, no.5, pp. 333-338, 2009.

[7] C.J. Stam, Nonlinear dynamical analysis of EEG and MEG, in Clinical Neurophysiology, vol. 116, no. 10, pp. 2266-2301, 2005

[8] D.G.L. Schutter, C. Leitner, J.L. Kenemans, and J. van Honk, Electrophysiological correlates of cortico-subcortical interaction: A cross-frequency spectral EEG analysis, in Clinical Neurophysiology, vol. 117, no. 2, pp. 381-387, 2006.

[9] Burrus, C. Sidney, et al, Introduction to wavelets and wavelet transforms: a primer, Vol. 23, Upper Saddle River: Prentice hall, 1998.

[10] A. Subasi, EEG signal classification using wavelet feature extraction and a mixture of expert model, in Expert Systems with Applications, vol.32 no.4, pp. 1084-1093, 2007.

[11] D. Lee, Analysis of phase-locked oscillations in multi-channel single-unit spike activity with wavelet cross-spectrum, J Neuroscience Meth., vol. 115, no.1, pp. 67-75, 2002.

[12] L.B. Nguyen, A. V. Nguyen, S. H. Ling, and H. T. Nguyen, A PSO-based neural network for detecting nocturnal hypoglycemia using EEG signals, in Proc. 2012 Int. Joint Conf. Neural Networks, 2012, pp. 1-6.

[13] J.N. Caviness, J.G. Hentz, V.G. Evidente, E. Driver-Dunckley, J. Samanta, P. Mahant, and C.H. Adler, Both early and late cognitive dysfunction affects the electroencephalogram in Parkinson's disease, in Parkinsonism Relat. Disord., vol. 13, no.6, pp. 348-354, 2007.

[14] P. Brown, Oscillatory nature of human basal ganglia activity: relationship to the pathophysiology of Parkinson's disease, in Mov. Disord. vol. 184, no. 4, pp 357-363, 2002.

[15] S.J. Palmer, P.W.H. Lee, Z.J. Wang, W.L. Au, and M.J. Mc Keown, θ, β but not α-band EEG connectivity has implications for dual task performance in Parkinsons disease, in Parkinsonism Relat. Disord, vol 16, 2010, pp. 393-397.

[16] G.G. Knyazev, J.L.G. Dennis, and J. van Honk, Anxious apprehension increases coupling of delta and beta oscillations, Int. J. Psychophysiology, vol. 61, no. 2, pp. 283-287, 2006.

The detection of Freezing of Gait in Parkinson's disease patients using EEG signals based on Wavelet Decomposition

A.M. Ardi Handojoseno, James M. Shine, Tuan N. Nguyen, *Member, IEEE*,
Yvonne Tran, Simon J.G. Lewis, Hung T. Nguyen, *Senior Member, IEEE*

***Abstract*— Freezing of Gait (FOG) is one of the most disabling gait disturbances of Parkinson's disease (PD). The experience has often been described as "feeling like their feet have been glued to the floor while trying to walk" and as such it is a common cause of falling in PD patients. In this paper, EEG subbands Wavelet Energy and Total Wavelet Entropy were extracted using the multiresolution decomposition of EEG signal based on the Discrete Wavelet Transform and were used to analyze the dynamics in the EEG during freezing. The Back Propagation Neural Network classifier has the ability to identify the onset of freezing of PD patients during walking using these features with average values of accuracy, sensitivity and specificity are around 75 %. This results have proved the feasibility of utilized EEG in future treatment of FOG.**

I. INTRODUCTION

After Alzheimer's disease (AD), Parkinson's disease (PD) is the second most prevalent neurodegenerative disorder which increases with age [1]. It is a slowly progressive neurologic disorder caused by degeneration of dopamine and other sub-cortical neurons in the substantia nigra, an area in the basal ganglia of the brain. Dopamine is one of neurotransmitters which help transmit a message to the striatum in the central area of the brain to initiate and control movement and balance.

The freezing of gait (FOG) is defined as a 'brief, episodic absence or marker reduction of forward progression of the feet despite the intention to walk' [2]. It was found to be the most distressing symptom of PD. It is a common cause of fall, interferes with daily activities, makes people with Parkinson's lose confidence in walking and significantly impairs quality of life [3]. It is one of the least understood symptoms in Parkinson's disease and empirical treatments are of poor efficacy, making it an important clinical problem [2], [4].

In recent years, a few attempts have been reported on the detection and prediction of FOG. Since leg oscillations are so common in episodes of freezing, they are used as a sign of the freezing's onset and as an indication that special treatment to 'un-freeze' needs to be done immediately [2], [5]. Two major different approaches are based on characterizing freezing of gait using spatiotemporal kinematic parameter of gait (an increased cadence, decreased stride length, and decreased angular excursion of leg joints) and based on frequency analysis of leg movement [6]. Some works have also been reported using an Electromyographic (EMG) pattern to detect the onset of FOG [7], [8]. A wearable device using on-body acceleration sensors to measure the patients' movement has been developed [9]. Functional MRI and virtual reality-based walking tasks were utilized in recent research to identify direct neural correlate underlying freezing behavior in a patient with PD [4].

Electroencephalogram (EEG) has been used to identify and analyze brain dysfunctions including Alzheimer Disease (AD) [10], Epilepsy [11], monitoring cerebral injury and recovery [12] and Parkinson's Disease [13]. To the best of our knowledge, there is no implementation of EEG for FOG detection except in a preliminary experiment [14] . In this paper, we present a methods for detection of FOG using EEG signals based on Wavelet decomposition and patterns recognition techniques. The propose features, subband Wavelet Energy and Total Wavelet Entropy, were chosen as they were reported has significant advantages in detecting changes in a short segment of EEG signals [15]. Complemented with the Multilayer Perceptron Neural Network, they showed a significant change in the brain signals before freezing.

II. METHODS

A. Experimental Setup and Data Acquisition

Twenty-six patients (age 69.8 $\pm$ 8.41) with idiopathic Parkinson's disease with significant FOG were recruited from the Parkinson's Disease Research Clinic at the Brain and Mind Research Institute, University of Sydney. All patients underwent a structured series of video-recorded timed up-and-go tasks (TUG). Freezing episodes were defined as the paroxysmal cessation of a patient's footsteps during a TUG task and were analyzed by two independent raters.

The EEG signals were obtained using a-4 channel wireless EEG system developed by UTS with sensors are located at occipital one (O1-primary visual receiving area), parietal four (P4-navigational movement area), central zero (Cz-primary motor area) and frontal zero (Fz- supplementary motor area). Only the differential channels O1-T4 and P4-T3 were used in this study. Raw data were acquired at sampling rate of 500 Hz in 1 to 2 hours periods for each patient and an epoch of 1

A.M. Ardi Handojoseno, Tuan N. Nguyen and H.T. Nguyen are with Faculty of Engineering and Information Technology, University of Technology, Sydney, Broadway, NSW 2007, Australia. AluysiusMariaArdi.Handojoseno@student.uts.edu, tnnguyen.uts@gmail.com, Hung.Nguyen@uts.edu.au

James M. Shine and Simon J.G. Lewis are with Parkinson's Disease Research Clinic, Brain and Mind Research Institute, University of Sydney, Level 4, Building F, 94 Mallet Street, Camperdown, NSW, 2050, Australia. mac.shine@sydney.edu.au, simonl@med.usyd.edu.au

Yvonne Tran is with the Key University Research Centre for Health Technologies, University of Technology, Sydney and the Rehabilitation Studies Unit, University of Sydney, Australia. Yvonne.Tran@uts.edu.au

second from individual freezing events was taken. Afterward EEGs data were divided into three groups. The first group was recorded prior to an onset of Freezing (normal walking). The second group is referred to a period of onset of FOG (5 seconds before freezing). The third group contains the EEG signals during the FOG. These data are then processed in three stages: preprocessing stage, feature extraction and selection stage, and classification stage.

B. Data Preprocessing

Based on visual inspection on raw data, data from 10 patients were selected and 40 samples of data from each chosen subject were taken for each group (i.e.1200 samples). Afterwards, EEGs were filtered using band-pass and band-stop butterworth IIR filters in order to eliminate low frequency noise and high frequency noise (BPF 0.5-60 Hz) and cancel out the 50 Hz line frequency (BSF 50 Hz). Then, a simple threshold filter was applied for further eliminated noise, based on comparison of the signal data with its neighbor and the standard deviation of the data.

C. Feature Extraction and Selection

Compared to a traditional Fourier Transform, Wavelet Transform has the advantages of time-frequency localization, multiscale zooming, and multirate filtering for detecting and characterizing transients since its building block functions are adjustable and adaptable [16]. It gives an excellent feature extraction from non-stationary signals such as EEGs. In this research, the discrete wavelet transforms (DWT) based on dyadic scales and positions is used. The DWT is defined as,

$$DWT(j,k) = \frac{1}{\sqrt{|2^j|}} \int_{-\infty}^{\infty} x(t)\psi(\frac{t-2^j k}{2^j})dt \qquad (1)$$

where 2^j and $k2^j$ are the scale (reciprocal of frequency) and translation (time localization) respectively.

In the procedure of multiresolution decomposition of signal $x(t)$ based on the DWT, each signal is simultaneously passed through a complementary high pass filter (HPF) and low pass filter (LPF) and is down sampled by 2. The outputs of the high pass and low pass filters provide the detail D_j with the frequency band $[f_m/2 : f_m]$ and the approximation A_j with the frequency band $[0 : f_m/2]$, respectively. Frequency subbands are related to the sampling frequency of the original signal f_s in which f_m=$f_s/2^{(l+1)}$ where l is the level of decomposition.

The Wavelet decomposition for a given EEG signal $x(t)$ that shows the DWT with their coefficients could be written

$$x(t) = \sum_{k=-\infty}^{\infty} A(k)\varphi_k(t) + \sum_{j=0}^{\infty}\sum_{k=-\infty}^{\infty} D(j,k)\psi_{j,k}(t) \qquad (2)$$

The EEG signals then can be considered as a superposition of different structures occurring on different time-scales at different times. For EEG sampled at 500 Hz, a six level decomposition results in a good match to the standard clinical EEG subbands: *delta* (A_6: 0-3.9 Hz), *theta* (D_6: 3.9-7.8 Hz), *alpha* (D_5: 7.8-15.6 Hz), *beta* (D_4: 15.6-31.3 Hz), *gamma* (D_3: 31.3-62.5 Hz). Two of the highest resolution components are noises: D_2 (62.5-125 Hz) and D_1 (125-250 Hz). Daubechies (db4) wavelets are selected as the wavelet function due to their smoothing feature which is suitable for detecting changes of the EEG signals. Reconstruction of these signals into five constituent EEG subbands is depicted in Fig.1.

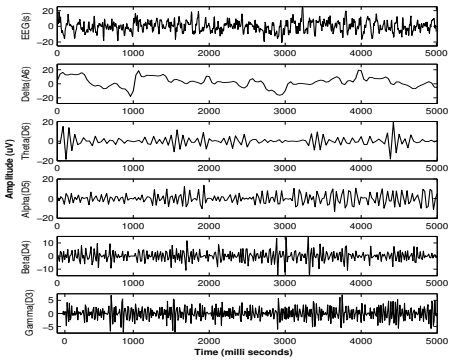

Fig. 1. Wavelet decomposition of EEG into five EEG subbands

The energy in these components and their wavelet coefficients are related to the energy of the original signal, according to Parseval's Theorm. This partition at different time (k) and in scale (j=1,....,l) can be presented as:

$$ED_j = \sum_{k=1}^{N} |D_{j,k}|^2, j = 1,....l \qquad (3)$$

$$EA_l = \sum_{k=1}^{N} |A_{j,k}|^2 \qquad (4)$$

where N is the number of the coefficients of the detail or approximation at each decomposition level.

The energy distribution diagrams of EEG subbands at channel O1 and P4 of three groups of signal: a) normal; b) onset; c) freezing shows that EEG wavelet energy increases before freezing in all subbands (Fig. 2). In comparison with the EEG signal from normal stage, subbands *alpha*, *beta*, and *gamma* of freezing stage have a bigger percentage of the values of the total energy of the signal.

Total energy of the wavelet coefficients will be

$$E_{tot} = EA_l + ED_j \qquad (5)$$

Normalization values of each subbands wavelet energy (WE) results in the Relative Wavelet Energy (RWE)

$$p_j = \frac{E_j}{E_{tot}} \qquad (6)$$

where E_j refers to ED_j and EA_l. Further analysis on the distribution energy using the Shannon information entropy theory reveals the shift of the degree of complexity of the

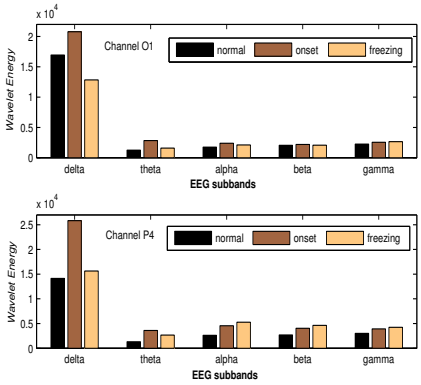

Fig. 2. Group means of wavelet energy of EEG subbands at O1 and P4

signal. Based on distribution of the RWE, the total wavelet entropy (TWE) is defined as [15]:

$$H(x) = -\sum_{j} p_{j,k} log p_{j,k} \quad (7)$$

Comparison of the TWE in three groups data (Fig.3) suggests that EEG activity in freezing stage is less regular (more complex) than in a normal condition in the occipital and parietal regions. Significant changes happen even between normal and onset with channel P4 appears as a stronger indicator of changing than channel O1.

Non-parametric statistical analysis the Wilcoxon Sum Rank Test was implemented to evaluate the statistical differences between those features of three groups of data and to select the significant one that differentiates those groups of data.

D. Classification

Based on the feature selection and their combination possibilities for classification, different Neural Networks with different set of inputs are developed. A three layer Back Propagation Neural Networks (BP-NN) is used, with 56% of the data trained by Levenberg Marquardt algoritm (25% and 19% of the data are used for validation and test, respectively). Tangent Sigmoid is chosen for activation function and training process is stopped by the validation set. The number of hidden nodes is selected between 4 to 7 depending on the number of inputs dimension and the number of training pairs. Twenty separated training and testing were done for each feature. Mean, standard deviation and the best result were recorded for further analysis.

III. RESULTS AND DISCUSSION

Statistical analysis indicates that group Normal differs from the other two groups (Onset and Freezing) at its Wavelet Energy subbands *delta*, *theta*, and *alpha* as well as their TWE (Table I). The higher subbands Wavelet Energy (*beta* and *gamma*) in channel O1 do not appear to be significantly

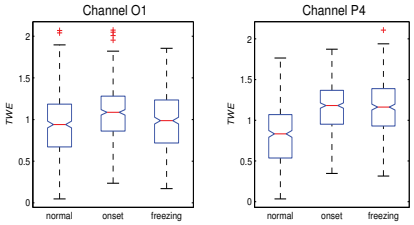

Fig. 3. The Box Plot of the TWE of three groups data of PD patients

different from each other as their confidence level less than 99% (p-value >0.01). However, all subbands wavelet energy at channel P4 are statistically different, suggesting this region has been deeply affected by the FOG. The degree of order of wavelet energy significantly increased from onset stage to freezing stage at occipital region (O1) in contrast with continuous decreasing regularity at parietal region (P4) as the general trend of dynamic from normal to freezing. This trend was contrary to the pattern of EEG signal of AD and epileptic patients during seizure which becomes more organized and has less complexity and chaoticity [10], [11].

While the subband *delta* is likely to be affected by noise, it is observed that the *theta* subband wavelet energy shows the most considerable difference between all three groups. It is consistent with a previous study of spectral analysis using Fast Fourier Transform on the same data in which *theta* appears as the most significant EEG subband affected by freezing [14]. However, contrary to Palmer's study [17] in which *beta* band EEG is found to be more important for dual task performance in PD which may lead to FOG, in this study *alpha* has a more significant contribution to task performance than *beta*.

For classification, four features of channel O1 were taken as they have a significantly high confidence level beyond criterium (p-value <0.01): WE *delta*, WE *theta*, WE *alpha* and TWE. All EEG subbands WE and TWE of channel P4 were implemented as inputs. Experiments were conducted for each location of brain (O1, P4) and combination of it.

The Back Propagation Neural Networks using Levenberg Marquardt algoritm for training shows a promising result in testing set as is indicated in Table II. Using only channel P4 has already given more than 76.57 % correct in classifying normal-onset. Performance was slightly increased in accuracy and specificity when it was combined with channel O1 to differentiate between normal and freezing. The success rate of differentiate between normal and onset (76.6 ± 3.4) is slightly higher than between normal and freezing (73.88 ± 79.6) implied that the neurological process of freezing in the brain started in 5 second periods before it appeared as freezing of gait. Compared to other works in different brain diseases such as AD and epilepsy which obtain accuracy up to 87.1 % [11] and sensitivity on average 83 % [18], clearly more research needs to be done to increase the performance of the system.

TABLE I

STATISTICAL CORRELATION ANALYSIS BETWEEN 3 DIFFERENT STAGES OF PD'S PATIENTS

Channel-Feature	mean±std Normal (N)	Onset (O)	Freezing (F)	*p*-value N-O	N-F	O-F
O1-WE δ	16939.779±26347.684	20781.927±28844.102	12840.539±21509.292	0.002	0.016	$\leq$ 0.001
O1-WE θ	1250.205±1496.056	2824.346±4010.260	1593.678±1997.817	$\leq$0.001	$\leq$0.001	$\leq$0.001
O1-WE α	1761.528±1828.380	2399.470 ±2168.370	2105.513±2200.471	$\leq$0.001	0.004	0.002
O1-WE β	2054.270±2776.284	2193.293±2729.281	2075.393±2411.743	0.028	0.174	0.290
O1-WE γ	2250.084±3129.022	2543.499 ±4003.021	2659.319±4233.292	0.339	0.083	0.373
O1-TWE	0.932±0.395	1.070±0.322	0.976± 0.353	$\leq$0.001	$\leq$0.001	$\leq$0.001
P4-WE δ	14132.911±20644.905	25843.544±32521.796	15637.085±18483.045	$\leq$0.001	$\leq$0.001	$\leq$0.001
P4-WE θ	1319.528±1366.631	3593.649±3857.009	2657.609±2045.397	$\leq$0.001	$\leq$0.001	0.002
P4-WE α	2622.983±2874.563	4546.447±3056.553	5271.596±3766.857	$\leq$0.001	$\leq$0.001	0.013
P4-WE β	2694.404±2835.144	4038.314±3000.283	4622.378±3257.461	$\leq$0.001	$\leq$0.001	0.007
P4-WE γ	3012.389±3562.820	3922.334±3108.741	4248.954±2950.425	$\leq$0.001	$\leq$0.001	0.020
P4-TWE	0.820±0.372	1.160±0.292	1.163±0.319	$\leq$0.001	$\leq$0.001	0.998

TABLE II

CLASSIFICATION RESULTS OF PROPOSED FEATURES USING BP-NN

Normal - Onset						
Inputs	Accuracy (%)		Sensitivity (%)		Specificity (%)	
	mean±std	best	mean±std	best	mean±std	best
O1	59.2±3.4	66.4	61.6±8.4	80.5	57.0±8.5	72.7
P4	76.6±3.4	81.6	74.2±6.8	86.8	78.9±7.3	89.7
O1,P4	75.0±3.4	80.3	72.0±7.0	87.3	77.2±5.4	88.6
Normal - Freezing						
Inputs	Accuracy (%)		Sensitivity (%)		Specificity (%)	
	mean±std	best	mean±std	best	mean±std	best
O1	52.1±3.9	57.9	54.2±11.9	74.4	50.2±9.4	76.3
P4	73.4±3.2	78.9	72.3±6.3	86.1	74.4±5.0	86.5
O1,P4	73.9±2.8	79.6	71.2±6.1	88.1	77.2±4.7	82.9

IV. CONCLUSIONS AND FUTURE WORK

We presented results of study of early detection of FOG in PD's patient using EEG signals. Complemented with special treatment such as sensory cuing, this classification system could be used in helping PD's patient with FOG to 'unfreeze' this symptom before it affected the movement. EEG subbands Wavelet Energy and Total Wavelet Entropy features can be used to represent changing during onset and freezing period. Classification done by BP-NN has a promising result and shows the feasibility of using EEGs for FOG detection. Moreover, this study support analysis of physiological brain dynamics during FOG. It may lead to better understanding of its underlying mechanism. Further exploration on other features, different area of the brain and classification methods will be our near future work before implementing it in a device.

REFERENCES

[1] A.E. Lang, "Foreword", in *Parkinson's disease: diagnosis and clinical management*, 2nd ed., S.A. Factor and W.J. Weiner, Eds., New York: Demos Medical Publishing, 2008, pp. xiii-xiv.

[2] J.G. Nutt, B.R. Bloem, N. Giladi, M. Hallet, F.B. Horak, and A. Niewboer, E.H. Miller, "Freezing of gait: moving forward on a mysterious clinical phenomenon", vol. 10, pp. 2011, *The Lancet Neurology*, pp. 734-744, 2011.

[3] J.H. Baker, "The symptom experience of patients with Parkinson's disease", *The Journal of Neuroscience Nursing*, vol. 38, pp. 51-57, 2006.

[4] J.M. Shine, S.L. Naishmith, and S.J.G. Lewis, "The pathophysiological mechanisms underlying freezing of gait in Parkinson's disease", *Journal of Clinical Neuroscience*, vol. 18, pp. 1154-1157, 2011.

[5] E. Johanov, E. Wang, L. Verhagen, M. Fredrickson, and R. Fratangelo, "deFOG- a real time system for detection and unfreezing of gait of Parkinson's patients", in *31th Annual International Conference of the IEEE EMBS*, 2009, pp. 5151-5154.

[6] A. Delval, A.H. Snijders, V. Weerdesteyn, J.E. Duysens, L. Defebvre, N. Giladi, B.R. Bloem, "Objective detection of subtle freezing of gait episodes in Parkinson's disease", *Movement Disorders*, vol. 25, no. 11, pp. 1684-1693, 2010.

[7] A. Niewboer, R. Dom, W. Weerdt, K. Desloovere, L. Janssens, and V. Stijn, "Electromyographic profiles of gait prior to onset of freesing episodes in patients with Parkinsons disease", *Brain*, vol. 127, pp. 1650-1660, 2004.

[8] M.B. Popovic, M.D. Jovicic, S. Radovanovic, I. Petrovic, and V. Kostic, "A simple method to assess freezing of gait in Parkinsons disease patients", *Brazilian Journal of Medical and Biological Research*, vol. 43, pp. 883-889, 2010.

[9] M. Bachlin, M. Plotnik, D. Roggen, D. Maidan, J.M. Hausdorff, N. Giladi, and G. Troster, "Wearable Assistant for Parkinsons Disease Patients with the Freezing of Gait Symptom", *IEEE Transactions on Information Technology in Biomedicine*, vol. 14, no. 2, pp. 436-446, 2010.

[10] L.R. Trambaiolli, T.H. Falk, F.J. Fraga, R. Anghinah, and A.C. Lorena, "EEG spectro-temporal modulation energy: a new feature for automated diagnosis of Alzheimer's disease", in *33rd Annual International Conference of the IEEE EMBS*, 2011, pp. 3828-3831.

[11] H. Adeli, S. Ghosh-Dastidar, and N. Dadmehr, "A Wavelet-Chaos Methodology for Analysis of EEGs and EEG Subbands to Detect Seizure and Epilepsy", *IEEE Transactions on Biomedical Engineering*, vol. 54, no. 2, pp. 205-211, 2007.

[12] H.C. Shin, X. Jia, R. Nickl, R.G. Geocadin, and N.V. Thakor, "A Subband-Based Information Measure of EEG During Brain Injury and Recovery After Cardiac Arrest", *IEEE Transactions on Biomedical Engineering*, vol. 55, no. 8, pp. 1985-1990, 2008.

[13] G.L. Sorensen, J. Kempfner, P. Jennum, and H.B.D. Sorensen, "Detection of arousals in Parkinson's disease patients", in *33rd Annual International Conference of the IEEE EMBS*, 2011, pp. 2764-2767.

[14] J. Shine, A. Handojoseno, T. Nguyen, S. Moore, S. Naismith, H. Nguyen, and S. Lewis, "Electroencephalographic abnormalities during freezing of gait in Parkinson's disease", *Journal of Neurophysiology*, submitted for publication.

[15] O.A. Rosso, S. Blanco, J. Yordanova, V. Kolev, A. Figliola, M. Schürmann, and E. Basar, "Wavelet entropy: a new tool for analysis of short duration brain electrical signals", *Journal of Neuroscience Methods*, vol. 105, pp. 65-75, 2001.

[16] C.S. Burrus, R.A. Gopinath, and H.Guo, *Introduction to wavelets and wavelet transforms: a primer*, New Jersey: Prentice-Hall, Inc., 1998. pp. 2-7.

[17] S.J. Palmer, P.W.H. Lee, Z.J. Wang, W.L. Au, and M.J. Mc Keown, "θ, β but not α-band EEG connectivity has implications for dual task performance in Parkinsons disease", *Parkinsonism and Related Disorder*, vol 16, 2010, pp.393-397.

[18] M.M. Hartmann, F. Fürba, H. Perko, A. Skupch, K. Lackmayer, C. Baumgartner, and T. Kluge, "EpiScan: Online seizure detection for epilepsy monitoring units", in *33rd Annual International Conference of the IEEE EMBS*, 2011, pp. 6096-6099.

Bibliography

Abásolo, D., Escudero, J., Hornero, R., Gómez, C., & Espino, P. 2008. Approximate entropy and auto mutual information analysis of the electroencephalogram in Alzheimers disease patients. *Medical & Biological Engineering & Computing*, **46**(10), 1019–1028.

Addison, P.S. 2010. *The illustrated wavelet transform handbook: introductory theory and applications in science, engineering, medicine and finance*. CRC Press.

Adeli, H., Ghosh-Dastidar, S., & Dadmehr, N. 2007. A Wavelet-Chaos Methodology for Analysis of EEGs and EEG Subbands to Detect Seizure and Epilepsy. *IEEE Transactions on Biomedical Engineering*, **54**(2), 205–211.

Ahissar, E., Vaadia, E., Ahissar, M., Bergman, H., Arieli, A., & Abeles, M. 1992. Dependence of cortical plasticity on correlated activity of single neurons and on behavioral context. *Science*, **257**(5075), 1412–1415.

Almeida, Q.J., & Lebold, C.A. 2010. Freezing of gait in Parkinson's disease: a perceptual cause for a motor impairment? *Journal of Neurology, Neurosurgery & Psychiatry*, **81**(5), 513–518.

Amboni, M., Cozzolino, A., Longo, K., Picillo, M., & Barone, P. 2008. Freezing of gait and executive functions in patients with Parkinson's disease. *Movement Disorders*, **23**(3), 395–400.

Androulidakis, A.G., Mazzone, P., Litvak, V., Penny, W., Dileone, M., Gaynor, L.M.F.D., Tisch, S., Di Lazzaro, V., & Brown, P. 2008. Oscillatory activity in the pedunculopontine area of patients with Parkinson's disease. *Experimental Neurology*, **211**(1), 59–66.

Arai, N., Lu, M.K., Ugawa, Y., & Ziemann, U. 2012. Effective connectivity between human supplementary motor area and primary motor cortex: a paired-coil TMS study. *Experimental Brain Research*, **220**(1), 79–87.

Arthur, J., & Brown, R. 2009. Parkinson's Disease. *Disability Studies Wiki CE*. Accessed: 11 August 2011.

Azevedo Coste, C., Sijobert, B., Pissard-Gibollet, R., Pasquier, M., Espiau, B., & Geny, C. 2014. Detection of Freezing of Gait in Parkinson Disease: Preliminary Results. *Sensors*, **14**(4), 6819–6827.

Baccalá, L.A., & Sameshima, K. 2001. Partial directed coherence: a new concept in neural structure determination. *Biological Cybernetics*, **84**(6), 463–474.

Baccald, L.A., & de Medicina, F. 2007. Generalized partial directed coherence. *Pages 163–166 of: Digital Signal Processing, 2007 15th International Conference on*. IEEE.

Bächlin, M., Roggen, D., Tröster, G., Plotnik, M., Inbar, N., Maidan, I., Herman, T., Brozgol, M., Shaviv, E., Giladi, N., *et al.* 2009. Potentials of Enhanced Context Awareness in Wearable Assistants for Parkinson's Disease Patients with the Freezing of Gait Syndrome. *Pages 123–130 of: ISWC*.

Bachlin, M., Plotnik, M., Roggen, D., Maidan, D., Hausdorff, J.M., Giladi, N., & Troster, G. 2010. Wearable Assistant for Parkinsons Disease Patients with the Freezing of Gait Symptom. *IEEE Transactions on Information Technology in Biomedicine*, **14**(2), 436–446.

Backer, J.H. 2006. The symptom experience of patients with Parkinson's disease. *Journal of Neuroscience Nursing*, **38**(1), 51–57.

Bakker, M., De Lange, F.P., Helmich, R.C., Scheeringa, R., Bloem, B.R., & Toni, I. 2008. Cerebral correlates of motor imagery of normal and precision gait. *Neuroimage*, **41**(3), 998–1010.

Baram, Y., Badarny, S., & Aharon-Peretz, J. 2006. Virtual Reality Feedback Cues for Improvement of Gait in Patients with Parkinsons Disease. *In: Proc. 10th International Congress of Parkinson's Disease and Movement Disorders*.

Bartels, A.L., & Leenders, K.L. 2009. Parkinson's disease: The syndrome, the pathogenesis and pathophysiology. *Cortex*, **45**(8), 915–921.

Bartels, A.L., de Jong, B.M., Giladi, N., Schaafsma, J.D., Maguire, R.P., Veenma, L., Pruim, J., Balash, Y., Youdim, M.B.H., & Leenders, K.L. 2006. Striatal dopa and glucose metabolism in PD patients with freezing of gait. *Movement disorders*, **21**(9), 1326–1332.

Belmonte, M.K., Allen, G., Beckel-Mitchener, A., Boulanger, L.M., Carper, R.A., & Webb, S.J. 2004. Autism and abnormal development of brain connectivity. *The Journal of Neuroscience*, **24**(42), 9228–9231.

Benoit, C.E., Dalla Bella, S., Farrugia, N., Obrig, H., Mainka, S., & Kotz, S.A. 2014. Musically cued gait-training improves both perceptual and motor timing in Parkinsons disease. *Frontiers in human neuroscience*, **8**.

Blinowska, K.J., & Zygierewicz, J. 2011. *Practical Biomedical Signal Analysis Using MATLAB®*. CRC Press.

Bloem, B.R., Hausdorff, J.M., Visser, J.E., & N.Giladi. 2004. Falls and Freezing of Gait in Parkinsons Disease: A Review of Two Interconnected, Episodic Phenomena. *Movement Disorders*, **19**(8), 871–884.

Burrus, C.S., Gopinath, R.A., Guo, H., Odegard, J.E., & Selesnick, I.W. 1998. *Introduction to wavelets and wavelet transforms: a primer*. Vol. 23. Prentice hall New Jersey.

Carlson, N.R. 2013. *Physiology of behavior*. 11th edition edn. Upper Saddle River, New Jersey: Pearson.

Catarino, A., Churches, O., Baron-Cohen, S., Andrade, A., & Ring, H. 2011. Atypical EEG complexity in autism spectrum conditions: a multiscale entropy analysis. *Clinical Neurophysiology*, **122**(12), 2375–2383.

Catarino, A., Andrade, A., Churches, O., Wagner, A.P., Baron-Cohen, S., & Ring, H. 2013. *Task-related functional connectivity in autism spectrum conditions: an EEG study using wavelet transform coherence*. Ph.D. thesis, BioMed Central.

Chong, R., Lee, K.H., Morgan, J., Mehta, S., Griffin, J., Marchant, J., Searle, N., Sims, J., & Sethi, K. 2011. Closed-Loop VR-Based Interaction to Improve Walking in Parkinsons. *Novel Physiotherapies*. Accessed: 11 August 2011.

Coben, R., Clarke, A.R., Hudspeth, W., & Barry, R.J. 2008. EEG power and coherence in autistic spectrum disorder. *Clinical Neurophysiology*, **119**(5), 1002–1009.

Cohen, M.I., Yu, Q., & Huang, W.X. 1995. Preferential correlations of a medullary neuron's activity to different sympathetic outflows as revealed by partial coherence analysis. *Journal of Neurophysiology*, **74**(1), 474–478.

Cohen, M.X. 2011. It's about Time. *Frontiers in Human Neuroscience*, **5**.

Cole, B.T., Roy, S.H., & Nawab, S.H. 2011. Detecting freezing-of-gait during unscripted and unconstrained activity. *Pages 5649–5652 of: Engineering in Medicine and Biology Society, EMBC, 2011 Annual International Conference of the IEEE*. IEEE.

Comon, P. 1994. Independent component analysis, a new concept? *Signal Processing*, **36**(3), 287–314.

Connor, C.M., Thorpe, S.K., Malley, M.J., & Vaughan, C.L. 2007. Automatic detection of gait events using kinematic data. *Gait Posture*, **25**(3), 469–474.

Constantinescu, R., Leonard, C., Deeley, C., & Kurlan, R. 2007. Assistive devices for gait in Parkinson's disease. *Parkinsonism & Related Disorders*, **13**(3), 133–138.

Crémers, J., D'Ostilio, K., Stamatakis, J., Delvaux, V., & Garraux, G. 2012. Brain activation pattern related to gait disturbances in Parkinson's disease. *Movement Disorders*, **27**(12), 1498–1505.

de Hemptinne, C., Ryapolova-Webb, E.S., Air, E.L., Garcia, P.A., Miller, K.J., Ojemann, J.G., Ostrem, J.L., Galifianakis, N.B., & Starr, P.A. 2013. Exaggerated phase–amplitude coupling in the primary motor cortex in Parkinson disease. *Proceedings of the National Academy of Sciences*, **110**(12), 4780–4785.

DeloitteAccessEconomicsPtyLtd. 2011 (October). *Living with Parkinson's Disease-update*. Tech. rept. Parkinson's Australia.

Delval, A., Snijders, A.H., Weerdesteyn, V., Duysens, J.E., Defebvre, L., Giladi, N., & Bloem, B.R. 2010. Objective detection of subtle freezing of gait episodes in Parkinson's disease. *Movement Disorders*, **25**(11), 1684–1693.

Demirci, O., Stevens, M.C., Andreasen, N.C., Michael, A., Liu, J., White, T., Pearlson, G.D., Clark, V.P., & Calhoun, V.D. 2009. Investigation of relationships between fMRI brain networks in the spectral domain using ICA and Granger causality reveals distinct differences between schizophrenia patients and healthy controls. *Neuroimage*, **46**(2), 419–431.

Deshpande, G., Libero, L.E., Sreenivasan, K.R., Deshpande, H.D., & Kana, R.K. 2013. Identification of neural connectivity signatures of autism using machine learning. *Frontiers in Human Neuroscience*, **7**.

Devos, D., Defebvre, L., & Bordet, R. 2010. Dopaminergic and non-dopaminergic pharmacological hypotheses for gait disorders in Parkinsons disease: Pharmacology of parkinsonian gait disorders. *Fundamental & Clinical Pharmacology*, **24**(4), 407–421.

Dietz, M.A., Goetz, C.G., & Stebbins, G.T. 1990. Evaluation of a modified inverted walking stick as a treatment for parkinsonian freezing episodes. *Movement Disorders*, **5**(3), 243–247.

Ding, X., & Lee, S.W. 2013. Changes of functional and effective connectivity in smoking replenishment on deprived heavy smokers: a resting-state FMRI study. *PloS One*, **8**(3), e59331.

Dorsey, E.R., Constantinescu, R., Thompson, J.P., Biglan, K.M., Holloway, R.G., Kieburtz, K., Marshall, F.J., Ravina, B.M., Schifitto, G., Siderowf, A., *et al.* 2007. Projected number of people with Parkinson disease in the most populous nations, 2005 through 2030. *Neurology*, **68**(5), 384–386.

Dubois, B., Burn, D., Goetz, C., Aarsland, D., Brown, R.G., Broe, G.A., Dickson, D., Duyckaerts, C., Cummings, J., Gauthier, S., *et al.* 2007. Diagnostic procedures for Parkinson's disease dementia: recommendations from the movement disorder society task force. *Movement Disorders*, **22**(16), 2314–2324.

Ellis, P.D. 2010. *The Essential Guide to Effect Sizes: An Introduction to Statistical Power*. Cambridge: Cambridge University Press.

Factor, S., & Weiner, W. 2007a. *Parkinson's Disease: Diagnosis & Clinical Management*. Demos Medical Publishing. Chap. Foreword, pages xiii–xiv.

Factor, S., & Weiner, W. 2007b. *Parkinson's Disease: Diagnosis & Clinical Management*. Demos Medical Publishing. Chap. The Unified Parkinsons Disease Rating Scale.

Fall, Per-Arne, Saleh, Avin, Fredrickson, Mats, Olsson, Jan-Edvin, & Granérus, Ann-Kathrine. 2003. Survival time, mortality, and cause of death in elderly patients with Parkinson's disease. A 9-year follow-up. *Movement Disorders*, **18**(11), 1312–1316.

Farge, M. 1992. Wavelet transforms and their applications to turbulence. *Annual Review of Fluid Mechanics*, **24**(1), 395–458.

Fling, B.W., Cohen, R.G., Mancini, M., Nutt, J.G., Fair, D.A., & Horak, F.B. 2013. Asymmetric pedunculopontine network connectivity in parkinsonian patients with freezing of gait. *Brain*, **136**(8), 2405–2418.

Follett, K.A., & Torres-Russotto, D. 2012. Deep brain stimulation of globus pallidus interna, subthalamic nucleus, and pedunculopontine nucleus for Parkinson's disease: which target? *Parkinsonism & Related Disorders*, **18**, S165–S167.

Foresee, F.D., & Hagan, M.T. 1997. Gauss-Newton approximation to Bayesian learning. *Pages 1930–1935 of: Proceedings of the 1997 international joint conference on neural networks*, vol. 3. Piscataway: IEEE.

Friston, K.J. 1994. Functional and effective connectivity in neuroimaging: a synthesis. *Human Brain Mapping*, **2**(1-2), 56–78.

Friston, K.J. 2011. Functional and effective connectivity: a review. *Brain Connectivity*, **1**(1), 13–36.

Friston, K.J., Harrison, L., & Penny, W. 2003. Dynamic causal modelling. *Neuroimage*, **19**(4), 1273–1302.

Frølich, L., Andersen, T.S., & Mørup, M. 2015. Classification of independent components of EEG into multiple artifact classes. *Psychophysiology*, **52**(1), 32–45.

Gancher, S. T. 2008. *Parkinson's Disease: Diagnosis and Clinical Management*. 2nd edition edn. New York: Demos Medical Publishing. Chap. Clinical Rating Scales, pages 135–143.

Gatev, P., Darbin, O., & Wichmann, T. 2006. Oscillations in the basal ganglia under normal conditions and in movement disorders. *Movement Disorders*, **21**(10), 1566–1577.

Geetha, G., & Geethalakshmi, S.N. 2011. EEG de-noising using sure thresholding based on wavelet transforms. *International Journal of Computer Applications*, **24**(6).

Gersch, W., & Goddard, G.V. 1970. Epileptic focus location: spectral analysis method. *Science*, **169**(3946), 701–702.

Geweke, J. 1982. Inference and causality in economic time series models.

Gibb, W.R.G., & Lees, A.J. 1988. A comparison of clinical and pathological features of young-and old-onset Parkinson's disease. *Neurology*, **38**(9), 1402–1402.

Giladi, N., & Niewboer, A. 2008. *Parkinson's Disease: Diagnosis and Clinical Management*. 2nd edition edn. New York: Demos Medical Publishing. Chap. Gait Disturbance, pages 55–63.

Giladi, N., Treves, T.A., Simon, E.S., Shabtai, H., Orlov, Y., Kandinov, B., Paleacu, D., & Korczyn, A.D. 2001. Freezing of gait in patients with advanced Parkinson's disease. *Journal of Neural Transmission*, **108**(1), 53–61.

Giladi, N., Tal, J., Azulay, T., Rascol, O., Brooks, D.J., Melamed, E., Oertel, W., Poewe, W.H., Stocchi, F., & Tolosa, E. 2009. Validation of the freezing of gait questionnaire in patients with Parkinson's disease. *Movement Disorders*, **24**(5), 655–661.

Goldstein, N. 2009. *Genes and Disease: Pakinson's Disease*. New York: Infobase Publishing.

Grinsted, A., Moore, J.C., & Jevrejeva, S. 2004. Application of the cross wavelet transform and wavelet coherence to geophysical time series. *Nonlinear Processes in Geophysics*, **11**(5/6), 561–566.

Gruzelier, J.H., Foks, M., Steffert, T., Chen, M.J.L., & Ros, T. 2014. Beneficial outcome from EEG-neurofeedback on creative music performance, attention and well-being in school children. *Biological Psychology*, **95**, 86–95.

Guevara, M.A., & Corsi-Cabrera, M. 1996. EEG coherence or EEG correlation? *International Journal of Psychophysiology*, **23**(3), 145–153.

Guyon, I., Li, J., Mader, T., Pletscher, P.A., Schneider, G., & Uhr, M. 2007. Competitive baseline methods set new standards for the NIPS 2003 feature selection benchmark. *Pattern Recognition Letters*, **28**(12), 1438–1444.

Guyon, I., Gunn, S., Nikravesh, M., & Zadeh, L.A. 2008. *Feature extraction: foundations and applications*. Vol. 207. Springer.

Han, J., Jeon, H.S., Jeon, B.S., & Park, K.S. 2006. Gait detection from three dimensional acceleration signals of ankles for patients with Parkinson's disease. *In: Proceedings of the International Special Topic Conference on Information Technology in Biomedicine*.

Han, J.H., Lee, W.J., Ahn, T.B., Jeon, B.S., & Park, K.S. 2003. Gait analysis for freezing detection in patients with movement disorder using three dimensional acceleration system. *Pages 1863–1865 of: Engineering in Medicine and Biology Society, 2003. Proceedings of the 25th Annual International Conference of the IEEE*, vol. 2. IEEE.

Handojoseno, A.M.A, Shine, J.M., Nguyen, T.N., Tran, Y., Lewis, S.J.G., & Nguyen, H.T. 2012. The detection of Freezing of Gait in Parkinson's disease patients using EEG signals based on Wavelet decomposition. *Pages 69–72 of: Engineering in Medicine and Biology Society (EMBC), 2012 Annual International Conference of the IEEE*. IEEE.

Handojoseno, A.M.A, Shine, J.M., Nguyen, T.N., Tran, Y., Lewis, S.J.G., & Nguyen, H.T. 2013. Using EEG spatial correlation, cross frequency energy, and wavelet coefficients

for the prediction of Freezing of Gait in Parkinson's Disease patients. *Pages 4263–4266 of: Engineering in Medicine and Biology Society (EMBC), 2013 35th Annual International Conference of the IEEE*. IEEE.

Handojoseno, A.M.A., Shine, J.M., Gilat, M., Nguyen, T.N., Tran, Y., Lewis, S.J.G., & Nguyen, H.T. 2014. Prediction of freezing of gait using analysis of brain effective connectivity. *Pages 4119–4122 of: Engineering in Medicine and Biology Society (EMBC), 2014 36th Annual International Conference of the IEEE*. IEEE.

Handojoseno, A.M.A., Shine, J.M., Nguyen, T.N., Tran, Y., Lewis, S.J.G., & Nguyen, H.T. 2015a. Analysis and prediction of the freezing of gait using EEG brain dynamics. *IEEE Transactions on Neural Systems and Rehabilitation Engineering*, **23**(5), 887–896.

Handojoseno, A.M.A., Gilat, M., Tran, Q., Chamtie, H., Shine, J.M., Nguyen, T.N., Tran, Y., Lewis, S.J.G., & Nguyen, H.T. 2015b. An EEG study of turning freeze in Parkinsons disease patients: the alteration of brain dynamic on the motor and visual cortex. *Pages 6618–6621 of: Engineering in Medicine and Biology Society (EMBC), 2015 Annual International Conference of the IEEE*. IEEE.

Handojoseno, A.M.A, Naik, G.R., Gilat, M., Shine, J.M., Nguyen, T.N., Tran, Y., Lewis, S.J.G., & Nguyen, H.T. 2015c. Detection of Freezing of Gait based on combination of Independent Component Analysis and Brain Effective Connectivity. *IEEE Journal of Biomedical and Health Informatics*. submitted.

Hashimoto, T. 2006. Speculation on the responsible sites and pathophysiology of freezing of gait. *Parkinsonism & Related Disorders*, **12**, S55–S62.

Haykin, S.S. 2009. *Neural networks and learning machines*. Vol. 3. Pearson Education Upper Saddle River.

Heinrichs-Graham, E., Wilson, T.W., Santamaria, P.M., Heithoff, S.K., Torres-Russotto, D., Hutter-Saunders, J.A.L., Estes, K.A., Meza, J.L., Mosley, R.L., & Gendelman, H.E. 2013. Neuromagnetic evidence of abnormal movement-related beta desynchronization in Parkinson's disease. *Cerebral Cortex*, bht121.

Heremans, E., Nieuwboer, A., & Vercruysse, S. 2013. Freezing of gait in Parkinsons disease: where are we now? *Current Neurology and Neuroscience Reports*, **13**(6), 1–9.

Hyvarinen, A. 1999. Fast and robust fixed-point algorithms for independent component analysis. *Neural Networks, IEEE Transactions on*, **10**(3), 626–634.

Hyvärinen, A., & Oja, E. 2000. Independent component analysis: algorithms and applications. *Neural Networks*, **13**(4), 411–430.

Hyvärinen, A., Karhunen, J., & Oja, E. 2004. *Independent component analysis*. Vol. 46. John Wiley & Sons.

Jennings, P.J. 1995. Evidence of incomplete motor programming in Parkinson's disease. *Journal of Motor Behavior*, **27**(4), 310–324.

Joseph, R. 1996. *Neuropsychiatry, neuropsychology, and clinical neuroscience: Emotion, evolution, cognition, language, memory, brain damage, and abnormal behavior* . Williams & Wilkins Co.

Jovanov, E., Wang, E., Verhagen, L., Fredrickson, M., & Fratangelo, R. 2009. deFOG-a real time system for detection and unfreezing of gait of Parkinson's patients. *Pages 5151–5154 of: Proceeding of the 31th Annual International Conference of the IEEE EMBS*.

Juri, C., Rodriguez-Oroz, M., & Obeso, J.A. 2010. The pathophysiological basis of sensory disturbances in Parkinson's disease. *Journal of the Neurological Sciences*, **289**(1-2), 60–65.

Killane, I., Fearon, C., Newman, L., McDonnell, C., Waechter, S., Sons, K., Lynch, T., & Reilly, R. 2015. Dual Motor-Cognitive Virtual Reality Training Impacts Dual-Task Performance in Freezing of Gait. *IEEE Journal of Biomedical and Health Informatics*, **19**(6), 1855–1861.

Knobl, P., Kielstra, L., & Almeida, Q. 2011. The relationship between motor planning and freezing of gait in Parkinson's disease. *Journal of Neurology, Neurosurgery & Psychiatry*, jnnp–2011.

Kompoliti, K., Goetz, C.G., Leurgans, S., Morrissey, M., & Siegel, I.M. 2000. "On" freezing in Parkinson's disease: resistance to visual cue walking devices. *Movement Disorders*, **15**(2), 309–312.

Kus, R., Kamiński, M., & Blinowska, K.J. 2004. Determination of EEG activity propagation: pair-wise versus multichannel estimate. *Biomedical Engineering, IEEE Transactions on*, **51**(9), 1501–1510.

Kuś, R., Ginter, J.S., & Blinowska, K.J. 2005. Propagation of EEG activity during finger movement and its imagination. *Acta Neurobiologiae Experimentalis*, **66**(3), 195–206.

Lachaux, J.P., Rodriguez, E., Martinerie, J., Varela, F.J., *et al.* 1999. Measuring phase synchrony in brain signals. *Human Brain Mapping*, **8**(4), 194–208.

Lachaux, J.P., Lutz, A., Rudrauf, D., Cosmelli, D., Le Van Quyen, M., Martinerie, J., & Varela, F. 2002. Estimating the time-course of coherence between single-trial brain signals: an introduction to wavelet coherence. *Neurophysiologie Clinique/Clinical Neurophysiology*, **32**(3), 157–174.

Langlois, D., Chartier, S., & Gosselin, D. 2010. An introduction to independent component analysis: InfoMax and FastICA algorithms. *Tutorials in Quantitative Methods for Psychology*, **6**(1), 31–38.

Lau, T.M., Gwin, J.T., McDowell, K.G., & Ferris, D.P. 2012. Weighted phase lag index stability as an artifact resistant measure to detect cognitive EEG activity during locomotion. *Journal of Neuroengineering Rehabilitation*, **9**(1), 1–9.

Lee, Y.Y., & Hsieh, S. 2014. Classifying Different Emotional States by Means of EEG-Based Functional Connectivity Patterns. *PloS one*, **9**(4), e95415.

Linazasoro, G. 1996. The apomorphine test in gait disorders associated with parkinsonism. *Clinical Neuropharmacology*, **19**(2), 171–176.

Loo, S.K., & Makeig, S. 2012. Clinical utility of EEG in attention-deficit/hyperactivity disorder: a research update. *Neurotherapeutics*, **9**(3), 569–587.

Lotte, F., Congedo, M., Lécuyer, A., Lamarche, F., Arnaldi, B., *et al.* 2007. A review of classification algorithms for EEG-based brain–computer interfaces. *Journal of Neural Engineering*, **4**.

Macht, M., Kaussner, Y., Möller, J.C., Stiasny-Kolster, K., Eggert, K.M., Krüger, H.P., & Ellgring, H. 2007. Predictors of freezing in Parkinson's disease: a survey of 6,620 patients. *Movement Disorders*, **22**(7), 953–956.

MacKay, D.J.C. 1992. Bayesian interpolation. *Neural Computation*, **4**(3), 415–447.

Mallat, S. 1999. *A wavelet tour of signal processing*. Academic Press.

Mancini, M., Priest, K.C., Nutt, J.G., & Horak, F.B. 2012. Quantifying freezing of gait in Parkinson's disease during the instrumented timed up and go test. *Pages 1198–1201 of: Engineering in Medicine and Biology Society (EMBC), 2012 Annual International Conference of the IEEE*. IEEE.

Matsui, H., Udaka, F., Miyoshi, T., Hara, N., Tamaura, A., Oda, M., Kubori, T., Nishinaka, K., & Kameyama, M. 2005. Three-dimensional stereotactic surface projection study of freezing of gait and brain perfusion image in Parkinson's disease. *Movement Disorders*, **20**(10), 1272–1277.

Mazilu, S., Hardegger, M., Zhu, Z., Roggen, D., Troster, G., Plotnik, M., & Hausdorff, J.M. 2012. Online detection of freezing of gait with smartphones and machine learning techniques. *Pages 123–130 of: Pervasive Computing Technologies for Healthcare (PervasiveHealth), 2012 6th International Conference on*. IEEE.

Mazilu, S., Blanke, U., Hardegger, M., Troster, G., Gazit, E., Dorfman, M., & Hausdorff, J.M. 2014. GaitAssist: A wearable assistant for gait training and rehabilitation in Parkinson's disease. *Pages 135–137 of: Pervasive Computing and Communications Workshops (PERCOM Workshops), 2014 IEEE International Conference on*. IEEE.

Melissant, C., Ypma, A., Frietman, E.E.E., & Stam, C.J. 2005. A method for detection of Alzheimer's disease using ICA-enhanced EEG measurements. *Artificial Intelligence in Medicine*, **33**(3), 209–222.

Mirowski, P., Madhavan, D., LeCun, Y., & Kuzniecky, R. 2009. Classification of patterns of EEG synchronization for seizure prediction. *Clinical Neurophysiology*, **120**(11), 1927–1940.

Misiti, M., Misiti, Y., Oppenheim, G., & Poggi, J.M. 2007. *Wavelets and their Applications*. Vol. 330. Wiley Online Library.

Molavi, M., & Bin Yunus, J. 2012. The effect of noise removing on emotional classification. *Pages 485–489 of: Computer & Information Science (ICCIS), 2012 International Conference on*, vol. 1. IEEE.

Moore, O., Peretz, C., & Giladi, N. 2007. Freezing of gait affects quality of life of peoples with Parkinson's disease beyond its relationships with mobility and gait. *Movement Disorders*, **22**(15), 2192–2195.

Moore, S.T., MacDougall, H.G., & Ondo, W.G. 2008. Ambulatory monitoring of freezing of gait in Parkinson's disease. *Journal of Neuroscience Methods*, **167**(2), 340–348.

Moreau, C., Ozsancak, C., Blatt, J.L., Derambure, P., Destee, A., & Defebvre, L. 2007. Oral festination in Parkinson's disease: biomechanical analysis and correlation with festination and freezing of gait. *Movement Disorders*, **22**(10), 1503–1506.

Morgan, J.C., Mehta, S.H., & Sethi, K.D. 2010. Biomarkers in Parkinsons Disease. *Current Neurology and Neuroscience Reports*, **10**(6), 423–430.

Morison, G., Tieges, Z., & Kilborn, K. 2012. Multiscale permutation entropy analysis of the EEG in early stage alzheimer's patients. *Pages 805–809 of: Biomedical Engineering and Sciences (IECBES), 2012 IEEE EMBS Conference on*. IEEE.

Mormann, F., Lehnertz, K., David, P., & Elger, C.E. 2000. Mean phase coherence as a measure for phase synchronization and its application to the EEG of epilepsy patients. *Physica D: Nonlinear Phenomena*, **144**(3), 358–369.

Mutlu, A.Y., & Aviyente, S. 2009. Inferring effective connectivity in the brain from EEG time series using dynamic bayesian networks. *Pages 4739–4742 of: Engineering in Medicine and Biology Society, 2009. EMBC 2009. Annual International Conference of the IEEE*. IEEE.

Nachev, P., Kennard, C., & Husain, M. 2008. Functional role of the supplementary and pre-supplementary motor areas. *Nature Reviews Neuroscience*, **9**(11), 856–869.

Nguyen, L.B., Nguyen, A.V., Ling, S.H., & Nguyen, H.T. 2012. An adaptive strategy of classification for detecting hypoglycemia using only two EEG channels. *Pages 3515–3518 of: Engineering in Medicine and Biology Society (EMBC), 2012 Annual International Conference of the IEEE*. IEEE.

Niazmand, K., Tonn, K., Zhao, Y., Fietzek, U.M., Schroeteler, F., Ziegler, K., Ceballos-Baumann, A.O., & Lueth, T.C. 2011a. Freezing of gait detection in parkinson's disease using accelerometer based smart clothes. *Pages 201–204 of: Biomedical Circuits and Systems Conference (BioCAS), 2011 IEEE*. IEEE.

Niazmand, K., Tonn, K., Zhao, Y., Fietzek, U.M., Schroeteler, F., Ziegler, K., Ceballos-Baumann, A.O., & Lueth, T.C. 2011b. Freezing of gait detection in parkinson's disease using accelerometer based smart clothes. *Pages 201–204 of: Biomedical Circuits and Systems Conference (BioCAS), 2011 IEEE*. IEEE.

Nicolaou, N., Hourris, S., Alexandrou, P., & Georgiou, J. 2012. EEG-based automatic classification of awakeversus anesthetizedstate in general anesthesia using Granger causality. *PLoS One*, **7**(3), e33869.

Nieuwboer, A., & Giladi, N. 2013a. Characterizing freezing of gait in Parkinson's disease: Models of an episodic phenomenon. *Movement Disorders*, **28**(11), 1509–1519.

Nieuwboer, A., & Giladi, N. 2013b. Characterizing freezing of gait in Parkinson's disease: models of an episodic phenomenon. *Movement Disorders*, **28**(11), 1509–1519.

Nieuwboer, A., Rochester, L., Herman, T., Vandenberghe, W., Emil, G.E., Thomaes, T., & Giladi, N. 2009. Reliability of the new freezing of gait questionnaire: agreement between patients with Parkinson's disease and their carers. *Gait & Posture*, **30**(4), 459–463.

Niewboer, A., Dom, R., Weerdt, W., Desloovere, K., Janssens, L., & Stijn, V. 2004. Electromyographic profiles of gait prior to onset of freesing episodes in patients with Parkinsons disease. *Brain*, **127**(7), 1650–1660.

Nolte, G., Bai, O., Wheaton, L., Mari, Z., Vorbach, S., & Hallett, M. 2004. Identifying true brain interaction from EEG data using the imaginary part of coherency. *Clinical Neurophysiology*, **115**(10), 2292–2307.

Nunez, P.L., & Srinivasan, R. 2006. *Electric fields of the brain: the neurophysics of EEG*. Oxford University Press.

Nutt, J.G., Bloem, B.R., Giladi, N., Hallett, M., Horak, F.B., & Nieuwboer, A. 2011a. Freezing of gait: moving forward on a mysterious clinical phenomenon. *The Lancet Neurology*, **10**(8), 734–744.

Nutt, J.G., Bloem, B.R., Giladi, N., Hallett, M., Horak, F.B., & Nieuwboer, A. 2011b. Freezing of gait: moving forward on a mysterious clinical phenomenon. *The Lancet Neurology*, **10**(8), 734–744.

Okuma, Y. 2006. Freezing of gait in Parkinsons disease. *Journal of Neurology*, **253**(7), vii27–vii32.

Okuma, Y. 2014. Practical approach to freezing of gait in Parkinson's disease. *Practical Neurology*, **14**(4), 222–230.

Olbrich, S., Olbrich, H., Adamaszek, M., Jahn, I., Hegerl, U., & Stengler, K. 2013. Altered EEG lagged coherence during rest in obsessive–compulsive disorder. *Clinical Neurophysiology*, **124**(12), 2421–2430.

Omidvarnia, A., Mesbah, M., O'Toole, J.M., Colditz, P., & Boashash, B. 2011. Analysis of the time-varying cortical neural connectivity in the newborn EEG: A time-frequency approach. *Pages 179–182 of: Systems, Signal Processing and Their Applications (WOSSPA), 2011 7th International Workshop on*. IEEE.

Ortiz, E., Stingl, K., Münßinger, J., Braun, C., Preissl, H., & Belardinelli, P. 2012. Weighted phase lag index and graph analysis: preliminary investigation of functional connectivity during resting state in children. *Computational and Mathematical Methods in Medicine*, **2012**.

Ozaki, T. 2012. *Time series modeling of neuroscience data*. CRC Press.

Penfield, W., & Welch, K. 1951. The supplementary motor area of the cerebral cortex: a clinical and experimental study. *AMA Archives of Neurology & Psychiatry*, **66**(3), 289–317.

Pereda, E., Quiroga, R.Q., & Bhattacharya, J. 2005. Nonlinear multivariate analysis of neurophysiological signals. *Progress in Neurobiology*, **77**(1), 1–37.

Picot, A., Charbonnier, S., & Caplier, A. 2012. On-line detection of drowsiness using brain and visual information. *Systems, Man and Cybernetics, Part A: Systems and Humans, IEEE Transactions on*, **42**(3), 764–775.

Popovic, M.B., Jovicic, M.D., Radovanovic, S., Petrovic, I., & Kostic, V. 2010. A simple method to assess freezing of gait in Parkinsons disease patients. *Brazilian Journal of Medical and Biological Research*, **43**, 883–889.

Porcaro, C., Zappasodi, F., Rossini, P.M., & Tecchio, F. 2009. Choice of multivariate autoregressive model order affecting real network functional connectivity estimate. *Clinical Neurophysiology*, **120**(2), 436–448.

Press, C., Cook, J., Blakemore, S.-J., & Kilner, J. 2011. Dynamic modulation of human motor activity when observing actions. *The Journal of Neuroscience*, **31**(8), 2792–2800.

Priestley, M.B. 1996. Wavelets and Tiem-dependent Spectral Analysis. *Journal of Time Series Analysis*, **17**(1), 85–103.

Quian Quiroga, R. 2009. Bivariable and multivariable analysis of EEG signals. *Quantitative EEG analysis: Methods and applications*, 109–120.

Rahman, S., Griffin, H.J., Quinn, N.P., & Jahanshahi, M. 2008. The factors that induce or overcome freezing of gait in Parkinsons disease. *Behavioural Neurology*, **19**(3), 127–136.

Reed, C.L. 1998. Evidence for movement preprogramming and on line control in differentially impaired patients with parkinson's disease. *Cognitive Neuropsychology*, **15**(6-8), 723–745.

Rosenblum, M.G., Pikovsky, A.S., & Kurths, J. 1996. Phase synchronization of chaotic oscillators. *Physical Review Letters*, **76**(11), 1804.

Rosso, O.A. 2007. Entropy changes in brain function. *International Journal of Psychophysiology*, **64**(1), 75–80.

Rowe, J.B., & Siebner, H.R. 2012. The motor system and its disorders. *Neuroimage*, **61**(2), 464–477.

Rubinstein, T.C., Giladi, N., & Hausdorff, J.M. 2002. The power of cueing to circumvent dopamine deficits: a review of physical therapy treatment of gait disturbances in Parkinson's disease. *Movement Disorders*, **17**(6), 1148–1160.

Saarni, S.I., Härkänen, T., Sintonen, H., Suvisaari, J., Koskinen, S., Aromaa, A., & Lönnqvist, J. 2006. The impact of 29 chronic conditions on health-related quality of life: a general population survey in Finland using 15D and EQ-5D. *Quality of Life Research*, **15**(8), 1403–1414.

Saito, Y., & Harashima, H. 1981. Tracking of information within multichannel EEG record causal analysis in EEG. *Recent advances in EEG and EMG data processing*, 133–146.

Sameshima, K., & Baccalá, L.A. 1999. Using partial directed coherence to describe neuronal ensemble interactions. *Journal of Neuroscience Methods*, **94**(1), 93–103.

Sanei, S., & Chambers, J.A. 2008. *EEG Signal Processing*. John Wiley & Sons.

Schaafsma, J.D., Balash, Y., Gurevich, T., Bartels, A.L., Hausdorff, J.M., & Giladi, N. 2003. Characterization of freezing of gait subtypes and the response of each to levodopa in Parkinson's disease. *European Journal of Neurology*, **10**(4), 391–398.

Schack, B., & Krause, W. 1995. Dynamic power and coherence analysis of ultra short-term cognitive processesA methodical study. *Brain Topography*, **8**(2), 127–136.

Schlögl, A. 2006. A comparison of multivariate autoregressive estimators. *Signal Processing*, **86**(9), 2426–2429.

Schneider, T., & Neumaier, A. 2001. Algorithm 808: ARfitA Matlab package for the estimation of parameters and eigenmodes of multivariate autoregressive models. *ACM Transactions on Mathematical Software (TOMS)*, **27**(1), 58–65.

Semmlow, J.L. 2011. *Biosignal and Medical Image Processing*. CRC press.

Seth, A.K. 2005. Causal connectivity of evolved neural networks during behavior. *Network: Computation in Neural Systems*, **16**(1), 35–54.

Shannon, C.E. 1948. Bell System Tech. J. 27 (1948) 379; CE Shannon. *Journal of Bell System Technology*, **27**, 623.

Shin, H.C., Jia, X., Nickl, R., Geocadin, R.G., & Thakor, N.V. 2008. A Subband-Based Information Measure of EEG During Brain Injury and Recovery After Cardiac Arrest. *IEEE Transactions on Biomedical Engineering*, **55**(8), 1985–1990.

Shine, J.M., Naismith, S.L., & Lewis, S.J.G. 2011. The pathophysiological mechanisms underlying freezing of gait in Parkinsons disease. *Journal of Clinical Neuroscience*, **18**(9), 1154–1157.

Shine, J.M., Moore, S.T., Bolitho, S.J., Morris, T.R., Dilda, V., Naismith, S.L., & Lewis, S.J.G. 2012. Assessing the utility of freezing of gait questionnaires in Parkinsons disease. *Parkinsonism & Related Disorders*, **18**(1), 25–29.

Shine, J.M., Naismith, S.L., & Lewis, S.J.G. 2013a. The differential yet concurrent contributions of motor, cognitive and affective disturbance to freezing of gait in Parkinson's disease. *Clinical Neurology and Neurosurgery*, **115**(5), 542–545.

Shine, J.M., Moustafa, A.A., Matar, E., Frank, M.J., & Lewis, S.J.G. 2013b. The role of frontostriatal impairment in freezing of gait in Parkinson's disease. *Frontiers in Systems Neuroscience*, **7**.

Shine, J.M., Handojoseno, A.M.A., Nguyen, T.N., Tran, Y., Naismith, S.L., Nguyen, H., & Lewis, S.J.G. 2014. Abnormal patterns of theta frequency oscillations during the temporal evolution of freezing of gait in Parkinsons disease. *Clinical Neurophysiology*, **125**(3), 569–576.

Shoushtarian, M., Murphy, A., & Iansek, R. 2011. Examination of central gait control mechanisms in Parkinson's disease using movement-related potentials. *Movement Disorders*, **26**(13), 2347–2353.

Silberstein, P., Pogosyan, A., Kühn, A.A., Hotton, G., Tisch, S., Kupsch, A., Dowsey-Limousin, P., Hariz, M.I., & Brown, P. 2005. Cortico-cortical coupling in Parkinson's disease and its modulation by therapy. *Brain*, **128**(6), 1277–1291.

Simuni, T., & Hurtig, H. 2008. *Parkinsons Disease: Diagnosis and Clinical Management*. 2nd edition edn. New York: Demos Medical Publishing. Chap. Levodopa: A pharmalogic Miracle Four Decades Later, pages 471–490.

Sitnikova, E., Hramov, A.E., Koronovsky, A.A., & van Luijtelaar, G. 2009. Sleep spindles and spike–wave discharges in EEG: their generic features, similarities and distinctions disclosed with Fourier transform and continuous wavelet analysis. *Journal of Neuroscience Methods*, **180**(2), 304–316.

Skudlarski, P., Jagannathan, K., Anderson, K., Stevens, M.C., Calhoun, V.D., Skudlarska, B.A., & Pearlson, G. 2010. Brain connectivity is not only lower but different in schizophrenia: a combined anatomical and functional approach. *Biological Psychiatry*, **68**(1), 61–69.

Snijders, A.H. 2012. *Tackling freezing of gait in Parkinson's disease*. Nijmegen, the Netherlands: [Donders Institute for Brain, Cognition and Behaviour, Radboud University Medical centre, Nijmegen, the Netherlands].

Snijders, A.H., Leunissen, I., Bakker, M., Overeem, S., Helmich, R.C., Bloem, B.R., & Toni, I. 2011. Gait-related cerebral alterations in patients with Parkinsons disease with freezing of gait. *Brain*, **134**(1), 59–72.

Sporns, O. 2011. *Networks of the Brain*. MIT press.

Sporns, O., Chialvo, D.R., Kaiser, M., & Hilgetag, C.C. 2004. Organization, development and function of complex brain networks. *Trends in Cognitive Sciences*, **8**(9), 418–425.

Stam, C.J., Nolte, G., & Daffertshofer, A. 2007. Phase lag index: assessment of functional connectivity from multi channel EEG and MEG with diminished bias from common sources. *Human Brain Mapping*, **28**(11), 1178–1193.

Staudinger, T., & Polikar, R. 2011. Analysis of complexity based EEG features for the diagnosis of Alzheimer's disease. *Pages 2033–2036 of: Engineering in Medicine and Biology Society, EMBC, 2011 Annual International Conference of the IEEE*. IEEE.

Subasi, A. 2007. EEG signal classification using wavelet feature extraction and a mixture of expert model. *Expert Systems with Applications*, **32**(4), 1084–1093.

Suchan, B., Zoppelt, D., & Daum, I. 2003. Frontocentral negativity in electroencephalogram reflects motor response evaluation in humans on correct trials. *Neuroscience Letters*, **350**(2), 101–104.

Sullivan, G.M., & Feinn, R. 2012. Using effect size-or why the P value is not enough. *Journal of Graduate Medical Education*, **4**(3), 279–282.

Supekar, K., Menon, V., Rubin, D., Musen, M., & Greicius, M.D. 2008. Network analysis of intrinsic functional brain connectivity in Alzheimer's disease. *PLoS Computational Biology*, **4**(6), e1000100.

Tas, C., Cebi, M., Tan, O., Hızlı-Sayar, G., Tarhan, N., & Brown, E.C. 2015. EEG power, cordance and coherence differences between unipolar and bipolar depression. *Journal of Affective Disorders*, **172**, 184–190.

Teolis, A. 1998. *Computational signal processing with wavelets*. Springer Science & Business Media.

Thatcher, R.W., North, D., & Biver, C. 2005. EEG and intelligence: relations between EEG coherence, EEG phase delay and power. *Clinical Neurophysiology*, **116**(9), 2129–2141.

Theiler, J., Eubank, S., Longtin, A., Galdrikian, B., & Farmer, J.D. 1992. Testing for nonlinearity in time series: the method of surrogate data. *Physica D: Nonlinear Phenomena*, **58**(1), 77–94.

Trambaiolli, L.R., Falk, T.H., Fraga, F.J., Anghinah, R., & Lorena, A.C. 2011. EEG spectro-temporal modulation energy: a new feature for automated diagnosis of Alzheimer's disease. *Pages 3828–3831 of: Proceeding of the 33rd Annual International Conference of the IEEE EMBS*.

Tripoliti, E.E., Tzallas, A.T., Tsipouras, M.G., Rigas, G., Bougia, P., Leontiou, M., Konitsiotis, S., Chondrogiorgi, M., Tsouli, S., & Fotiadis, D.I. 2013. Automatic detection of freezing of gait events in patients with Parkinson's disease. *Computer Methods and Programs in Biomedicine*, **110**(1), 12–26.

Übeyli, E.D. 2009. Combined neural network model employing wavelet coefficients for EEG signals classification. *Digital Signal Processing*, **19**(2), 297–308.

Van Drongelen, W. 2006. *Signal processing for neuroscientists: an introduction to the analysis of physiological signals*. Academic Press.

Velik, R., Hoffmann, U., Zabaleta, H., Marti, J.F., & Keller, T. 2012. The effect of visual cues on the number and duration of freezing episodes in Parkinson's patients. *Pages 4656–4659 of: Engineering in Medicine and Biology Society (EMBC), 2012 Annual International Conference of the IEEE*. IEEE.

Velu, P.D., Mullen, T., Noh, E., Valdivia, M.C., Poizner, H., Baram, Y., & de Sa, V.R. 2013. Effect of visual feedback on the occipital-parietal-motor network in Parkinsons disease with freezing of gait. *Frontiers in Neurology*, **4**.

Vinck, M., Oostenveld, R., van Wingerden, M., Battaglia, F., & Pennartz, C. 2011. An improved index of phase-synchronization for electrophysiological data in the presence of volume-conduction, noise and sample-size bias. *Neuroimage*, **55**(4), 1548–1565.

Vogl, T.P., Mangis, J.K., Rigler, A.K., Zink, W.T., & Alkon, D.L. 1988. Accelerating the convergence of the back-propagation method. *Biological Cybernetics*, **59**(4-5), 257–263.

Walter, D.O., & Adey, W.R. 1965. Analysis of brain-wave generators as multiple statistical time series. *Biomedical Engineering, IEEE Transactions on*, 8–13.

Walton, C.C., Shine, J.M., Hall, J.M., OCallaghan, C., Mowszowski, L., Gilat, M., Szeto, J.Y.Y., Naismith, S.L., & Lewis, S.J.G. 2015. The major impact of freezing of gait on quality of life in Parkinsons disease. *Journal of Neurology*, **262**(1), 108–115.

Waser, M., Deistler, M., Garn, H., Benke, T., Dal-Bianco, P., Ransmayr, G., Grossegger, D., & Schmidt, R. 2013. EEG in the diagnostics of Alzheimers disease. *Statistical Papers*, **54**(4), 1095–1107.

Weiss, D., Klotz, R., Govindan, R.B., Scholten, M., Naros, G., Ramos-Murguialday, A., Bunjes, F., Meisner, C., Plewnia, C., Krüger, R., *et al.* 2015. Subthalamic stimulation modulates cortical motor network activity and synchronization in Parkinsons disease. *Brain*, **138**(3), 679–693.

Welch, P.D. 1967. The use of fast Fourier transform for the estimation of power spectra: a method based on time averaging over short, modified periodograms. *IEEE Transactions on Audio and Electroacoustics*, **15**(2), 70–73.

WHO, *et al.* 2004. *Atlas: country resources for neurological disorders 2004: results of a collaborative study of the World Health Organization and the World Federation of Neurology*. Tech. rept. Geneva: World Health Organization. Accessed: 11 August 2011.

Wichmann, T., Smith, Y., & Vitek, J. L. 2007. *Parkinson's Disease: Diagnosis and Clinical Management*. 2nd edition edn. New York: Demos Medical Publishing. Chap. Basal Ganglia: Anatomy and Physiology, pages 245–265.

Wieler, M. 2003. *Freezing of gait in Parkinson's disease*. Master Thesis, Departement of Medicine, University of Alberta.

Wiener, N. 1956. The Theory of Prediction. *Modern Mathematica*, 165–190.

Wikström, S., Pupp, I.H., Rosén, I., Norman, E., Fellman, V., Ley, D., & Hellström-Westas, L. 2012. Early single-channel aEEG/EEG predicts outcome in very preterm infants. *Acta Paediatrica*, **101**(7), 719–726.

Wolters, E.Ch., & Bosboom, J.L.W. 2007. *Parkinsonism and Related Disorders*. 2nd edn. VU University Press. Chap. Parkinson's Disease, pages 143–158.

Wright, S. 1921. Correlation and causation. *Journal of Agricultural Research*, **20**(7), 557–585.

Xizheng, Z., Ling, Y., & Weixiong, W. 2010. Wavelet Time-frequency Analysis of Electroencephalogram (EEG) Processing. *International Journal of Advanced Computer Science and Applications*, **1**(5), 1–5.

Yelnik, J. 2002. Functional Anatomy of the Basal Ganglia. *Movement Disorders*, **17 (Suppl.3)**, S15–S21.

Yom-Tov, E., & Inbar, G.F. 2003. Detection of movement-related potentials from the electro-encephalogram for possible use in a brain-computer interface. *Medical and Biological Engineering and Computing*, **41**(1), 85–93.